THE INTERPLAY BETWEEN THE TUMOUR SUPPRESSOR P53 AND ITS NEGATIVE REGULATORS MDM2 AND MDMX

by

Qinyan Song

Submitted in partial fulfilment of the requirements
for the degree of Doctor of Philosophy

at

Dalhousie University
Halifax, Nova Scotia
August 2020

DEDICATION PAGE

For my family

For Jiani

For my mentors

For my friends

TABLE OF CONTENTS

LIST OF TABLES

LIST OF FIGURES

ACKNOWLEDGEMENTS

First of all, I would like to thank Dr. Paul Liu for providing me with an opportunity to work in his lab as a graduate student where I have benefited from the friendly, proactive and self-motivated learning environment. I especially want to thank him for his patience and supervision during the course of my graduate studies. I would also like to thank Dr. Jan Rainey to be my co-supervisor and for his wealth of knowledge that helped me to understand the basis of solution state NMR. Paul and Jan have been excellent mentors and I want to thank them for providing guidance on my research and scientific writing. The opportunities that Paul and Jan have provided me to attend national and international conferences are very helpful for me to grow as an independent, professional researcher. I would also like to thank my committee members, Drs. Stephen Bearne, Vanya Ewart and David Langelaan, who provided me with numerous helpful comments and suggestions. I am especially thankful for their encouragement throughout my graduate program.

I am also grateful to my former and current colleagues in the Liu and Rainey labs who helped me to grasp many key aspects of science and familiarize with many of the research techniques. I treasure the friendship and happy moments with all of them, including Drs. Xudong Dai and Lingling Xu who helped with my research project from the start. I would also like to thank Mr. Ian Burton and Dr. Tara Sprules for their expertise in NMR spectroscopy and handling of the NMR spectrometer at the National Research Council and the Quebec/Eastern Canada High Field NMR Facility. I want to like to thank Dr. Stephen Bearne for providing me with the access of his ITC and DSC instruments. I would also like to thank Roisin for her continuous support throughout my degree program. Finally, I would like to thank Natural Sciences and Engineering Research Council for funding this work.

Above all I want to thank my parents for their love and continuous support, for giving me a chance to pursue my study at the highest level. I was fortunate to meet and marry my wife Jiani here in Halifax; it must be our destiny to come across each other in a country far away from home. Her love and encouragements are invaluable for supporting me over the difficult times.

LIST OF ABBREVIATIONS AND SYMBOLS USED

δ	Chemical shift
Δδ	Secondary chemical shift
ε	Molar extinction coefficient
ℓ	Path length
[θ]	Mean residue ellipticity
AD	Acidic domain
AE	Anion exchange
Amp	Ampicillin
CBD	Chitin binding domain
CD	Circular dichroism
CE	Cation exchange
CSP	Chemical shift perturbation
dH_2O	Distilled water
DBD	DNA-binding domain
DNA	Deoxyribonucleic acid
DTT	Dithiothreitol
D_2O	Deuterium oxide
DSC	Differential scanning calorimetry

DSS	Sodium trimethylsilylpropanesulfonate
EDTA	Ethylenediaminetetraacetic acid
FPLC	Fast protein liquid chromatography
g	Relative centrifugal force
H_6	Hexahistine
hetNOE	Heteronuclear Overhauser effect
IMAC	Immobilized metal affinity chromatography
HSQC	Heteronuclear single quantum coherence
IPTG	Isopropyl β-D-1-thiogalactopyranoside
IARC	International Ageny for Research on Cancer
ITC	Isothermal titration calorimetry
K_d	Dissociation constant
LB	Lysogeny broth
MDM2	Mouse double minute 2 homolog
MDMX	Mouse double minute X homolog
Mer	2-mercaptoethanol
mtDNA	Mitochondrial DNA
MW	Molecular weight
MWCO	Molecular weight cut off

NES	Nuclear export signal
NLS	Nuclear localization signal
NMR	Nuclear magnetic resonance
Ni-NTA	Nickel-nitrilotriacetic acid
NRC	National Research Council
OD	Optical density
OLD	Oligomerization domain
PAGE	polyacrylamide gel electrophoresis
PBD	p53-binding domain
PCR	Polymerase chain reaction
PDB	Protein data bank
PRD	Proline rich domain
PRE	Paramagnetic relaxation enhancement
PTM	Post-translational modification
Pu	Purine
QANUC	Quebec/Eastern Canada High Field NMR Facility
RD	Regulatory domain
RT	Room temperature
SDS	Sodium dodecyl sulphate

SUMO	Small ubiquitin-like modifier
TCS	Thrombin cleavage site
TCEP	tris(2-carboxyethyl)phosphine
TD	Transactivation domain
TEMPO	2,2,6,6-tetramethyl-1-piperidinyloxy
TROSY	Transverse relaxation optimized spectroscopy
Ub	Ubiquitin
UV-Vis	Ultraviolet–visible
WT	Wild type
z	Net charge
ZFD	Zinc finger domain

ABSTRACT

p53 is a crucial tumour suppressor that is dysfunctional in most types of cancer. The *TP53* gene is frequently mutated in many cancers, resulting in loss of p53 expression or production of mutant p53 proteins that are unable to inhibit tumour development. In cancer where wild-type p53 is expressed, tumour cells develop mechanisms to prevent activation of p53. Inactivation of p53 is commonly achieved through upregulation of the negative regulators MDM2 and MDMX, which directly inhibit p53 activity and promote p53 degradation. Restoration of p53 tumour-suppressive function can effectively inhibit tumour progression and stimulate tumour regression, which provides an attractive target for cancer therapy.

Prior studies have detailed the mechanism of MDM2- and MDMX-mediated p53 inhibition by focusing on the inhibitory complex formed between the p53-binding domain of MDM2 or MDMX and the p53 transactivation domain. However, emerging evidence suggests that the acidic domains of MDM2 and MDMX play key roles in regulating p53 ubiquitination and DNA interaction. In this study, I further characterized the interaction between acidic domain of MDM2 and the DNA-binding domain of p53 using calorimetric techniques and NMR spectroscopy. Adding new context to this intermolecular interaction, I demonstrated that the acidic domain of MDM2 can directly bind to the p53 C-terminal regulatory domain. I also evaluated the role of the p53 transactivation domain in regulating the interaction between the acidic domain of MDM2 and the p53 DNA binding domain. Importantly, I have newly demonstrated that the acidic domain of MDMX is a direct intermolecular binding partner for the MDM2 p53-binding domain. Through these findings, I have proposed a new working model for the interplay between the tumour suppressor p53 and its negative regulators MDM2 and MDMX while highlighting some important questions that need to be addressed in future studies.

CHAPTER 1: INTRODUCTION

The research goal of this thesis is to characterize the role of domain-domain interactions between the tumour suppressor p53 and its negative regulators MDM2 and MDMX in regulating the activity of p53. Compromised p53 activity is frequently found in cancers either through mutation in the *TP53* gene to alter its function or overexpression of the negative regulators MDM2 or MDMX to inactivate p53 (Brown, Lain, Verma, Fersht, & Lane, 2009). For these reasons, reactivation of p53 is a promising strategy for cancer treatment. In order to identify therapeutic targets and develop better drug molecules, great effort has been made exploring the relationship between structure and function for p53 and both MDM2 and MDMX. In particular, the central region of either MDM2 or MDMX has shown to have the ability to regulate p53 activity and stability (Bista, Petrovich, & Fersht, 2013; Cheng, Song, Chen, & Chen, 2014; Cross et al., 2011; Wei, X. et al., 2016). Thus, further characterization of the central regions of MDM2 and MDMX is needed to understand their structural and functional relationship with p53. In this chapter, I briefly introduce p53, MDM2 and MDMX in the context of both physiological and pathological conditions, followed by a brief overview of the objectives for this thesis.

1.1 Cancer

Cancer is one of the most frequently diagnosed diseases across the globe. From a worldwide perspective, the International Agency for Research on Cancer estimated that in 2020 there would be 19 million newly diagnosed patients and 10 million deaths from cancer (Bouaoun et al., 2016). In Canada alone, it is estimated that there will be 225,800 new cancer patients and 83,300 deaths from cancer in 2020 (Brenner et al., 2020). Moreover, about half of Canadians will develop cancer in their lifetimes and 1 in 4 will die as a result of cancer. Correspondingly, in 2019

cancer was the number one cause of death in Canada. Cancer therefore represents a major health and financial issue both in Canada and worldwide.

Cancer is caused by genetic alterations that drive the transformation of normal human cells into malignant and malfunctioning cells (Hanahan, D. & Weinberg, 2000). Cells in our body are under constant stress, such as exposure to ionizing radiation, and generation of reactive oxygen species can lead to accumulation of genetic damage to promote cancer development (Storz, 2005; Thomas et al., 1994). Under normal conditions, these damaged cells are either subjected to DNA damage repair or undergo apoptosis (Roos, Thomas, & Kaina, 2016). If these two mechanisms fail, accumulation of genetic damage can trigger oncogenic transformation to promote cancer development. These mutations lead to elevation of cancer-promoting functions (oncogenes) or abatement cancer-preventing functions (tumour suppressor genes) that together provide survival and growth benefits for the cancer cells (Klein, 1988).

As proposed by Hanahan, Douglas & Weinberg (2011), cancer is the result of acquisition of a series of biological capacities that provide cells with the ability to sustain continuous proliferation; evade growth suppression; resist to cell death; promote replicative immortality; stimulate angiogenesis; activate invasion and metastasis; reprogram energy metabolism; and, escape from the host immune defense. Each of these fundamental traits necessary for cancer cells requires disruption of cellular signaling pathways in healthy cells that favour the homeostasis of normal cellular and tissue architecture. Genetic alternations that benefit cancer growth require accumulation of mutations for key target genes. Of these, *TP53* is the one of the most frequently mutated genes and, correspondingly, its gene product the p53 tumour suppressor is one of the most broadly affected proteins in cancer cells (Baker et al., 1989; Hollstein, M., Sidransky, Vogelstein, & Harris, 1991; Hollstein, M. C., Metcalf, Welsh, Montesano, & Harris, 1990; Iggo, Gatter,

Bartek, Lane, & Harris, 1990; Nakai, Misawa, Toguchida, Yandell, & Ishizaki, 1992; Nigro et al., 1989; Takahashi et al., 1989).

1.2 p53 tumour suppressor

In 1979, it was discovered that a 53 kDa protein from the host cell, which was given the name p53, was associated with the large T-antigen of tumour DNA virus, Simian Virus 40 (SV-40) (Kress, May, Cassingena, & May, 1979; Lane & Crawford, 1979; Linzer & Levine, 1979). Following the first successful cloning of p53 in 1984, it was first demonstrated that the cloned p53 possesses oncogenic activity (Eliyahu, Raz, Gruss, Givol, & Oren, 1984; Jenkins, Rudge, & Currie, 1984; Parada, Land, Weinberg, Wolf, & Rotter, 1984). Subsequent studies soon showed that tumour viruses could inactivate and neutralize p53 (Ben David, Prideaux, Chow, Benchimol, & Bernstein, 1988; Mowat, Cheng, Kimura, Bernstein, & Benchimol, 1985; Wolf & Rotter, 1984), which paved the road for further characterization of its tumour suppressive function. Sequencing of a murine wild-type p53 in 1988 further confirmed that the original p53 clone was a tumour-associated p53 mutant rather than a functional protein (Eliyahu et al., 1988; Finlay et al., 1988). In 1989, studies from different research groups confirmed that p53 can suppress E1A- and Ras-mediated oncogenic transformation, at which point p53 was first classified as a tumour suppressor protein (Eliyahu, Michalovitz, Eliyahu, Pinhasi-Kimhi, & Oren, 1989; Finlay, Hinds, & Levine, 1989; Hinds, Finlay, & Levine, 1989). Later, it was confirmed that tumours frequently harbour p53 mutations or deletions, consistent with its role as a tumour suppressor (Menon et al., 1990; Nigro et al., 1989). In the same year, inherited germline mutations of the *TP53* gene were discovered as the primary driving force of Li-Fraumeni Syndrome (Li, F. P. & Fraumeni, 1982; Malkin et al., 1990; Pirollo, Srivastava, Blattner, Zou, & Chang, 1990). The patients of this

autosomal dominant syndrome are more susceptible to develop multiple types of cancer at an early age. The tumour-suppressive function of p53 was further demonstrated experimentally by generation of p53 knockout mice, where these mice, despite of normal development and essentially the same appearance as wild-type mice, suffer from spontaneous tumour growth at early ages (Donehower, L. A. et al., 1992). These early studies highlighted the importance of this tumour suppressor and, till today, have fueled 40 years of research on p53.

1.2.1 The functions of the p53 protein

p53 is a transcription factor that is maintained at low level in unstressed cells (Chernov, Bean, Lerner, & Stark, 2001; Farmer et al., 1992; Maltzman & Czyzyk, 1984; Pietenpol et al., 1994; Price & Calderwood, 1993; Schärer & Iggo, 1992). Upon stress-induced stimulation, p53 is quickly stabilized and localized to the nucleus (Marchenko et al., 2010). Interestingly, emerging evidence suggests that stable fractions of p53 are localized to the mitochondria, where the protein exerts site-specific functions (Vaseva & Moll, 2009) (Figure 1.1). The existence of distinct pools of p53 highlighted the importance of p53 in regulating diverse pathways inside the cell.

Nuclear p53

The most well-established function of p53 is the ability to induce transcription of downstream genes that are involved in diverse signaling pathway in response to stress, such as cell cycle arrest (e.g. p21), DNA-damage repair (e.g. p53R2) and apoptosis (e.g. BAX) (Andrysik et al., 2017; Chipuk et al., 2004; Fischer, 2017; Tebaldi et al., 2015; Yamaguchi et al., 2001). The p53 protein directly binds to the p53 response elements, i.e. the consensus binding site in the

genomic DNA, where it recruits multiple components of the transcription machinery (Beckerman & Prives, 2010). Recruitment of chromatin modifiers such as histone acetyl transferases (e.g CBP/p300 & GCN5) and histone methyl transferases (e.g. PRMT1 & CARM1) help to modify chromatin structure and promote recruitment of the transcription factor TFIID, which consists of TATA-binding protein (TBP) and multiple TBP-associated factors (An, Kim, & Roeder, 2004; Ard et al., 2002; Avantaggiati et al., 1997; Barlev et al., 2001; Beckerman & Prives, 2010; Chen, X., Farmer, Zhu, Prywes, & Prives, 1993; Coleman et al., 2017; Farmer, Colgan, Nakatani, Manley, & Prives, 1996; Liu, X., Miller, Koeffler, & Berk, 1993; Scolnick et al., 1997; Thut, Chen, Klemm, & Tjian, 1995; Truant, Xiao, Ingles, & Greenblatt, 1993; Wang, T. et al., 2001). Once bound, TFIID nucleates the formation of pre-initiation complex, including RNA polymerase II and several other transcription factors, to promote transcription (Beckerman & Prives, 2010; Louder et al., 2016). In the absence of functional p53, TFIID cannot effectively recognize the promoters, leading to insufficient transcription initiation due to inefficient pre-initiation complex assembly (Coleman et al., 2017; Xing, Sheppard, Corneillie, & Liu, 2001). Thus, cancer-associated p53 mutations that abolish its transcriptional activity will ensure survival of cancer cells through alteration of p53 downstream signaling.

In addition to its transcriptional activity, another critical nuclear function of p53 is direct control of the DNA-damage response. p53 can directly upregulate genes involved in DNA-damage repair (Andrysik et al., 2017; Fischer, 2017). Moreover, it is directly involved in DNA-damage repair pathways, including nucleotide-excision repair, mismatch repair and double-strand break repair (Williams & Schumacher, 2016). This activity of p53 is achieved through direct interaction with many of the proteins involved in DNA repair and finetunes their specific activity, which leads to improved fidelity in the DNA-damage repair process. Interestingly, it has been demonstrated

that p53 possesses intrinsic 3' - 5' exonuclease activity that is important for DNA-damage repair and proofreading during DNA replication (Huang, P., 1998; Lilling, Elena, Sidi, & Bakhanashvili, 2003; Skalski, Lin, Choi, & Brown, 2000). The multitude and complexity of p53 activity in the DNA-damage response highlights the significance of p53 in maintaining genome integrity and prevention of oncogenic transformation, which lead to its being promoted as "the guardian of the genome" (Lane, 1992).

Cytoplasmic p53

The most notable function of cytoplasmic p53 is its transcription-independent tumour-suppressive activity. Early studies demonstrated that p53 could induce apoptosis in absence of transcriptional activity (Caelles, Helmberg, & Karin, 1994; Ding et al., 1998; Haupt, Y., Rowan, Shaulian, Vousden, & Oren, 1995). It was later confirmed that this activity is mediated by mitochondrial outer membrane permeabilization (Arima et al., 2005; Marchenko, Zaika, & Moll, 2000; Mihara et al., 2003; Moll, Marchenko, & Zhang, 2006). This pro-apoptotic activity of p53 is achieved through direct interaction with Bcl-2 family proteins. In the cytosol, p53 is normally sequestered by the anti-apoptotic protein Bcl-xL, which binds to p53 and prevents p53-mediated apoptosis (Chipuk, Bouchier-Hayes, Kuwana, Newmeyer, & Green, 2005; Follis, A. V. et al., 2014; Follis, Ariele Viacava et al., 2013). Under stress, expression of the BH3-only protein PUMA is induced and results in cytosolic accumulation, where it directly associates with Bcl-xL to induce a conformational change of Bcl-xL and disrupt the p53-Bcl-xL complex (Chipuk et al., 2005; Follis, Ariele Viacava et al., 2013). Free p53 quickly associates with the pro-apoptotic proteins BAX and BAK, resulting in mitochondrial outer membrane permeabilization and apoptosis

(Chipuk et al., 2004; Follis, Ariele Viacava et al., 2015; Leu, Dumont, Hafey, Murphy, & George, 2004).

Recent evidence suggests that cytosolic p53 can achieve apoptosis through an alternative mechanism. Cytoplasmic p53 is found to localize to the endoplasmic reticulum (ER) at specialized contact domains between the ER and mitochondria (mitochondria-associated membrane). Upon stress stimulation, p53 accumulates at these sites to modulate Ca^{2+} homeostasis. p53 can also directly interact with and stimulate the activity of sarco/ER Ca^{2+}-ATPase pump, resulting in increased uptake of Ca^{2+} ions into the ER lumen and promotion of subsequent transfer to mitochondria. The accumulation of Ca^{2+} ions then quickly overloads the mitochondria and alters mitochondrial morphology, which promotes the release of caspase cofactors and results in induction of mitochondria dependent apoptosis (Giorgi et al., 2015).

Mitochondrial matrix p53

It is intriguing that a pool of p53 is also localized to the mitochondrial compartments, including the intermembrane space and the matrix (Bergeaud et al., 2013). Mitochondrial p53 transport requires the protein to cross multiple layers of mitochondrial membrane. There are three known mechanisms to translocate p53 into mitochondria: 1) through direct interaction with the carrier RecQ helicase-like protein 4, which has an N-terminal mitochondrial transport signal and binds to the translocase of the outer membrane 20 to facilitate p53 translocation into the mitochondria (De et al., 2012); 2) proteolytic cleavage of p53 in the cytoplasm through the activity of a heterodimeric endoprotease p90 & p40, which unveils a cryptic mitochondrial transport signal that helps its localization to the mitochondria (Boopathi, Srinivasan, Fang, & Avadhani, 2008);

and, 3) through the redox carrier protein coiled-coil-helix-coiled-coil-helix domain containing 4, which binds p53 to facilitate active mitochondrial translocation (Zhuang et al., 2013). Once imported, mitochondrial membrane could serve as a physical barrier to allow subcellular partitioning of its activity.

The mitochondrial p53, in part, serves to maintain the integrity of the mitochondrial genome. In the mitochondrial matrix, p53 is found to co-localize with mitochondrial DNA (mtDNA) and the replication apparatus (Bakhanashvili, M. et al., 2008b). p53 has been shown to directly associate with DNA polymerase γ and provide a proofreading function during DNA replication to maintain mtDNA integrity (Bakhanashvili, M. et al., 2008b; Bakhanashvili, M. et al., 2008a; Bakhanashvili, Mary, Grinberg, Bonda, & Rahav, 2009; Gupta et al., 2014). Several studies demonstrated that p53 directly participates in mtDNA repair pathways (Achanta et al., 2005; Chen, D., Yu, Zhu, & Lopez, 2006; de Souza-Pinto, Harris, & Bohr, 2004). p53 was found to directly interact with the DNA repair complex to enhance base excision repair activity (Wong, T. S. et al., 2009). In the presence of single-stranded DNA-binding proteins, p53 can effectively hydrolyze the 8-oxo-7,8-dihydro-2-deoxy-guanosine (8-oxo dG) presented at the 3'-end of DNA, a hallmark of oxidative stress, through its intrinsic 3'-5' exonuclease activity. Moreover, p53 was shown to control mtDNA copy number, which serves to maintain the normal mitochondrial functions (Lebedeva, Eaton, & Shadel, 2009).

Beside its role in directly regulating mtDNA, p53 can associate with ATP synthase to regulate mitochondrial respiration and reactive oxygen species generation (Bergeaud et al., 2013). It achieves this function by direct interaction with oligomycin sensitivity-conferring protein, a subunit of the F_1F_o-ATP synthase complex. In this case, p53 promotes O_2 consumption while reducing production of reactive oxygen species, thereby decreasing oxidative stress in the

mitochondria. Furthermore, p53 can facilitate the assembly of F_1F_o-ATP synthase, thus maintaining mitochondrial function.

1.2.2 Structure organization of the p53 protein

Human p53 is a 43.7 kDa protein consisting of 393 amino acids that coexists as monomer, homodimer and homotetramer inside the cell (Gaglia, Guan, Shah, & Lahav, 2013). The protein consists of five functional domains: an N-terminal transactivation domain (TD) that can be further divided into two subdomains TD1 and TD2, a proline-rich domain (PRD), a DNA-binding domain (DBD), an oligomerization domain (OD), and a regulatory domain (RD) at the C-terminus (Figure 1.2, A). Note that there is a ~ 30 residue spacer sequence between the DBD and the OD. The modular domain structure of p53 makes it a great receptor for diverse signals, where each domain can perform the tasks independently or multiple domains can work simultaneously to mediate downstream responses.

Transactivation domain (TD)

The TD is the central hub for protein-protein interactions with numerous proteins to mediate diverse downstream effects, including chromatin modifiers (e.g., CBP/p300), DNA damage repair proteins (e.g., BRCA2), core transcription machinery (e.g., TBP, Tfb1), and p53 negative regulators (e.g. MDM2/MDMX) (Chen, X. et al., 1993; Farmer et al., 1996; Fuchs, Adler, Buschmann, Wu, & Ronai, 1998; Kussie et al., 1996; Momand, Zambetti, Olson, George, & Levine, 1992; Moynahan, Pierce, & Jasin, 2001; Paola et al, 2006; Popowicz, Czarna, & Holak, 2008; Rajagopalan, S., Andreeva, Rutherford, & Fersht, 2010; Scolnick et al., 1997; Shvarts et al.,

1996; Shvarts et al., 1997; Thut et al., 1995; Truant et al., 1993). Importantly, removal of the TD completely abolish the function of p53 (Raj & Attardi, 2017), highlighting its critical role in promoting p53 activity.

The TD, spanning the N-terminal 60 residues, can be further divided into two subdomains that spans p53 residues 1 – 40 and 41 – 60, namely the TD1 and TD2 subdomains (Candau et al., 1997; Zhu, Zhou, Jiang, & Chen, 1998). Both the TD1 and TD2 subdomains are intrinsically disordered segments that only exhibit minimal α-helical character but undergo a disordered to ordered transition by adopting amphipathic helices once bound to binding partners such as CBP/p300 and MDM2 (Krois, Ferreon, Martinez-Yamout, Dyson, & Wright, 2016; Kussie et al., 1996; Lee et al., 2000). In the MDM2/p53 complex, TD1 adopts a short amphipathic helix allowing the side chains of three key hydrophobic residues, F19, W23 and L26, to penetrate deeply into the hydrophobic cleft of MDM2 (Kussie et al., 1996) (Figure 1.3, A). In the CBP/p53 complex, the key contact residues are F19, L22, W23, L25 and L26 of TD1, whose side chains mediate hydrophobic and cation-π contacts with CBP (Krois et al., 2016) (Figure 1.3, B). It is clear that both MDM2 and CBP can bind to the same sequence on TD1, which highlights the potential for TD1 to participate in a dynamic network that interacts with many proteins using same sequence.

Both TD1 and TD2 subdomains can bind cooperatively to the CBP, with each subdomain adopting an amphipathic helix that binds to the hydrophobic surface on the CBP (Krois et al., 2016) (Figure 1.3, B). Furthermore, both the TD1 and TD2 subdomains have been shown to bind to the same hydrophobic cleft of MDM2 or MDMX, suggesting that the TD1 and TD2 subdomains share some degree of sequence redundancy in mediating protein-protein interactions (Bochkareva et al., 2005; Shan, Li, Bruschweiler-Li, & Bruschweiler, 2012). Moreover, the TD2 subdomain forms an amphipathic helix involving key contacts driven by residues I50, W53, F54 and E56 that

bind the p62 and Tfb1 subunits of transcription factor II H (Paola et al., 2006). In addition, the TD2 subdomain can mimic single-stranded DNA, where the side chains of W53 and F54 mimic nucleotide bases and directly interact with single-stranded DNA binding proteins that are important for DNA replication and damage repair (e.g. RPA70 and PC4) (Bochkareva et al., 2005; Rajagopalan, S., Andreeva, Teufel, Freund, & Fersht, 2009). Interestingly, recent data suggest that TD2 can weakly interact with p53 DBD and modulate its DNA-binding specificity (He et al., 2019; Krois, Dyson, & Wright, 2018). The diverse function of the TD stresses its critical role in promoting p53 activity.

Proline rich domain (PRD)

The PRD, consisting of residues 61 – 90, is significantly enriched in proline content and has the propensity to adopt a polyproline II helix structure that serves as a rigid linker to point the TD away from the DBD (Baptiste, Friedlander, Chen, & Prives, 2002; Huang, F. et al., 2009). With five repeats of the PXXP motif, it was shown that the PRD can serve as a binding site for SH3 (Src homology 3) domains and appeared to affect the interaction with the histone acetyl transferase p300 (Dornan, Shimizu, Burch, Smith, & Hupp, 2003; Toledo et al., 2006). There was some evidence suggesting that the PRD modulates MDM2-mediated p53 degradation, p53 transcription activation, and transcription-independent apoptosis (Berger, Vogt Sionov, Levine, & Haupt, 2001; Dornan et al., 2003; Edwards, Hananeia, Eccles, Zhang, & Braithwaite, 2003; Zhu, Jiang, Zhou, Zhu, & Chen, 1999). However, PRD-mediated downstream effects have not been well studied and the structural and functional role of the PRD remains to be evaluated.

DNA-binding domain (DBD)

The DBD, spanning residues 100 – 292, is responsible for sequence specific DNA binding (Cho, Gorina, Jeffrey, & Pavletich, 1994; Pavletich, Chambers, & Pabo, 1993). Being a structured region, the structure of DBD has been widely studied (Cañadillas et al., 2006; Cho et al., 1994). The general shape of the DBD is a β-sandwich-like structure that contains two antiparallel β-sheets and a loop-sheet-helix motif packed tightly against one end of the β-sandwich (Figure 1.2, B and 1.3, C). The two antiparallel β-sheets consist of four (S1, S3, S8 and S5) and five (S6, S7, S4, S9 and S10) β-strands, respectively, and the β-sandwich structure is highly twisted toward either end of the β-sheets. The β-sheets at one end of the β-sandwich are tightly packed to adopt a compact β-barrel-like fold, and, in contrast, the other end is opened up to accommodate the loop-sheet-helix motif and two large loops. The two large loops L2 and L3 are held together by a tetrahedrally-coordinated Zn^{2+} ion through four residues, including three cysteines and one histidine. In addition, the L2 loop also contains a short helix (H1) that accommodates the structural histidine residue. The Zn^{2+} ion is structurally important for maintaining the correct folding of the DBD. Loss of the Zn^{2+} ion destabilized the structure of the DBD and compromised DNA binding activity. The loop-sheet-helix motif contains the S2-S2' β-hairpin, L1 loop and helix 2 (H2). The H2 packs tightly against the S2-S2' β-hairpin and L1 loop makes contact with H2 through hydrogen bonds (H-bonds). The loop-sheet-helix motif is anchored to the β-sandwich via the S10 strand, which forms a small, three-strand β-sheet together with the S2-S2' β-hairpin. The residues from S2 and S2' strands form extensive hydrophobic contact with a hydrophobic pocket formed by the S1, S3 and S8 strands, which further stabilizes the loop-sheet-helix motif.

The DBD makes specific contact with p53 binding sites on the genomic DNA. Typically, the binding sites consist of four copies of the consensus sequence Pu-Pu-Pu-C-(A/T) and are

orientated in pairs (Wang, Y., Schwedes, Parks, Mann, & Tegtmeyer, 1995). The major part of the core β-sandwich structure is not directly involved in DNA binding, rather it serves as the structural support for the loop-sheet-helix motif and L3 loop that are responsible for the DNA interaction. The L1 loop and H2 helix from the loop-sheet-helix motif fit into the major groove and the L3 loop provides an arginine residue that intercalates into the adjacent minor groove. The residues that make direct contact with DNA are K120, R273, A276, C277, R280, R283 (from the loop-sheet-helix motif) and S241, R248 (from L3 loop). Interestingly, the DBD can promote self-association into a dimer once bound to DNA (Veprintsev et al., 2006). The residues involved in the DBD domain-domain interaction are clustered to the L3 Loop and H1, including the highly conserved E171 and R174 that form inter-domain salt bridges. Importantly, cancer derived p53 mutations are commonly found in the DNA contact surface (loop-sheet-helix motif and L3 loop) of the DBD, where these mutations either directly or indirectly abolish DNA binding activity (Joerger, Ang, & Fersht, 2006).

Interestingly, the DBD can directly associate with pro- and anti-apoptotic Bcl-2 family proteins in the cytoplasm. The interaction is driven by specific interaction between the DNA-binding surface of the DBD and a complementary surface on Bcl-2 family proteins (Follis, A. V. et al., 2014; Follis, Ariele Viacava et al., 2015). Under normal condition, cytoplasmic p53 is sequestered by Bcl-xL through the DBD that prevents p53 activity at the mitochondria (Chipuk et al., 2005; Follis, Ariele Viacava et al., 2013; Vaseva & Moll, 2009). When the cell is under stress, BH3-only protein PUMA accumulates in the cytosol and directly bind to the BH3 groove of Bcl-xL. The interaction then promotes Bcl-xL to undergo a conformational change that lead to p53 release (Follis, Ariele Viacava et al., 2013). The free p53 is localized to the mitochondria outer membrane to activate the pro-apoptotic Bcl-2 family proteins Bax and Bak, which promote

mitochondrial outer membrane permeabilization and result in subsequent apoptosis (Chipuk et al., 2004; Follis, A. V. et al., 2014; Follis, Ariele Viacava et al., 2015; Leu et al., 2004).

Oligomerization domain (OD)

The oligomerization domain contains a structured region spanning residues 325 – 356 (Clore et al., 1994). Interestingly, a dimer is formed through co-translational dimerization of p53 monomer, which the dimers then assemble into tetramer post-translationally (Chris et al., 2002). The OD tetramer adopts a dimer of dimer conformation (Figure 3, D). Each dimer forms an anti-parallel β-sheet flanked by two antiparallel α-helices, where each monomer contributes one β-strand and one α-helix connected by a tight turn formed by a single glycine residue (G334). The two dimers are brought together by extensive hydrophobic interactions and salt bridges at the two pairs of antiparallel α-helices. The two antiparallel β-sheets, on the other hand, are exposed on the surface of the tetramer and do not participate in tetramerization. Additionally, mutation of key residues within the tetramerization interface results in a dimer that is structurally identical to the dimer within the tetramer (Davison et al., 2001). Consequently, wild-type p53 encompassing the OD exists in a dynamic equilibrium of monomer, homodimer and homotetramer inside the cell, with the dimer being the dominant species owing to its very high affinity for dimerization (Gaglia et al., 2013; Rajagopalan, Sridharan, Huang, & Fersht, 2011). Furthermore, only the dimeric and tetrameric forms of p53 are transcriptionally active (Kawaguchi et al., 2005).

In addition to its structural role, the OD has important roles in subcellular localization. Immediately preceded by a bipartite nuclear localization signal (residues 305 – 322), the OD, on the other hand, contains a nuclear export signal (NES; residue 340 – 351) that is masked by its

tertiary and quaternary structure (Stommel et al., 1999). Proteins that disrupt p53 tetramerization (e.g. ARC, Apoptosis repressor with caspase recruiting domain) can expose the NES to facilitate cytoplasmic trafficking, resulting in subsequent transcription inhibition (Foo et al., 2007). In contrast, proteins that stabilize tetrameric p53 (e.g. 14-3-3) promote nuclear localization and subsequent transcriptional activation (Rajagopalan, Sridharan, Jaulent, Wells, Veprintsev, & Fersht, 2008).

Regulatory domain (RD)

Spanning residues 361 – 393, the C-terminal segment of p53 constitutes the regulatory domain (Kim et al., 2012; Laptenko et al., 2015a; Weinberg, Freund, Veprintsev, Bycroft, & Fersht, 2004; Yakovleva et al., 2001). Being a disordered region, the RD is rich in basic amino acids including six lysine and two arginine residues and is very important in regulating p53 stability and activity. Allowing it to achieve diverse functions, the RD is subjected to extensive post-translational modifications (PTMs), such as acetylation, methylation, sumoylation, ubiquitination and phosphorylation (DeHart, Chahal, Flint, & Perlman, 2014; Kruse & Gu, 2009; Meek & Anderson, 2009). The PTMs on the RD modulate its interaction with numerous binding partners to regulate p53 function. Importantly, if RD is deleted from p53, the resulting protein is deficient in promoter binding and transcription activation (Laptenko et al., 2015b; McKinney, Mattia, Gottifredi, & Prives, 2004).

The RD has the characteristics of a chameleon sequence, where the sequence can adopt different secondary structures depending on the structural context of the binding partner. The RD can form an α-helix when bound to S100B, whereas in complex with Sir2, a member of the family

of Sirtuin deacetylases, the same sequence adopts a β-strand conformation that forms a small β-sheet with the flanking β-strands from the enzyme (Avalos et al., 2002; Rustandi, Baldisseri, & Weber, 2000). Moreover, the sequence can retain significant disorder when bound to CDK2 and CBP (Lowe et al., 2002; Mujtaba et al., 2004). The structural plasticity of the RD allows it to interact with diverse proteins and mediate various downstream effects.

The RD mediates direct DNA contact and promotes p53 binding to DNA (Kim et al., 2012; Laptenko et al., 2015b; Weinberg et al., 2004; Zhou et al., 1999). The lysine and arginine residues mediate non-specific DNA contact through electrostatic interactions with the phosphate groups of the DNA backbone (Friedler, Veprintsev, Freund, von Glos, & Fersht, 2005; Laptenko et al., 2015b). The non-specific nature of the interaction allows p53 to perform one-dimensional diffusion on a target DNA molecule, promoting fast recognition of p53-specific promoter sequences (McKinney et al., 2004; Tafvizi, Huang, Fersht, Mirny, & van Oijen, 2011; Terakawa, Kenzaki, & Takada, 2012). PTMs on the RD modulate these non-specific interactions with DNA, resulting in rapid dissociation or sequence discrimination (Laptenko et al., 2015a; Weinberg et al., 2004).

1.2.3 Regulation of p53 activity

The normal function of a cell is maintained by constantly suppressing the activity of p53 (Chernov et al., 2001; Farmer et al., 1992; Maltzman & Czyzyk, 1984; Pietenpol et al., 1994; Price & Calderwood, 1993; Schärer & Iggo, 1992). In response to stress that disrupts normal cellular function, p53 accumulation promotes spatial and temporal functions such as cell cycle arrest, DNA-damage repair and apoptosis (Andrysik et al., 2017; Chipuk et al., 2004; Fischer, 2017; Tebaldi et al., 2015; Yamaguchi et al., 2001). The switch from p53 suppression to activation is a

key step that determines the ultimate fate of the cell. In the absence of p53 activation, accumulation of DNA damage will promote oncogenic transformation and facilitate cancer development (Donehower, L. A. et al., 1992; Menon et al., 1990; Nigro et al., 1989). In contrast, p53 overactivation is detrimental to cell survival and development (Ebrahim, Mulay, Anders, & Thomasova, 2015; Hall & Lane, 1997; Thomasova et al., 2015; Thomasova et al., 2016). Thus, p53 regulation is of fundamental importance for the cell and the whole organism.

Regulation of p53 stability is a key step that provides a frontline for controlling p53 activity. Under normal conditions, cellular p53 is maintained at a low level by MDM2 through the ubiquitin-proteasome pathway (Fuchs et al., 1998; Haupt, Y., Maya, Kazaz, & Oren, 1997; Honda, Tanaka, & Yasuda, 1997; Kubbutat, Jones, & Vousden, 1997; Rodriguez, Desterro, Lain, Lane, & Hay, 2000a). MDM2 is an E3 ubiquitin ligase that utilizes lysine as a substrate to conjugate ubiquitin onto the lysine side chain (Hershko & Ciechanover, 1998; Honda et al., 1997). Further conjugation of ubiquitin onto a pre-existing ubiquitin generates a poly-ubiquitin chain that can serve as a degradation signal for the 26S proteasome (Glickman & Ciechanover, 2002; Hershko & Ciechanover, 1998; Rodriguez, Desterro, Lain, Lane, & Hay, 2000b). The protein cargo is then actively imported in the lumen of the 26S proteasome and degraded to short peptide fragments, whereas the ubiquitin chain is released and recycled by the proteasome-associated deubiquitination enzyme.

An additional layer of regulation can be exerted on p53 by controlling its activity and subcellular localization without protein degradation. The negative regulator MDMX maintains a stable pool of nuclear p53, while suppressing its transactivation activity in an inactive protein complex (Jackson & Berberich, 2000; Stad et al., 2001). On the contrary, MDM2 contains a nuclear export signal that can facilitate nuclear-cytoplasmic shuttling that promotes p53 nuclear

export, thus preventing p53 transcription activity by physically separating the protein from genomic DNA (Inoue, Geyer, Howard, Yu, & Maki, 2001; Lohrum, Woods, Ludwig, Balint, & Vousden, 2001; Nie, Sasaki, & Maki, 2007; Roth, Dobbelstein, Freedman, Shenk, & Levine, 1998). In addition, p53 contains a nuclear export signal that is masked by the tertiary and quaternary structure of the OD (Stommel et al., 1999). The OD structure can be disrupted by anti-apoptotic protein apoptosis repressor with caspase recruitment domain to expose the nuclear export signal to promote cytoplasmic shuttling (Foo et al., 2007).

Control over p53 can be modulated and reversed by PTMs. For example, MDM2, as an E3 ubiquitin ligase, can only mono-ubiquitinate p53 on a lysine residue (Li, M. et al., 2003). The mono-ubiquitined p53 cannot be targeted for proteasomal degeneration but has been shown to be involved in regulating DNA binding and subcellular localization. Poly-ubiquitination and degradation of p53 requires MDM2 in complex with MDMX, a MDM2 homolog that lacks E3 ubiquitin ligase activity, or CBP/p300 that possesses E4 ubiquitin ligase activity to promote assembly of poly-ubiquitin chain (Badciong & Haas, 2002; Shi et al., 2009; Wang, X., Wang, & Jiang, 2011). To suppress the activity of MDM2, phosphorylation of T18 near the p53 N-terminus disrupts MDM2 binding and results in p53 stabilization (Jabbur et al., 2002; Schon, Friedler, Bycroft, Freund, & Fersht, 2002). Moreover, phosphorylation of multiple serine residues near the p53 N-terminus, such as S15, T18 and S20, promotes its association with CBP/p300, which can effectively compete with MDM2 interaction to activate p53 to promote transcription of downstream genes (Teufel, Bycroft, & Fersht, 2009).

1.2.4 The role of p53 in cancer

The main obstacle faced by cancer cells is the activation of tumour suppressors that inhibit cell cycle progression and promote apoptosis. To circumvent these problems, cancer cells were found to upregulate regulatory proteins that inhibit the activity of tumour suppressors or accumulate genetic mutations to produce non-functional tumour suppressors. Loss of tumour-suppressive functions confer growth and survival advantages for cancer cells that allow the cells to proliferate in the absence of any regulatory control.

As a crucial tumour suppressor, the *TP53* gene is frequently mutated and associated with more than 50% of all cancers, in which missense mutations in the DBD account for 80% of mutations identified in the *TP53* gene (Olivier, Hollstein, & Hainaut, 2010). Missense mutations cause a single nucleotide substitution in the *TP53* gene results in a codon that encodes for a different amino acid. Remarkably, six hotspot residues are frequently found in cancer cells harboring missense mutations, these include R175, G245, R248, R249, R273, and R282 (Mello & Attardi, 2013) (Figure 1.2, B and Figure 1.4, A). All six missense mutations are found to reside near the DNA-binding surface in the DBD (Figure 1.4, B). The missense mutations in R175, G245, R249 and R282 disrupt the tertiary structure of the DBD, leading it to adopt an altered conformation that prevents transcription of tumour suppressive genes (Friedler et al., 2004; Joerger et al., 2006; Mello & Attardi, 2013). On the other hand, R248 and R273 mutations block direct DNA contact so that the DBD cannot bind effectively to its target DNA (Eldar, Rozenberg, Diskin-Posner, Rohs, & Shakked, 2013; Wong, K. B. et al., 1999). Importantly, these p53 mutants are prone to aggregation and can seed the aggregation of the wild-type (WT) p53 (Bullock et al., 1997; Bullock, Henckel, & Fersht, 2000; Friedler, Veprintsev, Hansson, & Fersht, 2003). Thus, in addition to being transcriptionally inactive in tumour suppressor genes, the p53 misssense mutants

exert a dormant negative effect on WT p53. In addition to loss of function and dominant negative effects, these p53 misssense mutants also acquire oncogenic properties (gain of function) to facilitate cancer cell survival and growth (Olive et al., 2004; Oren & Rotter, 2010; van Oijen & Slootweg, 2000).

Patients harbouring mutated p53 often develop metastatic cancers that result in poor prognosis and high mortality rate (Donehower, Lawrence et al., 2019; Robles & Harris, 2010; Wang, M., Yang, Zhang, & Li, 2018). In case of the p53 R175H mutant, a study of mouse thymocyte harboring mutant p53 displayed enhanced interchromosomal translocation and impaired double-strand breaks repair by preventing recruitment of MRN/ATM to double-strand breaks, highlighting its role in promoting genome instability (Liu, D. P., Song, & Xu, 2010). Moreover, overexpression of the p53 R175H mutant promotes invasion and migration through activation of the EGFR/PI3K/AKT pathway (Dong, Xu, Jia, Li, & Feng, 2009). Furthermore, mutant p53 promotes expression of ID4 and leads to stabilization of mRNA encoding the angiogenic factors IL8 and GRO-α, which stimulate the angiogenic potential of cancer cells (Fontemaggi et al., 2009). Importantly, p53 mutants are often resistant to MDM2-mediated proteasomal degradation and result in significant protein accumulation in cancer cells (Li, D. et al., 2011; Lukashchuk & Vousden, 2007; Wiech et al., 2012). Cancer cells hijack the tumour suppressive functions of the p53 while converting it to an oncogenic protein that favors survival and growth.

1.3 MDM2 family proteins: MDM2 & MDMX

Despite the fact that mutations in the *TP53* gene are frequently found in cancers, there are many cancers that retain WT p53. In many cases, WT p53 is inactivated through the activity of its

negative regulators MDM2 and MDMX, which ultimately achieves the same outcome as p53 mutations: to inhibit the tumour-suppressive function of p53. Overexpression of MDM2 or MDMX is frequently found in many cancers, including liposarcoma, breast and colorectal cancers (Wade, Li, & Wahl, 2013). Both MDM2 and MDMX can inhibit p53 through direct protein-protein interactions that prevent recruitment of transcription co-activators (Chen, J., Lin, & Levine, 1995; Danovi et al., 2004; Kussie et al., 1996; Momand et al., 1992; Oliner, J. D. et al., 1993; Shvarts et al., 1996; Shvarts et al., 1997). Furthermore, MDM2 can promote p53 ubiquitination and subsequent degradation in the proteasome (Fang, Jensen, Ludwig, Vousden, & Weissman, 2000; Fuchs et al., 1998; Honda et al., 1997; Honda & Yasuda, 2000; Rodriguez et al., 2000a). Importantly, either MDM2 or MDMX knockout significantly impeded cancer cells growth in a p53-dependent manner (Feeley, Adams, Mitra, & Eischen, 2017; Haupt, S. et al., 2015), which highlights the significance of targeting MDM2/MDMX to block the interaction with p53 for treatment of cancers harboring WT p53.

The *mdm2* gene was discovered in a screen for amplified genes in transformed mouse cells to isolate factors associated with double minutes (fragments of extrachromosomal DNA) (Cahilly-Snyder, Yang-Feng, Francke, & George, 1987; Fakharzadeh, Trusko, & George, 1991). The MDM2 protein was subsequently identified as a negative regulator that inhibits and degrades p53 (Haupt, Y. et al., 1997; Kubbutat et al., 1997; Momand et al., 1992), which was recognized as an important factor in promoting cancer development. Interestingly, the *mdm2* gene is a transcription target of p53, thereby forming a feedback loop to keep p53 in check inside the cell (Picksley & Lane, 1993; Wu, X., Bayle, Olson, & Levine, 1993). The critical role of MDM2 as a regulator of p53 is supported by the fact that the early embryonic lethality of *mdm2*-null mice was completely rescued in a p53-null background (Jones, Roe, Donehower, & Bradley, 1995; Montes de Oca Luna,

R., Wagner, & Lozano, 1995). Importantly, amplification of the *mdm2* gene was observed in more than one-third of human sarcomas, and, to a lesser extent, in other cancers such as glioblastomas, leukemias, and breast carcinomas that retained WT p53 (Oliner, Jonathan D., Saiki, & Caenepeel, 2016). The paralogue MDMX, named for its homology with MDM2, was discovered in a mouse cDNA library screened for p53 binding proteins (Shvarts et al., 1996). The *mdmx* gene was originally believed to be regulated by other mechanisms, but emerging evidence suggests that this gene is also under the control of p53 (Phillips et al., 2010; Wei, C. et al., 2006). Similarly to *mdm2*, knockout of the *mdmx* gene in mice results in embryonic lethality owing to lack of cell proliferation and can be rescued by p53 loss (Migliorini et al., 2002; Parant et al., 2001). Hence, it appears that both MDM2 and MDMX can function in a regulatory feedback loop to keep p53 protein level and activity in check. These research studies highlight MDM2 and MDMX as key regulatory proteins for the p53 tumour suppressor.

1.3.1 Structural features of MDM2 and MDMX

MDM2 and MDMX are multi-domain proteins with molecular weights of 55.2 kD and 54.8 kDa, respectively. Importantly, both MDM2 and MDMX share similar domain organization and contain four functional domains interconnected by large disordered regions with minimal sequence conservation. The functional domains of MDM2 and MDMX include an N-terminal p53-binding domain (PBD), an acidic domain (AD), a zinc finger domain (ZFD) and a C-terminal Really Interesting New Gene (RING) domain (Figure 1.5, A and B). The domains function synergistically to regulate the activity and stability of p53.

p53-binding domain (PBD)

The PBDs of MDM2 and MDMX directly bind to the transactivation domain (TD) of p53 with nanomolar affinity (Pazgier et al., 2009). Being a crucial region for the function of MDM2 or MDMX, the PBDs drive the formation of inhibitory complexes between MDM2/MDMX and p53 to prevent recruitment of transcription machinery that inhibit the transcription of p53 target genes (Shvarts et al., 1996; Thut, Goodrich, & Tjian, 1997). Thus, inhibition of the interaction between p53 and MDM2/MDMX could stabilize p53, which leading to the activation of its downstream signaling pathways.

Kussie et al. first reported the structure of the MDM2 PBD in complex with a small peptide derived from the p53 TD (Kussie et al., 1996). The overall structure of the PBD resembles a distorted trough, in which a cleft is formed by a pocket of hydrophobic amino acids (Figure 1.6, A, green). The cleft is composed of four α-helices that make up the sides and the bottom, capped by three-stranded β-sheets at either end of the cleft. The TD peptide forms an amphipathic α-helix followed by an extended region. The α-helix mediates key contacts with the PBD, with the hydrophobic face of the helix being completely buried in the PBD cleft.

The PBD domain of MDM2 contains a structured region spanning residues 26 – 108. The overall fold consists of a structural repetition that can be separated into two portions, residues 26 – 70 and 71 – 108, each consisting of 3 β-strands and two α-helices, which fold together to form a globular structure with a hydrophobic core. The cleft is formed by a layer of hydrophobic amino acids that seals the bottom of the cleft. The PBD cleft contains 14 conserved hydrophobic amino acids that make van der Waals contacts to the TD. A 13 amino acid sequence (residue 17 – 29) from the TD binds the PBD, of which residues 18 – 26 adopt an amphipathic α-helix conformation.

On the hydrophobic face, three hydrophobic amino acids (F19, W23 and L26) have extended side chain conformations that allow for close packing to make van der Waals contacts with the hydrophobic core of the PBD. T18 forms multiple hydrogen bonds with D21 and is believed to help the initiation of the α-helix. Immediately after L26 lies the helix breaking proline (P27), which likely contributes to termination of the α-helix. The critical role of the three hydrophobic residues from the TD is evidenced by the fact that mutation of any of the three amino acids to alanine greatly inhibited the interaction with the PBD (Li, C. et al., 2010). Importantly, TD peptides which lack T18 are unable to bind the PBD, highlighting the critical role of T18 in stabilizing the interaction. Moreover, the interaction is greatly reduced when T18 is phosphorylated (Schon et al., 2002). In addition, the N-terminal region of the PBD contains a disordered region, spanning residues 1 – 25, which increases the thermostability of the PBD and exerts an inhibitory effect on TD binding (Worrall, Worrall, Blackburn, Walkinshaw, & Hupp, 2010). Moreover, the sequence spanning residues 17 – 24 forms a lid that can fold onto the hydrophobic cleft that blocks the access by the TD (Uhrinova et al., 2005).

The PBD of MDMX, spanning from residue 23 – 109, is structurally similar to the PBD of MDM2 (Popowicz et al., 2008). The overall fold preserves the key feature of the structure of the PBD of MDM2, where a structural repetition is found that can separate the domain into two portions of roughly 40 residues long and a hydrophobic cleft is formed by packing of the hydrophobic core (Figure 1.6, A cyan). The noticeable difference between the PBD of MDM2 and MDMX is that the cleft in MDMX is shallower than the cleft formed in MDM2. The side chain of Y99 points into the cleft whereas the side chain of Y100 at the equivalent position in the PBD of MDM2 protrudes to the side of the cleft. Moreover, the cleft is further narrowed down by the side chain of M53 at the other side of the cleft (larger than the corresponding L54 from the PBD of

MDM2). Despite the shallower cleft, the binding determinant is retained in the interaction between the PBD of MDMX and the TD. The key contacts are mediated by three hydrophobic residues F19, W23 and L26 of the TD that fill up the hydrophobic cleft. The side chains of F19 and W23 insert deeply into the cleft but the residues starting at L25 are shifted outward due to the shallower cleft created by the bulky side chains of M53 and Y99. Under stress conditions, the residue Y99 can be phosphorylated by c-Abl that creates a steric clash between the phosphate group and neighboring contact residues of the TD, thus inhibiting p53 binding (Chen, X. et al., 2016).

The PBD from either MDM2 or MDMX was demonstrated to bind a distant region from the canonical binding site within the p53 TD. The sequence spanning residues 49 – 54 binds the PBD cleft with micromolar affinity and adopts an α-helical conformation (Shan et al., 2012). This region contains three hydrophobic residues, I50, W53, and F54, that are inserted deeply into the PBD cleft. Consequently, the PBD can bind to both regions on the TD with a higher binding affinity. Interestingly, the TD sequence responsible for PBD binding is also required for direct interaction with transcription machinery, such as CBP/p300 and TBP (Chen, X. et al., 1993; Krois et al., 2016; Liu, X. et al., 1993). Thus, the TD-PBD interaction could prevent recruitment the transcription machinery and directly inhibit the transcriptional activity of p53.

Acidic domain (AD)

The central region of MDM2 and MDMX contains a highly charged sequence rich in glutamate and aspartate residues (Figure 1.5, B). In MDM2, the AD spans residues 222 – 303 and was shown to be required for the E3 ubiquitin ligase function of MDM2 (Argentini, Barboule, & Wasylyk, 2001; Cheng et al., 2014; Kawai, Wiederschain, & Yuan, 2003; Sdek et al., 2004; Yang,

L., Song, Cheng, Chen, & Chen, 2019). The MDM2 AD is highly acidic, with an isoelectric point of 3.08, and the sequence contains 14 aspartate and 14 glutamate residues. Moreover, there are 11 serine and 3 threonine residues that could potentially be phosphorylated (Hornbeck et al., 2015). Indeed, many kinases are known to phosphorylate the AD and regulate the activity of MDM2, such as casein kinase I & II and polo-like kinase (Allende-Vega, Dias, Milne, & Meek, 2005; Dias, Hogan, Ochocka, & Meek, 2009; Winter et al., 2004). Importantly, deletion of either partial or full-length AD abolished the ability of MDM2 to ubiquitinate p53 and prevented proteasomal degradation (Argentini et al., 2001; Cheng et al., 2014; Kawai et al., 2003). The AD directly interacts with the RING domain to stimulate the ubiquitin ligase activity by promoting ubiquitin discharge from the E2 ubiquitin conjugating enzyme (Cheng et al., 2014). In the same study, the authors found that a MDM2 mutant with an extra copy of AD results in hyperactivation of ubiquitin ligase activity, which further supports the fact that the AD is directly involved in the ubiquitination process. More importantly, the tumour suppressors p14arf and retinoblastoma protein were shown to bind the AD and inhibit the activity of MDM2 (Bothner et al., 2001; Hsieh et al., 1999; Midgley et al., 2000; Pomerantz et al., 1998; Sdek et al., 2004; Zhang, Y., Xiong, & Yarbrough, 1998), highlighting the critical role of the AD in maintaining the proper function of MDM2.

Besides its activity in stimulating MDM2-mediated ubiquitination of p53, the AD also directly interacts with p53 to inhibit its DNA-binding activity (Yu et al., 2006). The AD binds to the p53 DBD with micromolar affinity to induce a conformational change to expose the Pab240 epitope, an indicator of a mutant-like conformation (Cross et al., 2011; Yu et al., 2006). Of note, p53 mutants that harbour missense mutations in the DBD accumulate to significantly higher concentration in cancer cells (Li, Dun et al., 2011; Lukashchuk & Vousden, 2007; Nagata et al., 1999; Peng et al., 2001). Furthermore, these mutants were shown to bind more tightly to the AD

to inhibit p53 ubiquitination and degradation (Yang, L. et al., 2019). Furthermore, these authors found that introducing extra copies of the AD can effectively restore the ubiquitin ligase activity of MDM2 to promote ubiquitination and degradation of mutant p53.

The acidic domain of MDMX (ADX) spans residues 190 – 300 (Figure 5, B). Despite their similar name, the ADX and the AD have low sequence homology. The ADX contains four conserved tryptophan residues whereas the AD only contains one tryptophan residue that is not conserved through evolution. Moreover, the ADX contains many arginine and lysine residues while the AD does not have any positively charged residues. The WWW sequence 190 – 210 contains a stretch of hydrophobic amino acids, including three key tryptophan residues, and was demonstrated to have an auto-regulatory effect on MDMX (Bista et al., 2013). This region can directly interact with the PBD from the same MDMX molecule to weaken the interaction with the TD. The tryptophan residues W200 & W201 are critical for the binding to the hydrophobic cleft and compete with the p53 TD. Of note, the same region can also bind to the p53 DBD to prevent p53 from binding to DNA and tryptophan residues W200 & W201 are important for mediating this interaction (Wei, X. et al., 2016). This interaction is further stimulated by CK1α, which binds the ADX and phosphorylate S289 (Chen, L., Li, Pan, & Chen, 2005; Wu, S., Chen, Becker, Schonbrunn, & Chen, 2012).

Zinc finger domain (ZFD)

The ZFDs of MDM2 and MDMX are found immediately adjacent to the C-terminal of the AD. The ZFD of both proteins have significant sequence homology and are well conserved, with the four cysteine residues coordinating a zinc ion. The solution structure of the MDM2 ZFD was

previously determined (Kostic, Matt, Martinez-Yamout, Dyson, & Wright, 2006), consisting of four β-strands and a 3_{10} helix. The four β-strands form two β-hairpins and the indole group of W303 is packed between the hairpins, which makes up the core of the structure. The cysteine residues involved in coordinating the zinc ion are found within the loops that connect the two β-hairpins (Figure 1.6B).

The ZFD of MDM2 is a key region in regulating the activity of MDM2 towards p53. Importantly, ribosomal proteins such as L5, L11 and L23 directly interact with the ZFD and inhibit MDM2-mediated ubiquitination of p53 (Dai & Lu, 2004; Jin, Itahana, O'Keefe, & Zhang, 2004; Zhang, Y. et al., 2003). A crystal structure of the ZFD-L11 complex shows that the ZFD structurally mimics rRNA and binds to the rRNA binding pocket on L11 (Zheng et al., 2015). Interestingly, despite the fact that the ZFD has significant sequence homology for MDMX, the structural feature that allows L11 binding is missing and MDMX cannot bind to L11 (Gilkes, Chen, and Chen, 2006). Of note, the cysteine residues maintaining the structurally important zinc ion are frequently mutated in many cancers and disrupt the tertiary structure of the MDM2 ZFD (Lindstrom, Jin, Deisenroth, White Wolf, & Zhang, 2007). These missense mutants of the ZFD cannot bind to L11 and L5 and escape their inhibitory effect on MDM2, which allows MDM2 to be fully functional in binding to and suppressing the activity of p53.

Really Interesting New Gene Domain (RING)

The C-terminal RING domain of MDM2 is necessary for the intrinsic E3 ubiquitin ligase activity of the protein and is needed for homodimerization and heterodimerization with the RING domain of MDMX to form functional dimers (Fang et al., 2000; Kostic et al., 2006; Linke et al.,

2008; Sharp, Kratowicz, Sank, & George, 1999; Tanimura et al., 1999). The RING domain of MDM2 and MDMX functions as an adaptor protein that binds to an E2 ubiquitin-conjugating enzyme and p53, resulting in transfer of ubiquitin to the p53 protein and subsequent degradation by the proteasome (Linke et al., 2008). Of note, MDMX can homodimerize at high concentration but lacks intrinsic E3 ubiquitin ligase activity (Bista et al., 2013; Egorova, Mis, & Sheng, 2014). The heterodimer of the MDM2/MDMX RING domain has higher ubiquitin ligase activity as compared to the MDM2 RING domain homodimer. Moreover, the MDM2 RING domain homodimer is rapidly degraded in the proteasome, whereas the MDM2/MDMX heterodimer forms a stable complex that can efficiently ubiquitinate p53 to promote its proteasomal degradation (Kawai, Lopez-Pajares, Kim, Wiederschain, & Yuan, 2007; Kostic et al., 2006; Linke et al., 2008; Sharp et al., 1999).

The structure of the MDM2 and MDMX RING domain heterodimer has been solved (Linke et al., 2008). The RING domain structures of MDM2 and MDMX are nearly identical and fold into a compact structure, with two zinc ions stabilizing the structure of the RING domain for each monomer (Figure 1.6, C). The dimerization interface is formed from three β-strands of each monomer to make up the core, such that the core of the heterodimer is effectively a six-stranded β-barrel filled by the side chains of hydrophobic residues from each monomer. Notably, the structure of the RING heterodimer is similar to the structure of the RING homodimer of MDM2, with a C_α rmsd of 1.9 Å (Kostic et al., 2006; Linke et al., 2008). The RING domain heterodimer and homodimer both exhibit highly positively charged surfaces (Figure 1.6, D). Of note, the AD of MDM2, with its highly negatively charged character, can bind to the RING domain to stimulate the E3 ubiquitin ligase activity of MDM2 (Cheng et al., 2014).

1.3.2 Targeting MDM2 and MDMX for cancer therapy

The key roles of MDM2 and MDMX in regulating activity and stability of p53 make them attractive targets for therapeutic intervention of cancers expressing WT p53. The most popular drug molecules of this nature are MDM2 antagonists that are designed to bind the PBD and neutralize the interaction with the p53 TD. Nutlin-3, a *cis*-imidazoline analog, is one of the first small molecules discovered that binds the MDM2 PBD with nanomolar affinity (Vassilev et al., 2004). This molecule mimics the three key contact residues F19, W23 and L26 from the p53 TD and intercalates deeply into the hydrophobic cleft (Figure 1.7). The discovery of nutlin molecules sparked the development of better and more effective MDM2 antagonists specifically targeting the PBD. Unfortunately, many small molecules targeting MDM2 cannot effectively bind the hydrophobic cleft of MDMX PBD, owing to its shallower nature (Popowicz et al., 2008) (Figure 1.7). More recently, a novel molecule was discovered to interact with the PBD of both MDM2 and MDMX to promote homo- and hetero-dimerization of the PBD, resulting in simultaneous p53 activation (Graves et al., 2012). Last but not least, small stapled α-helical peptides that structurally mimic the p53 TD have been discovered that can inhibit both the PBD of MDM2 and MDMX to release p53 from inhibition and rescue the activity of WT p53 (Chang et al., 2013). As of now, alternative small molecule inhibitors that specifically target the PBD of MDMX are continuously being discovered (Liu, Y. et al., 2019; Zhang, Q., Zeng, & Lu, 2014).

The PBD antagonists block the interaction between p53 and MDM2/MDMX but have no effect on the E3 ubiquitin ligase activity of the MDM2 RING domain. Moreover, these compounds often have undesirable nonspecific effects when used at higher concentration, owing to their effect on normal cells. Thus, blocking the activity of the RING domain may have more therapeutic benefits, as this could stabilize the protein without p53 functional overactivation. Specifically, this

would allow p53 to be retained in the inactive state in normal cells by the interaction between the TD and the PBD that inhibits p53 transactivation. Indeed, a new category of drug molecules targeting the E3 ubiquitin ligase activity of MDM2 has been developed (Herman et al., 2011; Yang, Y. et al., 2005). These small molecules bind to the RING domain of MDM2 and inhibit its E3 ubiquitin ligase activity, resulting in p53 stabilization to promote cell cycle arrest and apoptosis. If desired, these compounds could be used in combination with the PBD antagonists to further stimulate p53 activity.

Importantly, cancers expressing mutant p53 often lead to accumulation of high protein level of mutant p53. The gain of function effects of p53 mutants promote cancer cell growth and invasion that can result in poor prognosis (Do et al., 2012; Freed-Pastor et al., 2012; Kalo et al., 2012; Olive et al., 2004; Petitjean et al., 2007; Song, Hollstein, & Xu, 2007; Song & Xu, 2007). p53 mutants were shown to escape MDM2-mediated ubiquitination and degradation (Lukashchuk & Vousden, 2007; Wiech et al., 2012; Yang, L. et al., 2019). Hence, MDM2 antagonists will provide little advantage in treating cancers expressing mutant p53, as blocking the interaction between the two will have no effect on p53 stability. Instead, MDM2 E3 ubiquitin ligase reactivation for cancer cells expressing mutant p53 under this circumstance will have significant therapeutic advantage by promoting degradation of mutant p53, which could abolish the deleterious gain of function effects.

1.4 Research objectives

As detailed above, the p53 pathway is essential for maintaining normal cell function. The interplay between p53 and its inhibitors MDM2 and MDMX, when out of balance, is responsible for many types of cancers and thus presents a target for cancer therapy. These three proteins

contain multiple domains that have been assigned important structural and functional roles in previous studies. However, many of the structural features underpinning these domain functions remain uncharacterized. This thesis details a series of studies that describe and evaluate the interactions between different domains of p53, MDM2 and MDMX.

The modular structures of p53, MDM2 and MDMX make it possible to dissect and study their domain-domain interactions individually. Taking advantage of this modularity, the experiments described herein primarily focus on individual domains rather than full-length proteins to enable protein production and facilitate downstream experiments. In chapter 2, I address the question of whether the MDM2 AD is a direct binding partner for the DBD and RD of p53. I found that the AD can bind both the DBD and the RD, leading me to propose a model that the AD is a key sequence element to promote enzyme-substrate recognition to facilitate p53 ubiquitination. In chapter 3, I investigate the role of p53 TD in regulating the interaction between the AD and the DBD. I found that the TD2 motif can directly interact with the DBD and compete with the AD for DBD binding. This inhibitory effect can be modulated by the interaction between the TD and the MDM2 PBD. Based upon this, I propose that the TD-PBD interaction is required prior to establishing the interaction between the AD and the DBD. In chapter 4, I test the hypothesis that the MDMX AD (ADX) can bind to the MDM2 PBD (PBD2). I found that the ADX can bind PBD2 and inhibit the TD-PBD2 interaction. Moreover, I identified two binding sites within the ADX sequence that can bind to PBD2. Thus, I propose that the ADX is a crucial region that regulates both MDM2 and MDMX.

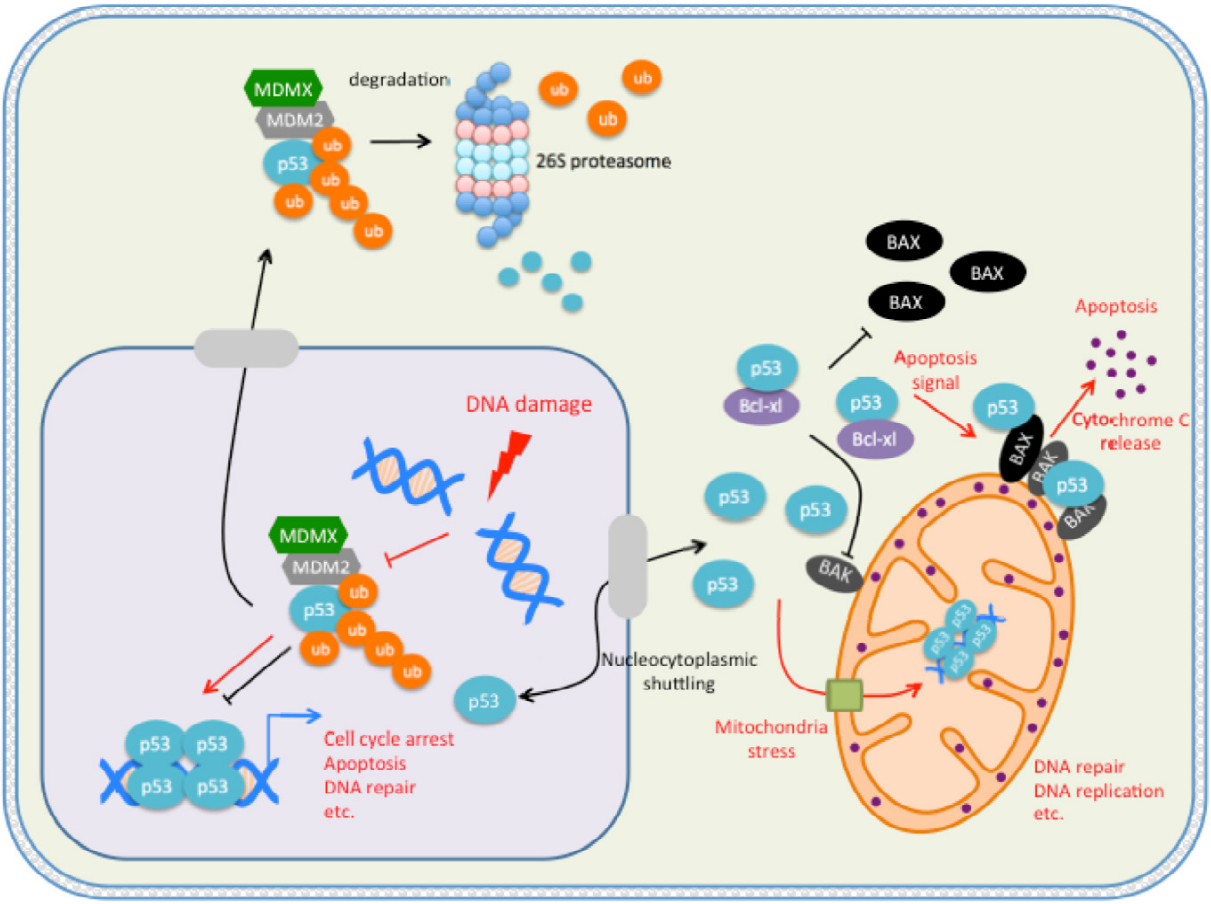

Figure 1.1: Schematic diagram showing the core p53 pathway. The p53 protein has two distinct pools: nuclear and cytoplasmic. Under normal conditions, p53 is constantly inhibited by its negative regulators MDM2 and MDMX. The MDM2-MDMX-p53 complex is inactive and is rapidly ubiquitinated by the intrinsic ubiquitin ligase activity of MDM2. p53 ubiquitination triggers active nuclear export and promotes degradation in the 26S proteasome. In the presence of stress stimuli, such as DNA damage, p53 is stabilized and binds efficiently to target DNA as a tetramer to initiate transactivation of downstream genes. In the cytoplasm, another pool of p53 is involved in a transcription-independent pathway. Under normal conditions, a pool of cytoplasmic p53 is sequestered by the antiapoptotic protein Bcl-xL to prevent it from interacting with proapoptotic protein Bax and Bak. Once p53 is activated, it is released from Bcl-xL inhibition and binds to Bax and Bak, which promotes protein oligomerization at the mitochondrial outer membrane to allow membrane permeabilization and cytochrome c release. Leakage of cytochrome C into the cytosol drives the formation of the apoptosome to promote mitochondria-mediated apoptosis. Interestingly, a fraction of p53 can also be actively transported into the mitochondrial matrix to promote DNA repair and facilitate DNA replication of the mitochondrial genome.

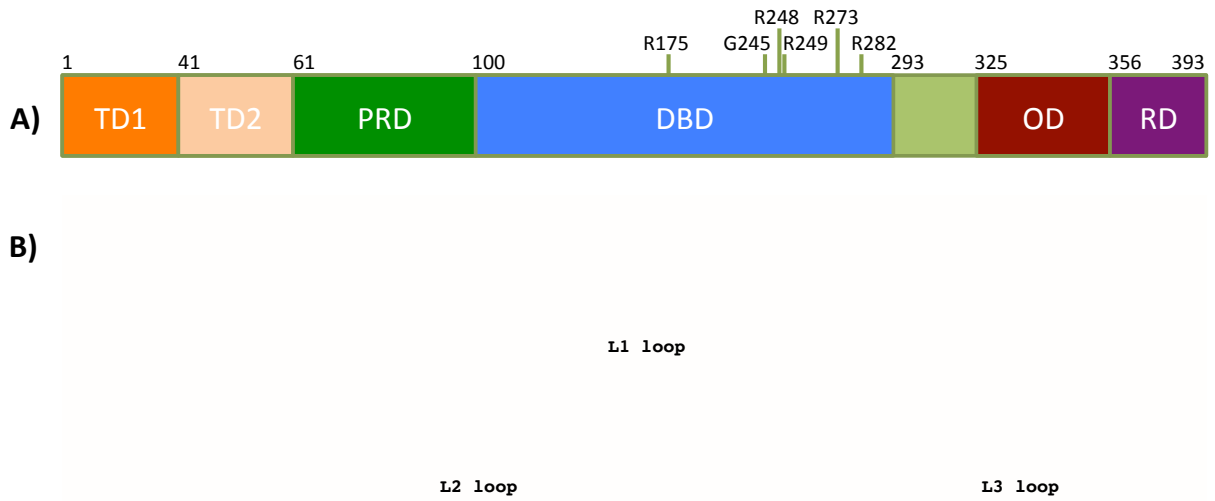

Figure 1.2: p53 domain organization and sequence conservation. A) Schematic diagram showing the domain organization of the 393aa p53 protein. TD1: transactivation domain 1; TD2: transactivation domain 2; PRD: Proline rich domain; DBD: DNA binding domain; OD: oligomerization domain and RD: regulatory domain. B) Sequence alignment of p53 across six species. The structural topology of p53, based upon Cho et. al, 1994, is illustrated above the sequence alignment. The six residues, R175, G245, R248, R249, R273 and R282, that are most frequently mutated in cancer are indicated with red circles beneath the alingment. Notably, all six sites reside in the DBD.

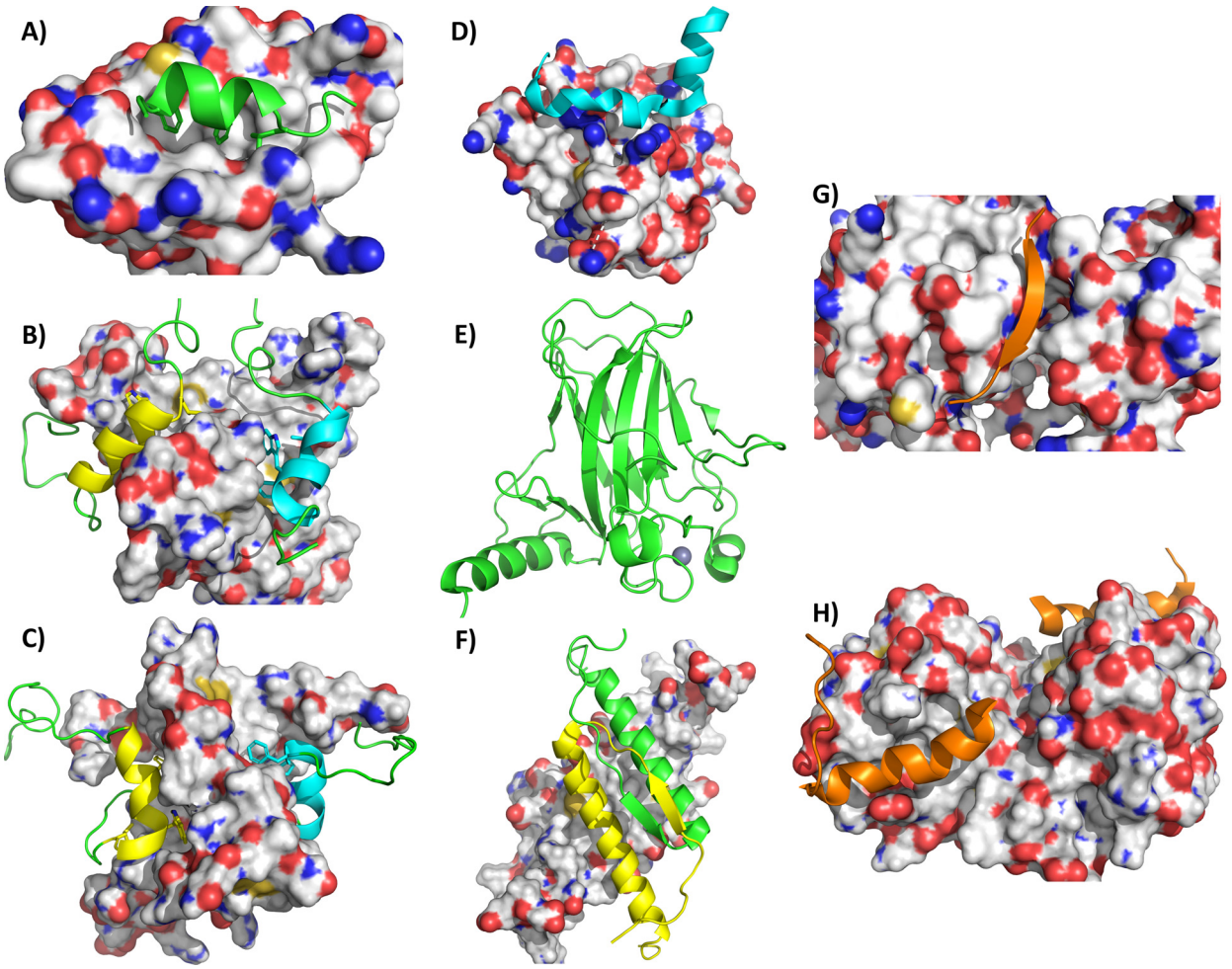

Figure 1.3: Solved structures of the p53 domains. A) p53 TD1 (cartoon) bound to the MDM2 p53-binding domain (surface), with the key contact residues of TD1 (F19, W23 and L26) colored in yellow (Kussie et al., 1996. PDB ID: 1YCR). B) and C) Solution structure of the p53 TD (cartoon) bound to the CBP-TAZ1 and CBP-TAZ2 (surface) (Krois et al., 2016. PDB ID: 5HOU and 5HPD). Hydrophobic residues from TD1 (orange, F19, W23 and L26) and TD2 (cyan, I50, W53 and F54) that were involved in the direct interaction are highlighted with their side chains. D) p53 TD2 (cartoon) bound to the RPA70N (surface) (Bochkareva et al., 2005. PDB ID:2B3G) E) Solution structure of the p53 DBD with the bound zinc ion indicated as a grey sphere (Perez-Canadillas et al, 2006. PDB ID: 2FEJ). F) Solution structure of the p53 OD (Clore et al., 1994. PDB ID: 2J0Z). Two monomers are shown as surface and the other two monomers were shown as cartoon. G) p53 RD (cartoon) bound to the Sir2 enzyme (surface) (Avalos et al. 2002. PDB ID: 1MA3). H) Solution structure of p53 RD (cartoon) bound to the S100B (surface) (Rustandi, Baldisseri and Weber. 2000. PDB ID: 1DT7).

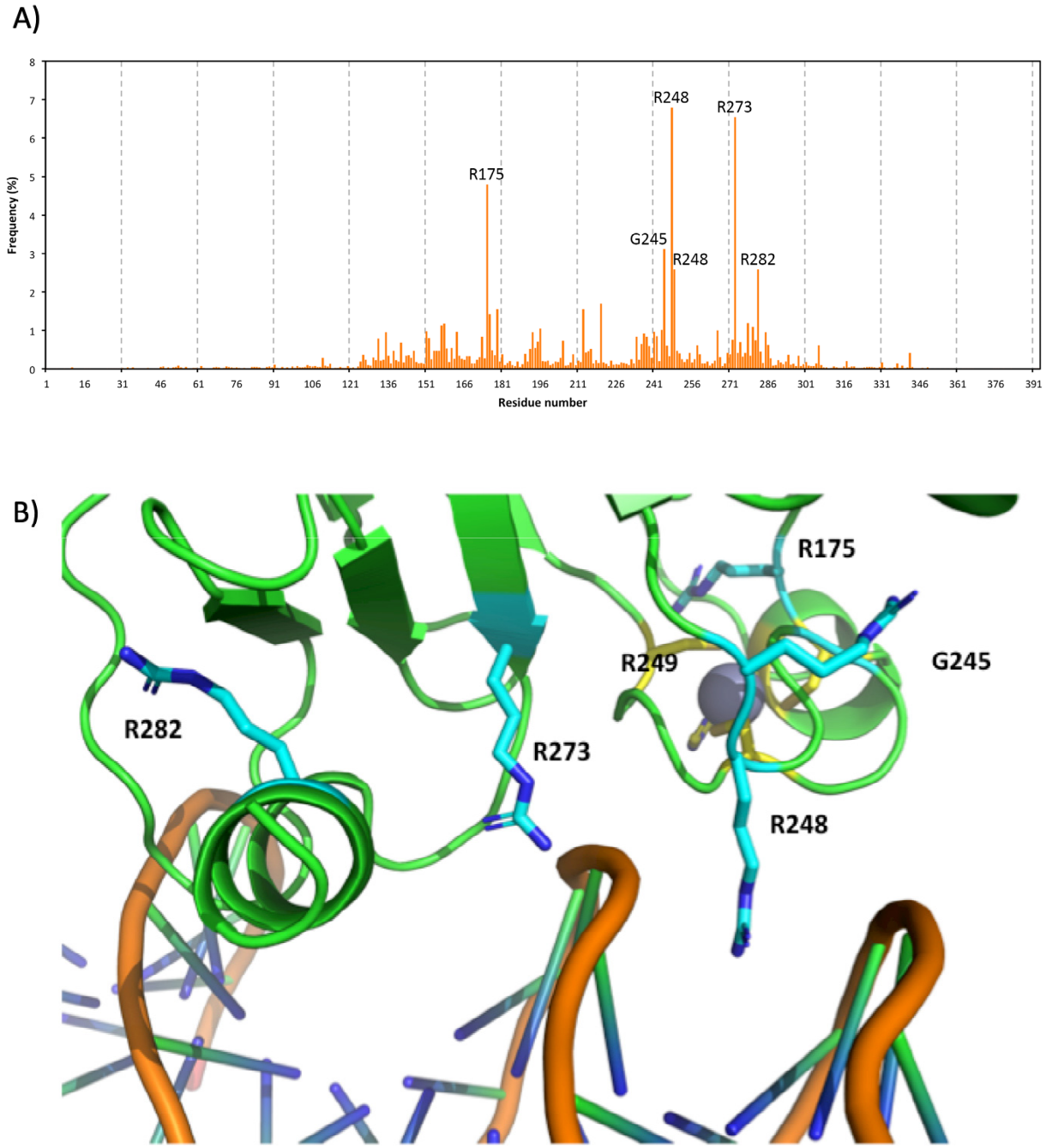

Figure 1.4: p53 mutations are frequently localized to the central DNA-binding domain. A) Frequency of somatic point mutations, with the 6 most frequent mutants of p53 found in human cancers specifically indicated. N = 28866; data from the IARC TP53 Database (http://www-p53.iarc.fr/). B) Location of the six key p53 cancer-associated mutations on the DBD: R175, G245, R248, R249, R273 and R282 (cyan). R175, G245, R249 and R282 are not directly involved in DNA-binding, instead serving to maintain the structural integrity of the DBD. The guanidium groups of the R273 and R248 side chains are involved in key contacts with DNA.

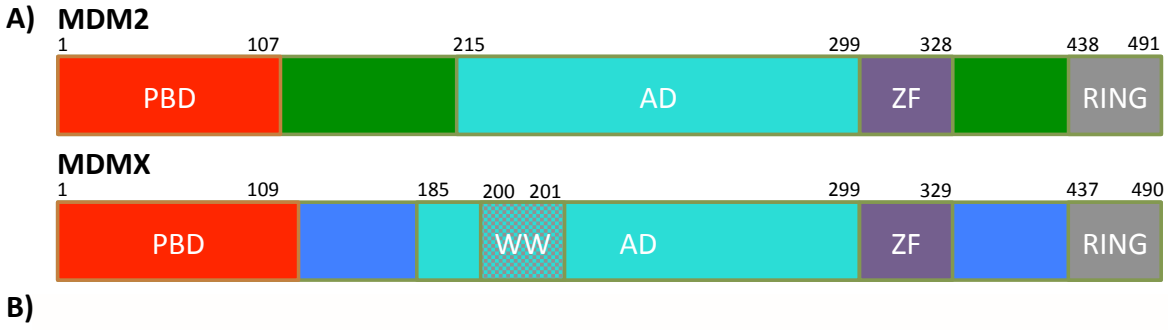

Figure 1.5: Domain organization and sequence conservation of the homologous proteins MDM2 and MDMX. A) Schematic diagram showing the domain organization of MDM2 and MDMX. PBD: p53-binding domain; AD: acidic domain; ZF: zinc finger domain; and RING: really interesting new gene domain. The two conserved tryptophan residues for the MDMX AD are highlighted. B) Sequence alignment of human MDM2 and MDMX. The amino acid sequences for the individual domains of each protein is coloured according the schematic diagram.

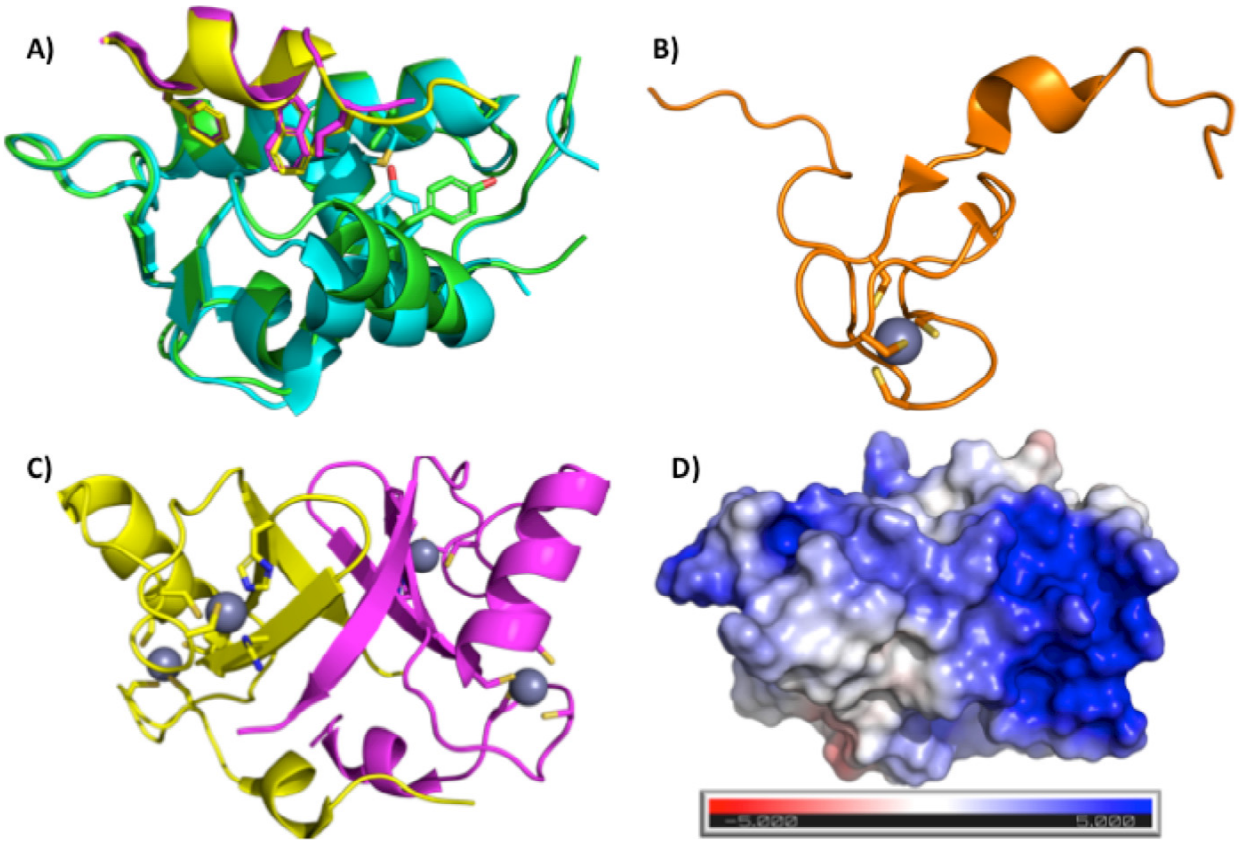

Figure 1.6: Solved structures of the MDM2/MDMX domains. Overlay of the MDM2 and MDMX p53-binding domain crystal structures in complex with p53 TD peptide. The key p53 contact residues (F19, W23 and L26) as well as the residues Y100/Y99 and M53/L54 of MDM2/MDMX, respectively, are highlighted (Kussie et al., 1996. and Popowicz, Czarna and Holak, 2008. PDB ID: 1YCR and 3DAB for MDM2 and MDMX, respectively). B) Solution structure of the MDM2 ZF domain (Yu et al, 2006. PDB ID: 2C6A) with cysteine side chains that bind to the structural zinc ion (grey sphere) highlighted. C) Crystal structure of the MDM2/MDMX RING domain heterodimer (Linke et al., 2008. PDB ID: 2VJE) coloured by protein in yellow (MDM2) and magenta (MDMX). The cysteine and histidine side chains that bind to the structural zinc ion (grey sphere) are highlighted. D) An electrostatic surface potential (generated with APBS, Jurrus et al., 2018) representation of the MDM2/MDMX RING domain heterodimer (PDB ID: 2VJE).

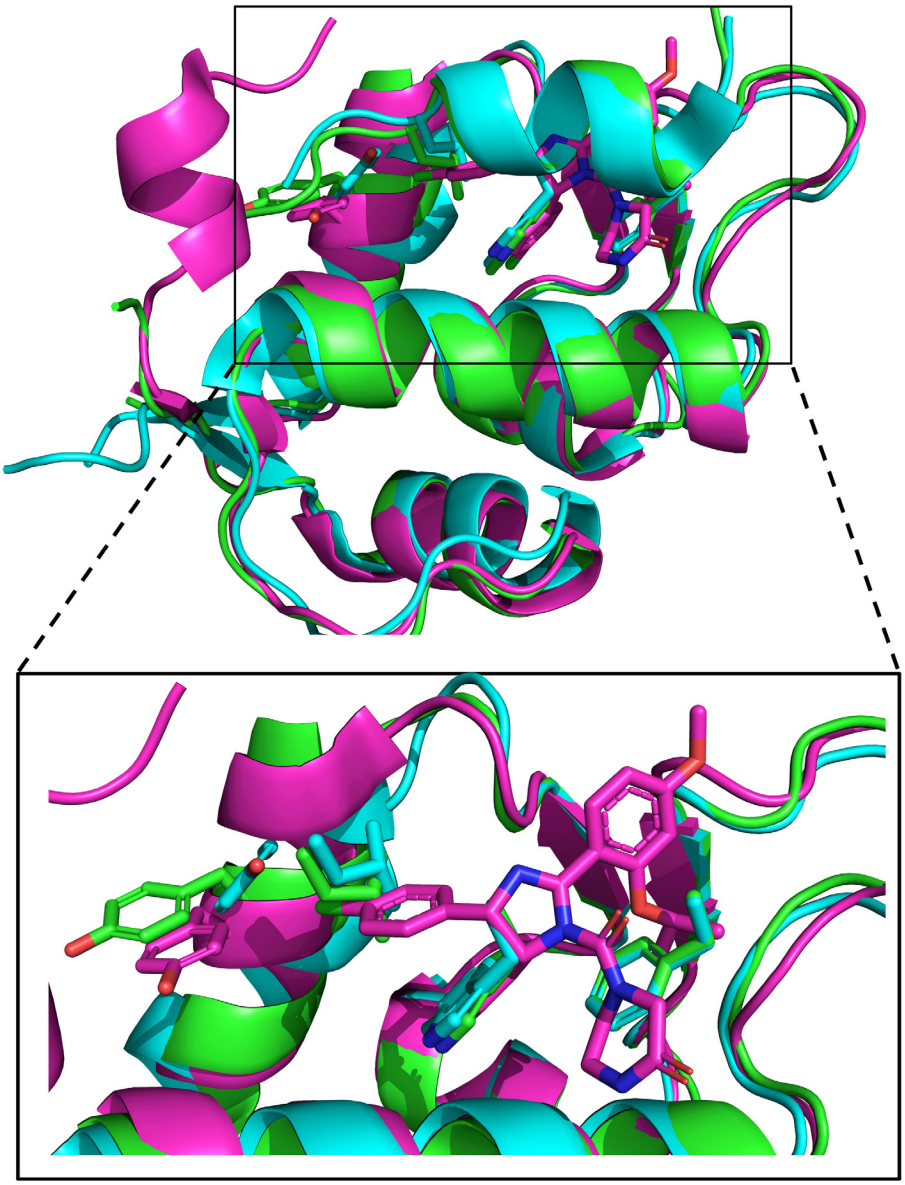

Figure 1.7: Superposed structures of the MDM2/MDMX PBD in complex with p53 TD peptide and nutlin-3a. Top panel: cartoon representation of the superposed structures of MDM2-p53, MDMX-p53 and MDM2-nutlin-3a (green, cyan and magenta respectively). The key p53 contact residues (F19, W23 and L26) as well as the residue Y100/Y99 of MDM2/MDMX, respectively, are highlighted. Bottom panel: Zoomed-in view of the p53-binding pocket showing the side chains of the key p53 contact residues (F19, W23 and L26) as well as the residue Y100/Y99 of MDM2/MDMX (PDB ID: 1YCR, 3DAB and 4HG7).

CHAPTER 2: STRUCTURAL INSIGHT INTO THE MECHANISM BY WHICH THE MDM2 ACIDIC DOMAIN PROMOTES P53 UBIQUITINATION.

2.1 Introduction

As detailed in Chapter 1, p53 is a tumour suppressor protein responsible for maintaining genome integrity and preclude cancer development (Sandor, Ambrus, & Ember, 1995; Vousden & Lu, 2002; Wang, 1999). In response to genotoxic and oncogenic stress, p53 is activated to promote cell-cycle arrest and apoptosis (Brugarolas et al., 1995; Buttgereit et al., 2001; Levine, 1997; Shaw et al., 1992; Wagner, Kokontis, & Hay, 1994; Yonish-Rouach et al., 1991). The p53 protein consists of five functional domains: an N-terminal transactivation domain, a proline-rich domain, a DNA-binding domain (DBD), an oligomerization domain, and a C-terminal regulatory domain (RD) (Figure 1.2). The activity of p53 is stringently regulated by its negative regulator MDM2; MDM2 expression is also induced by p53 to form a feedback loop that keeps p53 in check (Barak, Juven, Haffner, & Oren, 1993; Haupt, Maya, Kazaz, & Oren, 1997; Kubbutat, Jones, & Vousden, 1997; Midgley & Lane, 1997; Picksley & Lane, 1993; Wu, Bayle, Olson, & Levine, 1993).

MDM2 regulates p53 activity through multiple mechanisms. The N-terminal p53-binding domain of MDM2 directly binds to and sequesters the p53 transactivation domain to suppress its transcriptional activity (Chen, Lin, & Levine, 1995; Kussie et al., 1996; Momand, Zambetti, Olson, George, & Levine, 1992). The central acidic domain (AD) binds to the DBD to prevent it from interacting with target DNA (Cross et al., 2011; Yu, G. W. et al., 2006). More importantly, the MDM2 C-terminal RING domain can efficiently ubiquitinate p53, which promotes nuclear export of p53 and its subsequent degradation in the proteasome (Honda & Yasuda, 2000; Roth, Dobbelstein, Freedman, Shenk, & Levine, 1998). Consistent with its critical role in inhibiting p53, upregulation of MDM2 is a hallmark of many cancers and is frequently observed in cancers that

retain wild-type p53 (Bond et al., 2004; Leach et al., 1993; Momand, Jung, Wilczynski, & Niland, 1998; Oliner, Kinzler, Meltzer, George, & Vogelstein, 1992; Patterson et al., 1997; Reifenberger, Liu, Ichimura, Schmidt, & Collins, 1993).

It is well acknowledged that the catalytic unit for ubiquitin transfer resides within the MDM2 RING domain (Fang, Jensen, Ludwig, Vousden, & Weissman, 2000; Honda & Yasuda, 2000). However, it is unclear what regulates the processivity, the number of ubiquitin moieties that can be attached without releasing MDM2 from p53, and how the ubiquitin moiety is transferred onto p53 (Figure 2.1). There is emerging evidence suggesting that the MDM2 AD is essential for the activity of MDM2. Deletion or mutation of the AD were found to abolish the ubiquitin ligase activity of MDM2 and failed to mediate p53 ubiquitination and degradation (Argentini, Barboule, & Wasylyk, 2001; Cheng, Song, Chen, & Chen, 2014; Dolezelova, Cetkovska, Vousden, & Uldrijan, 2012; Kawai, Wiederschain, & Yuan, 2003; Ma et al., 2006). Moreover, the AD can directly bind to the RING domain to stimulate its catalytic activity (Cheng et al., 2014). Furthermore, MDM2 protein that was engineered to harbour multiple copies of the AD is hyperactive in mediating p53 ubiquitination (Cheng et al., 2014). More recently, cancer-derived p53 mutants were shown to bind to and sequester the AD to prevent p53 ubiquitination and subsequent proteasomal degradation (Yang, Song, Cheng, Chen, & Chen, 2019). Thus, the AD could potentially modulate the ubiquitination process of p53 by participating in intermolecular (i.e. the DBD and the RD) and intramolecular (i.e. the RING domain) interactions. Unfortunately, the function of the AD has been mostly studied *in vivo* and the structural-functional relationship in this domain is not well established.

In this chapter, I investigated the domain-domain interactions involving the AD, the DBD and the RD. Using NMR spectroscopy and ITC, I found that the AD can bind both the DBD and

the RD using a similar sequence motif while maintaining significant structural disorder. Moreover, the binding affinities for the AD-DBD and the AD-RD interactions are similar. Interestingly, I found that the structurally destabilized zinc-free DBD can bind to the AD with higher affinity. Taken together, our results suggest that the AD could potentially participate in a dynamic interaction network that serves to promote MDM2 mediated ubiquitination of p53, whereas structurally destabilized DBD could sequester the AD to inhibit p53 ubiquitination.

2.2 Materials and Methods

2.2.1 Materials

The codon optimized genes for human MDM2 (residues 1 – 491) and the MDM2 ADm5 (S240ES242ES246ES252ES256E) mutant were purchased from GENEWIZ (South Plainfield, NJ). The plasmid encoding CBD-SUMO-p53-FLAG (p53 residue 1 – 393) sequence was obtained from Miss Shenzhu Lin, a previous lab member of the Liu lab. The plasmid expressing the human p53 DBD (residues 94-312) was a gift from Cheryl Arrowsmith (Addgene plasmid # 24866; http://n2t.net/addgene:24866; RRID: Addgene_24866). The DNA oligonucleotide primers for cloning were obtained from Integrated DNA Technologies, Inc (Coralville, IA). The *E. coli* expression vector pETHS was created by a previous graduate student in the laboratory of Dr. Paul Liu by sub-cloning the hexahistidine-small ubiquitin modifier (H_6-SUMO) protein sequence followed by SapI and BamHI restriction sites into a pET-32 vector (Novagen; Darmstadt, Germany). The *E. coli* BL21 (DE3) and DH5α strains were purchased from New England Biolabs (Whitby, ON). Reagents and enzymes used for polymerase chain reaction (PCR), DNA phosphorylation, enzyme digestion and ligation were purchased from Fisher Scientific (Ottawa, ON) and Biobasic Inc (Markham, ON). Tris(2-carboxyethyl)phosphine (TCEP) and thrombin protease were purchased

from Cedarlane Laboratories (Burlington, ON). 12.5% Next gel solution was purchased from Amresco (Solon, OH). Sodium trimethylsilylpropanesulfonate (DSS), ascorbic acid, maleimide-TEMPO and 100× vitamin mix were purchased from Sigma-Aldrich Canada (Oakville, ON). 3.5 kDa and 14 kDa cutoff dialysis tubing were purchased from BioDesign Inc. of New York (Carmel Hamlet, NY). Uniformly ^{15}N-labeled ammonium chloride, uniformly ^{13}C-labeled D-glucose and deuterium oxide (D_2O; all isotopes at 99% enrichment) were purchased from Cambridge Isotope Laboratories (Tewksbury, MA). Ni-NTA resins were purchased from Takara Bio USA Inc. (Mountain View, CA). Hitrap Q sepharose HP (anion exchange), Hitrap SP sepharose HP (cation exchange) and Hitrap heparin HP columns were purchased from Fisher Scientific (Ottawa, ON). Amicon Ultra Centrifugal Filters were purchased from Fisher Scientific (Ottawa, ON). SUMO protease was produced in house using an expression plasmid constructed by a previous lab technician from the Liu lab. All other materials were purchased from Bioshop Canada Inc. (Burlington, ON) unless otherwise specified. Buffer compositions are listed in Table A4 in the Appendix.

2.2.2 Cloning and plasmid construction

The plasmid for expression of the AD (residue 215 – 300 of MDM2) with an N-terminal H_6-SUMO fusion was made by subcloning the gene into the pETHS vector using restriction enzymes SapI and BamHI. The plasmid for expression of the RD (residue 356 – 393 of p53) with an N-terminal CBD-SUMO fusion and a C-terminal TCS-H_6-FLAG tag was generated by site-directed mutagenesis from CBD-SUMO-p53-FLAG plasmid to remove the appropriate segment of the p53 sequence and incorporate the TCS-H_6 tag that precedes the FLAG tag sequence. Various mutant constructs of the AD were made by site-directed mutagenesis to exchange for the

desired DNA sequence. Sequence identity of each DNA target was confirmed by Sanger sequencing (Genewiz; South Plainfield, NJ). Forward and reverse primers used for DNA amplification are listed in Table A1 in the Appendix. Standard PCR thermocycling conditions for DNA amplification are highlighted in Table A2 in the Appendix. Plasmid constructs for *E. coli* expression are listed in Table A3 in the Appendix. All plasmids were stored at -20 °C.

2.2.3 Protein expression in E. coli

Protein expression was carried out using the *E. coli* BL21 (DE3) strain. For small scale test expression of each construct, a single colony was picked from an agar plate and grown in 3 mL LB medium supplemented with ampicillin (50 μg/ml) at 37 °C to an optical density at 600 nm (OD_{600}) of 0.6. Cultures were then treated with isopropyl β-d-1-thiogalactopyranoside (IPTG) at a final concentration of 0.8 mM to induce expression from the T7 promoter and allowed to grow for an additional 3 h at 37 °C after induction. For small scale test expression of the DBD construct, a single colony was picked from an agar plate and cells were grown in 3 mL LB medium with ampicillin (50 μg/ml) at 37 °C to an optical density at 600 nm (OD_{600}) of 0.6. The temperature was then lowered to 22 °C and the cells were further grown for 30 min. The culture was supplemented with 0.2 mM zinc sulphate and grown for an additional 30 min before induction. The culture was then treated with 0.5 mM IPTG to induce expression and allowed to grow for an additional 20 h at 22 °C after induction. For large scale expression of target proteins, a starter culture of *E. coli* (DE3) cells carrying the expression plasmids was grown for 12 h at 37 °C in a 125 mL Erlenmeyer flask containing 15 mL of LB medium with ampicillin (50 μg/ml). This was used to inoculate 1 L of LB medium with ampicillin (50 μg/ml) to an OD_{600} of 0.8. For expression of the AD constructs, expression was induced by addition of 0.5 mM IPTG to the culture and the cells were allowed to

grow for an additional 3 h at 37 °C. For expression of the DBD, the cells were further grown for 30 min at 22 °C, after which the culture was supplemented with 0.2 mM zinc sulphate or 0.2 mM cobalt chloride and continued to allow to grow for 30 min. The expression was induced by addition of 0.5 mM IPTG to the culture and hereafter the cells were grown for additional 18 h post-induction at 22 °C.

For expression of ^{13}C- and ^{15}N-enriched AD, *E. coli* (DE3) cells were grown in LB medium with ampicillin (50 μg/ml) to an OD_{600} of 0.8. The cells were harvested by centrifugation (4550 × g at 4 °C for 30 min) and resuspended in a ⅓ equivalent volume of minimal medium supplemented with 3 g/L $^{13}C_6$ D-glucose and 1 g/L $^{15}NH_4Cl$. Cells were then grown for 1 h at 37 °C and subsequently induced with the addition of 0.8 mM ITPG; thereafter, expression was carried out for 3 h at 37 °C. For expression of ^{2}H-, ^{13}C- and ^{15}N-enriched DBD, *E. coli* (DE3) cells were first grown in LB medium with ampicillin (50 μg/ml) to an OD_{600} of 0.8. Pelleted cells were collected by centrifugation (4550 × g at 4 °C for 30 min) and resuspended in a 1/3 equivalent volume of minimal medium constituted in 99% deuterium oxide supplemented with 3 g/L $^{13}C_6$ d-glucose and 1 g/L $^{15}NH_4Cl$. Cells were then grown for 1.5 h at 37 °C followed by 30 min inoculation at 22 °C. The cell culture was then supplemented with 0.2 mM zinc sulphate and cells were grown for an additional 30 min. Expression was subsequently induced by addition of 0.5 mM ITPG and cells were grown for 20 h at 22 °C. Following expression, cells were harvested by centrifugation (4550 × g at 4 °C for 30 min).

2.2.4 Nickel affinity chromatography

Cells expressing AD and RD constructs were resuspended in lysis buffer and lysed by French Pressure Cell Press (American Instrument Company, Silver Spring, MD). The soluble and

insoluble fractions were separated by centrifugation (30,000 × g at 4 °C for 1 hour). The soluble fraction was applied to a column packed with Ni-NTA agarose beads (Clontech Laboratories, Inc.) pre-equilibrated with the lysis buffer. The column was then washed with the denaturing lysis buffer followed by native lysis buffer wash. Finally, bound proteins were eluted with elution buffer, pooled and then cleaved overnight using SUMO protease (produced in house) while dialysing against cleavage buffer at room temperature (RT; ~ 22 °C). The cleaved AD was loaded onto a separate Ni-NTA column pre-equilibrated with cleavage buffer for reverse purification. The flow-through containing the pure protein was collected for further purification using fast performance liquid chromatography (FPLC), as detailed below. For the RD, the eluted protein is cleaved overnight using SUMO protease and thrombin protease while dialysing against cleavage buffer. The cleaved protein was collected for FPLC purification.

Cells expressing the DBD were resuspended in reducing lysis buffer and lysed using French Pressure Cell Press. The soluble and insoluble fractions were separated by centrifugation (30,000g at 10 °C for 1 hour). The soluble fraction was applied to a column packed with Ni-NTA agarose beads pre-equilibrated with the reducing lysis buffer. The column was then washed with the reducing lysis buffer, and bound proteins were eluted with elution buffer containing 2 mM β-mercaptoethanol. The eluted protein was pooled and cleaved overnight using thrombin protease while dialysing against cleavage buffer without reducing agent at RT. The cleaved protein was collected for subsequent purification using FPLC.

2.2.5 Fast performance liquid chromatography (FPLC)

The AD, ADm5, DBD and RD were purified according to the flowchart given in Figure 2.2. Briefly, protein solutions was loaded onto a HiTrap Q HP, a HiTrap SP HP or a Hitrap

heparin HP column pre-equilibrated with Buffer A at a constant flow rate of 1.5 mL/min on an Akta-purifier FPLC system (Amersham pharmacia biotech, Sweden). A linear NaCl gradient of 10-100% over a total volume of 125 mL at a flow rate of 1.5 mL/min was applied using Buffer A and B (buffer containing 1 mM Tris(2-carboxyethyl)phosphine was used for purification of the DBD) while monitoring the chromatogram at 280 nm. The peak corresponding to the target protein was collected, concentrated, flash frozen in liquid N_2 and stored at -80 °C until use.

Sample concentration was determined according to the Beer-Lambert law ($c=A\cdot\varepsilon^{-1}\cdot l^{-1}$), where c is concentration (M), A is the absorbance value, ε is the molar extinction coefficient (M^{-1}/cm^{-1}) and *l* is the pathlength (cm). Samples were 10 × diluted with 6 M guanidinium chloride and absorbance values were determined at 214 nm (peptide bond) and 280 nm (aromatic side chains) (Olis HP 8452 diode array UV spectrophotometer; Bogart, GA). The molar extinction coefficients at 214 nm (RD; ε = 70009 $M^{-1}\cdot cm^{-1}$) and 280 nm (AD; ε = 9970 $M^{-1}\cdot cm^{-1}$, ADm5; ε = 9970 $M^{-1}\cdot cm^{-1}$, and DBD; ε = 17420 $M^{-1}\cdot cm^{-1}$) were determined using the Prot pi | protein tool website server (https://www.protpi.ch/Calculator/ProteinTool). The concentrations for AD and DBD were determined using molar extinction coefficients at 280 nm and the concentration for RD (which has only one phenylalanine residue) was determined using its molar extinction coefficients at 214 nm.

2.2.6 Sodium dodecyl sulfate–polyacrylamide gel electrophoresis (SDS-PAGE)

Protein samples for SDS-PAGE were prepared by mixing an equal volume of the sample and 2x SDS-PAGE loading buffer. The samples were then incubated in a hot water bath (~ 95 °C) for 5 min and were centrifuged at 20,000 × g at RT for 5 min to pellet out insoluble debris. SDS-PAGE gels were prepared in house using 12.5% Next gel solutions. Samples were typically run at 200 V for 45 min in a Mini-Protean II cell (Bio-Rad Laboratories Inc.; Mississauga, ON) using a

Power Station 200 power supply (Labnet International Inc.; Edison, NJ). Gels were stained and visualized using Coomassie blue staining. Protein purity was estimated by densitometry using ImageJ (1.41 version) software.

2.2.7 Isothermal titration calorimetry (ITC)

ITC experiments were carried out using a VP-ITC instrument (Malvern Panalytical Ltd, Malvern, UK). The samples were dialysed against ITC buffer overnight at room temperature (~ 21 °C) and then filtered through a 0.2-μm syringe filter (CELLTREAT Scientific Products, Pepperell, MA) prior to experiments. Samples were degassed for 10 min at 19 °C with gentle stirring before loading. DBD was loaded in the sample cell at 150 μM. Following thermal equilibration at 20 °C and a 5 min delay, 36 serial injections of 8 μL of AD constructs (1.5 mM for wild-type and ADm5) were titrated into the cell with a 300 sec spacing between each injection and a stirring speed of 300 rpm. For experiments without added salt, samples were dialysed against 20 mM sodium phosphate, 1 mM TCEP and 0.025% w/v sodium azide. For titration of the AD by the DBD, the same experimental setup was followed except that 30 μM AD was used in the sample cell and 300 μM DBD was used in the syringe, of which 48 serial injections of 6 μL of the DBD constructs were titrated into the cell. For experiments using zinc-free DBD, the protein was prepared using a previously established protocol (Butler & Loh, 2003). Briefly, the zinc free DBD was generated by treating DBD with 1/33 volume of 10% v/v acetic acid (final pH ~ 4.3) and 1/100 volume of 0.5 M EDTA (pH 8.0) on ice for 1 min, thereafter 1.5 volumes of 0.5 M bis-tris propane (pH 6.8) was added to raise the pH to ~ 6.7. The ITC experiments in this case were performed using 24 serial injections of 500 μM AD into 50 μM zinc free DBD. For ITC experiments with the RD, the protein concentration was 200 μM in the sample cell (RD) and 2 mM in the syringe (AD or ADm5).

All experiments were performed in triplet and control experiments were conducted to measure heats of dilution and were used to correct the experimental binding isotherm for background heat effects. Data were analyzed using the ORIGIN software package (Origin 7 SR4 v7.0552; Malvern Panalytical Ltd, Malvern, UK). The corrected curves were fit to a one-site binding model according to the equation:

$$q_i = v \times \Delta H \times [P] \times \left(\frac{K_a[L]_i}{1 + K_a[L]_i} - \frac{K_a[L]_{i-1}}{1 + K_a[L]_{i-1}} \right)$$

as detailed in Leavitt & Freire, (2001).

2.2.8 Differential scanning calorimetry (DSC)

DSC experiments were carried out using a VP-DSC instrument (Malvern Panalytical Ltd, Malvern, UK). Samples were dialysed in ITC buffer overnight at room temperature (~ 21 °C) and then filtered through a 0.2-μm syringe filter prior to the experiments. The concentration for the DBD was kept at 50 μM in the absence and presence (100 μM) of the AD constructs. Samples were degassed for 10 min at 19 °C, with gentle stirring before loading. All experiments were performed in triplicate at a scan rate of 40 °C/h over a 10-50 °C range under a constant pressure of 35 psi, and the system was allowed to equilibrate at 10 °C for 15 min before scanning. Blank experiment with the AD (100 μM) was carried out as a control. Data analysis was performed using ORIGIN software (Origin 7 SR4 v7.0552; Malvern Panalytical Ltd, Malvern, UK). Owing to the irreversible aggregation of the DBD, the temperature at maximum height of the DSC peak that corresponds to the melting transition was used as an estimate for the T_m value.

2.2.9 Nuclear magnetic resonance (NMR) spectroscopy

Samples for NMR experiments were prepared in NMR buffer (Table B1). The samples were dialysed against NMR buffer in absence of 10% v/v D_2O and 1 mM DSS overnight at room temperature (RT ~ 21 °C) and then filtered through 0.2-micron syringe filter prior to the experiments. The D_2O stock solution of the NMR buffer with 10 mM DSS in 99% D_2O was prepared and filtered through 0.2-micron syringe filter. 1/10 volume of the D_2O stock solution of the NMR buffer was added to a final concentration of 10% v/v D_2O and 1 mM DSS.

The concentration of isotope-labeled AD was 150 μM for ^{1}H-^{15}N heteronuclear single quantum coherence (HSQC) experiments involving the DBD, which were carried out using a 500 MHz Bruker spectrometer equipped with a BBFO SmartProbe. For HSQC titration experiments of isotope-labeled AD (150 μM) with unlabeled RD, experiments were performed on a 700 MHz spectrometer. Triple resonance experiments for isotope-labeled AD (800 μM) were performed using a 500 MHz Varian INOVA spectrometer equipped with a HCN room temperature probe. Chemical shifts for the C', C_α, C_β, N and H_N nuclei were assigned using the standard suite of HNCO, HN(CA)CO, HNCACB and CBCA(CO)NH experiments(Sattler, Schleucher, & Griesinger, 1999) . The following experiments were all acquired on a 700 MHz Bruker Avance III spectrometer equipped with a TCI cyroprobe. {^{1}H} -^{15}N Steady-state heteronuclear NOE (hetNOE) experiment and triple-resonance experiments, including the HNCA and HNCO experiments, were acquired for 300 μM isotope-labeled AD in presence of 330 μM unlabeled DBD. A {^{1}H} -^{15}N steady-state hetNOE experiment was collected for 900 μM isotope-labeled AD. The {^{1}H}-^{15}N steady-state hetNOE experiments were acquired in an interleaved manner, with the reference spectrum acquired with a 5 sec relaxation delay whereas the NOE-enhanced spectrum was recorded with a 1 sec relaxation delay followed by a 4 sec proton pre-saturation.

All NMR experiments for isotope-labeled DBD were performed on an 700 MHz Bruker Avance III spectrometer equipped with a TCI cyroprobe except for triple-resonance experiments for the sample containing 300 μM isotope-labeled DBD in presence of 600 μM unlabeled AD, which were carried out using an 800 MHz Bruker Avance III spectrometer equipped with a TCI cyroprobe. Protein deuteration and transverse relaxation optimized spectroscopy (TROSY) (Pervushin, Riek, Wider, & Wuthrich, 1997; Salzmann, Pervushin, Wider, Senn, & Wuthrich, 1998) were employed for isotope-labeled DBD, owing to the unfavorable relaxation properties of a ~ 25 kD protein. Chemical shifts for the C_α, N and H_N nuclei were assigned using the TROSY-HNCA experiment for 300 μM isotope-labeled DBD in the presence and absence of 2 molar excess of unlabeled AD. TROSY-modified $\{^1H\}$-^{15}N hetNOE experiments of isotope-labeled DBD (300 μM) in the presence and absence of 2 molar excess of the unlabeled AD were acquired in an interleaved manner (Zhu, Xia, Nicholson, & Sze, 2000), the reference spectrum was acquired with a 5 sec relaxation delay whereas the spectrum with NOE enhancement was collected with a 1 sec relaxation delay followed by a 4 sec proton pre-saturation. ^1H-^{15}N TROSY experiments were performed for the isotope-labeled DBD with various unlabeled AD constructs.

Paramagnetic relaxation enhancement (PRE) experiments with isotope-labeled DBD were performed by incorporating a 2,2,6,6-tetramethyl-1-piperidinyloxy (TEMPO) spin label into the cysteine mutants AD^{S286C} or AD^{Q238C} using maleimide conjugation chemistry. Samples containing cysteine mutant AD proteins were dialysed against NMR buffer containing 1 mM TCEP instead of DTT for 12 h at room temperature. The reagent 4-maleimido-TEMPO was dissolved in 95% ethanol and added at 10 molar equivalents relative to the concentration of the AD cysteine mutant. Reactions were typically carried out at protein concentrations of 2 mM and were allowed to proceed at RT in the dark for 12 h with gentle shaking, after which excess spin label was removed by buffer

exchange using a 0.5 mL Zeba spin desalting column (Fisher Scientific; Ottawa, ON), with the final condition being NMR buffer in presence of 1 mM TCEP. The samples contained 160 μM of isotope-labeled DBD and 200 μM of the AD^{S286C} or AD^{Q238C} with spin-label. ^{1}H-^{15}N TROSY spectra of the samples with the active spin-label were acquired directly after buffer exchange. Immediately following the acquisition of a ^{1}H-^{15}N TROSY spectrum for each sample with active spin label, DTT and ascorbic acid were added, at final concentrations of 4 mM and 1 mM, respectively, to inactivate the spin label. The sample was then incubated for 30 min at RT and a second ^{1}H-^{15}N TROSY spectrum was acquired with the spin-label in the reduced state.

Full NMR experimental parameters, including triple resonance experiments that were acquired using non-uniform sampling of indirectly observed dimensions, are listed in Table A4 in the Appendix. Data were processed using Bruker TopSpin ver. 4.06 and NMRpipe (Delaglio et al., 1995). For NMR data collected by non-uniform sampling (NUS), NUS points were generated using the random sampling scheme prior to data collection. The NMR data generated with NUS were processed by iterative soft thresholding algorithm from NMRpipe to reconstruct the final spectra. ^{1}H frequencies were referenced to the internal standard DSS whereas ^{15}N and ^{13}C frequencies were indirectly referenced based on ^{1}H (Wishart et al., 1995 and Markley et al., 1998). Spectral visualization and analysis were carried out using CcpNmr Analysis version 2.3 (Vranken et al., 2005), including sequential backbone chemical shift assignment, secondary chemical shifts ($\Delta\delta$), intensity ratios derived from hetNOE (I_{sat}/I_{ref} of the signals from the spectrum with and without proton pre-saturation) and intensity ratios derived from PRE experiments (I_{para}/I_{dia} of the signals from the spectrum with the spin label at paramagnetic and diamagnetic states). Error estimates on hetNOE intensities (σ_{NOE}) were determined using:

$$\sigma_{NOE}/NOE = ((\sigma_{Isat}/I_{sat})^2 + (\sigma_{Iref}/I_{ref})^2)^{½}$$

as detailed in Farrow et al., (1994). Errors on PRE factors were similarly determined calculated based on the signal-to-noise ratios of the spectra. Chemical shift perturbations (CSPs) were determined using:

$$\Delta\delta_{HN} = \sqrt{\frac{\Delta\delta_H^2 + 0.2\Delta\delta_N^2}{2}}$$

as detailed in Williamson, (2013), of which CSPs that were greater than two standard deviations were considered significant. Chemical shift assignments were validated using the PANAV (Probabilistic Approach to NMR Assignment and Validation) web server (http://redpoll.pharmacy.ualberta.ca/PANAV) that implements the algorithm developed by Wang B, Wang Y and Wishart, (2010).

2.3 Results

2.3.1 Protein production and purification

Overexpression of the DBD, the RD and the AD constructs were carried out using *E. coli* expression system. All of the AD and the RD constructs contain an N-terminal H_6-SUMO fusion tag, as is frequently employed to enhance protein expression and to facilitate downstream purification (Marblestone et al., 2006). Each of these overexpressed SUMO-fusion proteins remained highly soluble after cell lysis and exhibited high metal-binding affinity for Ni-NTA purification (Figure 2.3). Protein samples of high purity were obtained using denaturing buffer containing 6 M urea as wash buffer. Of note, the fusion tag was efficiently cleaved by SUMO protease following 6 M urea treatment (Figure 2.3: AD, ADm5, AD^{S286C}, AD^{Q238C} & RD, lane SC). For the AD constructs, reverse purification using nickel-affinity chromatography followed by anion-exchange chromatography purification yielded proteins at 90 ~ 95% purity (Figure 2.3: AD,

ADm5, AD^{S286C} & AD^{Q238C}, lane AX). For the RD construct, cation-exchange chromatography purification yielded protein at ≥ 95% purity (Figure 2.3: RD, lane CX). The DBD construct contained an N-terminal H_6 tag followed by a thrombin cleavage site (TCS) to facilitate purification and straightforward removal of the H_6 tag by proteolysis with the protease thrombin. The overexpressed protein was partially soluble after cell lysis and the protein in the soluble fraction exhibited high binding-affinity for Ni-NTA purification (Figure 2.3). Following nickel-affinity purification, typical yields were of samples at > 70% purity (Figure 2.3: DBD, lane E). Following thrombin cleavage, most *E. coli* protein contaminants were removed by further purification using heparin-affinity chromatography to yield protein at ≥ 95% purity (Figure 2.3: DBD, lane HA). Of note, the thrombin-cleaved DBD contains a four amino acid spacer (G-S-H-M) at the protein N-terminus.

2.3.2 Chemical shift assignment and validation

Triple-resonance NMR experiments (listed in Table A5 in the Appendix) were performed to allow chemical shift assignment of the DBD, the DBD in complex with the AD, the AD and the AD in complex with the DBD (Table 2.1 & Table A6 – A9 in the Appendix). To validate my chemical shift assignments, the assigned chemical shifts were analysed using the PANAV (Probabilistic Approach to NMR Assignment and Validation) web server (http://redpoll.pharmacy.ualberta.ca/PANAV) that implements the algorithm developed by Wang B, Wang Y and Wishart (2010). The program reports information on chemical shift reference offsets, flagged mis-assignments and provides a global assignment quality score. The chemical shift reference offsets compensate for any potential referencing errors, the cut off re-referencing values are 1.0 ppm for C_α, C_β and C' nuclei and 1.5 ppm for N nuclei. Flagged mis-assignment showed these assignments

that are more than 4 standard deviations away from the expected values reported by Wang and Jardetzky (2001). The global assignment quality score CONA is a direct assessment of overall assignment quality, where proper assignment typically yields value of above 0.95 using a 6-residue fragment scan analysis. Based on the assessment by PANAV, my chemical shift assignment data (AD, AD in complex with unlabeled DBD, DBD and DBD in complex with unlabeled AD) are of high quality. Summary of the PANAV assessment report is presented in Table 2.2.

2.3.2 Interaction of the AD with p53 DBD

I have selected a segment of MDM2 encompassing residues 215 – 300 (referred to hereafter as the AD) based on prior studies which demonstrated the potential for this region to encompass a binding site for the p53 DBD (Cross et al., 2011; Yu, G. W. et al., 2006). The interaction between the AD and the DBD was examined using ITC, with the AD binding the DBD with $K_d \approx 21.7$ μM under our experimental conditions (Figure 2.4, A and Table 2.2). The AD is significantly enriched in glutamate and aspartate residues (14 aspartate and 14 glutamate residues out of 86 residues), leading to its low pI of ~ 3.07, and the DBD contains significant number of lysine and arginine residues (19 arginine and 8 lysine residues out of 219 residues; pI $\approx$ 8.23). I speculated that electrostatic interactions could play a critical role in mediating this interaction. To test this hypothesis, I performed ITC experiments in the absence of NaCl. Indeed, the affinity is stronger by an order of magnitude ($K_d \approx 1.4$ μM; Table 2.2), suggesting that charge plays an important role in the interaction between the AD and the DBD (Figure 2.4, B and Table 2.2).

The AD contains many phosphorylation sites that are crucial for MDM2 function (Blattner, Hay, Meek, & Lane, 2002). The electrostatic interaction shown above highlights the possibility that AD phosphorylation may serve to further strengthen its interaction with the DBD via

introduction of additional negative charges. To test this hypothesis, I produced the AD with glutamate mutations at five serine residues that are known phosphorylation sites (Hornbeck et al., 2015): S240E, S242E, S246E, S253E and S256E (referred to as the ADm5 construct). The interaction of ADm5 with the DBD was examined by ITC. The ADm5 binds the DBD with ~ 2 fold higher affinity than WT AD ($K_d \approx$ 13.3 μM as compared to $K_d \approx$ 21.7 μM; Table 2.2), consistent with the hypothesis that phosphorylation of the MDM2 AD could enhance its interaction with the p53 DBD.

After demonstrating that the AD and the DBD interact, I further evaluated the interaction using NMR experiments. The ^{1}H-^{15}N HSQC spectrum of the AD has very narrow peak dispersion (~ 0.8 ppm) in the proton dimension (Figure 2.5), a feature which is indicative of a disordered protein (Yao, Dyson, and Wright. 1997). To unambiguously validate this, I performed triple-resonance assignment that allowed near complete assignment of backbone resonances (Table 2.1). These data allowed assessment of secondary structure based on the based upon backbone ^{1}H, ^{13}C and ^{15}N alongside C_β chemical shifts. Specifically, I analysed the assigned chemical shifts (including H_N, N, C', C_α and C_β) using the δ2D webserver (Camilloni, De Simone, Vranken, & Vendruscolo, 2012) to estimate the secondary structure populations of individual amino acids as a function of the protein sequence. Consistent with the narrow H_N dispersion, this chemical shift-based secondary structural analysis clearly shows that the AD displays significant disordered structure with residual β-sheet structure at the C-terminal end of the sequence (Figure 2.6, B).

To identify the AD residues that are involved in the interaction with the DBD, I collected a ^{1}H-^{15}N HSQC spectrum of the AD in the presence of equimolar DBD and compared this to the spectrum for the AD. The HSQC spectrum of the AD in the presence of equimolar DBD showed little change in overall peak dispersion (Figure 2.5). Close inspection of the HSQC spectrum

revealed that the residues that underwent the most significant chemical shift perturbation clustered to residues 245 – 282 (Figure 2.6, A). It is interesting to note that the segment that spans residues 275 – 282 was significantly affected and the cross-peaks for residues V280 and Q282 were completely missing from the spectrum, suggesting that this region likely form a crucial contact with the DBD.

I showed that reduction of the buffer ionic strength stimulated the AD-DBD interaction (Table 2.2). To further evaluate the effect of ionic strength on the interaction between the AD and the DBD, I collected ^{1}H-^{15}N HSQC spectra of isotope-labeled AD in presence and absence of DBD using NMR buffer without NaCl. Interestingly, the overall peak dispersion is not affected by the change in salt concentration and the DBD-bound spectrum closely resembles the spectrum in presence of NaCl, suggesting that the overall conformation of the protein in the free or bound form is not dramatically affected (Figure 2.7, A and B). A notable difference is that the some of the amide cross-peaks were observed at much lower intensity, especially for the residues that underwent the most dramatic chemical shift changes and presumably at the binding site for the DBD. The weaker cross-peak intensity is in good agreement with an increase in binding affinity as this behaviour would be expected if more molecules of the AD are in the DBD-bound state, correlating with the formation of a slower-tumbling complex (~ 33.9 kDa for the AD-DBD complex vs. ~ 9.4 kDa for the AD at the unbound state) that would result in line broadening and a corresponding loss of signal intensity.

2.3.3 The AD and the DBD form a fuzzy complex

Despite the demonstration that the AD and the DBD bind with low micromolar affinity (Table 2.2), the chemical shift perturbations experienced by the AD upon binding to the DBD are not dramatic and the dispersion of the cross-peaks in the ^{1}H-^{15}N HSQC spectrum remains narrow

(Figure 2.5). Considering that the concentrations of the AD and the DBD (150 μM) used for the NMR experiments are ~ 6 times higher than the K_d, a significant fraction of the protein molecules would be in the bound form. These results suggest that the AD likely retains significant disorder in the DBD-bound form. To test this hypothesis, I assigned the backbone chemical shifts (including H_N, C_α, C' and N) of the AD in the presence of the DBD and analysed these data using δ2D webserver to estimate the secondary structure populations of individual amino acids. Indeed, the DBD-bound AD displayed a similar degree of structural disorder to that observed for the AD in absence of the DBD (Figure 2.6, B).

The disordered nature of the AD in the interaction with the DBD suggests that the AD should retain significant conformational dynamics once bound to the DBD. I probed the motion of the backbone amide groups on the ps-ns time scale by $\{^1H\}$-^{15}N steady state hetNOE experiments (Kay, Torchia, & Bax, 1989). Values of the HetNOE < 0.65 are typically held to be indicative of considerable structural flexibility on the ps timescale (Tjandra et al., 1995). The observed hetNOE enhancement factors for the AD in both the free and DBD-bound form are in the range of -1.5 to 0.3, which is indicative of a protein with a high degree of structural flexibility (Figure 2.6, C). Taken together, these data imply that the AD and the DBD likely adopt a dynamic fuzzy complex, in which one of the binding partners (i.e. AD) in the complex retains significant conformational dynamics (Tompa & Fuxreiter, 2008).

2.3.4 Defining the binding interface on the DBD for the AD

Based on the inference that the AD forms a random fuzzy complex when bound to the DBD, I speculated that the AD is unlikely to have a well-defined binding site on the DBD surface. To test this hypothesis, I further explored the interaction to determine the binding site on the DBD for the

AD. The DBD presents a considerable challenge for conventional NMR experiments owing to its unfavourable relaxation properties. Previous studies have demonstrated that transverse relaxation optimized spectroscopy (TROSY), a NMR technique that makes use of the cancellation between dipolar coupling and chemical shift anisotropy to reduce T_2 relaxation and produce spectra with sharp spectra lines (Pervushin et al., 1997), in combination with protein deuterium labelling can significantly improve spectral quality and allow for near-complete assignment of the DBD (Canadillas et al., 2006; Rasquinha, Bej, Dutta, & Mukherjee, 2017). The deuterium-labelled DBD was successfully produced for downstream NMR experiments (Figure 2.2). In order to identify the residues involved in the interaction with the AD, TROSY-based triple-resonance NMR experiments were performed to allow sequential assignment for the DBD in presence and absence of the AD.

The ^{1}H-^{15}N TROSY spectrum of the DBD is well dispersed over a range of ~ 4 ppm for the $^{1}H_N$ chemical shifts, with addition of the AD leading to observable chemical shift perturbations for majority of the cross-peaks (Figure 2.8). The residues in the DBD that underwent significant chemical shift changes upon binding to the AD are primarily localized to the N-terminus and the loop-sheet-helix motif (including L1 loop, H2 helix & S2-S2' β-hairpin; Figure 2.9, B). Specifically, significant changes were observed for S94, V97, S99 and T102 (from the N-terminal region), F113, L114 and G117 (from L1 loop), Y126 (from S2 strands), F134 (from S3 strand), S183, A189 and Q192 (from L3 loop), L201, D207 and R209 (flanking S5 strand), R249 (from L2 loop), C277, G293 and E294 (flank H2 helix), K291 (from H2 helix) and R306 and A307 (from the C-terminal region). The amide groups of the residues G117 and Y126 showed the most significant CSPs, suggesting that these two residues might be involved in direct contact with the AD. To evaluate potential structural changes of the DBD upon AD binding, the chemical shift data

(including H_N, N, C', C_α and C_β for all assignable residues) were analyzed using δ2D webserver to determine the secondary structure of the DBD at the per residue level (Figure 2.10).

In general, the overall fold of the DBD is largely unaffected when bound to the AD (Figure 2.10, A and B). However, a closer look at the data revealed subtle changes in the overall structure of the DBD (Figure 2.10, C). The loop-sheet-helix motif is more structured in the AD-bound form than the unbound DBD, with an apparent increase in α-helicity at the L1 loop and higher β-sheet content at the S2-S2' β-hairpin. A similar trend is observed for the L3 loop (flanking S8 and S9 strands), which gains significant β-sheet content when bound to the AD. On the other hand, the two loops connecting the H1 helix and S5 strand and flanking the S6 and S7 strands were less structured, with a noticeable decrease in β-sheet content. These noticeable differences of the DBD could be the result of binding induced conformational change caused by the AD, or a result of direct binding that modulate the conformational sampling in favour of one or more conformational states. To evaluate this change in structural content in relation to the conformational dynamics, $\{^1H\}$-^{15}N hetNOE experiments were performed to probe backbone dynamics of the DBD in presence and absence of the AD at ps-ns time scale. Clearly, the dynamics of the DBD is not affected by the interaction with the AD (Figure 2.11).

To more clearly define the AD binding site on the DBD, I performed PRE experiments using a nitroxide spin label (TEMPO). Two mutated versions of the AD were prepared, each having a single cysteine (AD^{Q238C} or AD^{S286C}) N- or C-terminal to the DBD binding site. The TEMPO spin label was then attached to the cysteine through maleimide coupling. Through observation of paramagnetic agent-induced enhancement of transverse relaxation, these spin labels serve to provide long-range distance restraints of up to 25 Å (Battiste and Wagner, 2000). ^1H-^{15}N TROSY spectra of the DBD in presence of either the AD^{Q238C} or AD^{S286C} were acquired for both active

(paramagnetic, I_{para}) and inactive (diamagnetic, I_{dia}) spin labels. The peak heights for all resonances were measured for both I_{para} and I_{dia} spin labels and the intensity ratio (I_{para}/I_{dia}) was used to identify the residues in proximity to the spin label. Resonance broadening is observed for many DBD backbone amide cross-peaks in the presence of spin-labeled AD^{Q238C} or AD^{S286C}, suggesting a direct interaction between the AD and the DBD (Figure 2.12 and 2.14). The residues in the DBD with amide cross-peaks broadened by the presence of each paramagnetic spin-labeled AD mutant were mapped onto the structure of the DBD (Figure 2.13 and 2.15). The largest PRE is observed for residues located in the N-terminal region, namely in the S1, S2, and S11 strands; L1, L3 loops; and, H2 helix. In particular, the residues that were significantly affected by the spin label were localized at or near the DNA binding surface of the DBD, suggesting that the AD could interfere with DNA binding activity of the DBD. This is in good agreement with literature findings that the AD inhibits the p53 DNA binding function (Cross et al., 2011).

If there is a preferred orientation of an AD in the AD-DBD complex, I expect different patterns of intensity loss when the spin label is on opposite ends of the AD peptide. In contrast, the PRE data showed that both spin-labelled AD^{Q238C} and AD^{S286C} constructs led to signal attenuations of many overlapping residues on the DBD. Moreover, the residues affected by the presence of these spin labels are not localized to a clear, defined region and cannot be accounted for by a single binding site on the DBD. The results indicate that the AD bind without any discernable orientation bias. Instead, these NMR data are consistent with a mechanism where the AD binds to the DBD with multiple conformations so that a significant region on the surface of the DBD is occupied by the AD. Furthermore, multiple bound conformations could allow the AD to engage in dynamic electrostatic interactions with the DBD. Indeed, PRE affected residues that are clustered around the surface-exposed lysine and arginine residues of the DBD (Figure 2.16). This binding mode is

in good agreement with the above-noted hypothesis of the formation of a fuzzy complex between the AD and the DBD, which would allow the AD to fluctuate without adopting any specific binding conformation but continues to interact specifically with the DBD.

2.3.5 The AD directly interacts with the C-terminal RD of p53

The DBD is positively charged (z = + 4.4 at pH 7.4) and I have demonstrated that electrostatic interactions facilitate the formation of a dynamic complex with the AD. Similarly, the RD is also positively charged with a net charge of z = + 4.7 at pH 7.4. Moreover, it has been demonstrated that both the DBD and the RD are directly ubiquitinated by MDM2 (Chan et al., 2006). Hence, it is plausible that the AD may bind to both the DBD and the RD to facilitate p53 ubiquitination. To test this hypothesis, ITC experiments were performed to evaluate the potential for interactions between the AD and the RD. Under the same experimental conditions used to characterize the DBD-AD interaction, the AD binds to the RD with a K_d of 21.3 μM (Figure 2.17, A and Table 2.10), similar to the value that I reported for the DBD (~ 21.3 μM; Table 2.2). Furthermore, the ADm5 mutant binds the RD with ~ 2× higher affinity ($K_d \approx 9.4$ μM; Figure 2.17, B and Table 2.2), which follows the trend observed for the interaction with the DBD (~ 13.3 μM; Table 2.2) . To further characterize this interaction, a ^{1}H-^{15}N HSQC-based titration was performed using ^{15}N-labeled AD and unlabeled RD (Figure 2.18). The data suggested that the residues that underwent the most significant chemical shift changes correspond well with the residues involved in the interaction with the DBD (residues 245 – 283) (Figure 2.19), suggesting that binding of the AD to the DBD or the RD are likely to be mutually exclusive (Figure 2.17, C). Thus, the data support the hypothesis that the AD is likely to be crucial for p53 ubiquitnation.

2.3.6 The AD-DBD interaction lowers the stability of the DBD and may preferentially bind to the partially-unfolded conformation of DBD

The NMR data suggested that although the DBD undergoes some degree of conformational rearrangement when bound to the AD, the overall fold of the DBD is maintained and its backbone dynamics are largely unaffected (Figure 2.10 and 2.11). In contrast to these findings, it has been reported that the AD can promote the adoption of a mutant-like conformation by the DBD that exposes the mutant-specific Pab240 epitope (residues 212 – 217, including part of the S7 strand), which is buried in the wild-type conformation but becomes exposed by denaturation or in mutant conformations (Cross et al., 2011 and Stephen & Lane, 1992). This obvious contradiction could be the result of the temperature used in our *in vitro* experiments (20 °C), which differs from the physiological temperature generally used for *in vivo* experiments. It is well known that the DBD is intrinsically unstable and undergoes spontaneous aggregation at near physiological temperature (Bullock et al., 1997; Nikolova, Henckel, Lane, & Fersht, 1998). Unfortunately, the intrinsic instability of the DBD prevented NMR experiments from being conducted at near-physiological temperature as the protein undergoes spontaneous aggregation. Instead, I used DSC to test for changes in the DBD melting temperature (T_m), where a destabilized mutant-like conformation of the DBD upon binding to the AD should be reflected by a decrease in T_m. The DSC thermogram data show that the apparent T_m for the DBD is lowered by 1.5 °C in presence of the AD (T_m = 42.1 ± 0.2 °C in the presence as compared to T_m = 43.6 ± 0.2 °C in the absence of the AD; Figure 2.20), suggesting that the AD may bind to and stabilize a mutant-like conformation of the DBD.

The favourable interaction of the AD with a mutant-like conformation of the DBD suggests that structurally-destabilized DBD mutants should bind the AD with higher affinity. Indeed, a previous study demonstrated that the AD binds more effectively to several DBD missense mutants,

including R175H, R273H, R248Q and D281G (Yang et al., 2019). The R175H mutant of the DBD displayed accelerated zinc loss and was shown to exist mainly in the zinc-free form at physiological temperature (Figure 2.21, A) (Butler & Loh, 2003; Yu, X. et al., 2014). I have selected zinc-free DBD (^{apo}DBD) for testing as the zinc-free form has similar structural and functional features to the R175H mutant and the mutation destabilizes the DBD but not the ^{apo}DBD (Butler and Loh, 2003). Moreover, this study presented a robust and straightforward protocol for producing the ^{apo}DBD from the DBD. Zinc chelation has also been shown to promote p53 to adopt a mutant-like conformation that can be recognized by the Pab240 antibody (Hainaut & Milner, 1993; Meplan, Richard, & Hainaut, 2000). Thus, zinc-free DBD is an excellent candidate to mimic the R175H mutant of the DBD. I tested the interaction between the zinc-free DBD and the AD using ITC. Remarkably, my ITC results showed that the AD binds the ^{apo}DBD with 3-fold higher affinity as compared to the DBD ($K_d \approx 8.1$ μM as compared to 21.3 μM; Figure 2.21, B and Table 2.2), suggesting that the AD can indeed preferentially bind the mutant DBD.

2.4 Discussion

The MDM2 AD plays an important role in promoting p53 ubiquitination and inhibiting the DNA-binding activity of p53, yet the precise structural & functional relationship of this region remains poorly understood. To our knowledge, there is only one other study that took a biophysical approach to investigate the structural and functional relationship of the AD on regulation of p53 activity (Grace et al., 2006). It has to be noted that the previous study experimented on short fluorescein-labeled peptide fragments derived from the AD, thus might not be representative of a full-length sequence.

In this study, I confirmed that the AD was able to directly bind the DBD. Moreover, I demonstrated that the interaction between the AD and the DBD is primarily electrostatic and can be facilitated by introducing additional negative charges on the AD. This result is in agreement with a previous paper by Friedler et al., (2005), which suggested that the DBD mediates protein binding with a strong electrostatic component. The significant contribution of electrostatic interactions to the binding affinity suggests that phosphorylation of key residues is likely to be important in fine-tuning the AD-DBD interaction. My NMR results suggest the sequence of the AD necessary for DBD binding lies within the region spanning residues 245 – 282. Importantly, this region contains numerous serine and threonine residues that were shown to be phosphorylated *in vivo* (Hornbeck et al., 2015), further supporting that phosphorylation is likely to be important for the function of the AD.

I found that the AD is an intrinsically disordered region and forms a dynamic fuzzy complex when bound to the DBD, where it retains significant structural disorder. Moreover, the entropy gain observed for the binding event directly reflects the coexistence of multiple alternative binding states of the AD in complex with the DBD (Table 2.10). Furthermore, the PRE and CSP data indicate that the AD can bind a large surface area on the DBD, including its DNA-binding surface. This observation supports the previous finding that the AD can effectively prevent p53-DNA interaction (Cross et al., 2011). In addition, the disordered nature of the AD could facilitate easy access by regulatory proteins that are responsible for p53 regulation, such as ribosomal protein L11 (Zhang et al., 2003), tumour suppressor p14ARF (Bothner et al., 2001) and retinoblastoma protein (Sdek et al., 2004). Binding of these proteins would serve to disrupt this important interaction, which could in turn help to stabilize and activate p53.

My data showed for the first time that both the AD and its phosphomimic mutant can directly bind the RD. The binding affinity for the AD-RD interaction is very similar to the AD-DBD interaction and, in both cases, the same sequence of AD is responsible for establishing a dynamic interaction with the DBD or the RD. Being the substrates for MDM2, both domains were shown to be ubiquitinated *in vivo* (Chan et al., 2006). More recently, the AD was shown to engage in an intramolecular interaction with the RING domain to facilitate p53 ubiquitination (Cheng et al., 2014). Thus, the AD can bind to the catalytic RING domain as well as its substrate. Moreover, the dynamic interaction may facilitate ubiquitin transfer from the RING domain to the DBD and the RD. Taken together, I proposed a model that the AD could form the basis of a dynamic network that connects the catalytic RING domain with the p53 substrate (the DBD and the RD) to promote efficient ubiquitination (Figure 2.22).

The AD has been shown to directly regulate the p53 DNA-binding activity by binding to the surface of the DBD and competing with the target DNA sequence (Cross et al., 2011). On the other hand, the electrostatic interactions between the RD and phosphate groups of the DNA backbone have been shown to promote one-dimensional sliding of p53 on DNA and directly controls site-specific DNA binding (Friedler et al., 2005, Laptenko et al., 2015 and Leith et al., 2012). Therefore, the AD could effectively prevent p53-DNA interaction by establishing direct contacts with the DBD and the RD. Thus, the MDM2 AD is likely to be a crucial region that regulates both the transcriptional activity and stability of p53. The critical role of the AD in regulation of p53 suggests this region can be subjected to therapeutic intervention to activate p53.

I noted that the T_m for the DBD is lowered when bound to the AD, suggesting that the AD may bind favourably to an altered conformation of the DBD that has lower thermostability as compared to the native conformation. I took the advantage of the structurally-destabilized ^{apo}DBD

that resembles the DBD R175H mutant and showed that it binds the AD with 3× higher affinity as compared to the WT DBD, supporting that the AD binds preferentially to a mutant-like structure of the DBD. Based on our model that the AD forms a dynamic network with the RING domain, the DBD and the RD to facilitate p53 ubiquitination, the higher binding affinity with the mutant DBD would likely have a deleterious effect on p53 ubiquitination by sequestering the AD. Indeed, a recent study showed that the AD could bind preferentially to several p53 DBD mutants *in vivo* and inhibit MDM2-mediated p53 ubiquitination (Yang et al., 2019). Importantly, accumulation of mutant p53 is a prominent feature of many cancers (Bartek et al., 1991, Inoue et al., 2012, Iggo et al., 1990). Moreover, emerging evidence suggest that some mutant p53 forms have gain of function effects that facilitate cancer cell growth and invasion (Dong et al., 2009, Fontemaggi et al., 2009, Gualberto et al., 1998, Kalo et al., 2012, Kollareddy et al., 2015, Liu et al., 2017, Olive et al., 2004, Oijen and Slootweg, 2000, Xu et al., 2008, Zhu et al., 2015, Zhang et al., 2013) Thus, disruption of the high affinity AD-DBD interaction in cancer cells expressing mutant p53 forms could potentially reactivate MDM2 to promote mutant p53 degradation, which may have therapeutic potential against cancers that accumulate gain-of-function mutant p53 forms.

Table 2.1: Chemical shift assignment reports.

DBD	
Atom type	Assignment
H_N*	197/204 (97%)
$N^{\perp}$	197/204 (97%)
C'	197/223 (88%)
C_α	215/223 (96%)
C_β	157/207 (76%)

DBD in complex with the AD	
Atom type	Assignment
H_N*	194/204 (95%)
$N^{\perp}$	194/204 (95%)
C'	187/223 (84%)
C_α	207/223 (93%)
C_β	164/207 (80%)

AD	
Atom type	Assignment
H_N*	81/82 (99%)
$N^{\perp}$	81/82 (99%)
C'	84/86 (98%)
C_α	84/86 (98%)
C_β	79/81 (98%)

AD in complex with the DBD	
Atom type	Assignment
H_N*	76/82 (93%)
$N^{\perp}$	76/82 (93%)
C'	76/86 (88%)
C_α	83/86 (97%)

* N-terminal HN was excluded.

⊥ Proline residues and N-terminal N were excluded.

Table 2.2: PANAV assessment reports for chemical shift assignments.

DBD (H_N, N, C_α, C_β, and CO)		
CONA Score (6-Resdue Scan)	0.99	> 0.95
Detected reference offsets	N: -0.75 ppm C_α: 0.31 ppm C_β: 0.85 ppm CO: 0.03 ppm	N: < ±1.5 ppm C_α: < ±1.0 ppm C_β: < ±1.0 ppm CO: < ±1.0 ppm
Number of assignments	963	
Number of deviant assignments	0	
Number of suspicious assignments	2	S127 C_α: 53.12 R248 N: 107.49
DBD + AD (H_N, N, C_α, C_β, and CO)		
CONA Score (6-Resdue Scan)	0.97	> 0.95
Detected reference offsets	N: -0.73 ppm C_α: 0.38 ppm C_β: 0.89 ppm CO: 0.07 ppm	N: < ±1.5 ppm C_α: < ±1.0 ppm C_β: < ±1.0 ppm CO: < ±1.0 ppm
Number of assignments	942	
Number of deviant assignments	0	
Number of suspicious assignments	2	S127 C_α: 53.17 R248 N: 107.44
AD (H_N, N, C_α, C_β, and CO)		
CONA Score (6-Resdue Scan)	1.00	> 0.95
Detected reference offsets	N: -0.91 ppm C_α: -0.31 ppm C_β: 0.52 ppm CO: -0.26 ppm	N: < ±1.5 ppm C_α: < ±1.0 ppm C_β: < ±1.0 ppm CO: < ±1.0 ppm
Number of assignments	409	
Number of deviant assignments	0	
Number of suspicious assignments	1	A300 N: 109.64

AD + DBD (H_N, N, C_α, and CO)		
CONA Score (6-Resdue Scan)	0.95 (1.00)*	> 0.95
Detected reference offsets	N: -0.72 ppm C_α: -0.86 ppm C_β: 0.00 ppm CO: -0.61 ppm	N: < 1.5 ppm C_α: < 1.0 ppm C_β: <1.0 ppm CO: <1.0 ppm
Number of assignments	315	
Number of deviant assignments	0	
Number of suspicious assignments	0	

*Reassessment after removal of N-terminal sequence STG that are not assignable.

Table 2.3: Parameters of the AD-DBD and the AD-RD interactions obtained from ITC.

Protein	K_d (μM)	ΔH (kcal·mol^{-1})	ΔS (cal·mol^{-1}·K^{-1})	n
With DBD				
AD	21.29 ± 0.58	-2.1 ± 0.2	14.1	0.75 ± 0.05
ADm5	13.31 ± 0.50	-5.2 ± 0.2	4.3	0.61 ± 0.08
With AD (low salt)				
DBD	1.37 ± 0.45	-7.1 ± 0.3	3.3	0.94 ± 0.05
With Apo DBD				
AD	8.30 ± 0.68	-2.2 ± 0.6	15.8	0.73 ± 0.06
With RD				
AD	21.35 ± 0.85	-1.5 ± 0.1	16.3	0.65 ± 0.05
ADm5	9.42 ± 0.80	-2.9 ± 0.1	13.1	0.52 ± 0.05

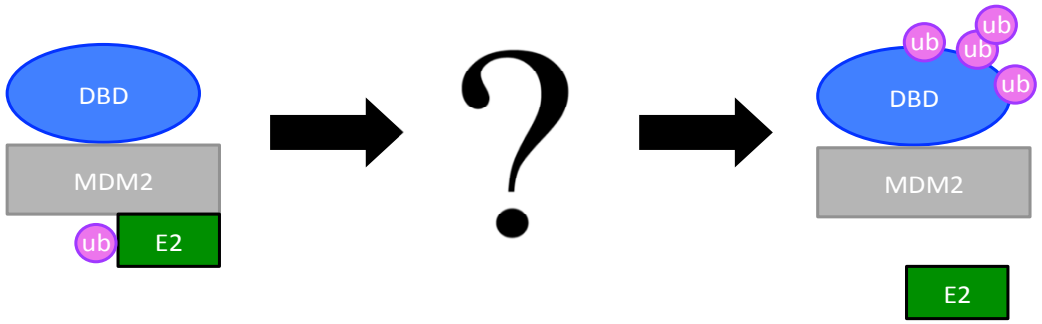

Figure 2.1: The underlying mechanism for p53 ubiquitination is unknown. p53 ubiquitination requires direct interaction between p53, MDM2 and ubiquitin-activated E2 ubiquitin-conjugating enzyme by which the ubiquitin moiety is conjugated onto several lysine residues across the p53 sequence.

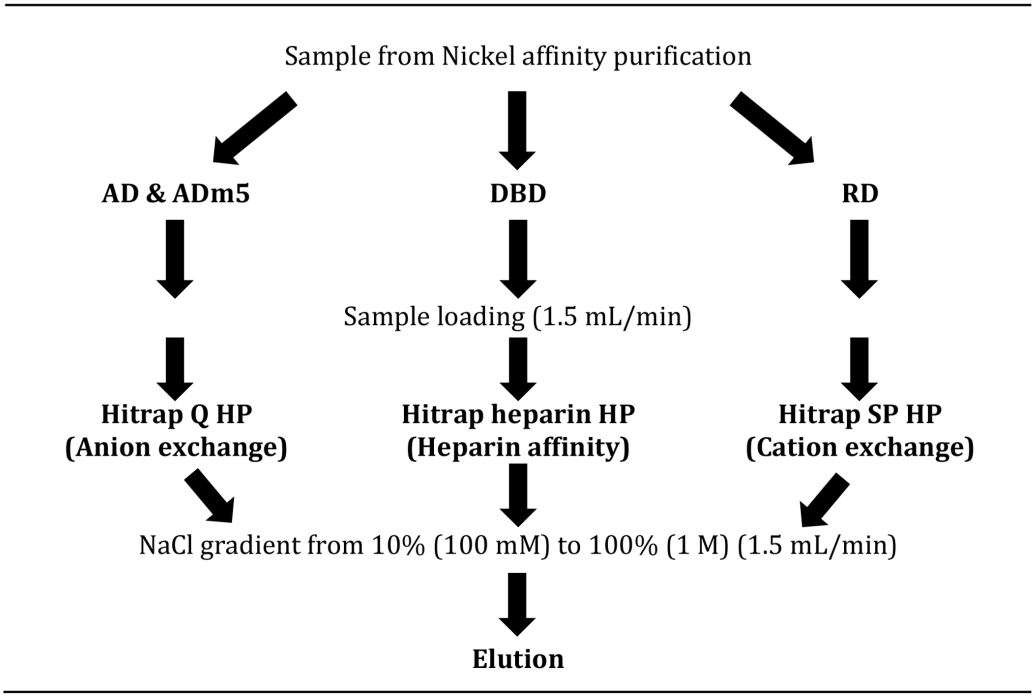

Figure 2.2: Schematic diagram showing the procedure for protein purification using FPLC.

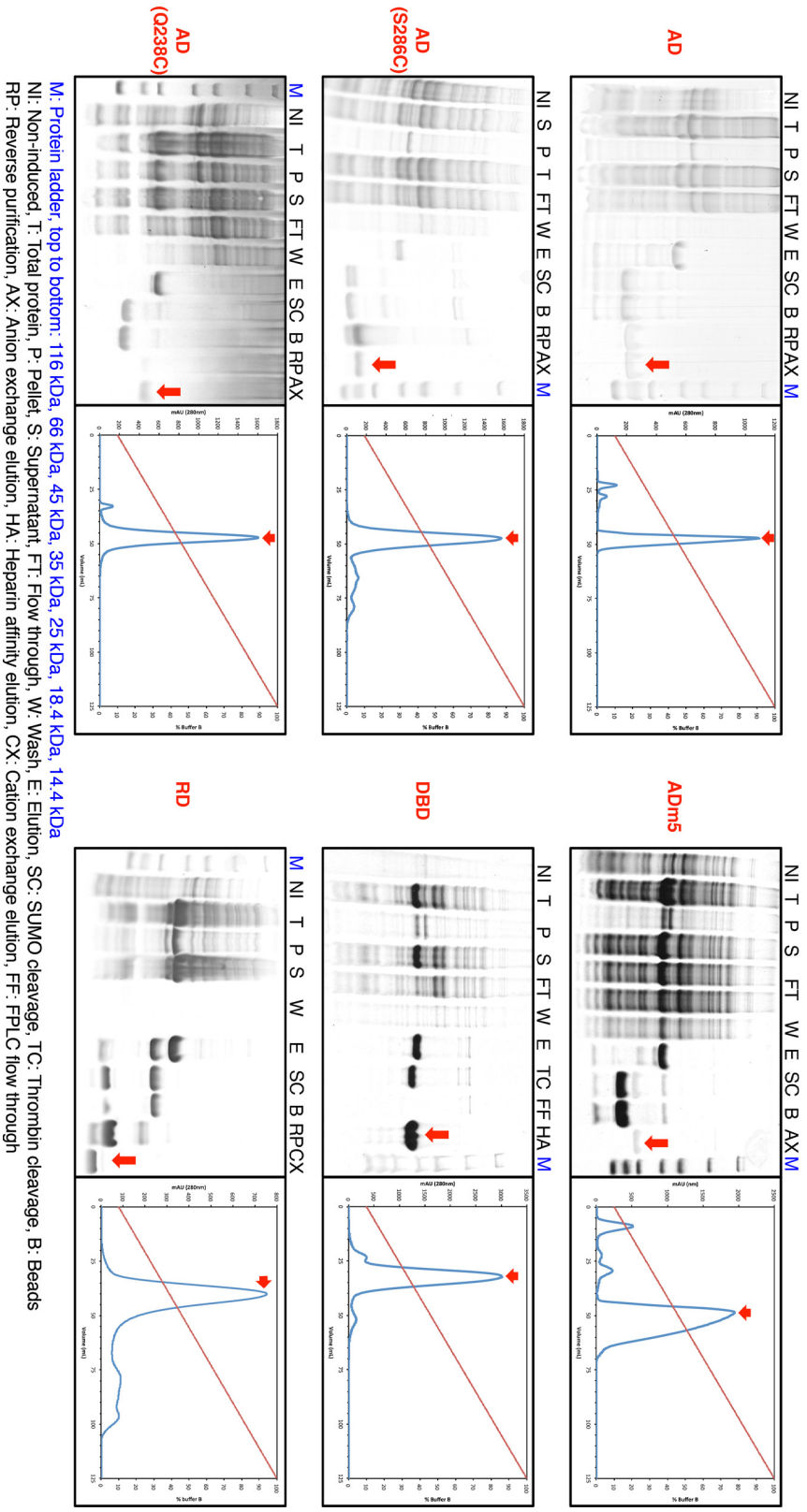

Figure 2.3: Expression and purification of recombinant proteins used in chapter 2. The gel pictures and chromatograms showed representative purification process of ^{15}N AD, ^{2}H-^{15}N DBD, natural abundant AD^{Q238C}, AD^{S286C}, ADm5 and RD.

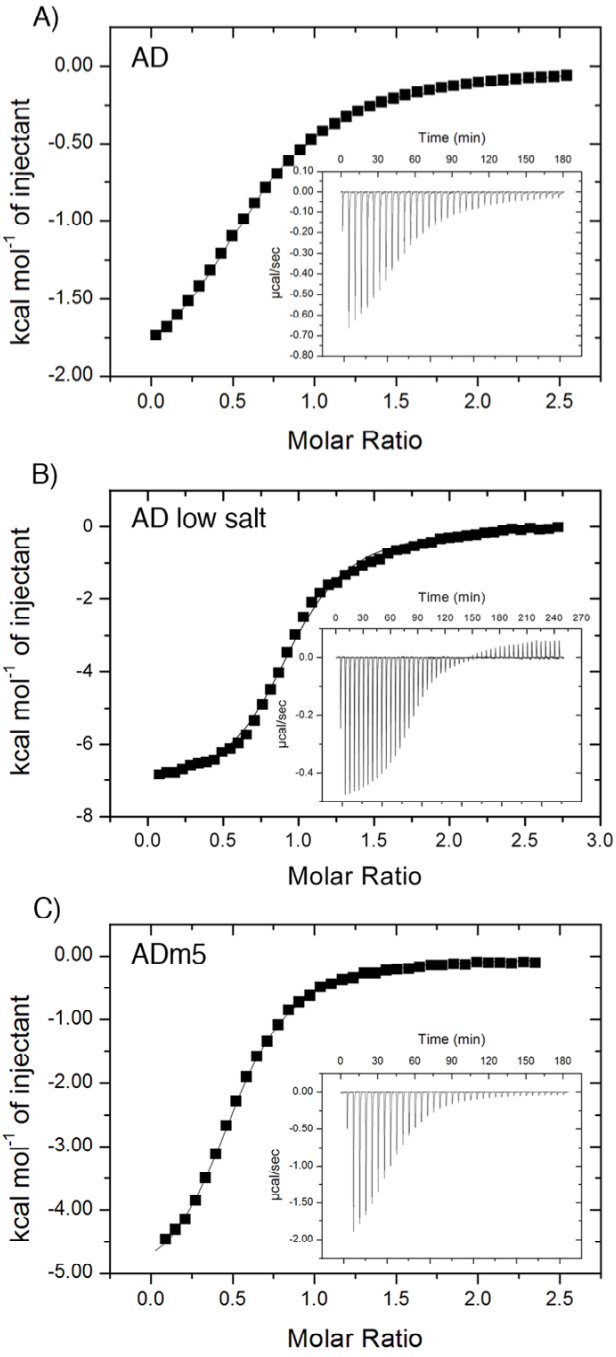

Figure 2.4: The MDM2 AD directly interacts with the p53 DBD. Isothermal titration calorimetry (ITC) analysis of: A) AD binding to the DBD, B) AD binding to the DBD in absence of NaCl, and C) ADm5 binding to the DBD. The integrated heat signals for each injection are plotted vs. molar ratio (squares), with fits to a one-site binding model shown (lines). Insets show the raw ITC data for the heat trace per injection vs time.

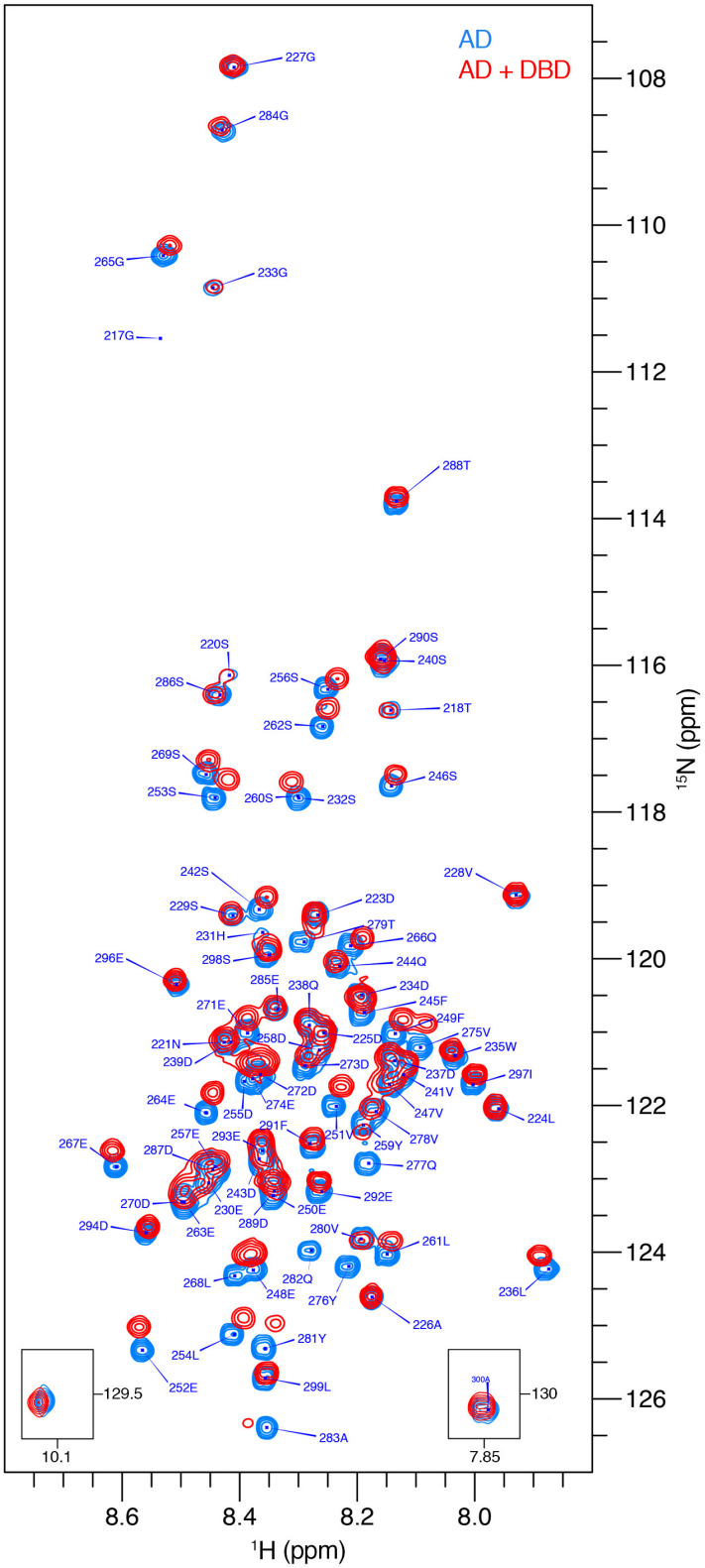

Figure 2.5: Comparison of the ^{1}H-^{15}N HSQC spectra of the AD in absence or presence of the DBD. The ^{1}H-^{15}N HSQC spectrum of the AD is annotated with resonance assignments.

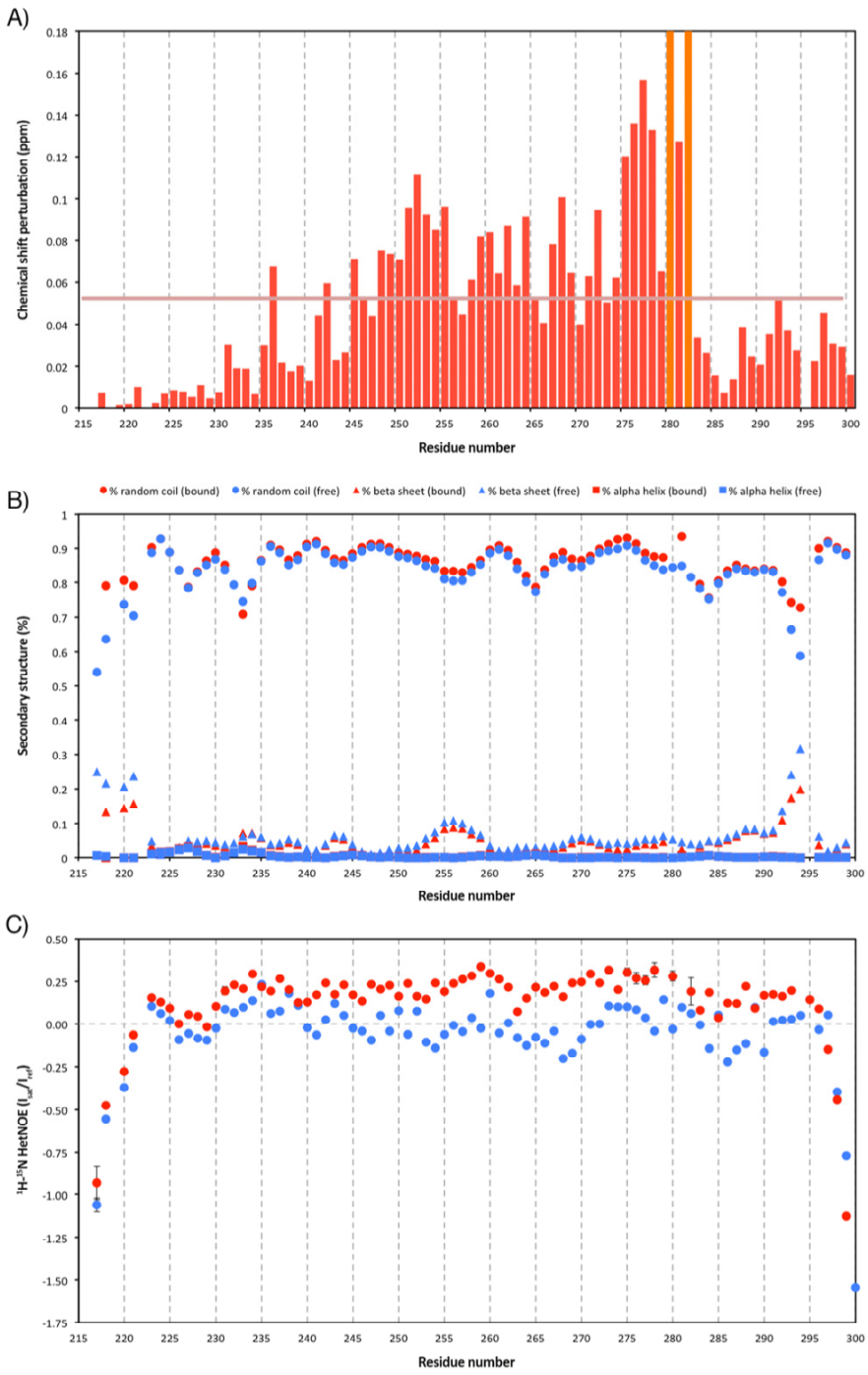

Figure 2.6: NMR analysis for the AD in absence (blue) or in presence of equimolar DBD (red). A) Chemical shift perturbation of the AD backbone amide chemical shifts as a function of residue number, threshold value is set to 2× standard deviation. The cross peaks for residues that were missing upon binding to the DBD are coloured in orange. B) The populations of secondary structure elements for the AD in the free and the DBD bound form (random coil: circle; β-sheet: triangle and α-helix: square) calculated using the δ2D method. C) {^{1}H}-^{15}N hetNOE values for each backbone amide of the AD in the free and the DBD-bound forms.

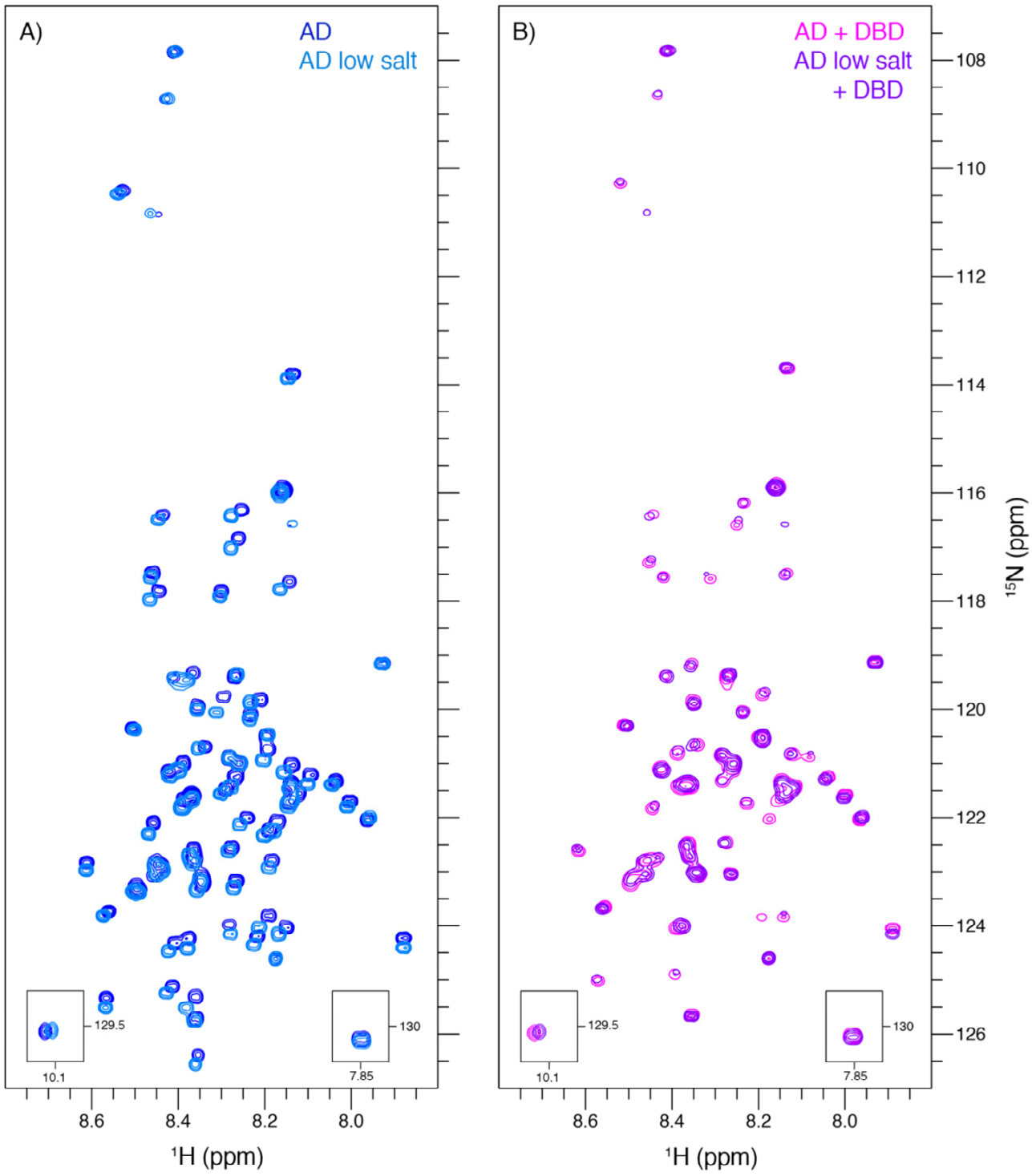

Figure 2.7: NMR analysis of the AD-DBD interaction under different salt concentrations. A) Comparison of ^{1}H-^{15}N HSQC spectra of the AD in the presence and absence of NaCl. B) Comparison of ^{1}H-^{15}N HSQC spectra of the AD in complex with the DBD in the presence and absence of NaCl.

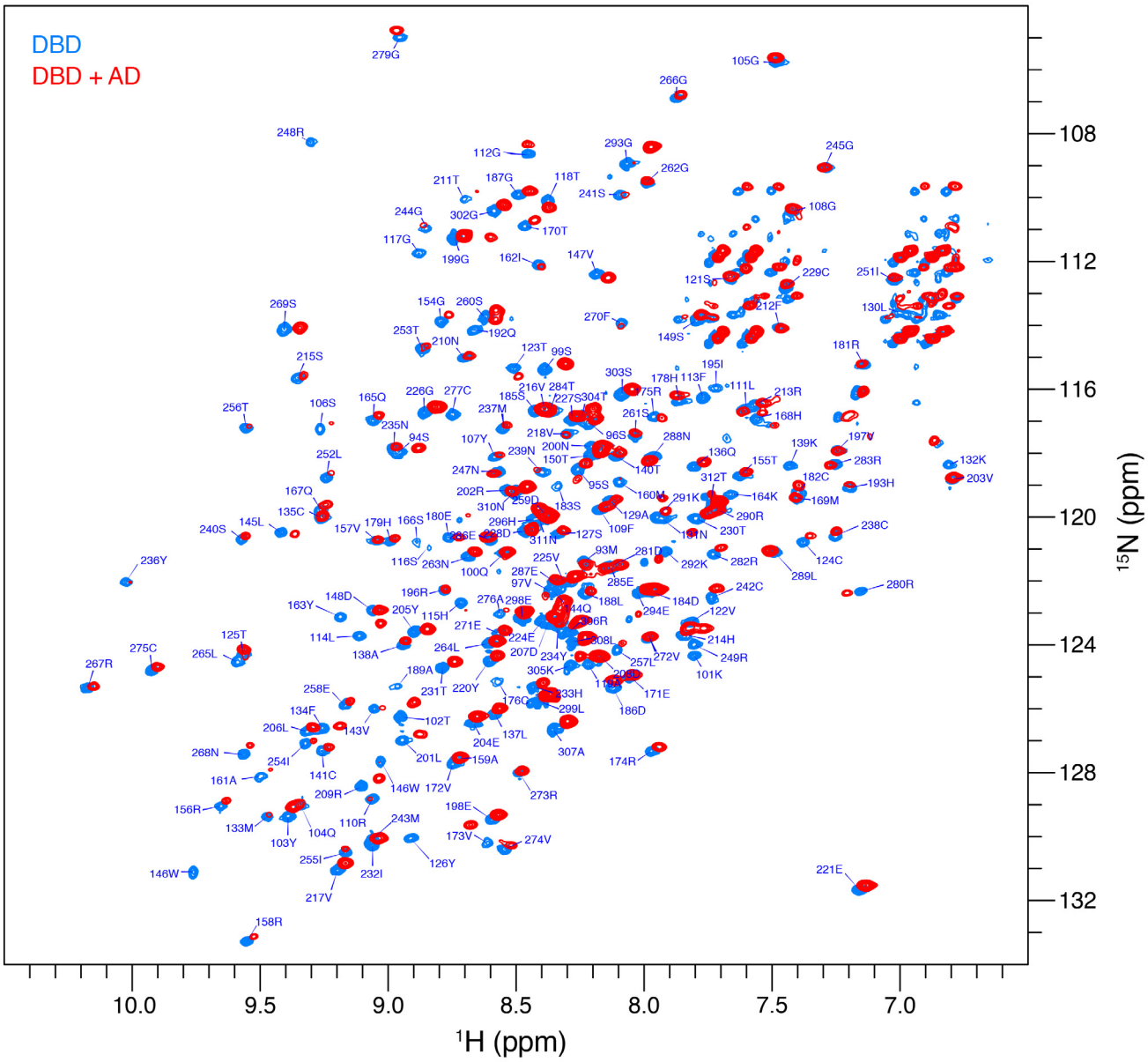

Figure 2.8: Comparison of ^{1}H-^{15}N TROSY spectra of the DBD in absence or presence of the AD.

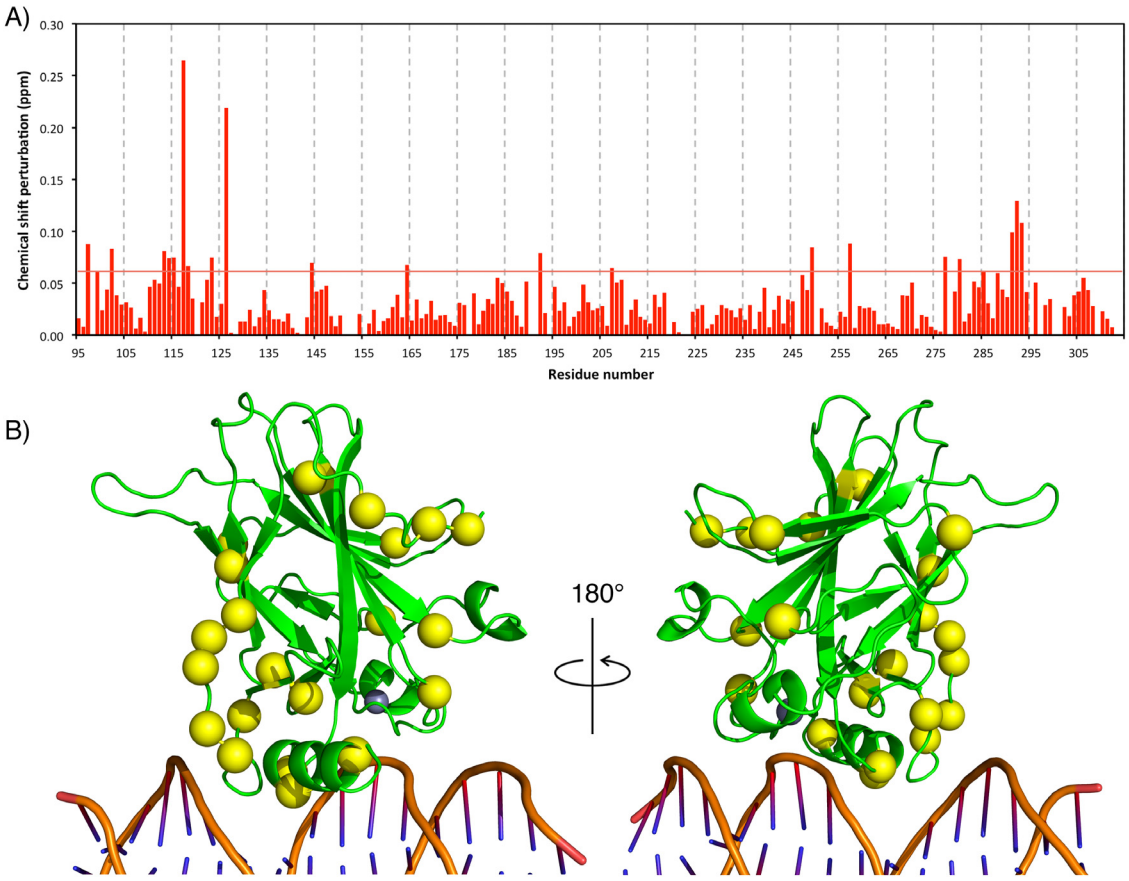

Figure 2.9: NMR chemical shift mapping reveals the binding site for the AD on the DBD. A) CSP values for the backbone amide resonances of the DBD in complex with the AD are plotted as a function of residue number. Threshold value is set to 2× standard deviation. B) The residues with perturbations larger than the threshold value are highlighted on the surface of the DBD structure as yellow spheres (Cho et al., 1994. PDB ID: 1TUP).

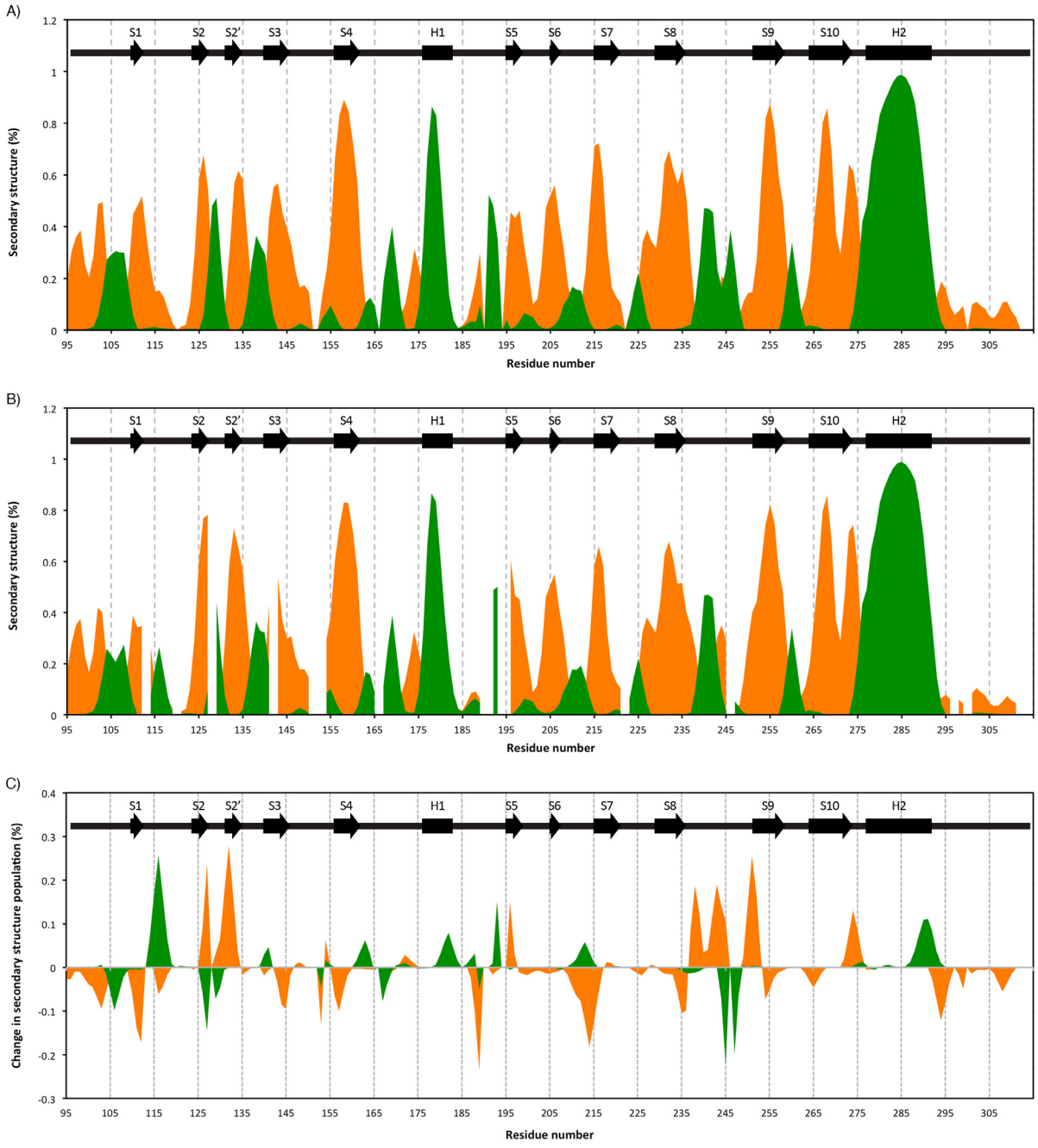

Figure 2.10: Secondary structure analysis of the DBD based on the NMR data. A) and B) The populations of secondary structure elements for the DBD in the free the AD bound form calculated with the δ2D method using the assigned backbone chemical shifts. α-Helical and β-sheet conformations are coloured green and orange, respectively. C) Population difference of secondary structure elements for the DBD when bound to the AD by subtracting A) from B). Topological diagrams showing the arrangement of secondary structure elements in the DBD (taken from Cho et al., 1994. PDB ID: 1TUP) are overlaid for reference at the top of each panel.

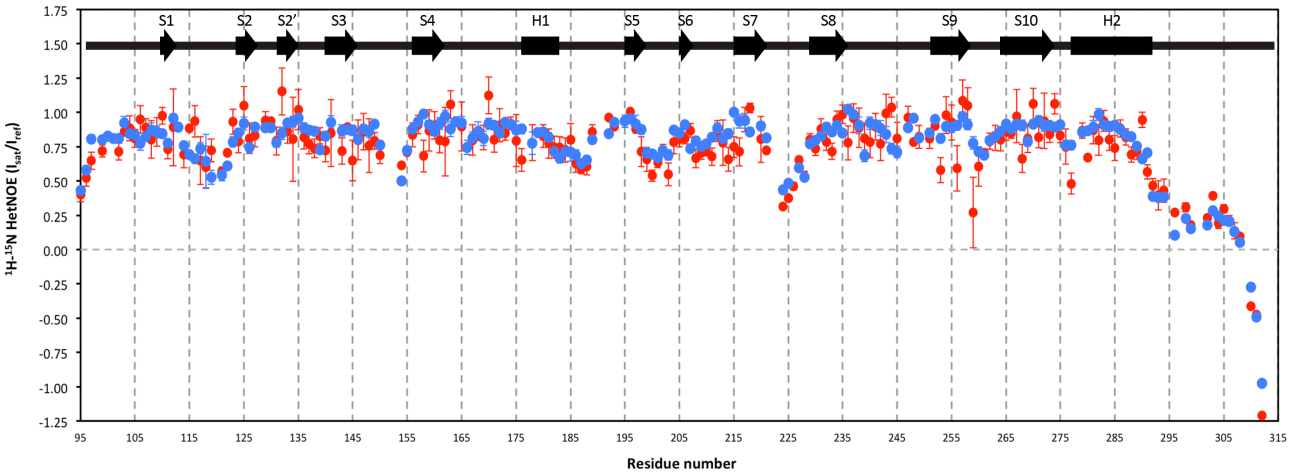

Figure 2.11: {^{1}H}-^{15}N hetNOE for the backbone amide of the DBD in absence (blue) and presence (red) of the AD. Topological diagrams showing the arrangement of secondary structure elements in the DBD (taken from Cho et al., 1994. PDB ID: 1TUP) is overlaid for reference at the top of the panel.

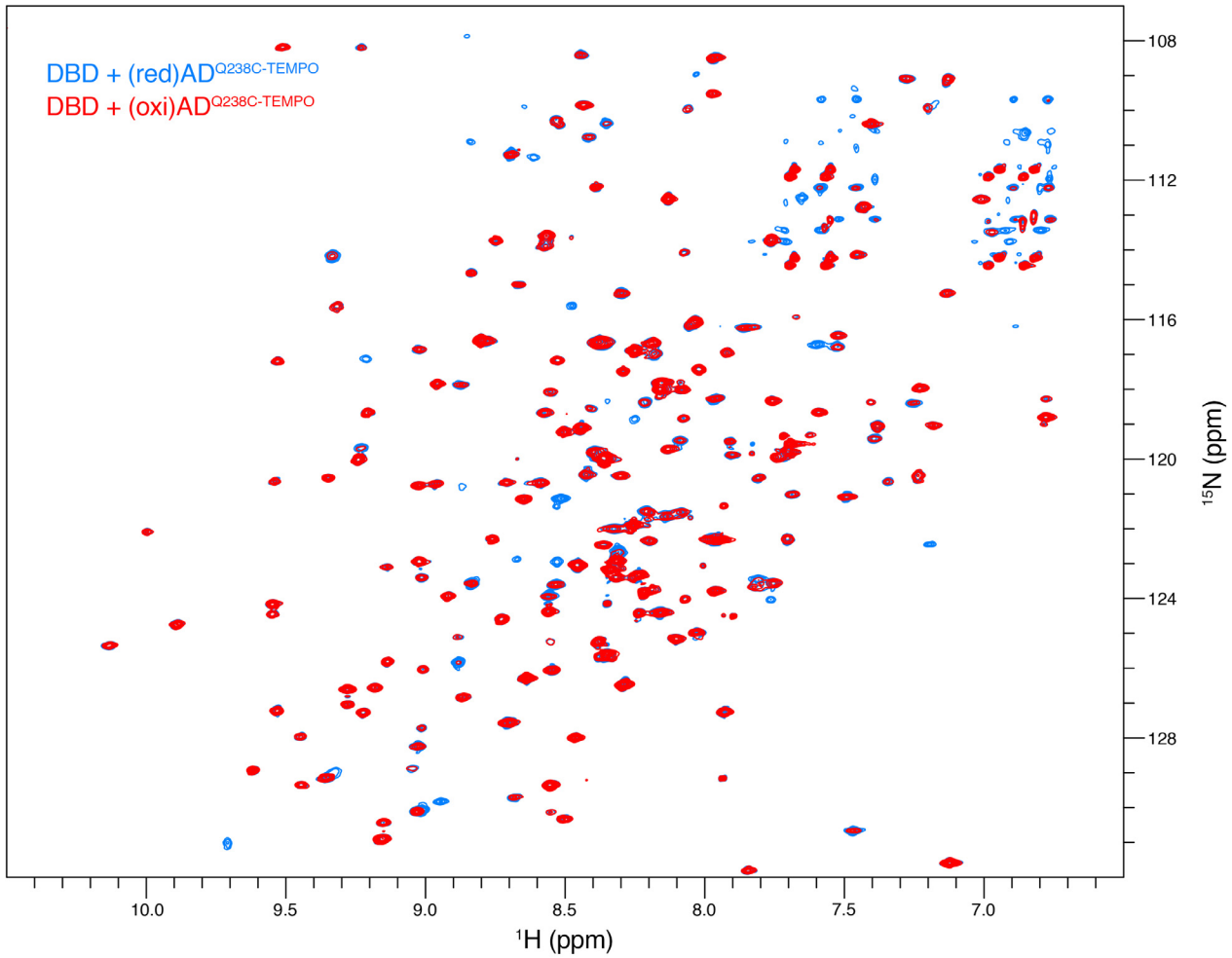

Figure 2.12: Comparison of ^{1}H-^{15}N TROSY spectra of the DBD in the presence of reduced or oxidized AD^{Q238C}-TEMPO.

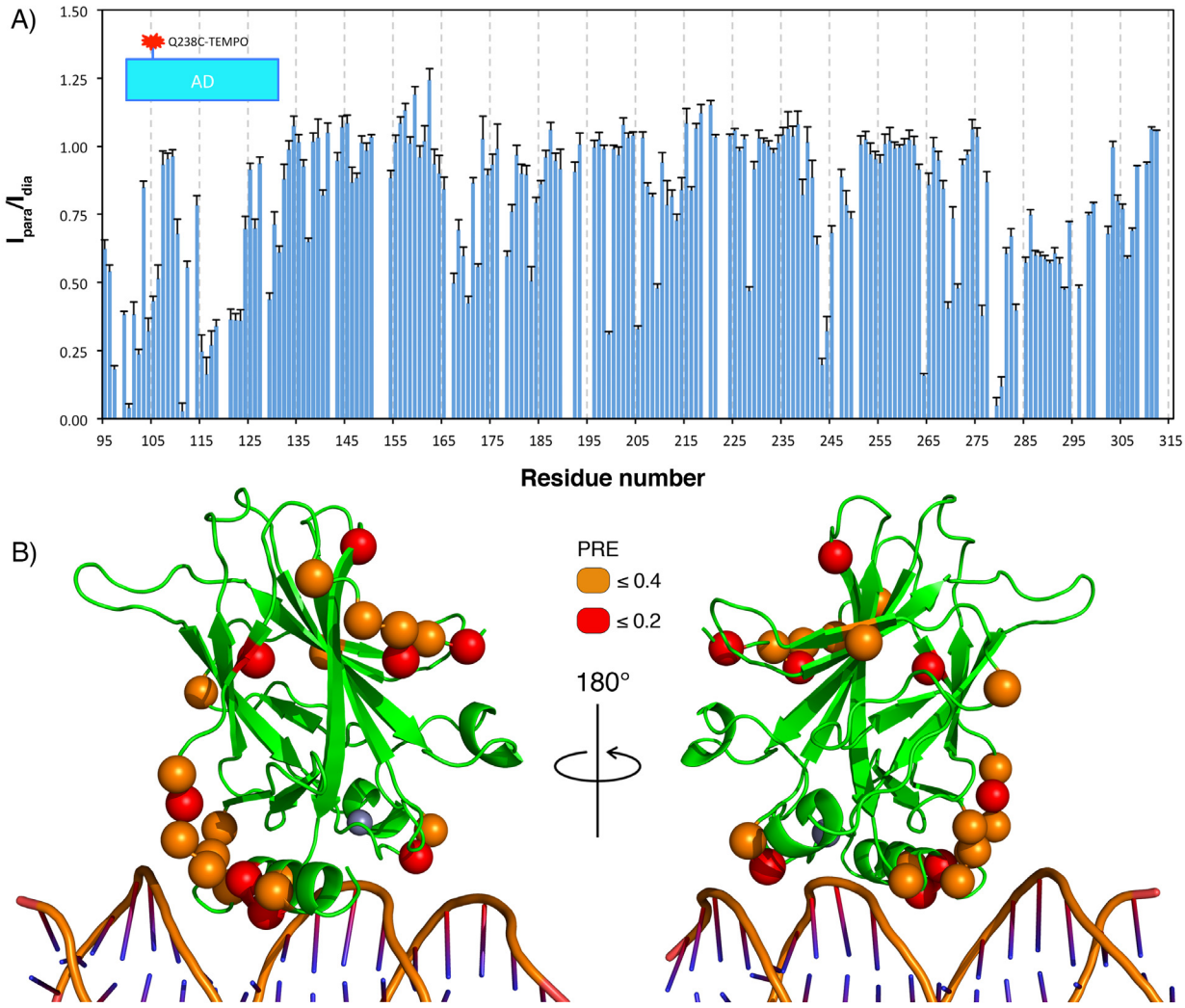

Figure 2.13: Analysis of PRE data of the DBD in complex with AD^{Q238C}-TEMPO. A) Intensity ratios for the backbone amide resonances of the DBD in complex with the AD^{Q238C}-TEMPO are plotted as a function of residue number. B) The residues that were significantly perturbed by the presence of a paramagnetic centre are mapped onto the structure of the p53 DBD (Cho et al., 1994. PDB ID: 1TUP).

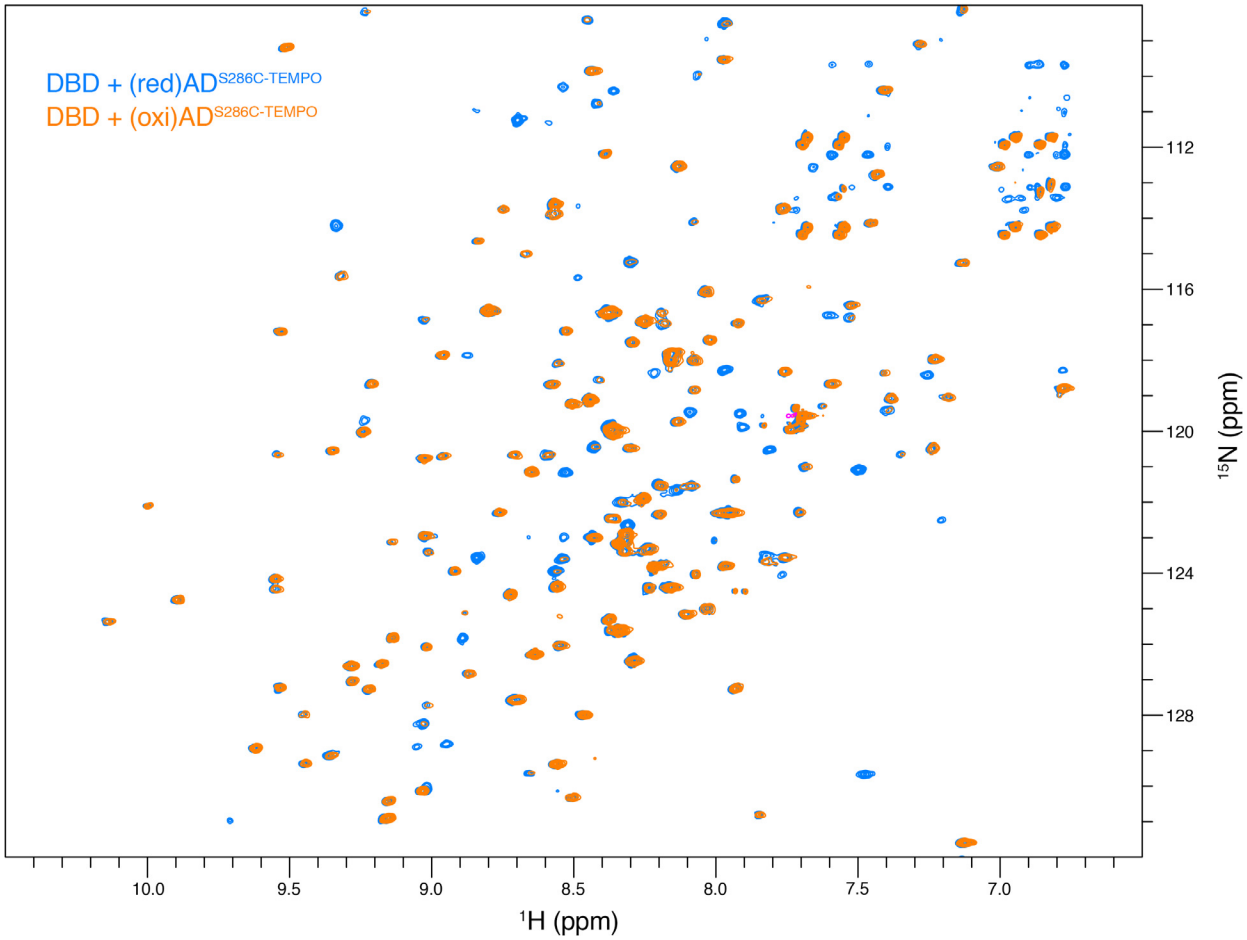

Figure 2.14: Comparison of ^{1}H-^{15}N TROSY spectra of the DBD in the presence of reduced or oxidized AD^{S286C}-TEMPO.

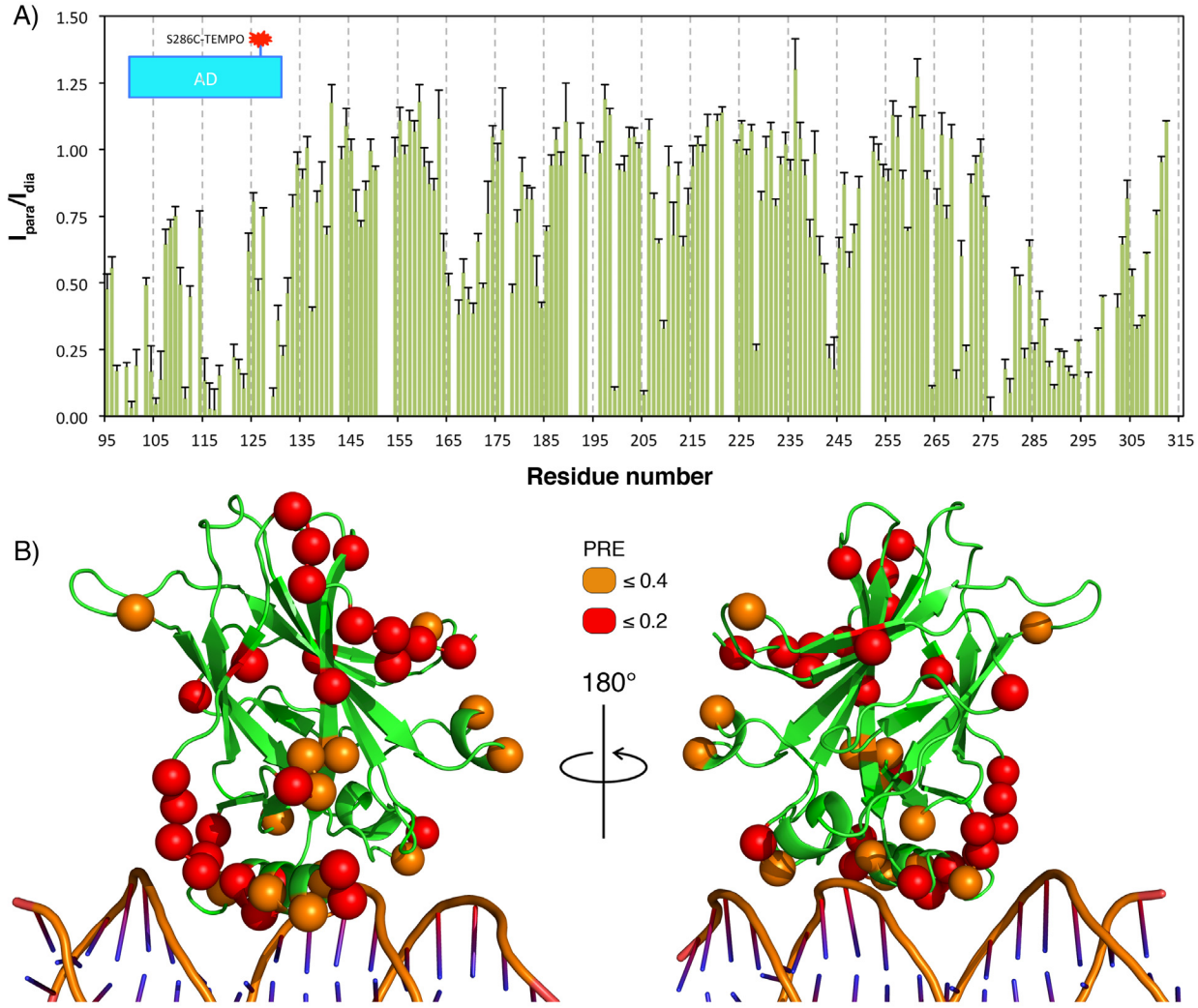

Figure 2.15: Analysis of PRE data of the DBD in complex with AD^{S286C}-TEMPO. A) Intensity ratios for the backbone amide resonances of the DBD in complex with the AD^{S286C}-TEMPO are plotted as a function of residue number. B) The residues that were significantly perturbed by the presence of a paramagnetic centre are mapped onto the structure of the p53 DBD (Cho et al., 1994. PDB ID: 1TUP).

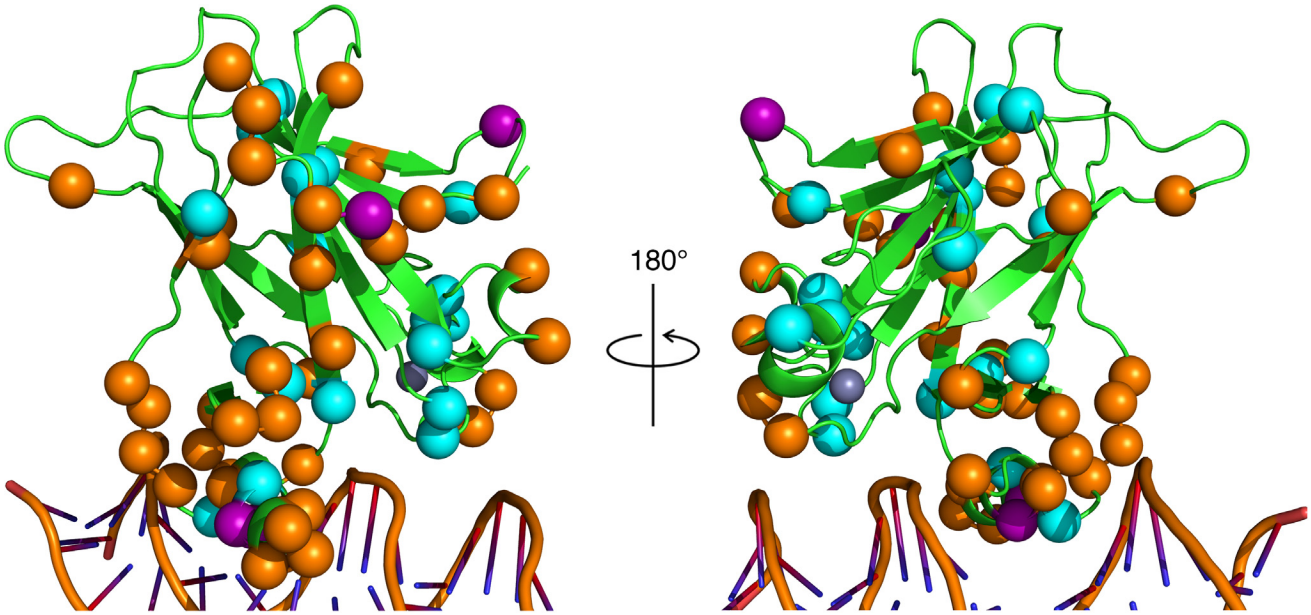

Figure 2.16: Observable PRE effect clusters around the lysine and arginine residues on the DBD. The residues that were significantly perturbed by PRE as well as the lysine and arginine residues were shown as spheres on the structure of the p53 DBD (Cho et al., 1994. PDB ID: 1TUP). Orange: residues affected by PRE; Cyan: lysine and arginine residues; Purple: lysine and arginine residues that were affected by PRE.

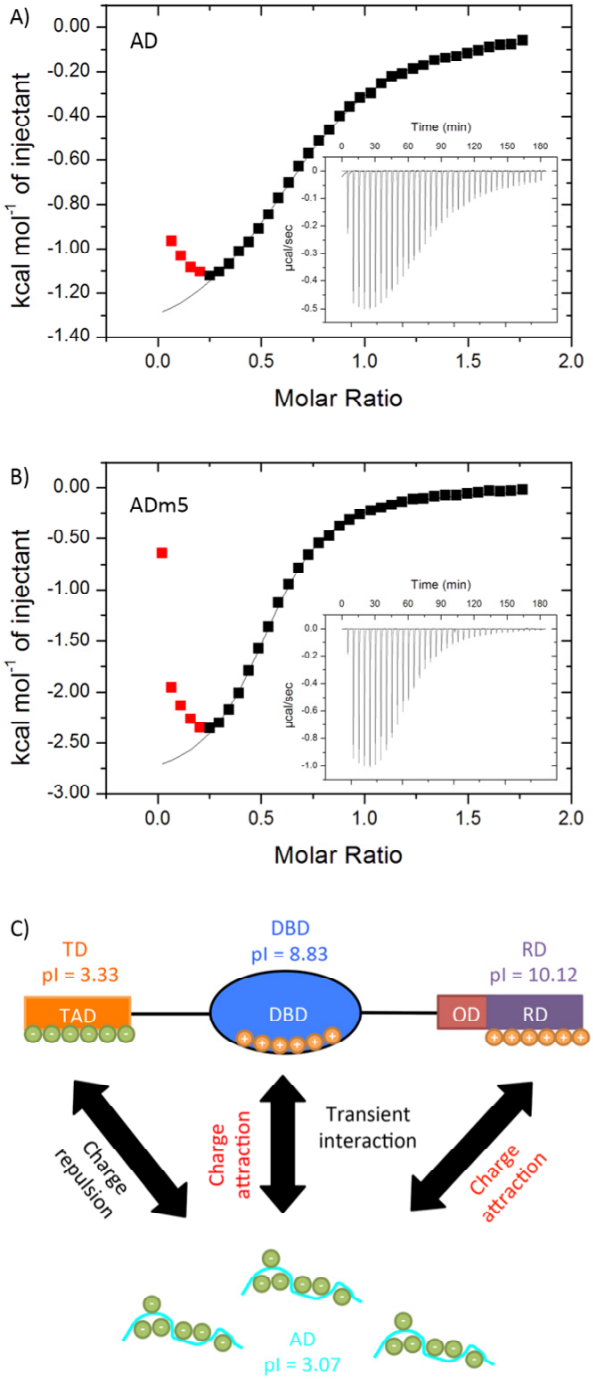

Figure 2.17: Interaction of the AD with the RD determined by ITC. ITC analysis of the AD (A) and ADm5 (B) binding to the RD. The data points coloured in red were omitted for analysis. The integrated heat signals for each injection are plotted vs. molar ratio (squares), with fits to a one-site binding model shown (lines). Insets show the raw ITC data for the heat trace per injection vs. time. C) Schematic diagram depicting the p53 protein domains and their respective isoelectric points. The role of electrostatic potential in the interaction with the AD is highlighted.

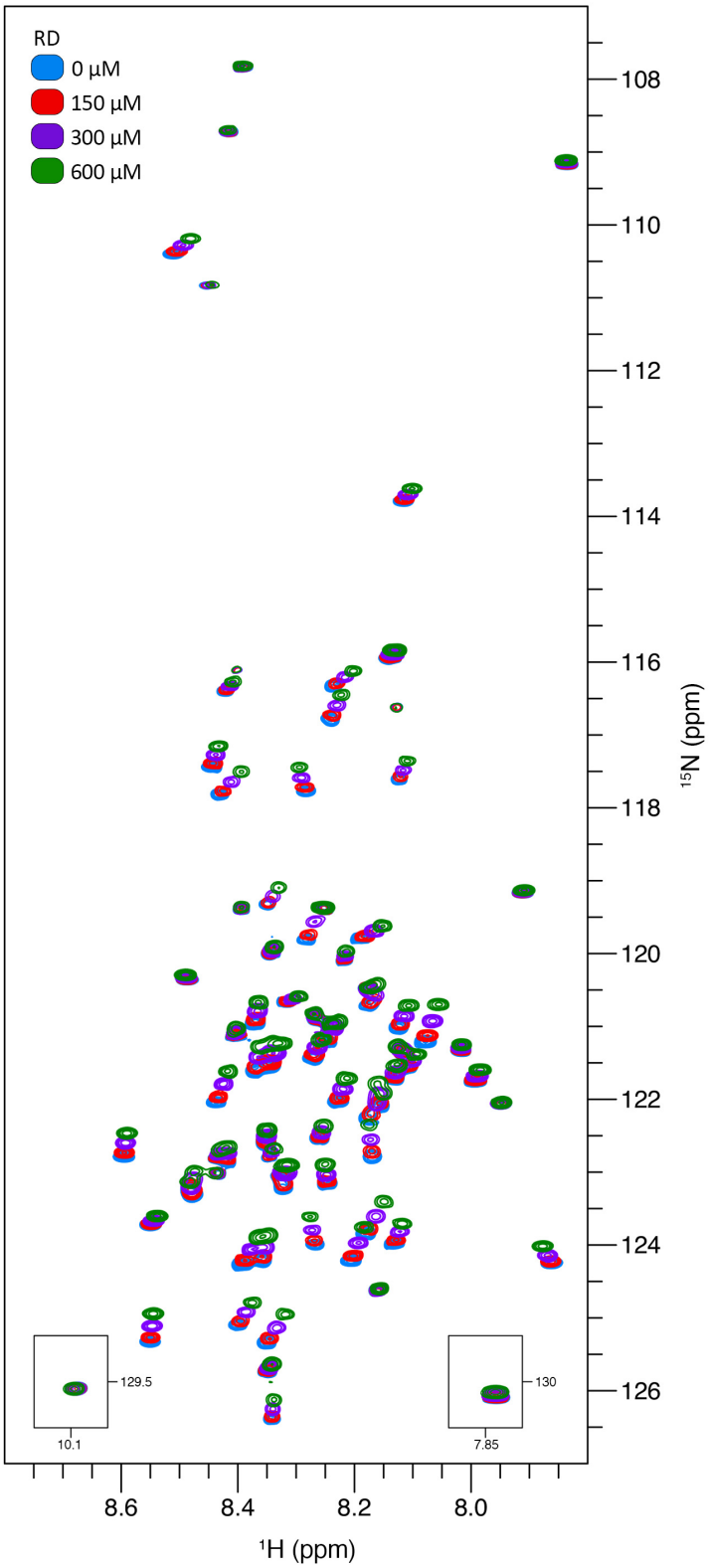

Figure 2.18: Overlaid ^{1}H-^{15}N HSQC spectra of the AD in the presence of increasing concentration of the RD.

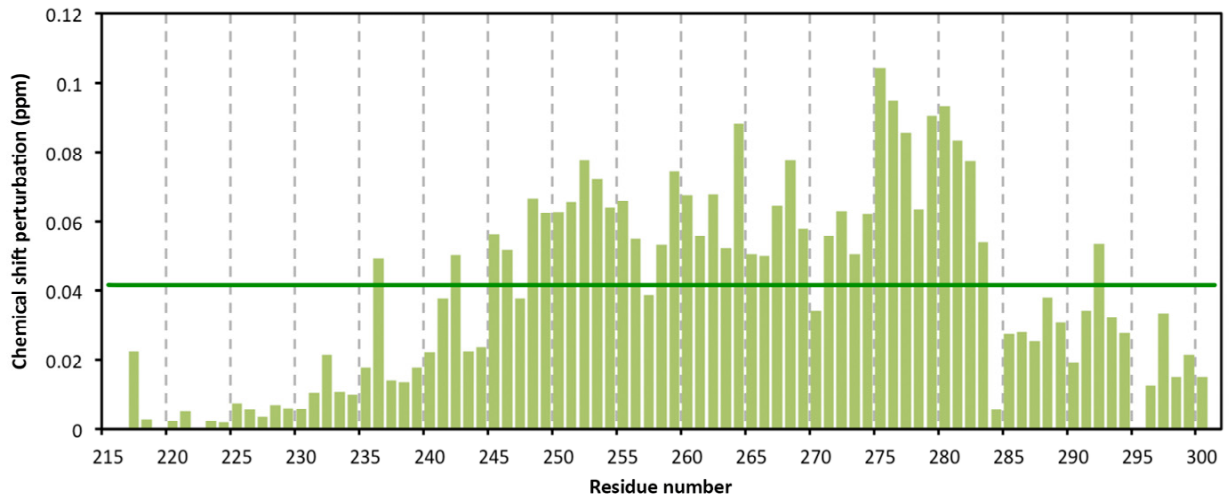

Figure 2.19: Interaction of the AD with the RD determined by CSP. CSP values for the backbone amide resonances of the DBD in complex with the AD are plotted as a function of residue number, threshold value is set to 2× standard deviation.

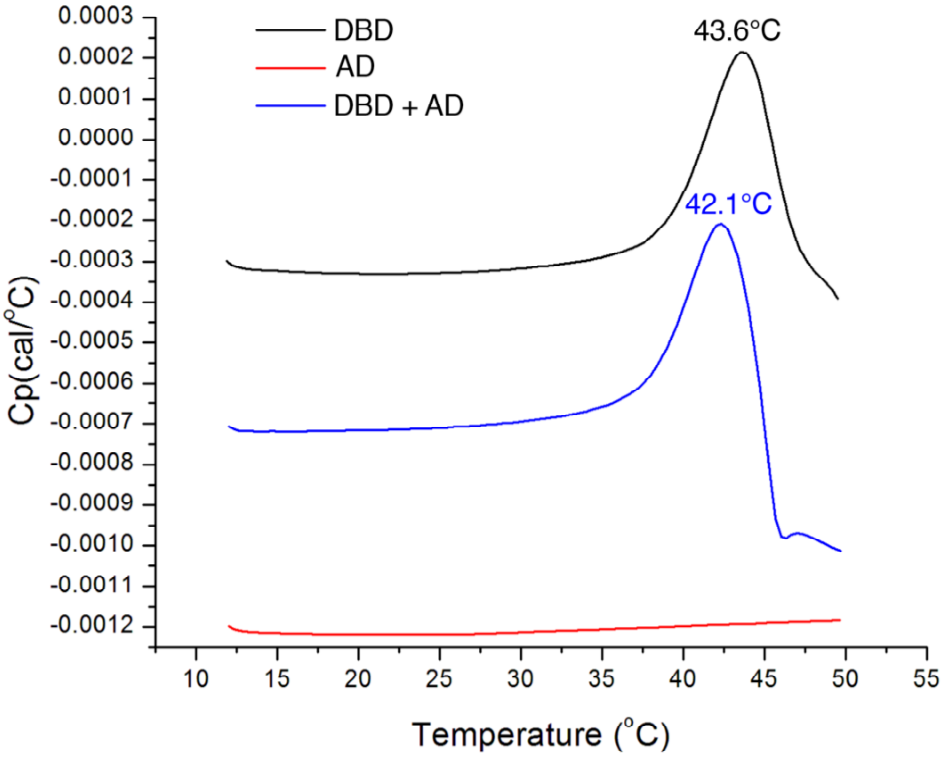

Figure 2.20: Measurement of DBD thermostability by DSC. Thermograms observed from the DSC experiments for the DBD in absence and presence of the AD. Data are shown without correction for the buffer baseline and are offset for clarity.

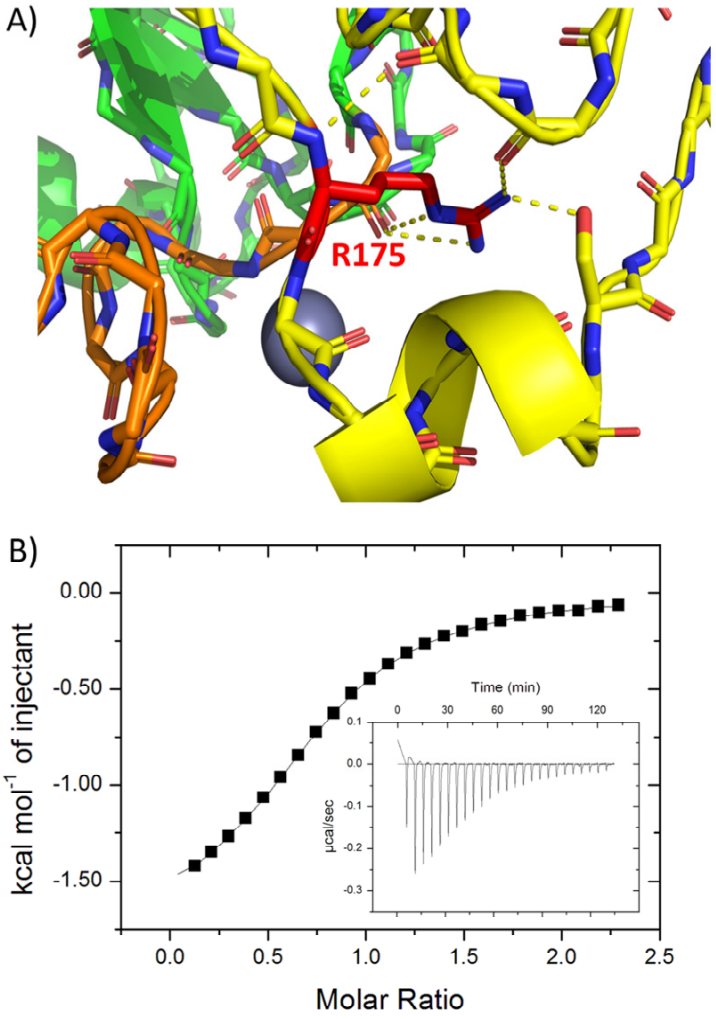

Figure 2.21: Interaction of the AD with the ^{Apo}DBD determined by ITC. A) Zoom in structure of the DBD highlighting the key contacts formed by the side chain of R175 (red) that near the zinc ion (grey sphere). L2 and L3 loops were coloured in yellow and orange, respectively. B) The integrated heat signals for each injection are plotted vs. molar ratio (squares), with fits to a one-site binding model shown (lines). Insets show the raw ITC data for the heat trace per injection vs. time.

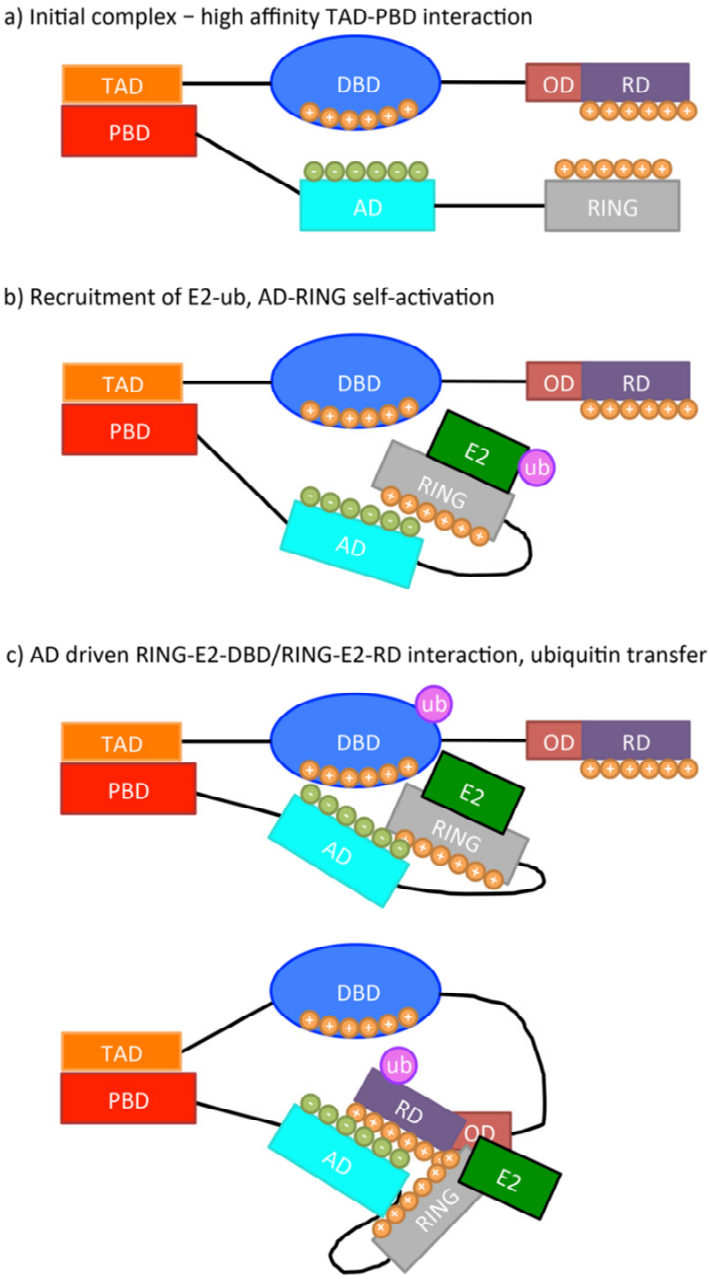

Figure 2.22: Proposed mechanism of ubiquitin transfer to p53. A) An initial complex is formed through the high affinity interaction between the p53 transactivation domain and the MDM2 p53-binding domain. B) Recruitment of ubiquitin activated E2 (E2-ub) to the RING domain. C) The AD activates RING-E2-ub complex and brings the complex to the p53 DNA binding domain or the regulatory domain to facilitate covalent attachment of the activated ubiquitin.

CHAPTER 3: THE TRANSACTIVATION DOMAIN (TD) OF P53 REGULATES THE INTERACTION BETWEEN ITS DNA-BINDING DOMAIN (DBD) AND THE ACIDIC DOMAIN (AD) OF MDM2

3.1 Introduction

The tumour suppressor protein p53 is crucial in mediating and regulating numerous cellular signalling pathways in response to stress and damage to promote cell cycle arrest, apoptosis and senescence (Bartke et al., 2001; Brown, Wei, & Sedivy, 1997; Chang et al., 1999; el-Deiry et al., 1993; Finlay, Hinds, & Levine, 1989; Harper, Adami, Wei, Keyomarsi, & Elledge, 1993; Marchenko, Zaika, & Moll, 2000; Mihara et al., 2003; Miyashita et al., 1994; Miyashita & Reed, 1995; Oda et al., 2000; Selvakumaran et al., 1994; Stambolic et al., 2001). The critical role of p53 in maintaining cellular homeostasis and genome integrity is evidenced by the fact that more than 50% of cancers harbour mutations in p53 (Harris, 1993; Petitjean et al., 2007). The structure of p53 is organized into five functional domains, including an N-terminal transactivation domain (TD), a proline-rich domain (PRD), a core DNA-binding domain (DBD), an oligomerization domain (OD), and a C-terminal regulatory domain (RD) (Figure 1.2). The DBD and the OD adopt well-folded structures whereas the TD and RD are intrinsically disordered regions and only fold into defined structures when bound to p53-binding partners (Krois, Ferreon, Martinez-Yamout, Dyson, & Wright, 2016; Kussie et al., 1996; Lee, Martinez-Yamout, Dyson, & Wright, 2010; Miller Jenkins et al., 2015; Rustandi, Baldisseri, & Weber, 2000). The TD contains two short motifs (TD1 and TD2) that serve as binding sites for numerous p53-binding proteins, such as MDM2, MDMX and CBP/p300 (Krois et al., 2016; Kussie et al., 1996; Lee et al., 2010; Popowicz, Czarna, & Holak, 2008). These interactions are crucial for the proper function of p53, which lead to transcription suppression, transcription activation, protein stabilization, or proteasomal degradation. Moreover,

the TD contains multiple serine and threonine residues that can be phosphorylated under different physiological conditions to fine-tune its activity and modulate downstream signalling (Armata, Garlick, & Sluss, 2007; Bulavin et al., 1999; Cai & Liu, 2008; Chao et al., 2003; Chao, Herr, Chun, & Xu, 2006; Chehab, Malikzay, Stavridi, & Halazonetis, 1999; Feng, Hollstein, & Xu, 2006; Jabbur, Huang, & Zhang, 2000; Loughery, Cox, Smith, & Meek, 2014; Pavithra et al., 2009; Saito et al., 2002; She, Chen, & Dong, 2000; Teufel, Bycroft, & Fersht, 2009; Zhao, Traganos, & Darzynkiewicz, 2008).

The E3 ubiquitin ligase MDM2 is a key negative regulator of p53, acting by promoting its ubiquitination and subsequent proteasomal degradation (Haupt, Maya, Kazaz, & Oren, 1997; Honda, Tanaka, & Yasuda, 1997; Kubbutat, Jones, & Vousden, 1997). MDM2 consists of four functional domains: an N-terminal p53-binding domain (PBD); an acidic, glutamate and aspartate rich domain (AD); a zinc-finger domain (ZF); and, a C-terminal Really Interesting New Gene (RING) domain (Figure 1.5). The PBD forms a hydrophobic cleft that allows the TD of p53 to bind with high affinity through the key residues F19, W23, and L26 from the TD1 motif to suppress its transcriptional activity (Kussie et al., 1996). The AD can bind to the DBD of p53 to prevent it from interacting with target DNA (Cross et al., 2011). Moreover, the AD is crucial for the E3 ubiquitin ligase activity of MDM2 (Cheng, Song, Chen, & Chen, 2014). The ZF domain serves as a binding site for the ribosomal proteins L5, L11, and L23, leading to p53 activation (Dai, M. S. & Lu, 2004; Dai, Mu-Shui et al., 2004; Jin, Itahana, O'Keefe, & Zhang, 2004; Lohrum, Ludwig, Kubbutat, Hanlon, & Vousden, 2003; Marechal, Elenbaas, Piette, Nicolas, & Levine, 1994; Zhang et al., 2003). The C-terminal RING domain possesses E3 ubiquitin ligase activity and is responsible for promoting p53 ubiquitination, with mono-ubiquitination promoting p53 nuclear export and with

poly-ubiquitination targeting p53 for proteasome degradation (Fang, Jensen, Ludwig, Vousden, & Weissman, 2000; Li et al., 2003).

In Chapter 2, I showed that the AD could directly bind to the surface of the DBD and it prefers to bind to the mutant-like over the wild-type structure of the DBD. As part of this study, I noticed that the AD binds the DBD with dramatically lower affinity in the presence of an intact TD. At the time this study was conducted, two studies showed that the intramolecular interaction between the TD and the DBD of p53 can modulate its association with specific and non-specific DNA sequences by binding to the DNA-binding surface of the DBD (He et al., 2019; Krois, Dyson, & Wright, 2018). The similar binding surface for both the p53 TD and MDM2 AD on the p53 DBD suggests that binding of these domains might be mutually exclusive. Thus, the TD could potentially serve as an intramolecular regulator of the interaction between the p53 DBD and the MDM2 AD.

The present chapter provides a detailed characterization of the interaction of the AD with the DBD in presence of the TD, allowing investigation of the potential role of the TD in modulating the AD-DBD interaction. I have detected a direct interaction between the TD and the DBD, where the TD binds the DNA binding surface of the DBD. Accordingly, the AD-DBD interaction is significantly weakened in the presence of an intact TD. I also demonstrate that the MDM2 PBD can weaken the interaction between the TD and the DBD and may, potentially, promote AD-DBD interaction. This work reveals that the TD inhibits the AD-DBD interaction and that the PBD may facilitate the AD-DBD interaction by binding to the TD.

3.2 Materials and Methods

3.2.1 Materials

The codon optimized gene for human MDM2 (residues 1 – 491) was obtained from GENEWIZ (South Plainfield, NJ) and the plasmid expressing the human p53 (residues 1-393) was a gift from Cheryl Arrowsmith (Addgene plasmid # 24859, http://n2t.net/addgene:24859; RRID: Addgene_24859). The oligonucleotide primers for cloning were obtained from Integrated DNA Technologies, Inc (Coralville, IA). All other materials used in this work have been listed in Chapter 2. All buffers were shown in Table A3 in the Appendix.

3.2.2 Cloning and plasmid construction

The plasmids for expression of the PBD and the TD with H_6-SUMO fusion tag were made by subcloning the gene into the pETHS vector using restriction enzymes SapI and BamHI. Deletion constructs of p53 were made by site directed mutagenesis to remove the DNA sequence in a desired manner using the Phusion High-Fidelity DNA polymerase (NEB; Whitby, ON) followed by subcloning into the pETHT vector using the restriction enzymes NdeI and BamHI. The pETHT vector was generated using restriction enzymes NdeI and BamHI from pE53D by removing the DBD gene sequence. Sanger sequencing was used to confirm the DNA sequence identity (Genewiz; South Plainfield, NJ). Forward and reverse primers used for DNA amplification are listed in Table A1 in the Appendix. Standard PCR thermocycling conditions were shown in Table A2 in the Appendix. Plasmid constructs for *E. coli* protein expression were listed in Table A3 in the Appendix. All plasmids were stored at – 20 °C.

3.2.3 Protein expression in E. coli

Protein expression was carried out using *E. coli* BL21 (DE3) strain. The protocol for expressing p53 constructs that contain the DBD (TPD; residues 1 – 312; containing the TD, the PRD and the DBD, T2PD; residues 32 – 312; containing the TD2 motif, the PRD and the DBD, PD; residues 61 – 312; containing the PRD and the DBD, and DBD, residues 94 – 312) was the same as for the DBD as described in section 2.2.3. Expression of the isotope-labelled and unlabelled AD, PBD (residues 1 – 125) and TP (residues 1 – 93; containing the TD and the PRD) was performed using the same protocol for expressing the AD as described in section 2.2.3. For expression of Co^{2+} bound DBD, cells were supplemented with 0.2 mM $CoSO_4$ instead of $ZnSO_4$ prior to induction with 0.5 mM IPTG. Note that ^{15}N labelled DBD (no ^{2}H labelling) is used in Chapter 3.

3.2.4 Nickel affinity chromatography

The protocol used for Ni-NTA purification is the same as described in section 2.2.4, from which the p53 constructs containing the DBD and the PBD construct were purified using the same conditions as for purification of the DBD. The TP was purified using the conditions applied for the AD. The AD, PBD and TP were further reverse-purified on Ni-NTA column whereas the TPD, T2PD, PD and DBD were directly used for FPLC purification.

3.2.5 Fast performance liquid chromatography (FPLC)

The AD and p53 constructs used in this work were purified similarly as described for purification of the AD and the DBD in section 2.2.3. Purification of the TP was performed using

the protocol for the AD, as described in section 2.2.3. The PBD was purified by passing the flow through from the Ni-NTA reverse purification through a pre-packed Hitrap Q sepharose column pre-equilibrated with cleavage buffer, using a peristaltic pump P-1 (Pharmacia Fine Chemicals, Sweden) connected to a 0.45 μm syringe filter at a constant flow rate of 1.5 mL/min. The flow through containing the purified protein was collected and concentrated.

Sample concentrations were determined according to the Beer-Lambert law using the protocol described in section 2.2.5. The concentration for the AD and the PBD was determined by using the molar extinction coefficient at 214 nm (ε AD = 156621 $M^{-1}\cdot cm^{-1}$ and ε PBD = 202624 $M^{-1}\cdot cm^{-1}$), the concentration for all other constructs was determined by using the molar extinction coefficient at 280 nm (ε TPD= 33920 $M^{-1}\cdot cm^{-1}$, ε T2PD = 28420 $M^{-1}\cdot cm^{-1}$ ε PD = 22920 $M^{-1}\cdot cm^{-1}$, ε DBD = 17420 $M^{-1}\cdot cm^{-1}$ and ε TP = 16500 $M^{-1}\cdot cm^{-1}$). All protein samples were flash frozen in liquid N_2 and stored in – 80 °C freezer before use.

3.2.6 SDS-PAGE

SDS-PAGE gels were run and visualized using the same conditions and protocols as in section 2.2.6.

3.2.7 Isothermal titration calorimetry

The ITC experiments were carried out using a VP-ITC instrument (Malvern Panalytical Ltd , Malvern, UK). Sample preparation protocol for ITC experiments was as described in section 2.2.7. For experiments measuring the affinity of the TPD, T2PD, PD or the DBD with the AD, a concentration of 0.200 mM was used in the sample cell. Following thermal equilibration at 20 °C

and an initial 5 min delay, 30 serial injections of 10 μL of the AD (2 mM) was titrated into the cell from the syringe under a constant stirring speed of 300 rpm with a 5 min spacing between each injection. All experiments were performed in duplicate and control experiments measuring the heat of dilution were used to correct for the background heat effects. Data analysis was performed using the ORIGIN software package (Origin 7 SR4 v7.0552; Malvern Panalytical Ltd, Malvern, UK) and corrected curve was fitted to a one-site binding model according to the equation:

$$q_i = v \times \Delta H \times [P] \times \left(\frac{K_a[L]_i}{1 + K_a[L]_i} - \frac{K_a[L]_{i-1}}{1 + K_a[L]_{i-1}} \right)$$

as detailed in Leavitt & Freire, (2001).

3.2.8 NMR spectroscopy

All samples were prepared in NMR buffer following the sample preparation protocols in section 2.2.99. ^{1}H-^{15}N HSQC experiments were carried out using an 500 MHz Bruker Avance spectrometer equipped with a BBFO SmartProbe. Experiments using 150 μM isotope-labeled AD were acquired in the presence or absence of 150 μM of each unlabeled p53 construct (TPD, T2PD, PD or DBD). Isotope-labeled TP (150 μM) was used for ^{1}H-^{15}N HSQC experiments in the presence or absence of equimolar DBD. All subsequent NMR experiments were performed on an 700 MHz Bruker Avance III spectrometer equipped with a TCI cryoprobe. Triple resonance experiments (HNCACB, CBCA(CO)NH, HNCO and HN(CA)CO) for isotope-labeled TP (800 μM) were performed and used for chemical shift assignment. Two ^{1}H-^{15}N HSQC spectra were collected for the PRE experiment: 150 μM isotope-labeled TP in presence of 225 μM DBD^{Zn} (diamagnetic) or DBD^{Co} (paramagnetic). ^{1}H-^{15}N HSQC spectra were also collected for 200 μM isotope labeled DBD in the absence or presence of 1.1 molar excess of TP. Finally, a ^{1}H-^{15}N HSQC spectrum was collected for 200 μM isotope-labeled DBD in the presence of 1.1 molar excess TP and 1.5 molar

excess PBD. Full NMR experimental parameters, including triple resonance experiments that were acquired using non-uniform sampling of indirectly observed dimensions, are listed in Table A4 in the Appendix. All spectral analysis was carried out as described in section 2.2.9.

3.3 Results

3.3.1 Protein production and purification

Protein overexpression were carried out using *E. coli* expression system. The AD, the PBD and the TP constructs contain an N-terminal H_6-SUMO fusion tag. Each of these overexpressed SUMO-fusion proteins remained highly soluble after cell lysis and exhibited high metal-binding affinity for Ni-NTA purification (Figure 3.1). Protein samples of the AD and the TP at a high purity were obtained using denaturing buffer containing 6 M urea as wash buffer. Of note, the fusion tag was efficiently cleaved by SUMO protease following 6 M urea treatment (Figure 3.1: AD & TP, lane SC). For the AD and the TP constructs, reverse purification using nickel-affinity chromatography followed by anion-exchange chromatography purification yielded proteins at 90 ~ 95% purity (Figure 3.1: AD & TP, lane AX). For the PBD construct, reverse purification using nickel-affinity chromatography is similarly followed by anion-exchange chromatography. However, flow through was collected instead of the elution, which typically yield protein at ≥ 90 % purity (Figure 3.1: PBD, lane FF). The p53 constructs (TPD, T2PD, PD and DBD) contained an N-terminal H_6 tag followed by a thrombin cleavage site (TCS) to facilitate purification and straightforward removal of the H_6 tag by proteolysis with the protease thrombin. The overexpressed protein was partially soluble after cell lysis and the protein in the soluble fraction exhibited high binding-affinity for Ni-NTA purification (Figure 3.1). Following nickel-affinity purification, typical yields were of samples at ⩾ 60% purity (Figure 3.1: TPD, T2PD, PD & DBD, lane E).

Following thrombin cleavage, most *E. coli* protein contaminants were removed by further purification using heparin-affinity chromatography to yield protein at ≥ 95% purity (Figure 3.1: TPD, T2PD, PD & DBD, lane HA). Of note, the thrombin-cleaved DBD contains a four amino acid spacer (G-S-H-M) at the N-terminus for all protein constructs.

3.3.2 Chemical shift assignment and validation

Triple-resonance NMR experiments (listed in Table A5 in the Appendix) were performed to allow chemical shift assignment of the TP (Table 3.1 & Table A10 in the Appendix). To validate my chemical shift assignments, the assigned chemical shifts were analysed using the PANAV. Based on the assessment by PANAV, my chemical shift assignment data are of high quality. Summary of the PANAV assessment report is presented in Table 3.2.

3.3.3 The TD2 motif of p53 inhibits the interaction between its DBD and the MDM2 AD.

To investigate the effect of the TD on the interaction between the DBD and the AD, I produced p53 constructs containing residues 1 – 312 (TPD; including the TD1 and the TD2 motifs of the TD, the PRD and the DBD), residues 32 – 312 (T2PD; including the TD2 motif, the PRD and the DBD), residues 61 – 312 (PD; including the PRD and the DBD) and residues 94 – 312 (DBD) (Figure 3.2, A). ITC experiments were performed to measure the affinity of the AD towards each of the p53 constructs (Figure 3.2, C – F). The affinity for the DBD and the PD to the AD are similar ($K_d \approx 24$ μM and 35 μM, respectively), suggesting that the PRD itself does not significantly affect the interaction between the DBD and the AD. I noted that the heat signature for the first few injections were endothermic for the PD as compared to the DBD, which were purely exothermic. It is likely that additional events are happening during the course of the AD-PD interaction.

However, there is no known interaction between the PRD and the DBD. Instead, it has been shown that the indole group of W93 can form a cation-π interaction with the guanidinium group of R174 (Figure 3.2, B), which in turn stabilizes the structure of the DBD (Nathan et al., 2011). In this NMR spectroscopy-based study, this cation-π interaction was shown to be dynamic, with a subpopulation of W93 existing in the unbound form. Thus, the observed endothermic heat signature could be attributed to a broken cation-π interaction between W93 and R174. The affinity of the AD towards the TPD, on the other hand, is much weaker than either the PD or DBD, and is on par with the affinity toward T2PD ($K_d \approx 111$ μM and 105 μM, respectively), suggesting that the TD2 motif rather than the TD1 motif contributed to the inhibition of the interaction between the AD and the DBD.

To further support the hypothesis that the TD serves as an intramolecular inhibitor of AD binding to the p53 DBD, I carried out NMR experiments with isotope-labeled AD in the presence and absence of equimolar amounts of each of TPD, T2PD, PD or DBD. The ^{1}H-^{15}N HSQC spectra for the AD in presence of the DBD or the PD were similar (Figure 3.3) agreeing well with the implication from ITC that the PRD did not dramatically affect the interaction between the AD and the DBD. The ^{1}H-^{15}N HSQC spectra for the AD in presence of TPD or T2PD, conversely, are significantly different from the spectra for the AD in presence of PD or DBD, with the cross-peaks shifting back towards their original positions (Figure 3.3). Close inspection of the spectra showed that the ^{1}H-^{15}N HSQC spectra for the AD in presence of TPD or T2PD are similar, despite the fact that the T2PD construct lacks the TD1 motif (Figure 3.4). This result shows that the TD2 motif, but not the TD1 motif, is the key determinant in exerting the inhibitory effect on the AD. Thus, our NMR results are in good agreement with the ITC data that – of all N-terminal regions of p53 – it is the TD2 motif that is responsible for inhibiting the interaction between the DBD and the AD.

Our results also suggest that the TD2 motif binds weakly to the DBD than the AD since the TD was unable to completely abolish the interaction between the AD and the DBD, despite that the fact that these two domains of p53 interact intramolecularly. In summary, these results show that the TD2 motif of p53 is capable of directly inhibiting the interaction between the AD and the DBD.

3.3.3 The TD2 motif binds weakly to the DBD.

I have identified a 30 amino acid sequence of the TD2 motif that can inhibit the AD-DBD interaction. Previous study suggested the possibility of a direct interaction between the TD and DBD (He et al., 2019; Krois, Dyson, & Wright, 2018). To identify the region that is important for interaction with the DBD, I used a TP construct containing the TD (residues 1 – 60) and the PRD (residues 60 – 93) and performed chemical shift assignment to identify and assign the chemical shifts of ^{1}H, ^{15}N, $^{13}C_{\alpha}$, $^{13}C_{\beta}$ and $^{13}C'$ nuclei for each residue. Of note, the TD contains two short motifs: the TD1 motif (residues 1 – 30) and the TD2 motif (residues 31 – 60). Two ^{1}H-^{15}N HSQC spectra were collected for the TP in the presence and absence of the DBD (Figure 3.5, A). The cross-peaks corresponding to the residues 45 – 55 from the TD2 motif underwent significant CSP in the presence of the DBD, whereas the cross-peaks corresponding to the residues from the TD1 motif or the PRD did not undergo noticeable chemical shift changes (Figure 3.6). This result suggest that the TD2 motif is responsible for the interaction with the DBD.

To further validate that the TD2 motif interacts with the DBD, I performed PRE experiments by collecting a set of ^{1}H-^{15}N HSQC spectra using isotope-labeled TD and unlabeled DBD prepared in either diamagnetic (zinc-bound) or paramagnetic (cobalt-bound) state. The metal ion is tetrahedrally-coordinated by side chains of histidine and cysteine residues (Cys-176, His-179, Cys-238, and Cys-242) and is in close proximity to DNA-binding surface of the DBD (Figure

3.3). The residues that underwent the most dramatic changes in cross-peak intensity were found to localize to the TD2 motif, suggesting that the TD2 motif likely binds the DNA-binding surface of the DBD (Figure 3.5, B). This result further supports the proposition that the TD2 motif can compete with the AD for DBD binding as the AD is shown to bind the DNA-binding surface of the DBD (section 2.3).

To further characterize this interaction, the ^{1}H-^{15}N TROSY spectra of the isotope-labeled DBD were acquired in the presence and absence of the TP (Figure 3.7). The CSP analysis suggest the residues of the DBD that are affected by the TP binding are localized to the DNA-binding surface (Figure 3.8, A & B). Furthermore, many of the DBD residues that are affected by the TP binding are also involved in the AD-DBD interaction (Figure 3.8, C). These results further support that the TD2 motif likely binds the DNA-binding surface of the DBD and competes with the AD. Taken together, all of these results suggest that the p53 TD, specifically the TD2 motif, can compete with the MDM2 AD for p53 DBD binding.

3.3.3 The PBD binds and sequesters the TD2 motif to promote the interaction between the DBD and the AD.

The PBD of MDM2 was previously shown to interact with both the TD1 and TD2 motifs of p53, despite the fact that the affinity for the TD2 motif is much weaker than the TD1 motif (Shan et al., 2012). Therefore, it is possible that sequestration of the TD2 motif by the PBD could facilitate the interaction between the AD and the DBD. To test this hypothesis, I collected a ^{1}H-^{15}N TROSY spectrum for the DBD in the presence of 1.1 molar excess of the TD with 1.5 molar excess of the PBD and compared it to the spectrum for the DBD in the presence of 1.1 molar excess of the TD (Figure 3.9). The spectrum for the DBD in presence of the TD and the PBD showed significantly

weaker CSP as compared to the spectrum for the DBD in presence of the TD, suggesting that the PBD can bind to the TD2 motif to prevent it from interacting with the DBD (Figure 3.9). Of note, the ^{1}H-^{15}N TROSY spectra of the DBD in the presence and absence of the PBD are near identical, suggesting that the PBD cannot directly bind to the DBD (Figure 3.10). Thus, the MDM2 PBD could bind to and sequester the TD2 motif of p53, exposing its DBD and allows the MDM2 AD to establish a more stable interaction with the DBD.

3.4 Discussion

The TD is intrinsically disordered and adopts an ensemble of transient conformations to facilitate interaction with diverse protein binding partners (Lum, Neuweiler, & Fersht, 2012; Wells et al., 2008). Our NMR data provide direct evidence that the TD directly interacts with the DBD and demonstrate that the TD interacts predominantly with the DNA-binding site. Indeed, this fits well in the context of recent studies showing that the TD directly competes with DNA for DBD binding and discriminates between the binding of specific and non-specific DNA sequences (He et al., 2019; Krois et al., 2018). Moreover, the TD2 motif was found to serve as single stranded DNA (ssDNA) mimic that binds to the ssDNA binding site of replication protein A and positive cofactor 4 (Bochkareva et al., 2005; Rajagopalan, Andreeva, Teufel, Freund, & Fersht, 2009) . Thus, it is likely that the p53 TD binds to its DBD by serving as an intramolecular DNA mimic.

Close inspection of the ^{1}H-^{15}N TROSY spectrum of the isotope-labeled DBD in complex with the TD reveals that the pattern of residues that undergoes chemical shift changes resembles that observed when the DBD is in complex with the AD. Moreover, the AD, similarly to the TD, can bind to the DNA-binding site of the DBD and compete with DNA (Cross et al., 2011). Here, I show that the TD2 motif of the TD inhibits the interaction between the AD and the DBD through

direct competition. The NMR data suggest that the TD cannot fully compete with the AD for DBD binding, implying that the intramolecular interaction between the TD and the DBD is much weaker than the intermolecular interaction with the AD. It must be noted that the protein constructs used in the current study lack the p53 C-terminal sequence (residues 313 – 393), which include the oligomerization domain and the regulatory domain. It is possible in the context of a full-length p53 in its oligomeric state that the TD from another subunit of the p53 oligomer could bind more tightly to the DBD and outcompete the AD. It is also possible that the higher local concentration of the TD in the p53 oligomer could allow it to bind more efficiently to the DBD and prevent the AD from interacting with the DBD.

The PBD of MDM2 binds the TD of p53 with high affinity and is responsible for the formation of the p53-MDM2 complex to promote p53 ubiquitination and degradation (Kubbutat et al., 1997; Kussie et al., 1996; Momand, Zambetti, Olson, George, & Levine, 1992). The interaction with the TD involves both the TD1 and TD2 motifs, of which the TD1 motif binds the PBD with much greater affinity that the TD2 motif (Shan et al., 2012). I speculated that the PBD could sequester both the TD1 and TD2 motifs to promote the interaction between the AD and the DBD. Indeed, our data provide compelling evidence that the PBD could stimulate the interaction between the DBD and the AD through direct interaction with the TD, including its TD1 and TD2 motifs. Thus, the maximum inhibitory effect of MDM2 likely requires both the PBD and the AD to act synergistically for establishing the interaction with p53. The results presented herein let us propose a model that an active domain-domain cross talk is necessary for the establishment of the p53-MDM2 complex, which the interaction between the PBD and the TD promotes the interaction between the AD and the DBD (Figure 3.11).

Previous studies have commonly focused on the interaction between the PBD and the TD1 motif of the TD. In this Chapter, I have clearly shown that the interaction between the PBD and TD2 motif also has the potential to play a significant role in modulating the activity of p53 by promoting direct interaction between the AD and the DBD. Our findings also have potential implications for the protein-binding characteristics of the DBD and the TD when interacting with other p53-binding proteins. Both regions have been shown to interact with pathophysiolologically important p53-binding proteins, such as Bcl-xL and BRCA2. The anti-apoptotic protein Bcl-xL can bind to and sequester cytoplasmic p53 by direct interaction with the DBD, whereas the Bcl-xL BH3 groove binds to the TD of p53 (Follis et al., 2014). BRCA2, a protein involved in DNA damage repair, can bind to the TD and the DBD of p53 through its OB domains and BRC repeats (Rajagopalan, Andreeva, Rutherford, & Fersht, 2010). Thus, synergistic binding interactions that simultaneously involve both the TD and the DBD of p53 may serve as a general mechanism for p53-binding proteins to bind p53.

Table 3.1: Chemical shift ssignment report for the TP.

Atom type	Assignment
H_N*	62/71 (87%)
$N^{\perp}$	62/71 (87%)
C'	76/93 (82%)
C_α	77/93 (83%)
C_β	76/93 (82%)

* N-terminal HN was excluded.

⊥ Proline residues and N-terminal N were excluded.

Table 3.2: PANAV assessment reports for chemical shift assignments.

TD* **(H_N, N, C_α, C_β, and CO)**		
CONA Score (6-Resdue Scan)	1.00	> 0.95
Detected reference offsets	N: -0.88 ppm C_α: 0.03 ppm C_β: 0.47 ppm CO: 0.09 ppm	N: < ±1.5 ppm C_α: < ±1.0 ppm C_β: < ±1.0 ppm CO: < ±1.0 ppm
Number of assignments	325	
Number of deviant assignments	0	
Number of suspicious assignments	0	

*Owing to the high proline content that cannot be assigned near the C-terminus of the sequence, only assignment for residues 1 – 74 were used for PANAV assessment.

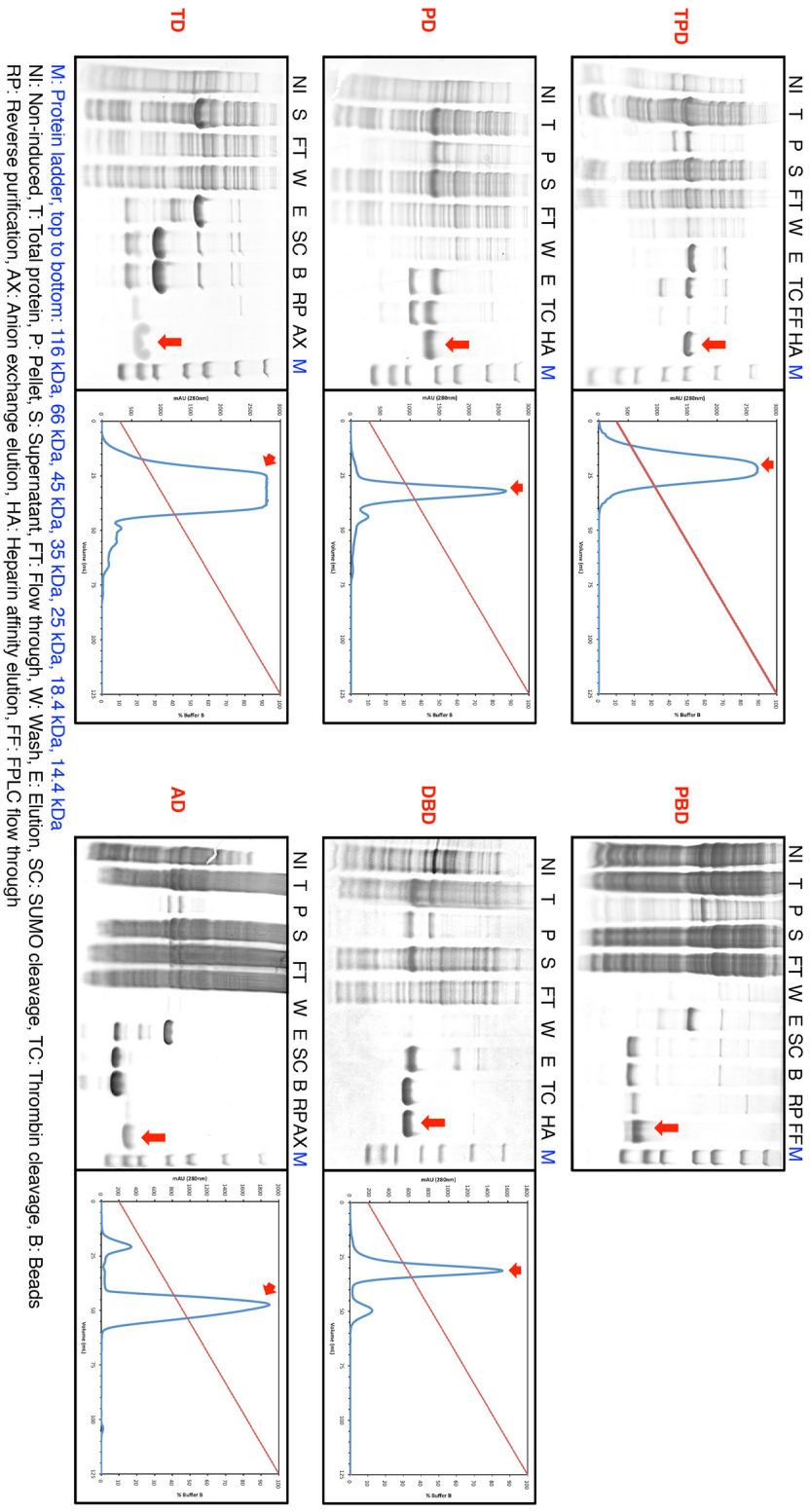

Figure 3.1: Expression and purification of recombinant proteins used in chapter 3. The gel pictures and chromatograms showed representative purification process of ^{15}N AD, ^{15}N TP, ^{15}N DBD, natural abundant TPD, PD.

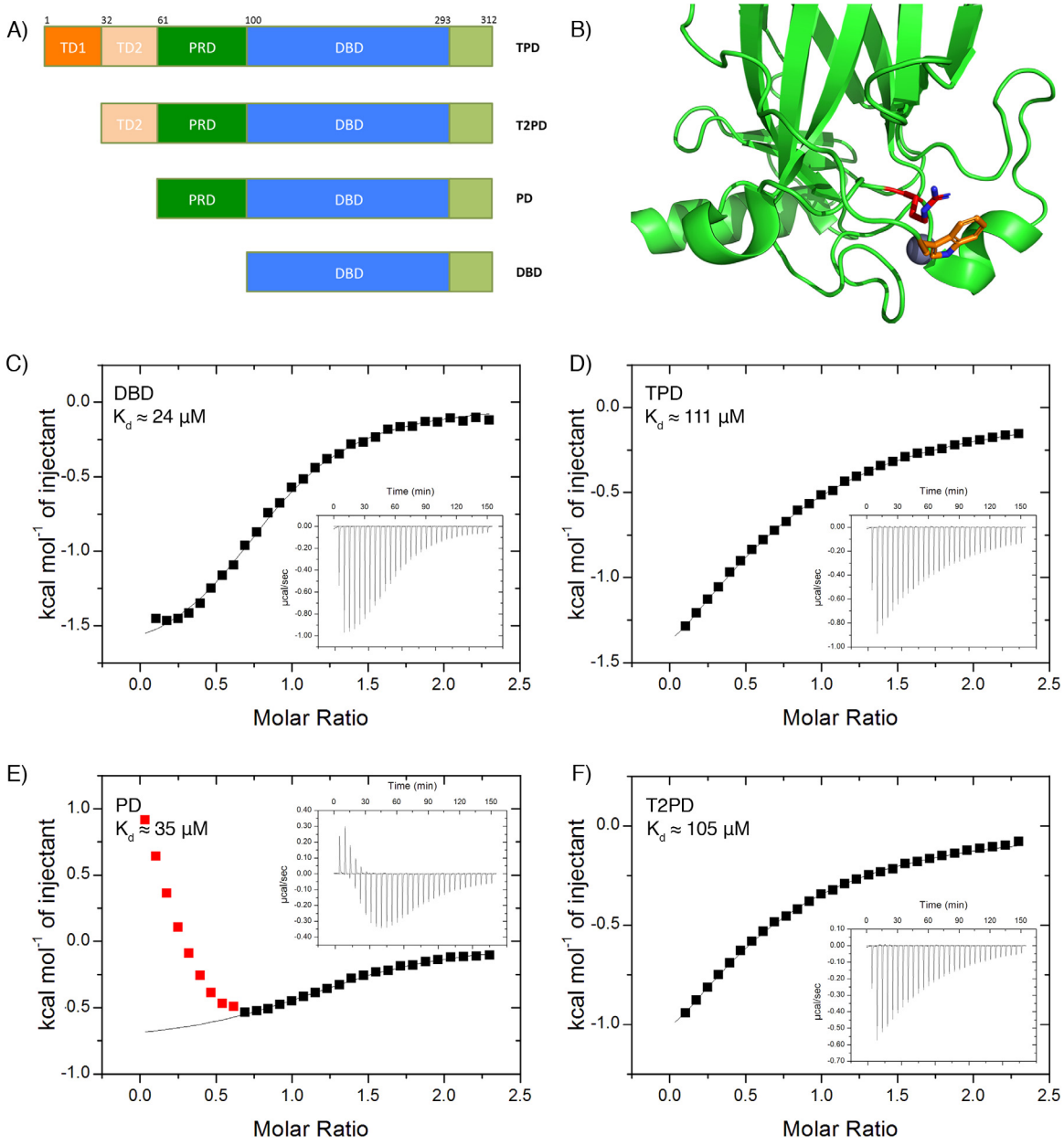

Figure 3.2: ITC studies of binding of the AD to various p53 constructs. A) Constructs used for ITC and NMR experiments. B) Crystal structure of the DBD highlighting the cation-π interaction between R174 (red) and W91 (orange) (Nathan et al., 2011. PDB ID: 2XWR). C), D), E) and F) ITC analysis of the AD binding to the various p53 constructs (DBD, PD, TPD and T2PD). The integrated heat signals for each injection are plotted vs. molar ratio (squares), with fits to a one-site binding model shown (lines). The data points highlighted in red were excluded from the fitting. Insets show the raw ITC data for the heat trace per injection vs. time.

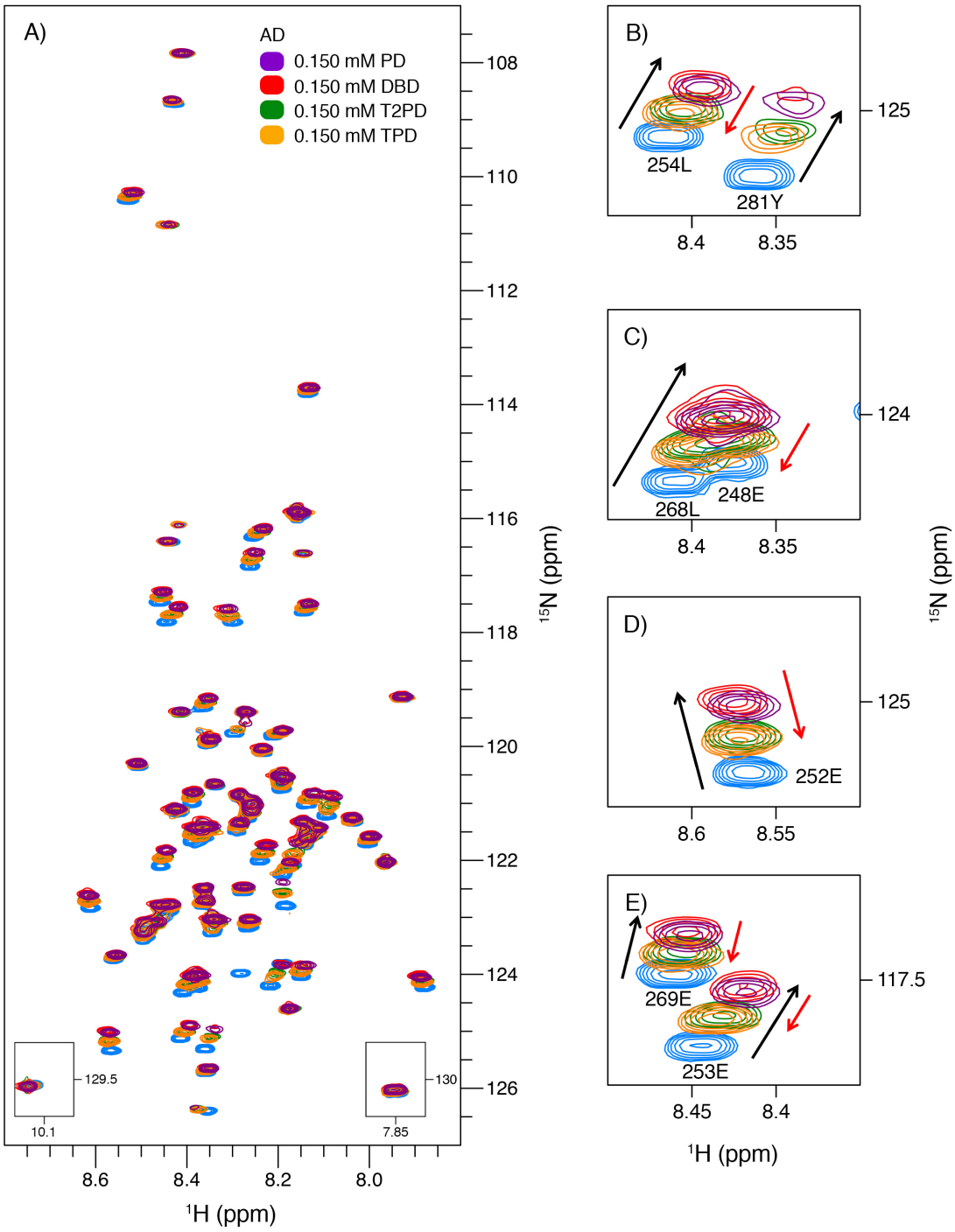

Figure 3.3: ^{1}H-^{15}N HSQC spectra of the AD in the presence and absence of various p53 constructs. A) ^{1}H-^{15}N HSQC spectra of the AD (blue) in the presence and absence of the PD (purple), DBD (red), T2PD (green) or TPD (yellow). B-E) Close-up view of a few AD residues that underwent significant CSP, binding to the PD or the DBD cause significant CSP (black arrow) as compared to the TPD or the T2PD (red arrow).

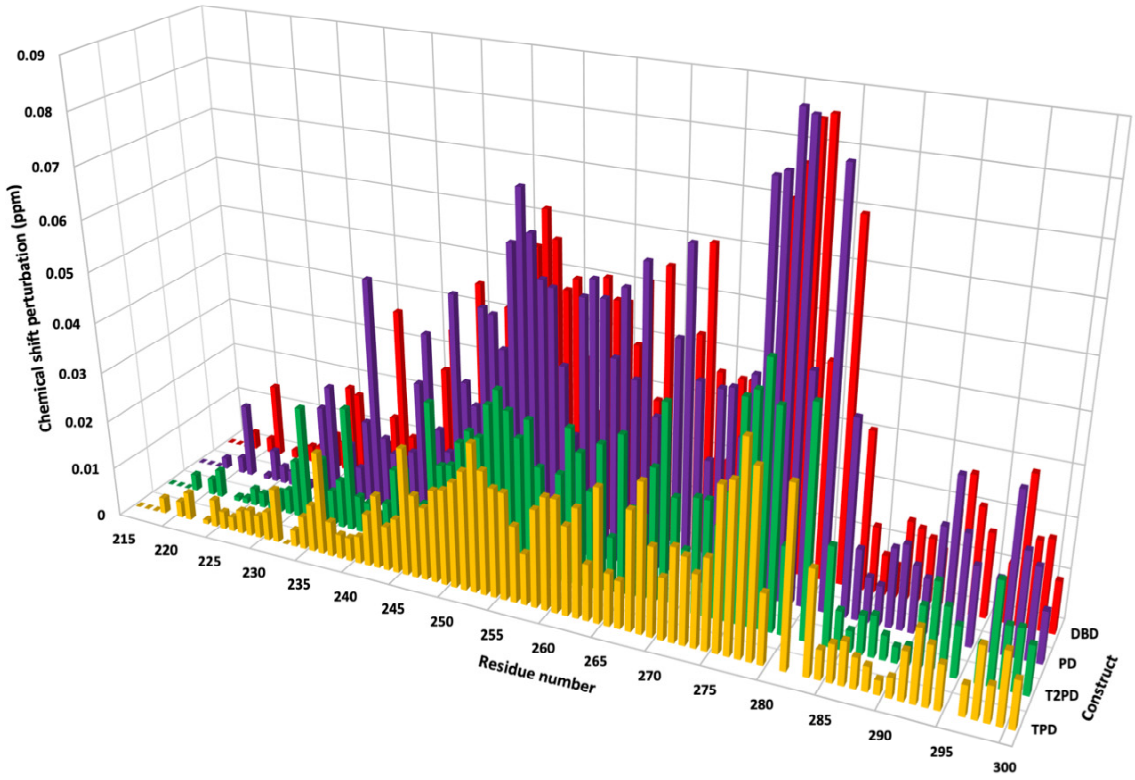

Figure 3.4: Chemical shift perturbation of the AD upon titration with various p53 constructs. TPD: including TD, PRD & DBD (yellow); T2PD: including TD2 motif, PRD & DBD (green); PD: including PRD & DBD. DBD (purple) and DBD (red).

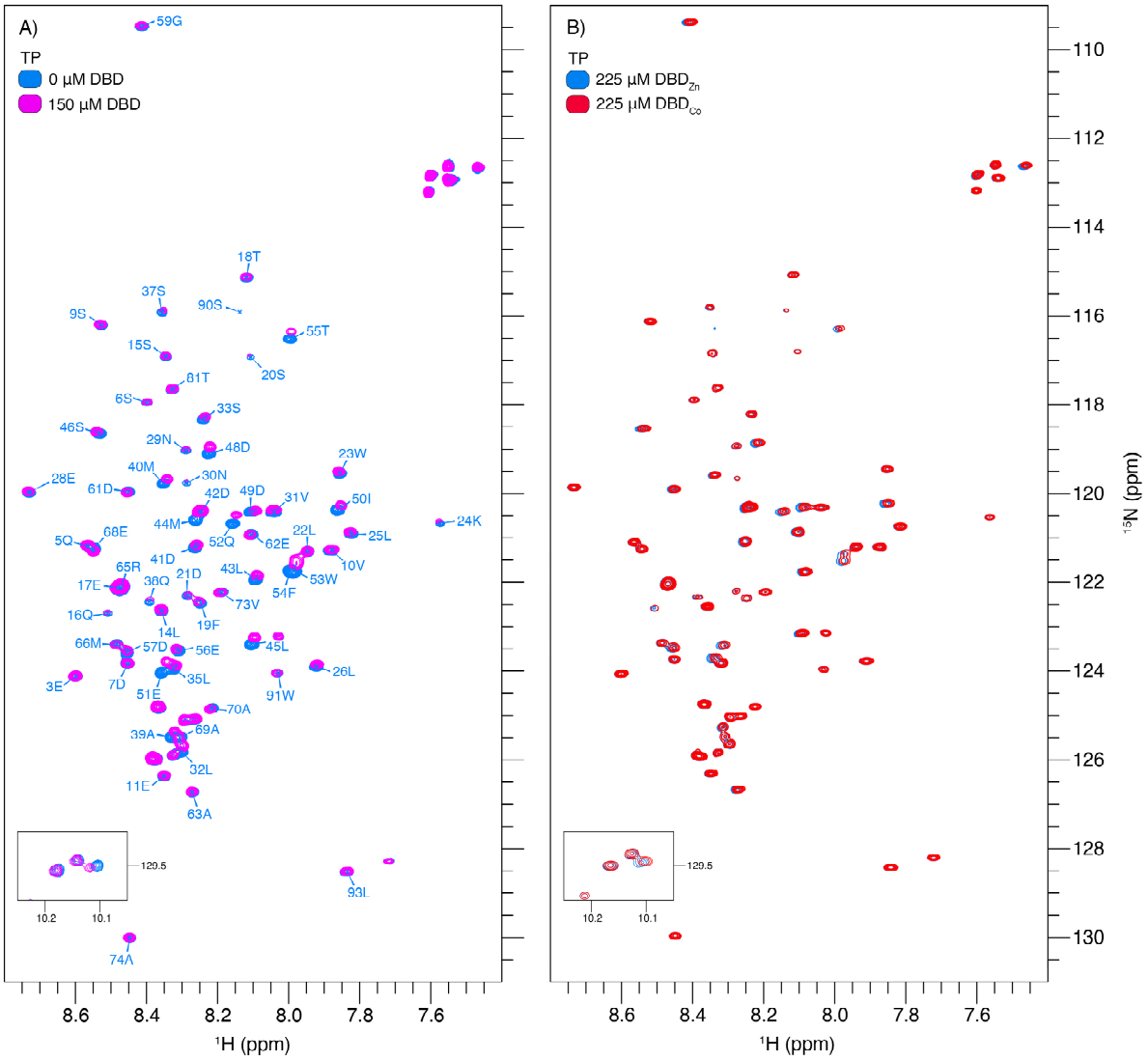

Figure 3.5: Overlaid ^{1}H-^{15}N HSQC spectra of the TP in complex with the DBD. A) ^{1}H-^{15}N HSQC spectra of the TP in absence and presence of the DBD. B) ^{1}H-^{15}N HSQC spectra of TP in presence of DBD_{Zn} (diamagnetic) or DBD_{Co} (paramagnetic).

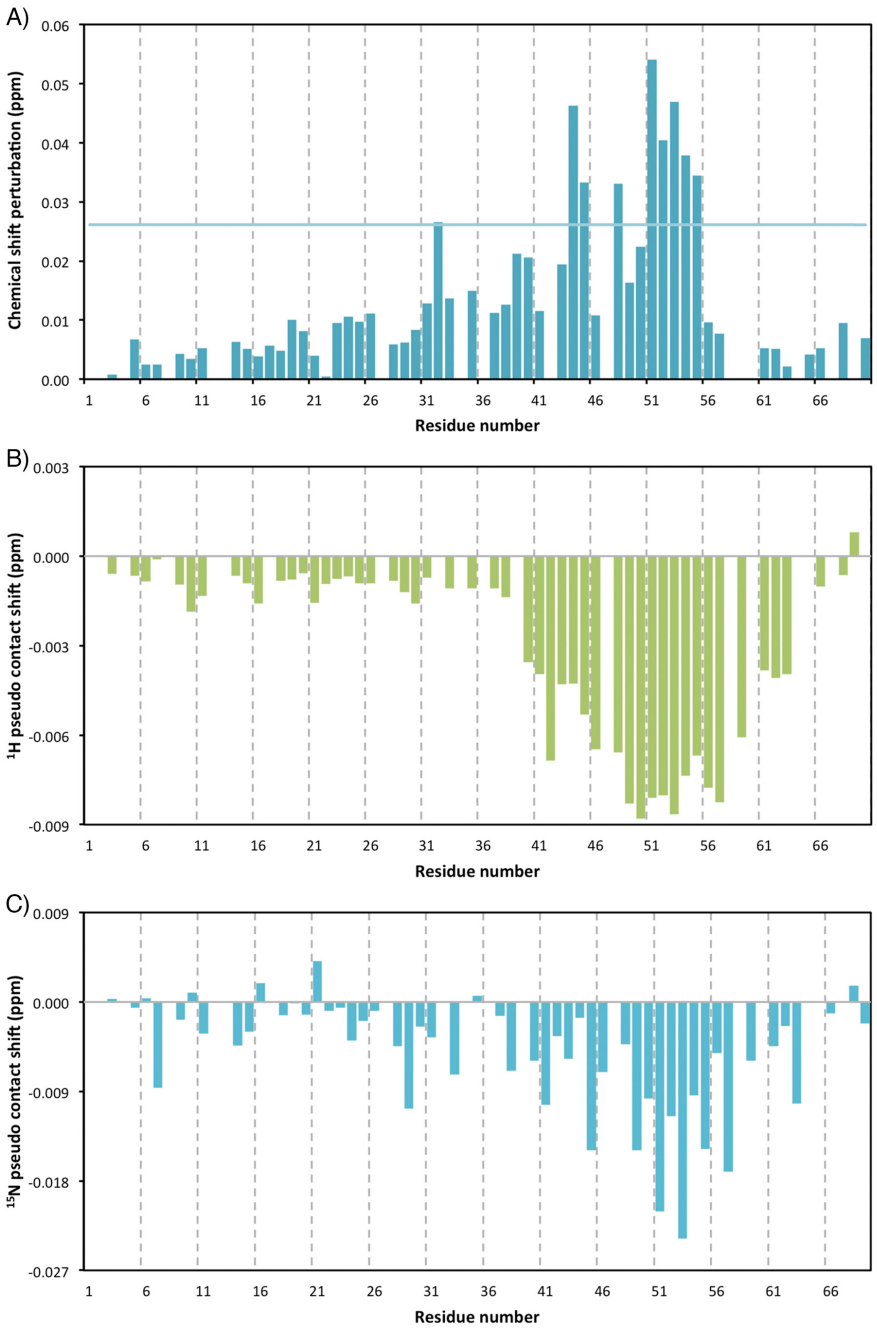

Figure 3.6: Chemical shift perturbations and pseudo contact shifts of the TP upon addition of the DBD. A) ^{1}H-^{15}N CSPs as a function of residue number for the TP in presence of the DBD. B) and C) $^{1}H_{N}$ and ^{15}N pseudo contact shifts as a function of residue number for the TD in presence of the equal concentration of either paramagnetic (Cobalt) or diamagnetic (Zinc) DBD. Threshold values are set to 2× standard deviation.

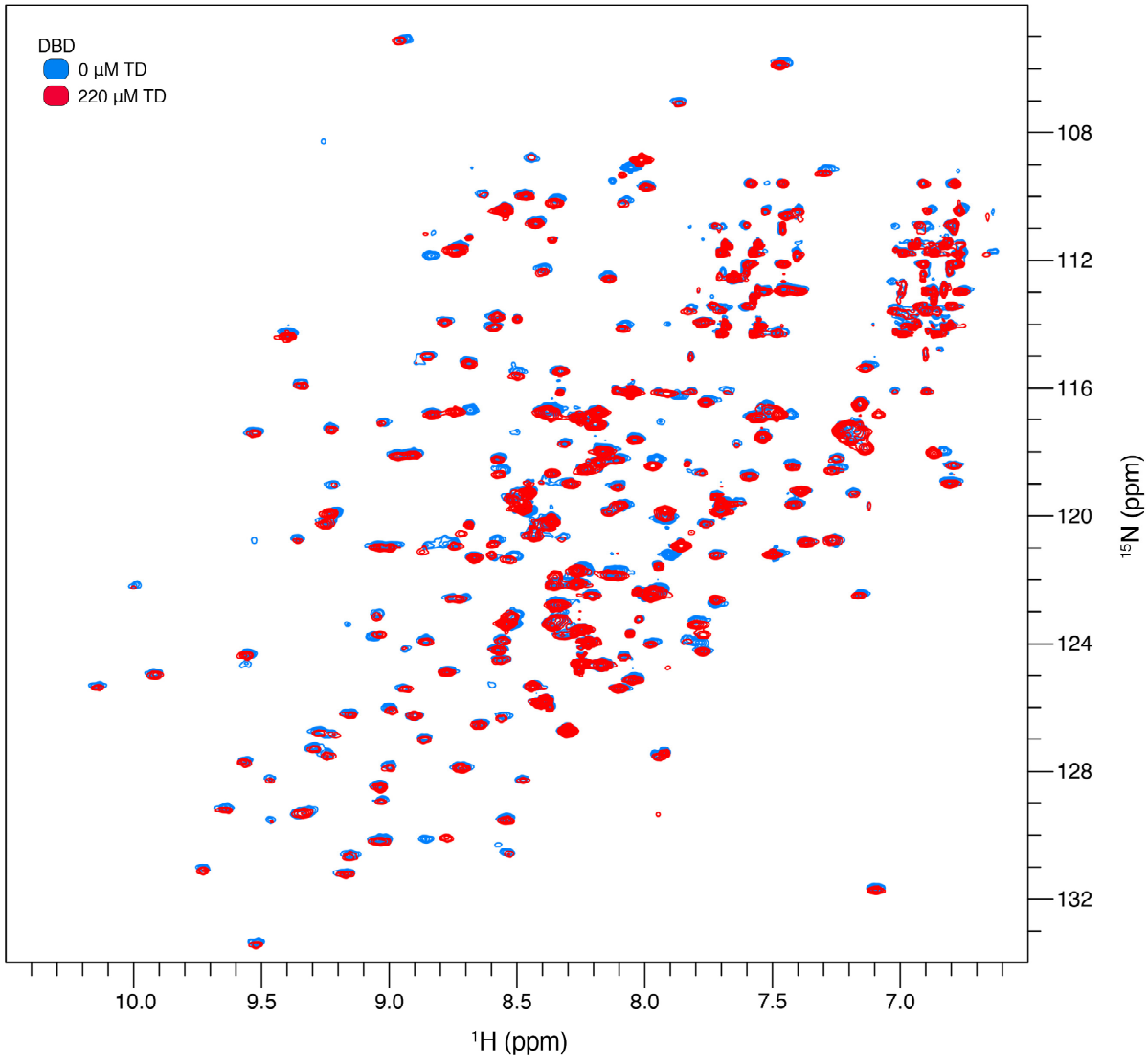

Figure 3.7: ^{1}H-^{15}N TROSY spectra of the DBD the presence and absence of the TP.

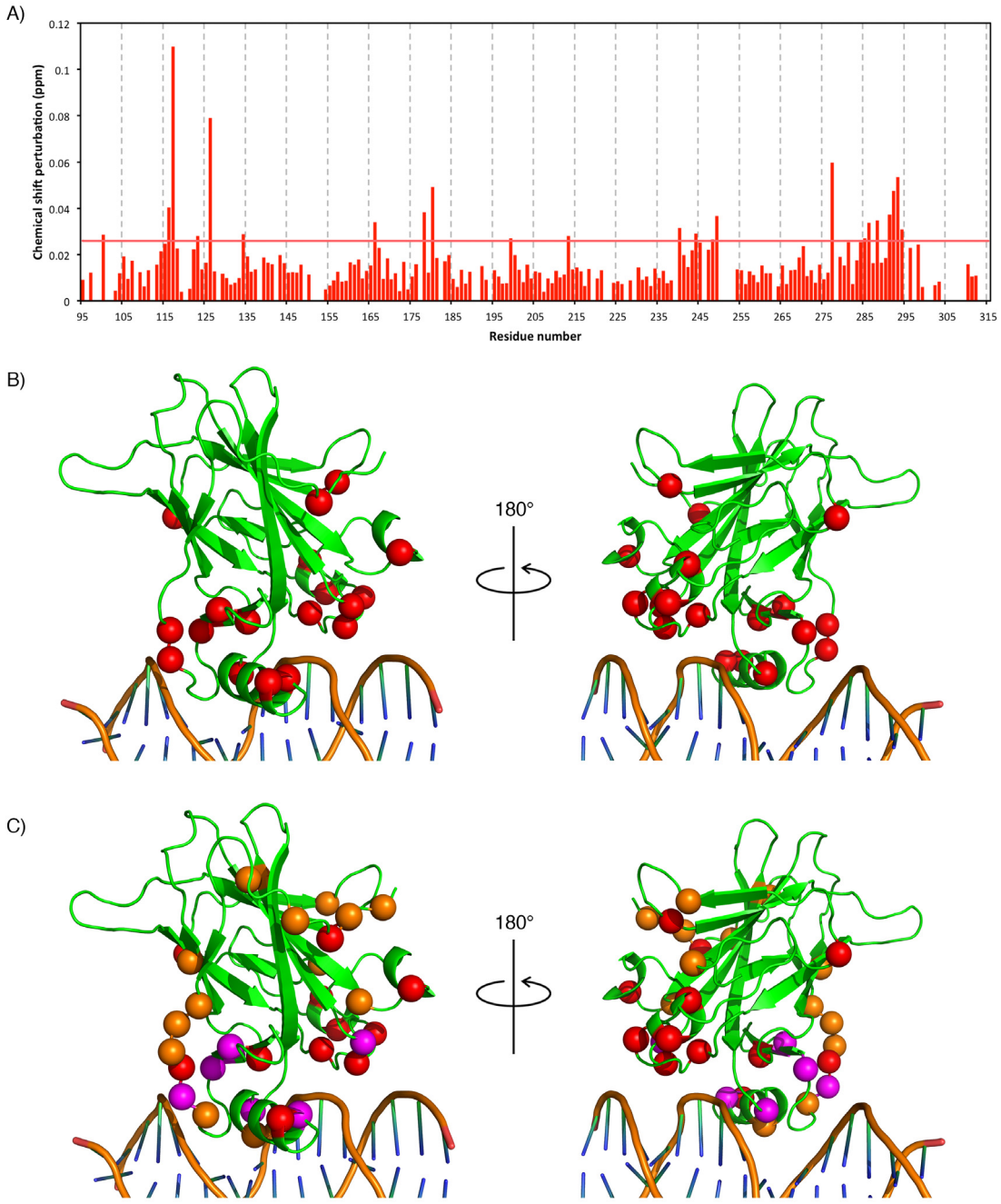

Figure 3.8: TD preferentially binds to the DNA-binding surface of the DBD. A) CSP values for the backbone amide resonances of the DBD in complex with the TP are plotted as a function of residue number. Threshold value is set to 2 The DBD assignment is taken from chapter 2. B) Mapping of the binding site on the DBD for the TP based on the CSP from A). C) Comparison of the binding site for the TP and the AD. The residues with perturbations larger than the threshold value are highlighted on the surface of the DBD structure as red (TP), orange (AD) and magenta (TP & AD shared) spheres (Cho et al., 1994. PDB ID: 1TUP).

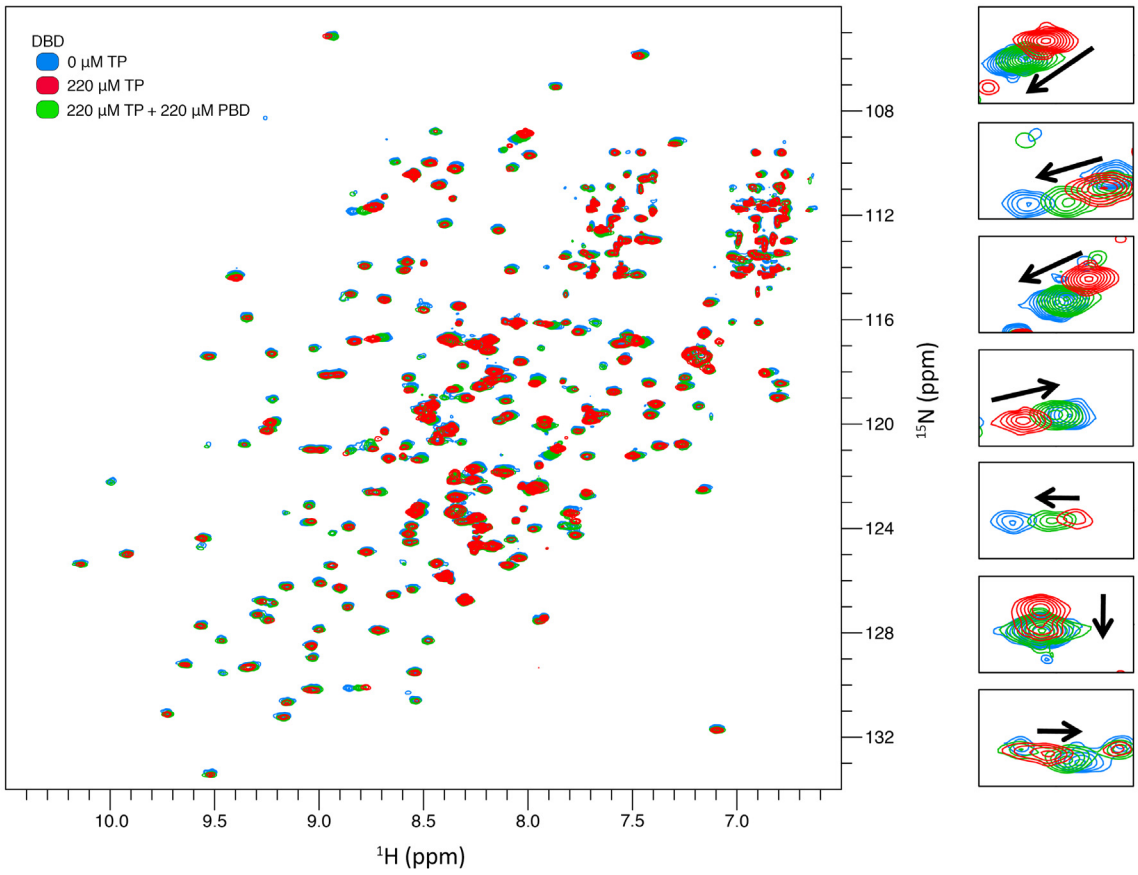

Figure 3.9: ^{1}H-^{15}N TROSY spectra of the DBD in the presence and absence of the TP or the TP and the PBD. Black arrow: change in CSPs of the DBD in presence of the TP and the PBD (green) as compared to the DBD in presence of the TP (red).

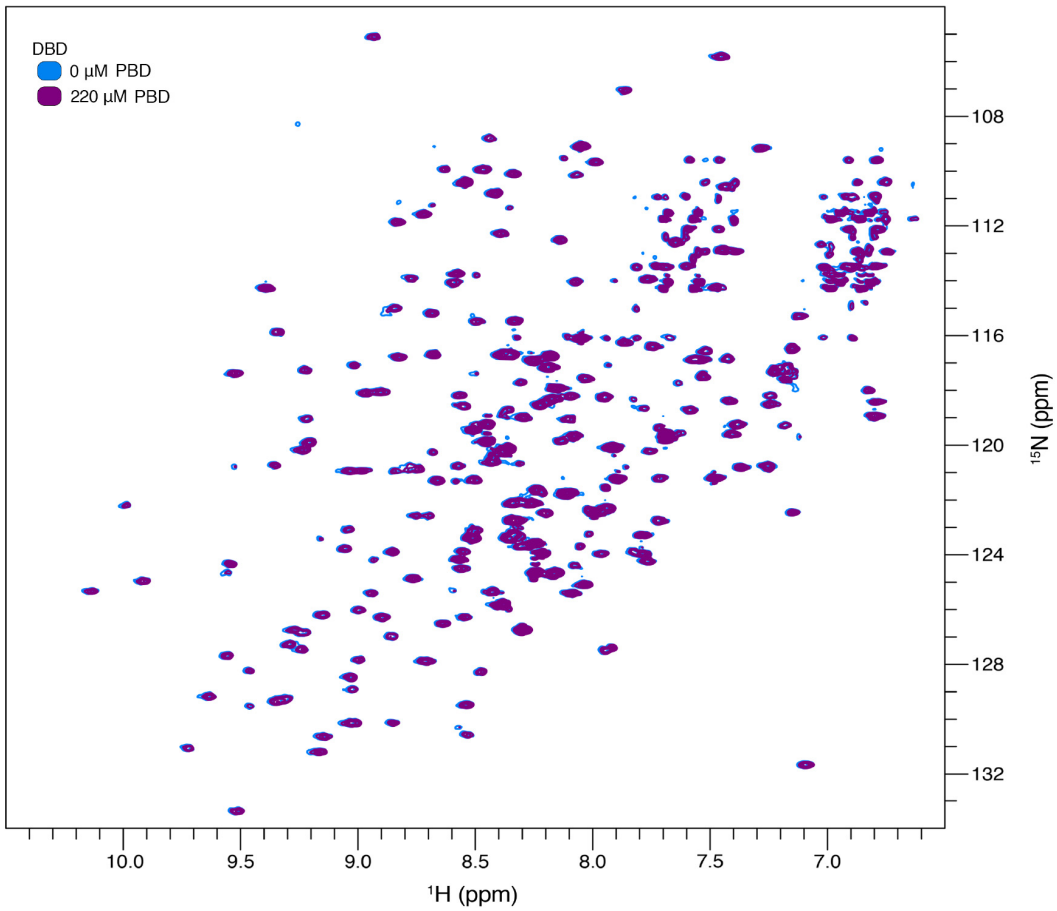

Figure 3.10: ^{1}H-^{15}N TROSY spectra of the DBD in the presence and absence of the PBD.

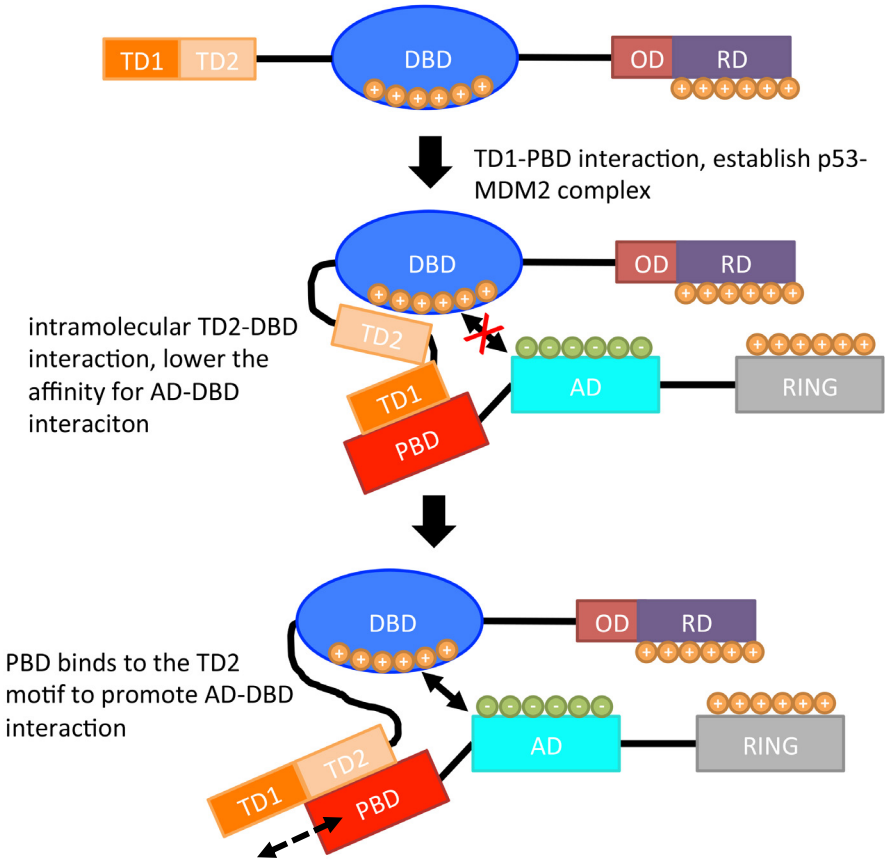

Figure 3.11: Proposed model for MDM2 activation. Initial p53-MDM2 complex requires high affinity interaction between the TD1 motif and the PBD. The TD2 motif forms a complex with the DBD to prevent AD binding. The PBD once bound to the TD1 could sequester the TD2 motif to expose the DBD, which in turn promote the interaction with its AD.

CHAPTER 4: THE ACIDIC DOMAIN OF MDMX BINDS TO AND PREVENTS THE PBD OF MDM2 FROM INTERACTING WITH P53 TRANSACTIVATION DOMAIN

4.1 Introduction

The homologous proteins MDM2 and MDMX are important negative regulators that tightly control the activity and stability of the tumour suppressor p53 in normal cells (Danovi et al., 2004; Fuchs, Adler, Buschmann, Wu, & Ronai, 1998; Honda, Tanaka, & Yasuda, 1997; Hu, Gilkes, Farooqi, Sebti, & Chen, 2006; Kubbutat, Jones, & Vousden, 1997; Momand, Zambetti, Olson, George, & Levine, 1992; Okamoto, Taya, & Nakagama, 2009; Oliner et al., 1993; Sharp, Kratowicz, Sank, & George, 1999; Shvarts et al., 1996; Shvarts et al., 1997). More importantly, MDM2 and MDMX are frequently upregulated in many types of cancers to promote cell survival and proliferation (Danovi et al., 2004; Laurie et al., 2006; Momand, Jung, Wilczynski, & Niland, 1998). Both proteins exert their function by sequestering p53 to prevent recruitment of transcription cofactors, thereby inhibiting the transcriptional activity of p53 (Kussie et al., 1996; Popowicz, Czarna, & Holak, 2008). Moreover, the proteins bind and inhibit the DNA-binding activity of p53 to prevent it from interacting with target DNA (Cross et al., 2011; Wei et al., 2016). In addition, MDM2 is an E3 ubiquitin ligase that can ubiquitinate multiple sites on p53 to promote nuclear export and proteasomal degradation (Honda et al., 1997). Unlike MDM2, MDMX is not a functional E3 ubiquitin ligase but instead heterodimerizes with MDM2 to boost its E3 ubiquitin ligase activity (Linke et al., 2008; Okamoto et al., 2009; Sharp et al., 1999).

MDM2 and MDMX contain three structural domains and a glutamate-aspartate rich (acidic) domain flanked by large disordered regions (Figure 1.5). The N-terminal p53-binding domain (PBD) adopts a globular SWIB-like fold and binds tightly to the p53 transactivation domain (TD) (Kussie et al., 1996; Popowicz et al., 2008). The central part of the protein contains a disordered acidic domain (AD) and a RanBP2 type zinc finger (ZF) domain, of which the AD has been shown to suppress the DNA-binding activity of p53 (Cross et al., 2011; Wei et al., 2016). The C-terminal region contains a Really Interesting New Gene (RING) domain. The RING domain of MDM2 possesses intrinsic E3 ubiquitin ligase activity, whereas – as noted above – the RING domain of MDMX is defective in mediating ubiquitination (Fang, Jensen, Ludwig, Vousden, & Weissman, 2000; Honda & Yasuda, 2000; Linares, Hengstermann, Ciechanover, Muller, & Scheffner, 2003). In addition, the RING domains of both MDM2 and MDMX can self-associate to form functional homodimers and heterodimers to promote the E3 ubiquitin ligase activity (Linke et al., 2008; Krostic et al., 2006).

The acidic domain of MDMX (referred to hereafter as ADX to distinguish it from the MDM2 AD), in addition to its role in inhibiting the DNA-binding activity of p53, was shown to serve as an auto-inhibitory element that forms an intramolecular interaction with the PBD to effectively disrupt the intermolecular interaction with the TD of p53 (Bista, Petrovich, & Fersht, 2013). The intramolecular interaction between PBD and ADX was shown to involve a tryptophan-rich motif (W3) spanning residues 194 – 206, within which the residues W200 and W201 were found to be crucial for mediating the interaction. Of note, the overall structure of the PBD from MDM2 (PBD2) is highly homologous to the structure of the PBD from MDMX (PBDX) (Kussie et al., 1996; Popowicz et al., 2008).

Moreover, both domains bind the p53 TD with a near-identical conformation (Figure 1.6, A). The high degree of structural and functional similarity between the PBD2 and the PBDX suggests that the ADX could potentially serve as a binding site for the PBD2.

In this Chapter, I detail a study aimed at characterizing the interaction between the ADX and the PBD2. I demonstrate that the ADX can directly bind to the PBD2 with micromolar affinity, with the interaction involving the W3 motif and the WF motif. The W3 motif is the primary binding site for the PBD2 whereas the WF motif can only weakly interact with the PBD2. I further demonstrate that the ADX can effectively compete with the TD for binding to the PBD, which is likely achieved by binding to the hydrophobic cleft of the PDB2. My results suggest that the ADX is an important regulatory element that modulates the interaction of both MDM2 and MDMX with p53.

4.2 Material and methods

4.2.1 Materials

The codon-optimized genes for human MDM2 (residues 1 – 491) and the MDMX ADX (residues 181 – 300) were obtained from GENEWIZ (South Plainfield, NJ). The DNA primers for cloning were obtained from Integrated DNA Technologies, Inc (Coralville, IA). All other materials used in this work are as listed previously in section 2.2. Recombinant TP produced and purified as detailed in Chapter 3 was used.

4.2.2 Cloning and plasmid construction

The plasmids for expressing the PBD and the TP were constructed as described in section 3.2.2. The expression plasmid for the ADX (residue 180 – 300) construct was produced by subcloning the codon-optimized gene into the pETHS vector using the

restriction enzymes SapI and BamHI. Mutation and deletion constructs (ADXAA: W200A/W201A and ADXD: truncation to residues 228 – 300) were generated by site-directed mutagenesis to remove or mutate, resulting in the desired DNA sequence, using the Phusion High-Fidelity DNA polymerase (NEB; Whitby, ON). Sanger sequencing was used to confirm the DNA sequence identity (Genewiz; South Plainfield, NJ). Forward and reverse primers used for DNA amplification are listed in Table A1 in the Appendix. Standard PCR thermocycling conditions are listed in Table A2 in the Appendix. Plasmid constructs for *E. coli* expression are listed in Table A3 in the Appendix. All plasmids were stored at – 20 °C.

4.2.3 Protein expression in E. coli

Protein expression was carried out using *E. coli* BL21 (DE3) strain. Expression of the isotope-labelled and unlabelled ADX constructs was performed using the same protocol for expressing the AD as described in section 2.2.3.

4.2.4 Nickel affinity chromatography

The protocol used for Ni-NTA purification is the same as described in section 2.2.4, The ADX constructs were purified using the same conditions as for purification of the AD.

4.2.5 Fast performance liquid chromatography (FPLC)

The ADX constructs used in this work were purified similarly as described for purification of the AD in section 2.2.3. Sample concentrations were determined according to the Beer-Lambert law using the protocol described in section 2.2.5. The concentration

for the ADXD was determined by using the molar extinction coefficient at 214 nm (ε = 104411 M^{-1} cm^{-1}), the concentration for all other constructs was determined by using the molar extinction coefficient at 280 nm (ε_{ADX} = 23490 M^{-1} cm^{-1}, ε_{ADXAA} = 12490 M^{-1} cm^{-1}). All protein samples were flash frozen in liquid N_2 and stored in – 80 °C freezer before use.

4.2.6 SDS-PAGE

SDS-PAGE gels were run and visualized using the same conditions and protocols detailed in section 2.2.6.

4.2.7 Circular dichroism spectroscopy

Far-UV CD spectra from 260 – 185 nm for the ADX were recorded at 20 °C using Olis DSM20 CD spectrophotometer (Bogart, GA) with a data pitch of 1 nm and all optical slits set at a band pass of 5.0 nm, with ellipticity acquired using integration time as a function of high volts in Olis SpectralWorks version 5.888.272. Samples (50 μM) were prepared in 20 mM phosphate buffer, pH 7 in quartz cuvettes (0.5 mm path length; Hellma Canada Limited; Concord, ON). All data were collected in triplicate, averaged and blank subtracted. The raw data were further processed using the CAPITO webserver (Wiedemann, Bellstedt, & Görlach, 2013) and the final values were reported as mean residue ellipticity [θ]. CD data in [θ] format were analysed using the BeStSel algorithm (Micsonai et al, 2018).

4.2.8 Isothermal titration calorimetry

ITC experiments were carried out using a VP-ITC instrument (Malvern Panalytical Ltd, Malvern, UK). The sample preparation protocol for ITC experiments was as described in section 2.2.8. For experiments measuring the affinity of the TP, ADX and ADXD for the PBD, 100 μM PBD was used in the sample cell. For experiments measuring the affinity of the TP for the PBD in presence of the ADX, concentrations of 100 μM PBD and 110 μM ADX were used in the sample cell. Following thermal equilibration at 20 °C and an initial 5 min delay, 30 serial injections of 10 μL of 1 mM solution of the TP, 1 mM solution of the ADX or a 2 mM ADXD solution were titrated into the sample cell from the syringe under a constant stirring speed of 300 rpm with a 5 min spacing between injections. All experiments were performed in duplicate and control experiments measuring the heat of dilution were used to correct for the background heat effects. Data analysis was performed using the ORIGIN software package (Origin 7 SR4 v7.0552; Malvern Panalytical Ltd, Malvern, UK) and corrected curve was fitted to a one-site binding model according to the equation:

$$q_i = v \times \Delta H \times [P] \times \left(\frac{K_a[L]_i}{1 + K_a[L]_i} - \frac{K_a[L]_{i-1}}{1 + K_a[L]_{i-1}} \right)$$

as detailed in Leavitt & Freire, (2001).

4.2.9 NMR spectroscopy

Samples were prepared in NMR buffer following the protocol described in section 2.2.9. Unless otherwise specified, experiments were performed on an 700 MHz Bruker Avance III spectrometer equipped with a TCI cryoprobe. ^{1}H-^{15}N HSQC experiments of 150 μM isotope-labeled ADX or ADXAA were performed in the presence or absence of 300

μM of PBD2. A ^{1}H-^{15}N HSQC experiment was also acquired for 150 μM isotope-labeled ADX in the presence of 150 μM PBD2 and 225 μM TP. ^{1}H-^{15}N HSQC experiments of 100 μM isotope-labeled PBD in the presence or absence of 300 μM unlabeled TP, ADX, ADXAA or ADXD were similarly collected. Triple-resonance experiments (HNCACB, CBCACONH, HNCO and HNCACO) for isotope-labeled PBD2 (400 μM) were performed to allow chemical shift assignment. ^{1}H-^{15}N HSQC spectra of 100 μM isotope-labeled ADXD in the presence or absence of 1.1 molar excess of PBD2 were collected on an 500 MHz Bruker Avance spectrometer equipped with a BBFO probe. Triple resonance experiments (HNCACB, CBCACONH, HNCO and HNCACO) for isotope-labelled ADX (380 μM) were performed for chemical shift assignment, which were acquired using an 800 MHz Bruker Avance III HD spectrometer equipped with a TCI cryoprobe. Full NMR experimental parameters, including triple resonance experiments that were acquired using non-uniform sampling of indirectly observed dimensions, are listed in Table A4 in the Appendix. All spectral analysis was carried out as described in section 2.2.9.

4.3 Results

4.3.1 Protein production and purification

Protein overexpression were carried out using *E. coli* expression system. The ADX constructs contain an N-terminal H_6-SUMO fusion tag. Each of these overexpressed SUMO-fusion proteins remained highly soluble after cell lysis and exhibited high metal-binding affinity for Ni-NTA purification (Figure 4.1). Further reverse purification using nickel-affinity chromatography followed by anion-exchange chromatography purification yielded proteins at 90 ~ 95% purity (Figure 4.1: ADX, ADXAA, and ADXD lane AX).

4.3.2 Chemical shift assignment and validation

Triple-resonance NMR experiments (listed in Table A5 in the Appendix) were performed to allow chemical shift assignment of the ADX (Table 4.1 & Table A11 in the Appendix). To validate my chemical shift assignments, the assigned chemical shifts were analysed using the PANAV. Based on the assessment by PANAV, the chemical shift assignment data are of high quality. Summary of the PANAV assessment report is presented in Table 4.2.

4.3.1 The ADX is intrinsically disordered

A previous study showed that the intramolecular interaction between the ADX and the PBD of MDMX involves a conserved WWW (W3) motif that contains the key W200 and W201 residues and spans residues 190 – 210, where they mapped the interaction site to amino acids 194 – 206 (Bista et al., 2013). To assess whether additional conserved regions within the ADX exist, I performed multiple sequence alignment of MDMX across six different species (Figure 4.2). Clearly, an additional region resides downstream of the W3 motif that shows a high degree of sequence conservation (sequence spanning residues 228 – 243). This region contains the conserved four hydrophobic amino acid sequence L/M-W-F-L (and was herein referred to as the WF motif) flanked by polar and acidic residues. The C-terminal region (residue 250 – 300) is highly enriched in acidic residues, but has poor sequence conservation and lacks any clustering of conserved hydrophobic residues similar to that seen in the W3 and the WF motifs.

I expressed and purified an ADX construct spanning MDMX residues 181 – 300 that contains the conserved W3 and WF motifs (Figure 4.1). Since the ADX has not been

previously characterized except for the W3 motif, I first tested whether the ADX adopts any secondary structure by CD spectropolarimetry. The CD spectra of intrinsically disordered proteins have a negative band at ~ 200 nm and an ellipticity close to zero at 222 nm, features that are distinct from folded proteins and which make it possible to identify partially or fully disordered proteins (Chemes, Alonso, Noval, & de Prat-Gay, 2012). The CD spectrum of ADX exhibited a strong negative band below 200 nm, suggesting that ADX contains a significant proportion of disordered content (Figure 4.3B). The CD spectrum also clearly shows a negative band at 222 nm, which is consistent with an α-helical contribution. The negative band at 208 that would also be expected is not apparent and is likely obscured by the presence of β-sheet content in the protein that may allow signal averaging near this wavelength. To estimate the secondary structure content for ADX, the CD data was further analysed by using the BeStSel web server (Micsonai et al, 2018). From this analysis, the ADX is estimated to be composed of ~ 47 % disordered structure, ~ 30 % helical and turn-like structures, and ~24 % β-sheet structure. It should be noted that the BeStSel algorithm is designed to accurately determine β-sheet content for folded proteins and the authors stated that spectra of disordered proteins could be biased towards antiparallel β-sheets, which lead to higher β-sheet structure content in disordered proteins (Micsonai et al, 2018).

To characterize the ADX in more depth, I performed NMR experiments on the ADX (Figure 4.3, C). The ^{1}H-^{15}N HSQC spectrum was dominated by signals clustered in a narrow region (~ 1 ppm) in the proton dimension, which is characteristic of an intrinsically disordered protein. Of note, two signals were very distinct from the remaining signals of the spectrum and could be easily assigned to W201 and F202 based on previously

published data for the W3 motif (residue 181 – 209) (Bista M. et al, 2013). To elucidate the structural features of ADX, I performed chemical shift assignment to identify and assign the ^{1}H, ^{15}N, $^{13}C_{\alpha}$, $^{13}C_{\beta}$ and $^{13}C'$ chemical shifts for each residue (Table 4.1 and 4.2). The data were further analysed using the δ2D webserver to determine the secondary structure populations of individual amino acids as a function of the protein sequence (Camilloni, De Simone, Vranken, & Vendruscolo, 2012). The chemical shift data are consistent with a scenario where ADX is an intrinsically disordered region, as the sequence has significant random-coil propensity (up to 85%) (Figure 4.4). Moreover, the δ2D analysis revealed significant amounts of residual structure in the ADX. The sequences spanning residues 199 – 206 and 237 – 242, which belong to the W3 and WF motifs, adopt α-helical character (up to 30% and 10% for W3 and WF motifs). In addition, extended β character and polyproline II (PPII) structure are observed throughout most of the protein sequence (up to 30% and 15%, respectively). Of note, the W3 and WF motifs lack the extended β character and PPII structure. The result suggests that, although the ADX is flexible, it has a propensity for adopting an extended structure, whereas the W3 and WF motifs are relatively more compact.

4.3.2 The ADX directly binds the PBD2 through the W3 and the WF motifs

To determine whether ADX can directly interact with PBD2, I carried out ITC experiments. I found that the ADX can indeed directly bind to the PBD2 with a K_d of ~ 6.8 μM (Figure 4.6, B). Noticeably, a significant heat of dilution was observed when ADX was titrated into buffer, suggesting that the protein might exist as oligomers at higher concentration (Figure 4.6, A). To further characterize the interaction between the PBD2

and the ADX, I acquired a ^{1}H-^{15}N HSQC spectrum of the ADX in presence of 2 molar excess of PBD2 (Figure 4.5). Under these conditions, significant resonance broadening was observed for 25 consecutive non-proline amino acids spanning residues 187 – 211, which encompasses the W3 motif (Figure 4.6, C). NMR signals of the WF motif, specifically the sequence spanning residues 239 – 242, were also broadened in the PBD2-bound state (Figure 4.6, C). The average cross-peak intensities for the residues of the W3 and WF motifs in the PBD2-bound state are consistently less than 30% of those in the PBD2-free state, indicating that these residues experience chemical exchange near the intermediate timescale. This suggests that, even in the bound state, the W3 and WF motifs were not stabilized in a single bound conformation. On the other hand, a significant fraction of C-terminal region (residues 250 – 300) did not show any difference between the free and bound forms indicating a lack of involvement in the interaction with PBD2.

4.3.3 The WF motif directly interacts with the PBD2

To evaluate whether the changes in resonances of the WF motif are caused direct binding to the PBD2, I first tested an ADX construct containing W200A & W201A mutations (ADX_{AA}) to disrupt the binding of the W3 motif to the PBD2. This strategy was based upon the fact that the W3 motif was found to bind the hydrophobic cleft of PBDX with the hydrophobic side-chains of W200 and W201, forming the primary driving force for the interaction between the W3 motif and PBDX (Bista et al., 2013). I collected and compared the ^{1}H-^{15}N HSQC spectrum of the ADX_{AA} to that for the WT ADX. Substitution of the two consecutive tryptophan residues by alanine resulted in a striking difference in the spectrum, with many cross-peaks from the segment spanning residues 198 – 213 not

assignable by direct comparison (Figure 4.7, A and Figure 4.8, A). The difference in signal pattern is likely attributable to the hydrophobic and aromatic nature of the tryptophan residues, which could potentially promote local interactions and secondary structuring within or between ADX molecules through hydrophobic or π-π interactions. Indeed, ITC showed that ADX at high concentration could potentially be forming oligomers that dissociate upon dilution (Figure 4.6, A), supporting the idea that the ADX might exist as higher order oligomers at the concentration (380 μM) used for the NMR experiments. On the other hand, the C-terminal half (residue 250 – 300) experiences little change upon mutation and was presumably not involved in the self-association process.

In order to identify the residues of the ADX_{AA} that potentially be involved in the interaction with PBD2, a ^{1}H-^{15}N HSQC spectrum of the ^{15}N-ADX_{AA} in presence of 2 molar excess of the PBD2 was acquired (Figure 4.7, B). The WF motif, specifically residues 240 – 242 experienced chemical shift perturbations and resonance broadening upon addition of 2 molar excess of the PBD (Figure 4.8, B). However, the changes experienced by the WF motif are minor suggesting that the WF motif could only weakly interact with the PBD2. Importantly, significant difference was also observed for the W3 motif despite the fact that the two crucial tryptophan residues were mutated to alanine, indicating that additional residues from the W3 motif are involved in establishing the interaction with the PBD2. Unfortunately, due to the significant change in the cross-peak pattern caused by W200A & W201A mutation, many of the cross-peak belonging to the W3 motif could not be assigned using the WT ADX assignment and prevented further analysis.

To further characterize the interaction between the WF motif and the PBD2, I produced a W3 motif-deletion construct (ADXD; residues 211 – 300) (Figure 4.1).

Comparison of the ^{1}H-^{15}N HSQC spectra of the ADXD and the ADX_{AA} showed minor differences near the WF motif whereas most cross-peaks from the ADXD overlapped with the ADX_{AA} counterpart but different from the WT ADX, suggesting that W200A & W201A mutations cause dramatic change to both W3 and W1 motifs (Figure 4.9, A and 4.10, A). This result indicates the W200 and W201 residues likely have additional function such as controlling the local structuring of the ADX, specifically the W3 and W1 motifs. The ^{1}H-^{15}N HSQC spectrum of ADXD in the presence of equimolar of the PBD2 showed modest chemical shift changes for the WF motif (Figure 4.9, B and 4.10, B). Further ITC experiment showed heat signatures that did not yield a clear binding isotherm, suggesting that the ADXD bind only weakly to the PBD2 (Figure 4.12, C).

To further examine this interaction, I acquired ^{1}H-^{15}N HSQC spectra for the PDB2 in the absence and presence of 3 molar excess of ADXD (Figure 4.11). Direct comparison of the spectra showed modest chemical shift changes for many signals, in agreement with a weak interaction between the ADXD and the PBD2. To determine the location of the potential binding site for the ADXD, triple-resonance experiments were carried out, allowing chemical shift assignment to identify the residues that underwent significant chemical shift changes upon ADXD binding (Tables 4.1 and 4.2). Unfortunately, I was not able to achieve full assignment owing to poor spectral quality. Despite these challenges, many residues that underwent chemical shift changes when bound to the ADXD could be identified. Visible chemical shift changes were mainly observed for residues near the p53-binding cleft, suggesting that the ADXD directly binds to PBD2 and likely competes with the TD (Figure 4.12, A and B).

4.3.4 The ADX effectively competes with TD for binding to the PBD2

To further evaluate the interaction between the ADX and PBD2, I carried out ^{1}H-^{15}N HSQC experiments for the ^{15}N-labeled PBD2 in the absence and presence of 3 molar excess of either the ADX or TD. Addition of the ADX or the TD led to significant resonance broadening for majority of the dispersed PBD2 signals belonging to the structured region and only the signals for the residues from the disordered region were visible (Figure 4.13 and 4.14). This observation is very different from the spectrum for the PBD2 in presence of the ADXD (Figure 4.11). The results suggest that neither TD nor ADX bind to form a stable complex with the PBD2, which instead likely sampling multiple conformations that exchange at the intermediate timescale. Moreover, significant spectral overlap was observed between PBD2 in complex with the ADX or the TD (Figure 4.15), suggesting that the two proteins may occupy the same binding site on the PBD2 (i.e. the canonical p53 binding pocket).

To test whether the ADX could inhibit the TD-PBD2 interaction, I acquired a ^{1}H-^{15}N HSQC spectrum of the ADX in the presence of equimolar PBD2 and 1.5 times molar excess of TD. Remarkably, the spectrum completely overlapped the spectrum of the ADX in the free state (Figure 4.16), indicating that the TD binds the PBD2 with higher affinity and effectively blocks the interaction between the ADX and the PBD2. The X-ray crystal structure of the PBD2-TD complex showed that the TD specifically binds to the hydrophobic cleft of PBD2 (Kussie et al., 1996). Thus, disruption of the interaction with the ADX suggests that the hydrophobic cleft is likely to be the binding site for the ADX. To determine whether the ADX could compete with the TD, I conducted ITC experiments

by titrating the TD into the pre-existing ADX-PBD2 complex. Indeed, the binding affinity for the TD towards the PBD2 in the presence of the ADX is dramatically reduced (~ 18-fold, $K_d \approx 3.6$ μM as compared to $K_d \approx 210$ nM), suggesting that the ADX can compete with the TD for PBD2 binding (Figure 4.17, A and B).

4.4 Discussion

I have shown that a significant portion of the central region of MDMX, which encompasses the acidic domain, is disordered but displays some degree of α-helical character near the W3 motif. Furthermore, I have identified a highly conserved motif (the W1 motif) that is located C-terminal to the previously characterized W3 motif. Based on the previous finding that the W3 motif could form an intramolecular interaction with the PBDX, I hypothesized that the same region will also bind to the MDMX homolog MDM2. Indeed, I found that the ADX can directly interact with the PBD2. My results demonstrate that both of the conserved motifs, W3 and WF, from ADX can interact with the PBD2. I further showed that the ADX can directly compete with the TD of p53 for binding to the PBD2. My data suggest that the WF motif likely binds to the PBD2 with very low affinity. It must be noted that the WF motif contains a few conserved threonine and serine residues that could potentially be phosphorylated. It is possible that upon phosphorylation the WF motif could bind more tightly to the PBD2. Together, my results demonstrate that the W3 and WF motifs from the ADX are likely to have direct roles in modulating the activity of both MDM2 and MDMX.

The dual motifs within the MDMX acidic domain suggests that the affinity for PBDX will likely be stronger than the value reported previously with only the W3 motif.

Importantly, my results suggest that MDMX could potentially suppress the activity of MDM2 by forming an inactive complex through the PBD2-ADX interaction to prevent p53 binding. Moreover, the affinity of this intermolecular interaction is likely to be strengthened as MDMX and MDM2 could form a high affinity heterodimer through their C-terminal RING domains (Kostic, Matt, Martinez-Yamout, Dyson, & Wright, 2006). It is also possible that PBD2 and PBDX could simultaneously bind to the W3 and WF motifs, further suppressing the activity of MDMX-MDM2 heterodimer. It is well acknowledged that MDMX is responsible for maintaining a basal pool of inactive p53 (Jackson & Berberich, 2000). The current findings suggest that this ability might be achieved through sequestering of MDM2 by the acidic domain of MDMX to prevent its interaction with p53, which provides a possible explanation for several studies showing that MDMX can inhibit MDM2-mediated p53 degradation (Jackson & Berberich, 2000; Mancini et al., 2004; Stad et al., 2001).

The highly disordered structure of the ADX in combination with the dual motifs suggest that ADX is likely to be a potential binding site for other proteins besides MDMX and MDM2. A previous study showed that the portion of MDMX comprising residues 128 - 444, which encompass the ADX and the Zinc figure domain, directly interacts with Smad to inhibit its transcriptional activity (Kadakia, Brown, McGorry, & Berberich, 2002). Moreover, this study reported that p300 could bind to and sequester this MDMX fragment to activate Smad. These results point to the possibility that the ADX could bind to both Smad and p300. Chen and coworkers showed that, under normal conditions, the ADX binds to casein kinase 1α (CK1α) and phosphorylates S289, which stimulates the MDMX-p53 interaction (Chen, L. et al., 2005; Wu et al., 2012). In contrast, DNA damage disrupted

the CK1α–MDMX interaction and, in turn, resulted in p53 release from the complex. More recently, Wei et al. (2016) reported that the ADX can directly bind to the p53 DNA-binding domain to regulate DNA binding, and that the interaction is further cooperatively stabilized with CK1α. Thus, the ADX is likely to have many important functions inside the cell.

It has been shown that the PBDX can be phosphorylated at Y99 by the stress activated kinase c-Abl, with the phosphate group structurally restraining the interaction with the TD of p53 by imposing steric clashes at its hydrophobic pocket (Chen, X. et al., 2016). Thus, phosphorylation in this manner would be likely to inhibit the intramolecular interaction with its own ADX, as the interaction is similarly mediated through the binding of ADX to the hydrophobic cleft of PBDX (Bista et al., 2013). Hence, phosphorylation of Y99 on MDMX PBD likely has dual effects: first to inhibit the direct interaction between MDMX and p53 and second to inhibit the direct interaction between MDMX and ADX, resulting in enhanced MDM2-ADX interaction.

In combination with the literature findings, our results have led to the following model of for p53 activation (Figure 4.18). Under normal condition, p53 is inhibited by MDM2 and MDMX heterodimer and CK1α stably associates with the ADX, preventing it from interacting with the PBD. In response to stress, CK1α dissociates from the ADX and promote it to interact with the PBD of MDM2 or MDMX and weakens the interaction with p53. Y99 phosphorylation of MDMX by c-abl inhibits the intramolecular interaction between ADX and its own PBD. The ADX can then freely interact with MDM2, which can be brought into in spatial proximity through the formation of a heterodimer by the C-terminal RING domains (Linke et al., 2008). Together, this could greatly weaken the interaction between the MDM2-MDMX heterodimer and p53. Meanwhile, transcription

coactivators could come into play to bind the TD and outcompete the MDM2-MDMX heterodimer to promote p53 activation and trigger downstream signaling.

Table 4.1: Chemical shift assignment reports.

ADX	
Atom type	**Assignment**
H_N*	116/117 (99%)
$N^{\perp}$	116/117 (99%)
C'	118/120 (98%)
C_α	118/120 (98%)
C_β	107/111 (96%)
PBD2	
Atom type	**Assignment**
H_N*	92/120 (77%)
$N^{\perp}$	92/120 (77%)
C'	85/125 (68%)
C_α	96/125 (77%)
C_β	89/119 (75%)
Atom type	

* N-terminal HN was excluded.

⊥ Proline residues and N-terminal N were excluded.

Table 4.2: PANAV assessment reports for chemical shift assignments.

ADX (H_N, N, C_α, C_β, and CO)		
CONA Score (6-Resdue Scan)	1.00	> 0.95
Detected reference offsets	N: -0.55 ppm C_α: -0.61 ppm C_β: 0.52 ppm CO: -0.51 ppm	N: < ±1.5 ppm C_α: < ±1.0 ppm C_β: < ±1.0 ppm CO: < ±1.0 ppm
Number of assignments	575	
Number of deviant assignments	0	
Number of suspicious assignments	0	
PBD2 (H_N, N, C_α, C_β, and CO)		
CONA Score (6-Resdue Scan)	1.00	> 0.95
Detected reference offsets	N: 0.53 ppm C_α: -0.69 ppm C_β: 0.57 ppm CO: -0.32 ppm	N: < ±1.5 ppm C_α: < ±1.0 ppm C_β: < ±1.0 ppm CO: < ±1.0 ppm
Number of assignments	463	
Number of deviant assignments	0	
Number of suspicious assignments	1	F55 CB: 32.93

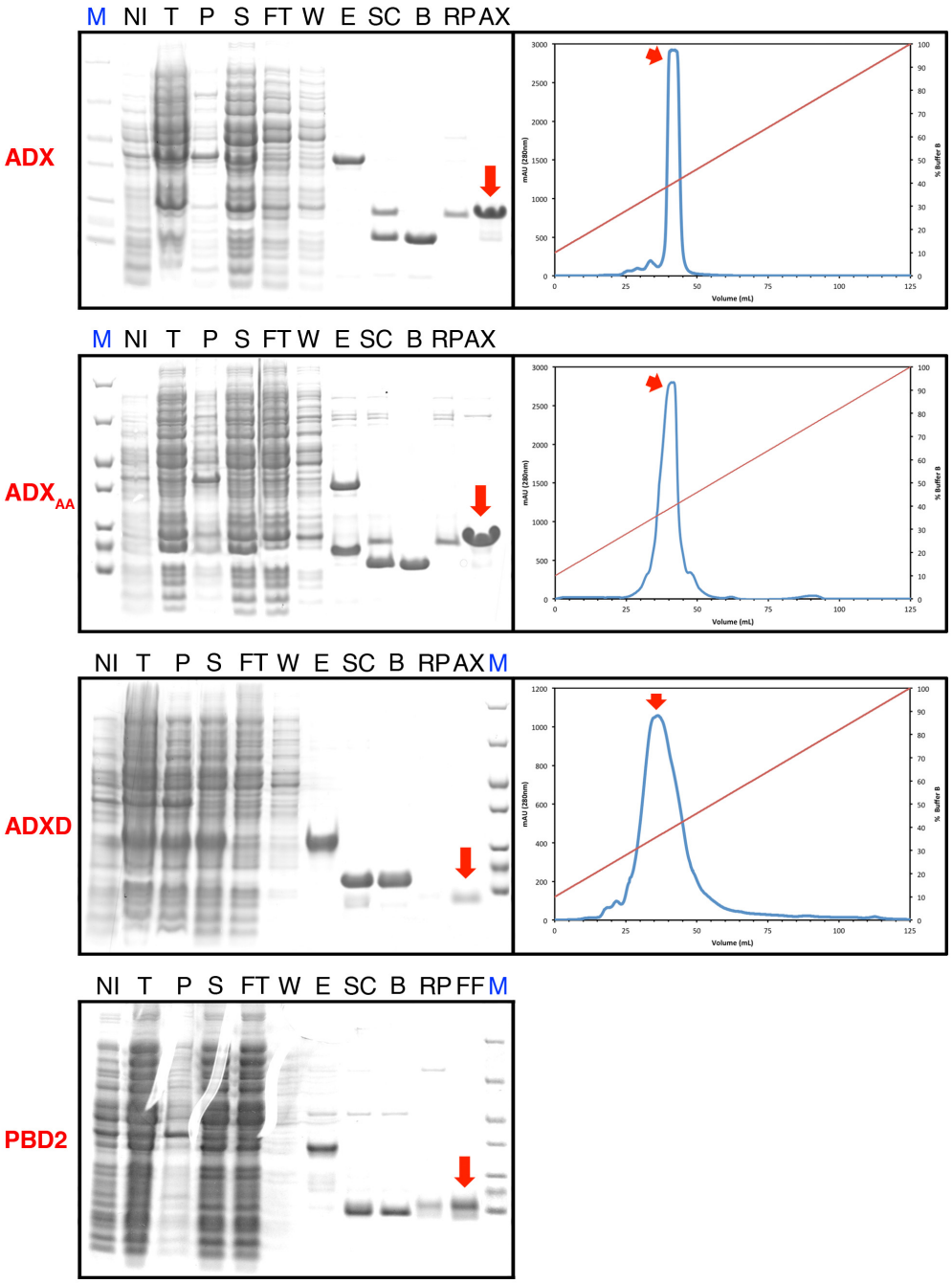

M: Protein ladder, top to bottom: 116 kDa, 66 kDa, 45 kDa, 35 kDa, 25 kDa, 18.4 kDa, 14.4 kDa
NI: Non-induced, T: Total protein, P: Pellet, S: Supernatant, FT: Flow through, W: Wash, E: Elution,
SC: SUMO cleavage, B: Beads, RP: Reverse purification, AX: Anion exchange elution, FF: FPLC flow through

Figure 4.1: Expression and purification of recombinant proteins used in chapter 4. The gel pictures and chromatograms showed representative purification process of ^{15}N-labelled ADX, ^{15}N-labelled ADX$_{AA}$, ^{15}N-labelled ADXD and ^{15}N-labelled PBD.

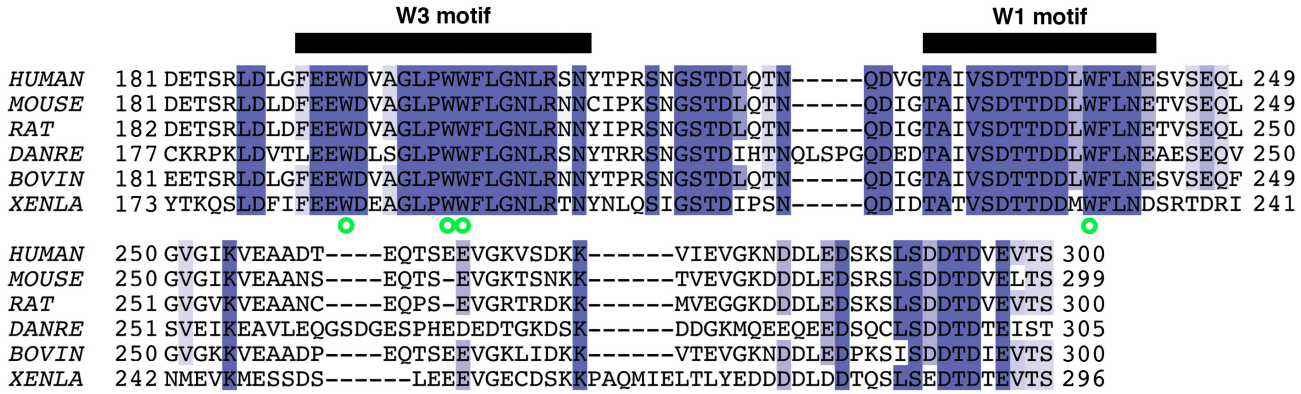

Figure 4.2: Multiple sequence alignment of the MDMX acidic domain from six different species. The W3 and WF motifs are delineated by black bars and the conserved tryptophan residues are indicated with green circles.

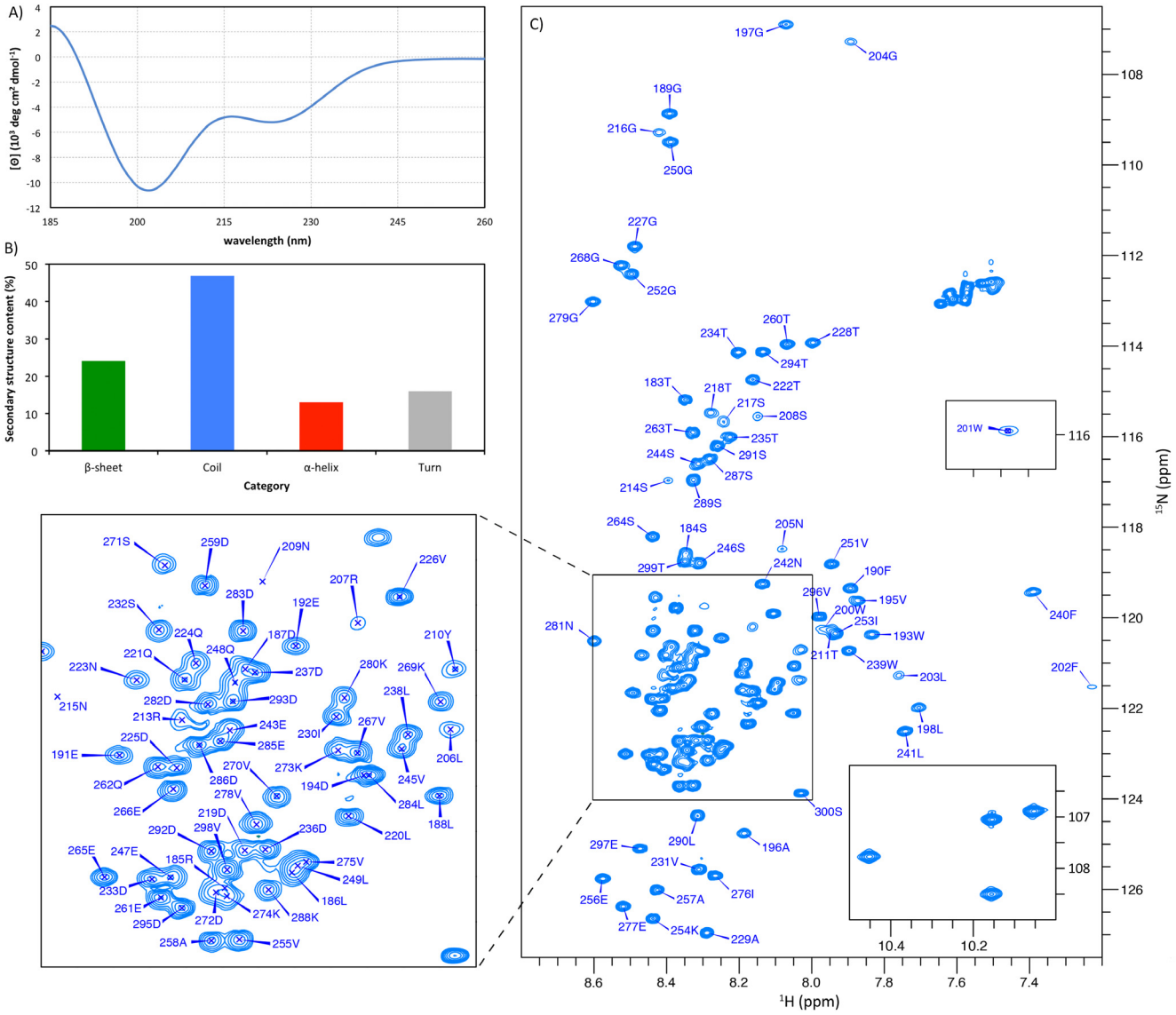

Figure 4.3: CD and NMR analysis revealed the ADX as a disordered region. A) Far-UV CD spectrum of ADX. B) Bar graph showing the percentage of secondary structural elements for the ADX calculated using the BeStSel webserver based on the CD data. C) Assigned ^{1}H-^{15}N HSQC spectrum of the ADX.

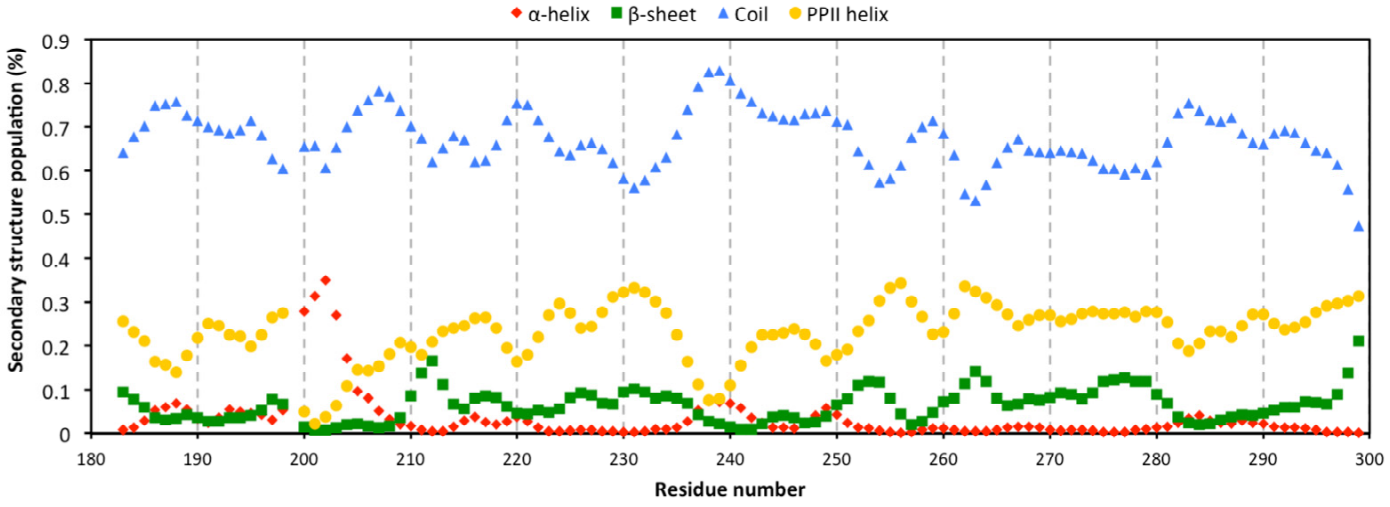

Figure 4.4: Secondary structure population of the ADX as a function of amino acid residue. The secondary structure population was calculated using the δ2D webserver based on the backbone chemical shifts (H_N, N, C', C_α) and C_β shifts. Red diamond: α-helix; green square: β-sheet; yellow circle PPII helix and blue triangle: random coil.

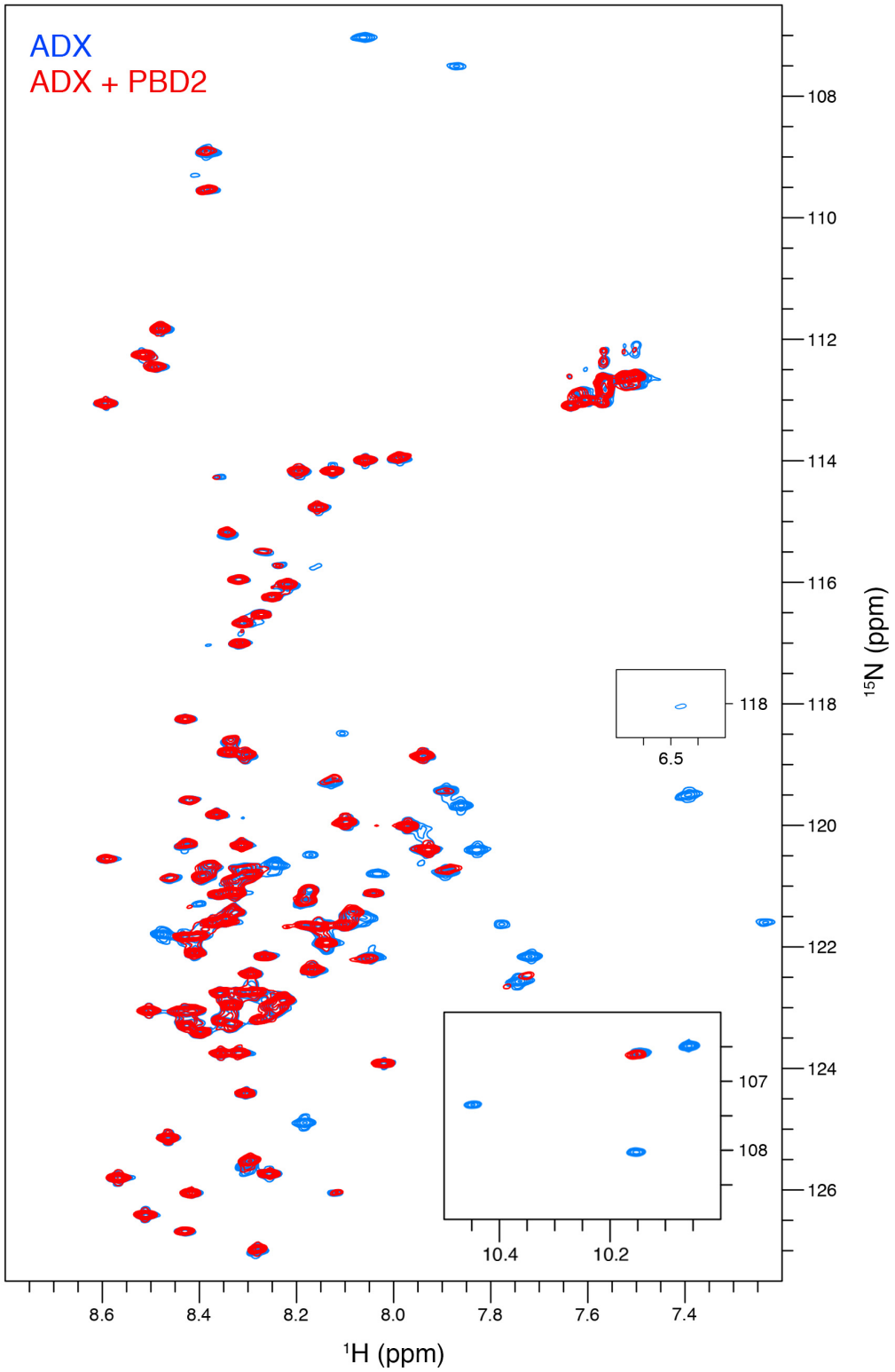

Figure 4.5: ^{1}H-^{15}N HSQC spectra for the ADX in the presence and absence of the PBD2.

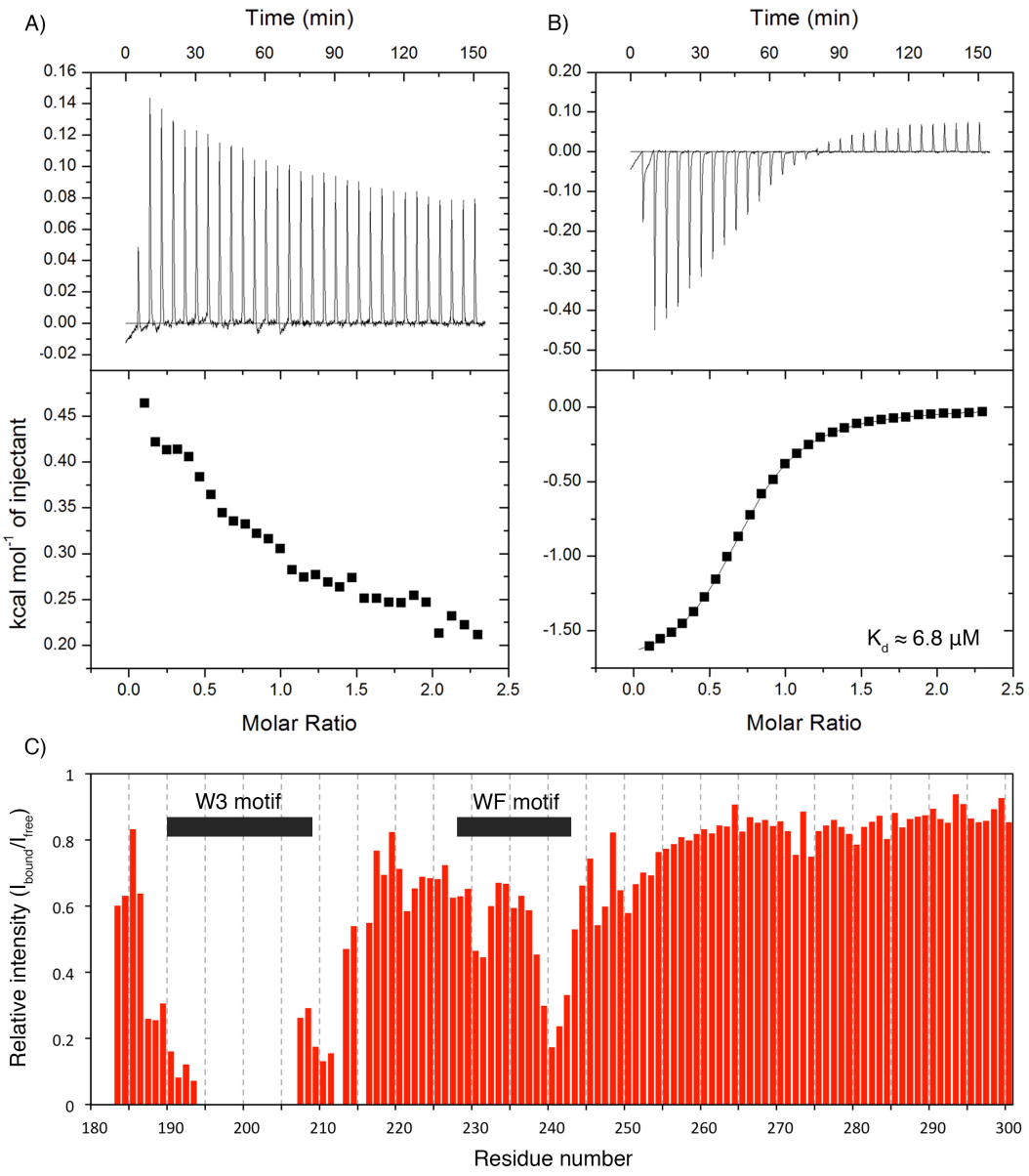

Figure 4.6: Thermodynamic and backbone-level characterization of the interaction between ADX and PBD2. A) ITC analysis showing the dilution heat upon injection of ADX into buffer. B) ITC analysis of ADX interaction with PBD2. C) Intensity ratio of the backbone amide cross-peaks of ADX in the presence vs. absence of PBD2, with the locations of the W3 and W1 motifs delineated.

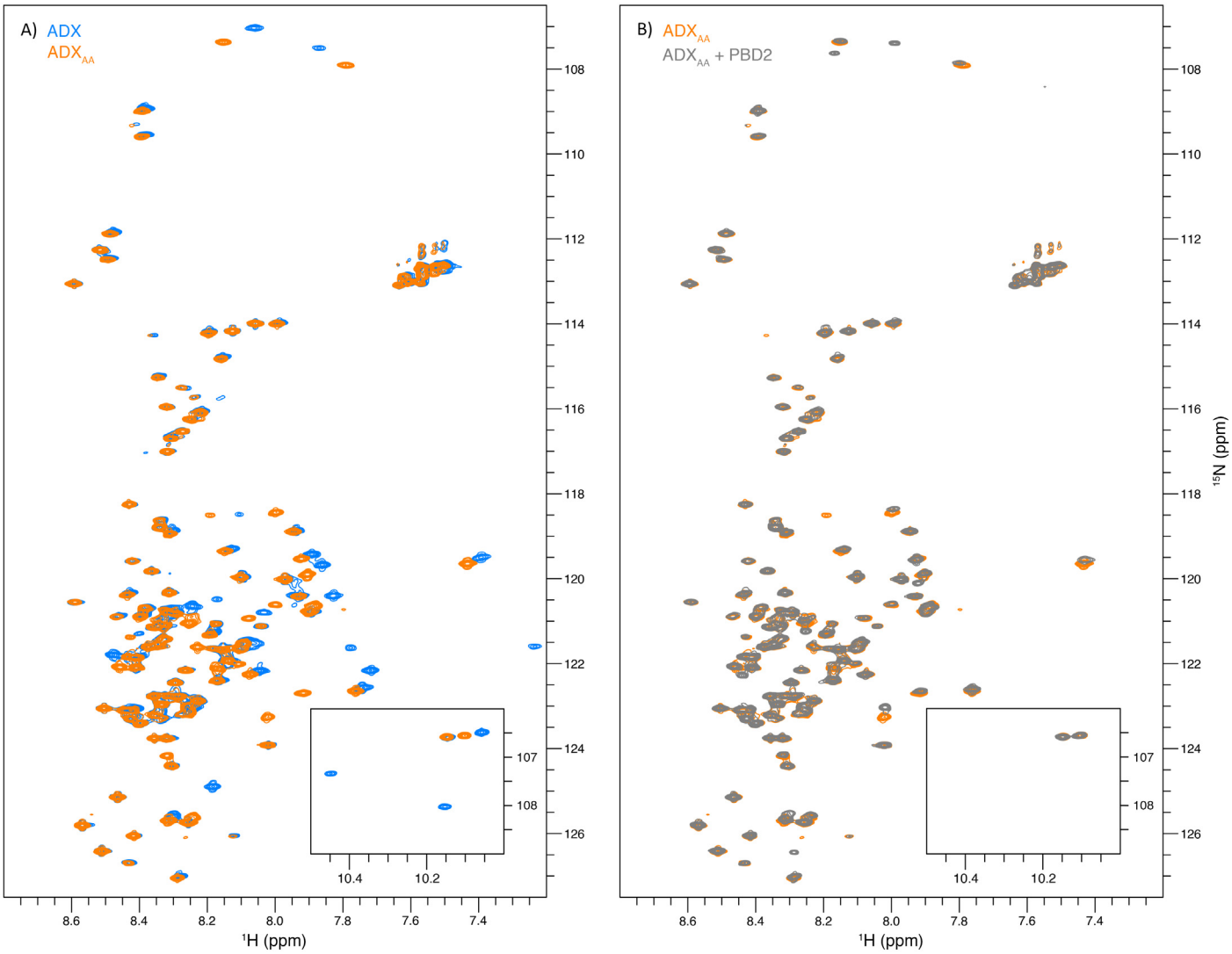

Figure 4.7: Comparison of the ^{1}H-^{15}N HSQC spectra of the ADX_{AA} with the ADX or the ADX_{AA} when bound to the PBD2. A) Comparison of the ^{1}H-^{15}N HSQC spectra for the ADX (blue) and ADX_{AA} (orange). B) Comparison of the ^{1}H-^{15}N HSQC spectra for the ADX_{AA} in the presence (grey) and absence (orange) of 2 molecular excess of the PBD2.

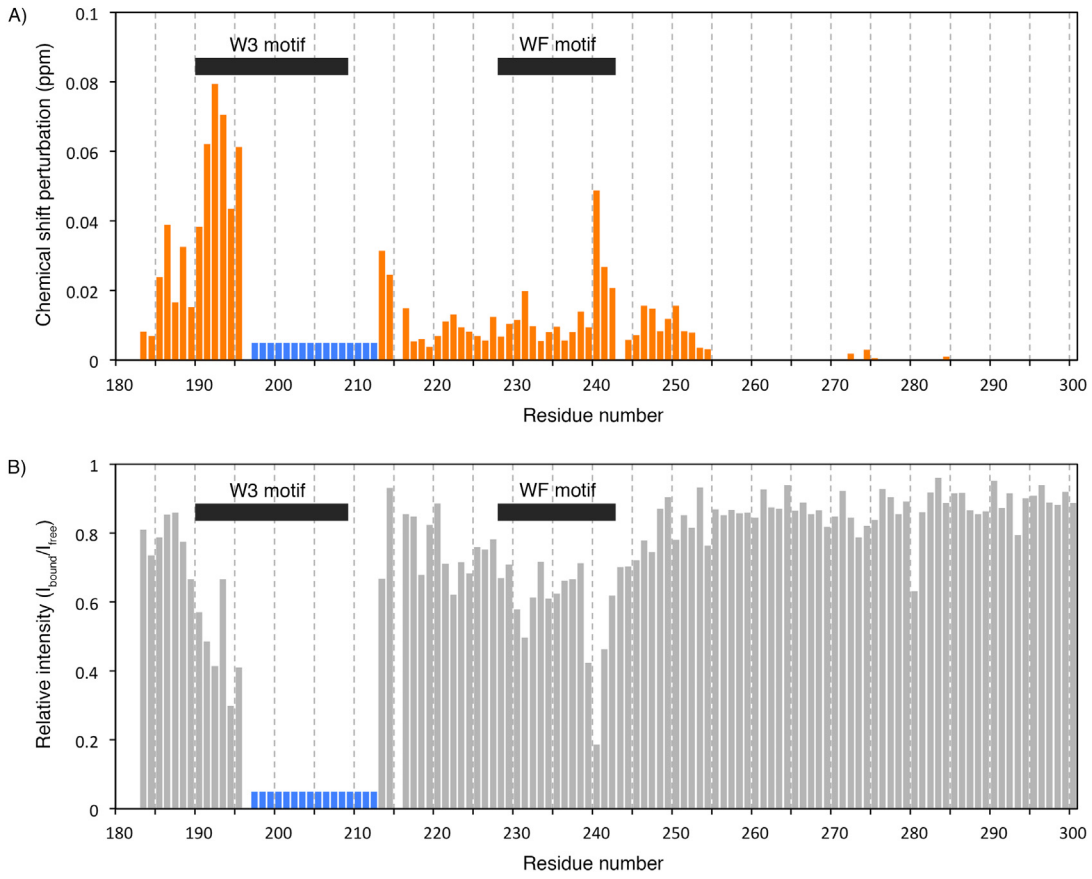

Figure 4.8: Sequence specific analysis of the NMR data for the ADX_{AA}. A) Chemical shift difference for the ADX_{AA} in comparison to the ADX. B) Intensity differences for the cross peaks of the ADX_{AA} in the presence and absence of 2 molar excess PBD2. W3 and WF motif were indicated with black bars. ADX_{AA} residues that cannot be assigned based on the assignment from the ADX were indicated with blue bars.

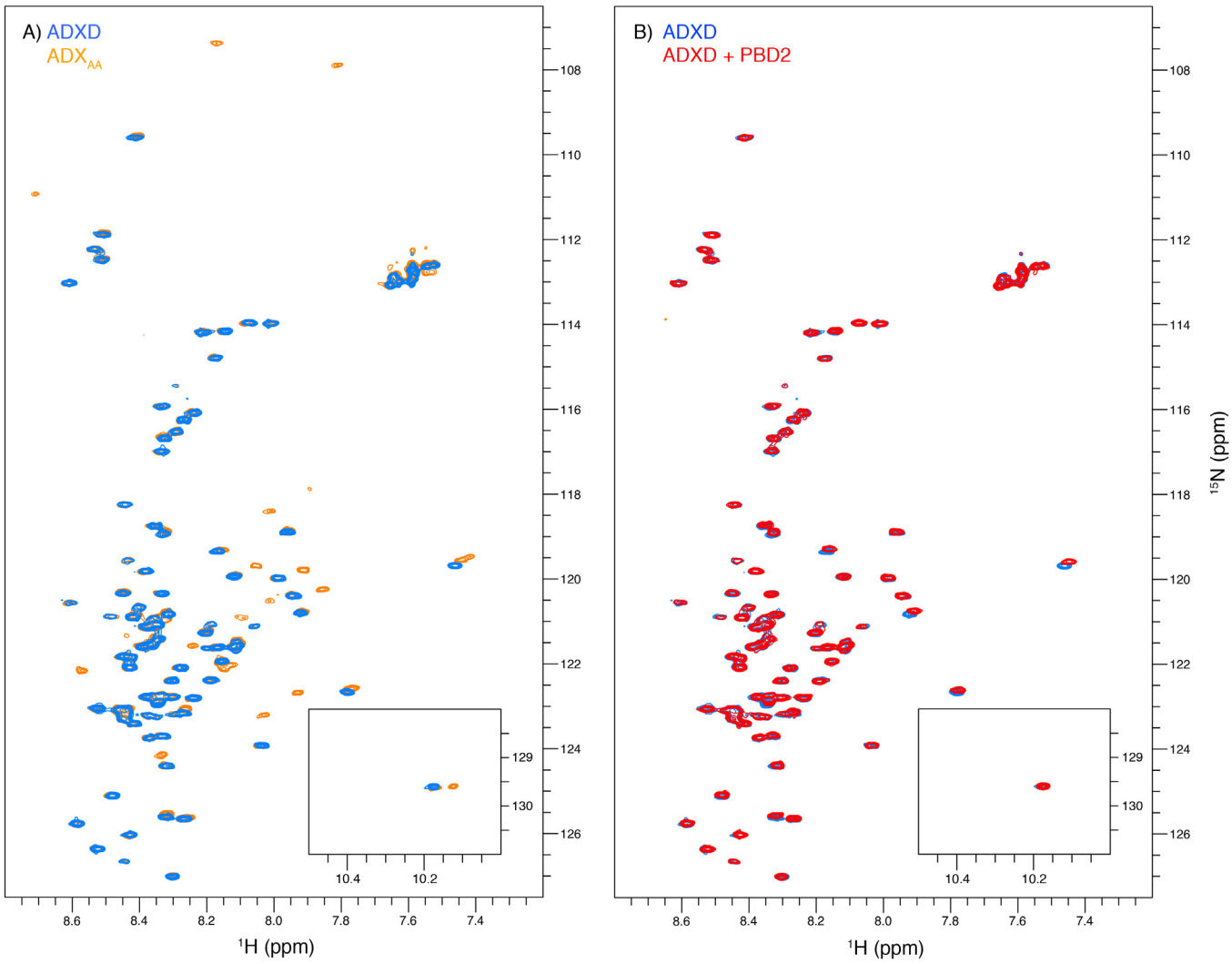

Figure 4.9: Comparison of the ^{1}H-^{15}N HSQC spectra for the ADXD with the ADX$_{AA}$ or the ADXD in the presence of the PBD2. A) Comparison of the ^{1}H-^{15}N HSQC spectra for the ADXD (blue) and ADX$_{AA}$ (orange). B) Comparison of the ^{1}H-^{15}N HSQC spectra for the ADXD in the presence (red) and absence (blue) of 2 molecular excess of the PBD2.

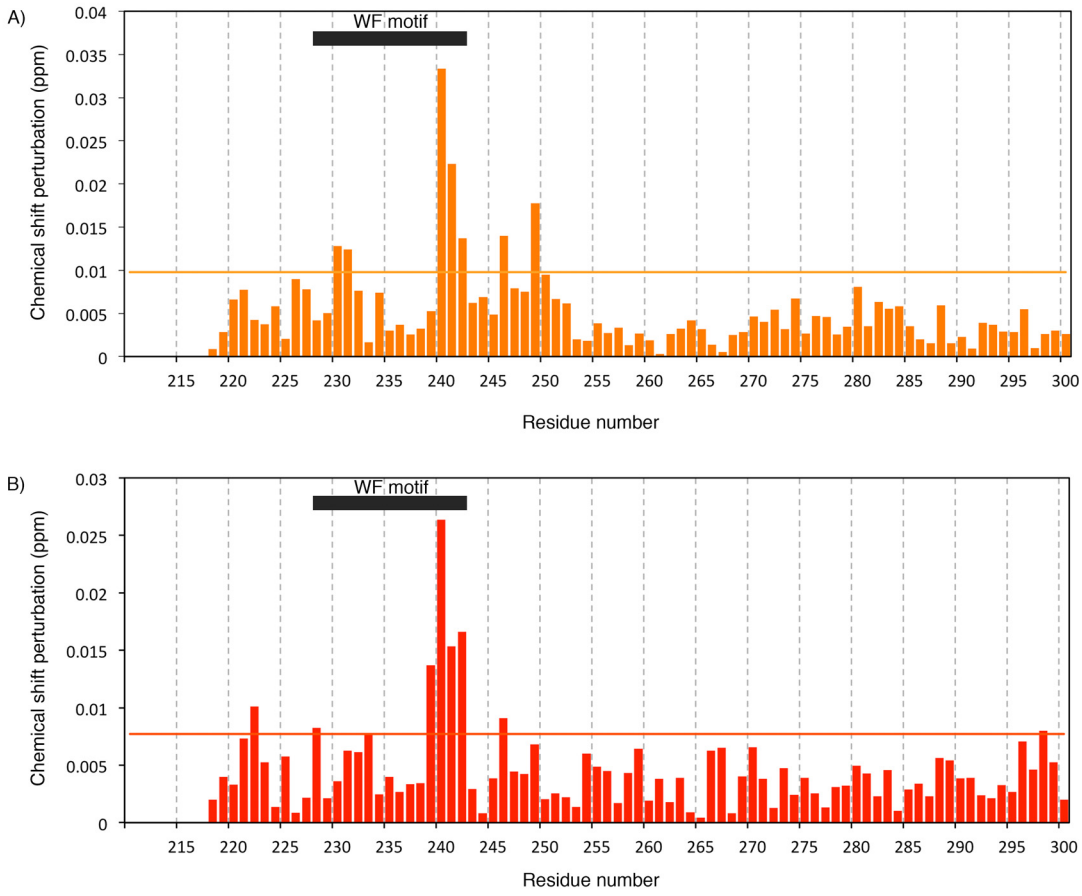

Figure 4.10: Sequence specific analysis of the NMR data for the ADXD. A) Chemical shift perturbation for the ADXD in comparison to the ADX_{AA} and B) Chemical shift perturbation for the ADXD in the presence and absence of 1.1 molar excess PBD2. WF motif was indicated with a black bar.

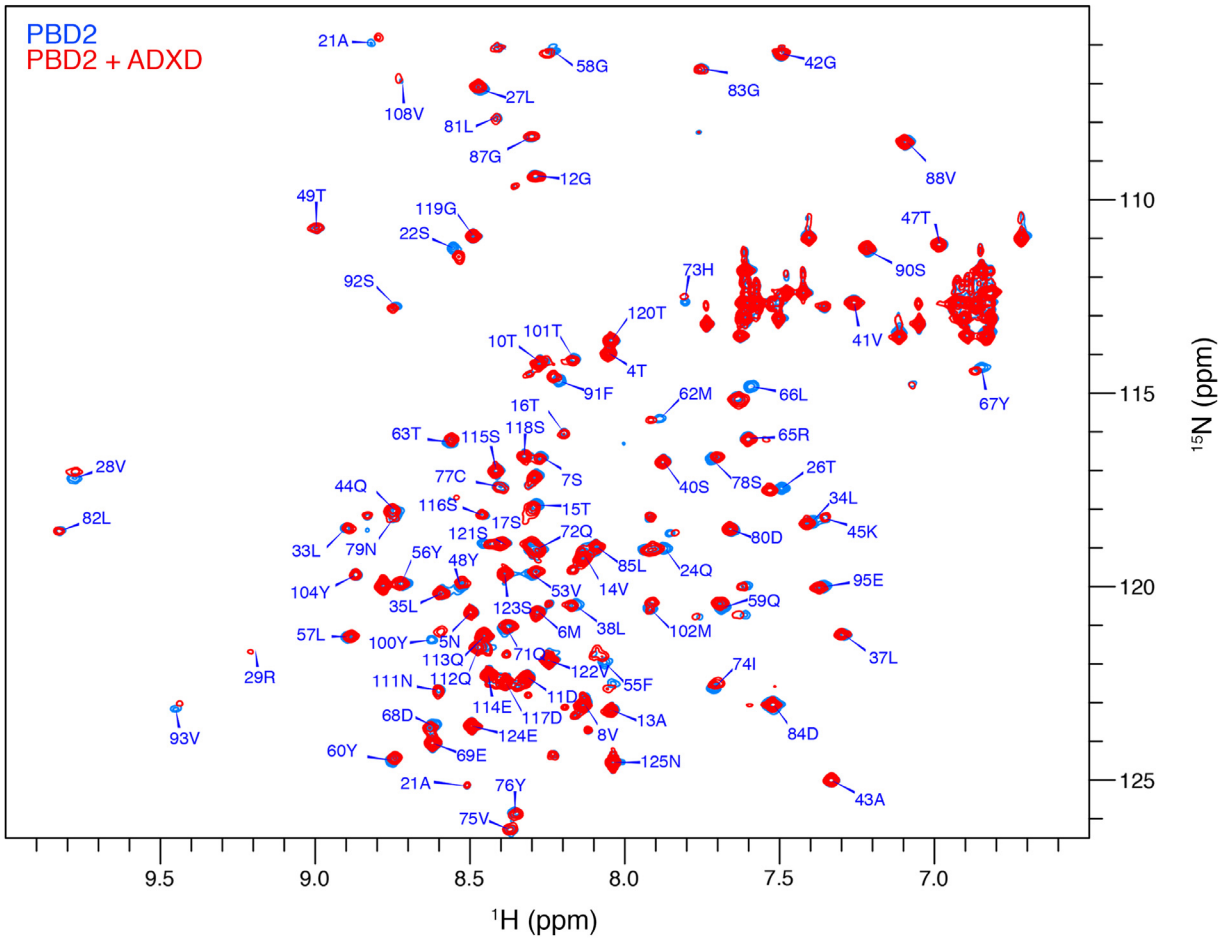

Figure 4.11: Comparison of the ^{1}H-^{15}N HSQC spectra of PBD2 in the presence and absence of ADXD.

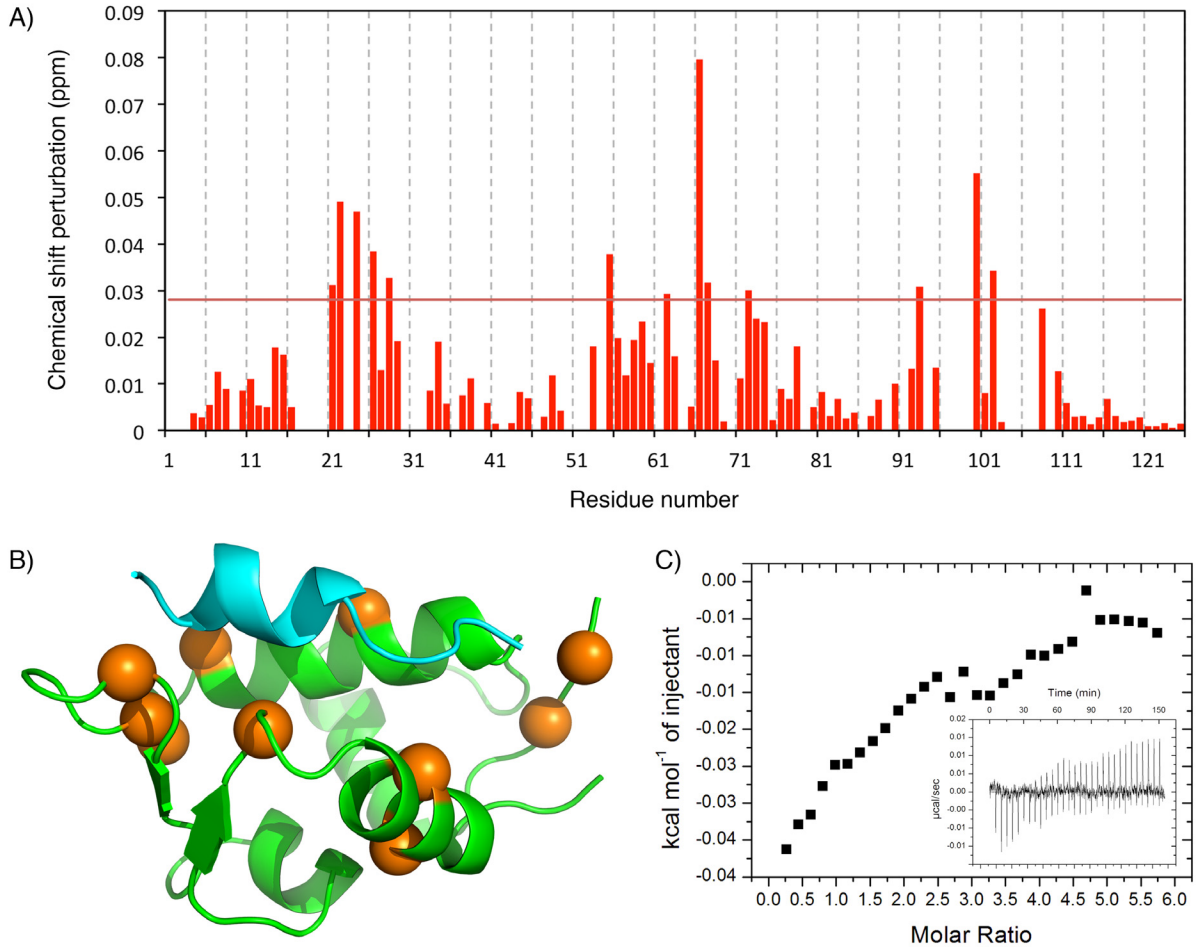

Figure 4.12: Probe the interaction between the ADXD and the PBD2. A) Analysis of chemical shift changes experienced by the individual residues from the PBD2 when bound to the ADXD. B) Mapping of the residues that underwent most significant chemical shift changes onto the crystal structure of an MDM2-p53 complex (Kussie et al., 1996. PDB ID: 1YCR). The MDM2 PBD and the p53 peptide were coloured green and cyan respectively. C) ITC analysis of interaction between the PBD2 and the ADXD.

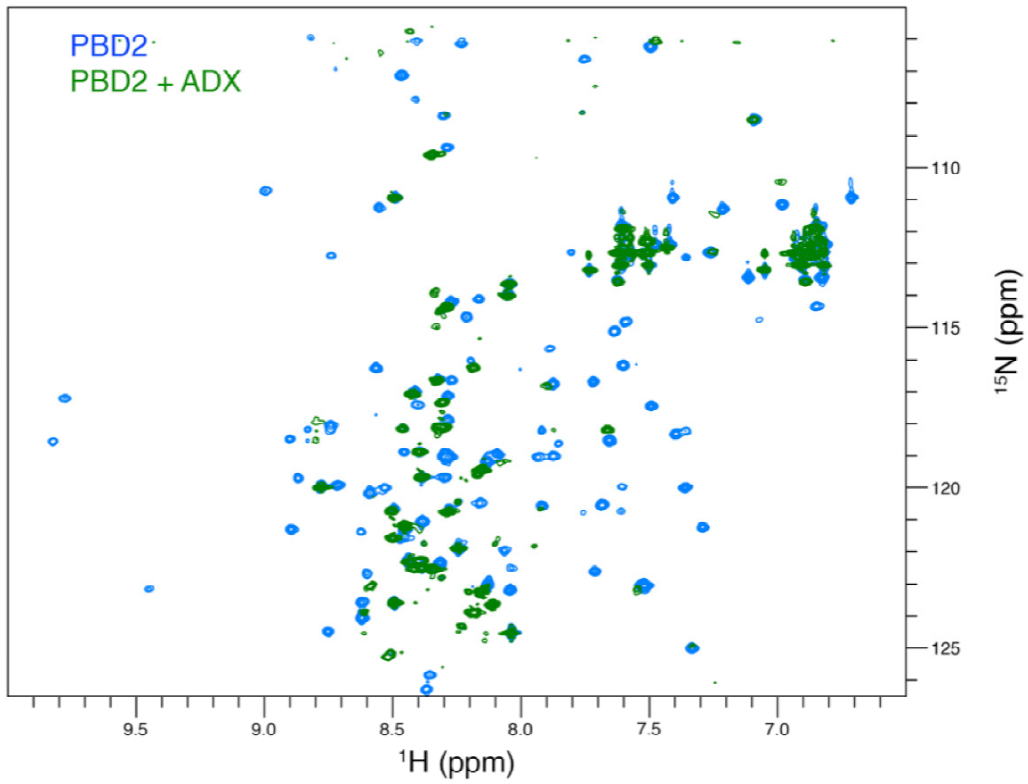

Figure 4.13: Comparison of the ^{1}H-^{15}N HSQC spectra of PBD2 in the presence and absence of the ADX.

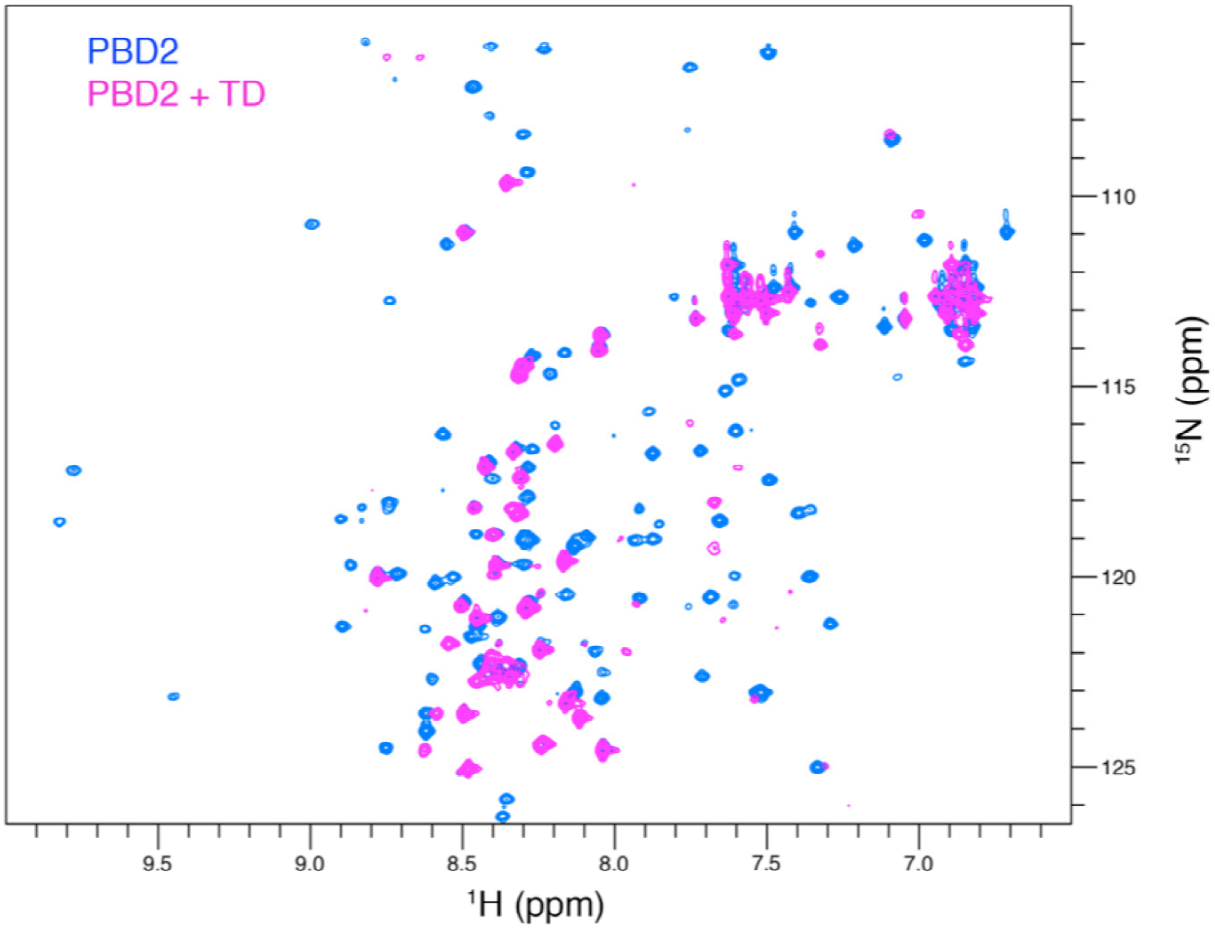

Figure 4.14: Comparison of the ^{1}H-^{15}N HSQC spectra of PBD2 in the presence and absence of the TD.

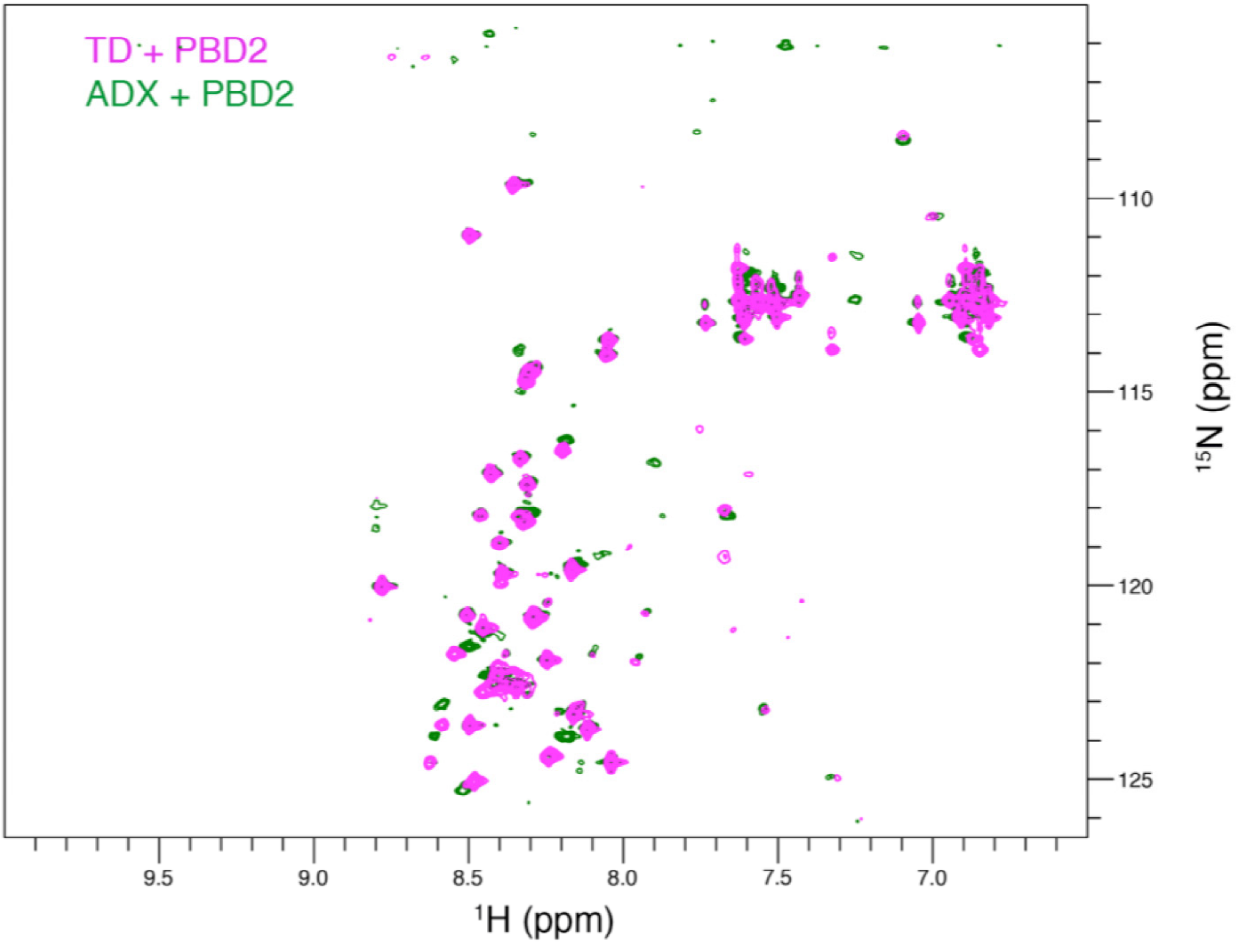

Figure 4.15: Comparison of the ^{1}H-^{15}N HSQC spectra of PBD2 in the presence of the ADX or the TD.

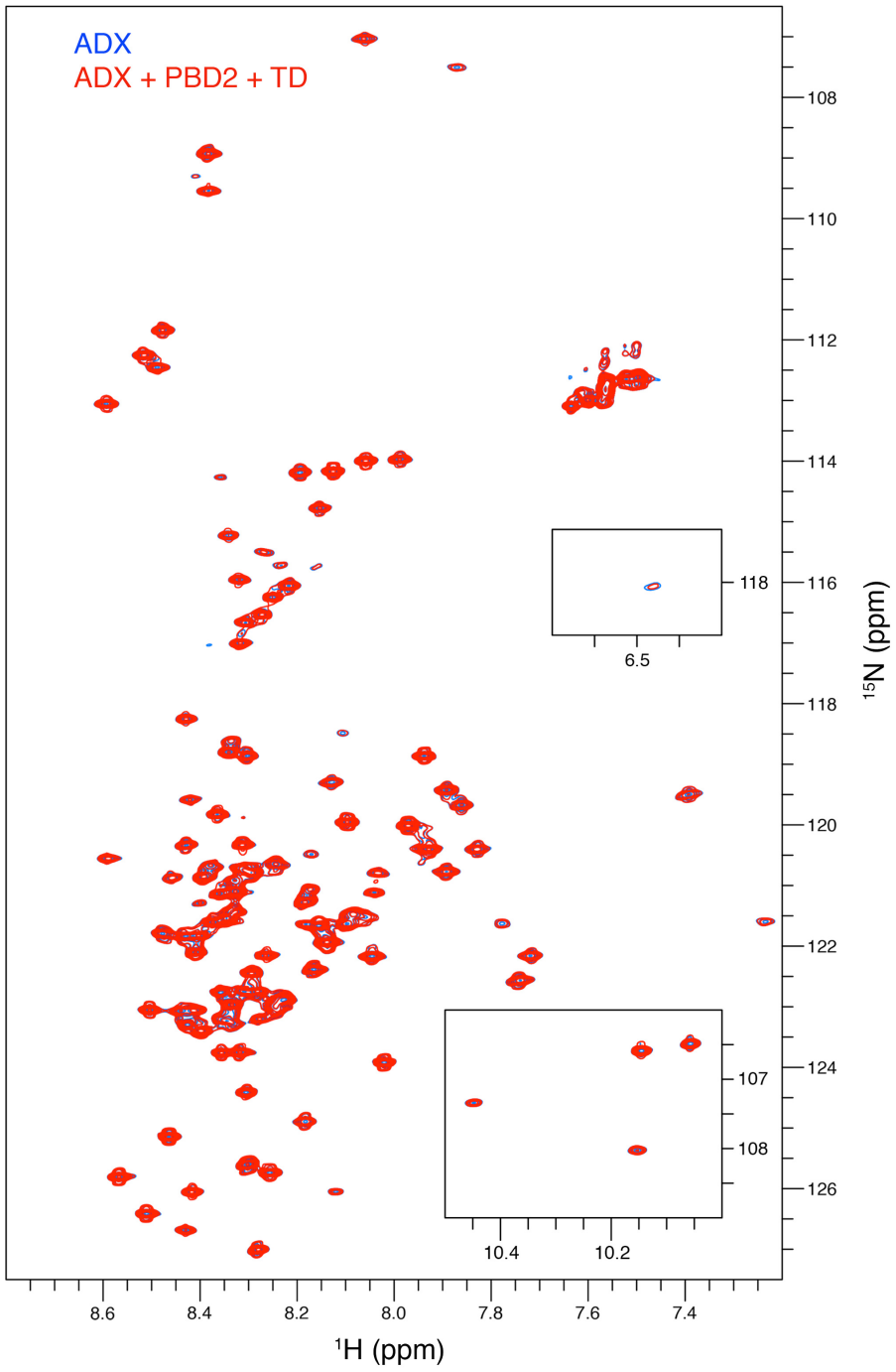

Figure 4.16: Comparison of the ^{1}H-^{15}N HSQC spectra of ADX in the presence or absence of the PBD2 and the TD.

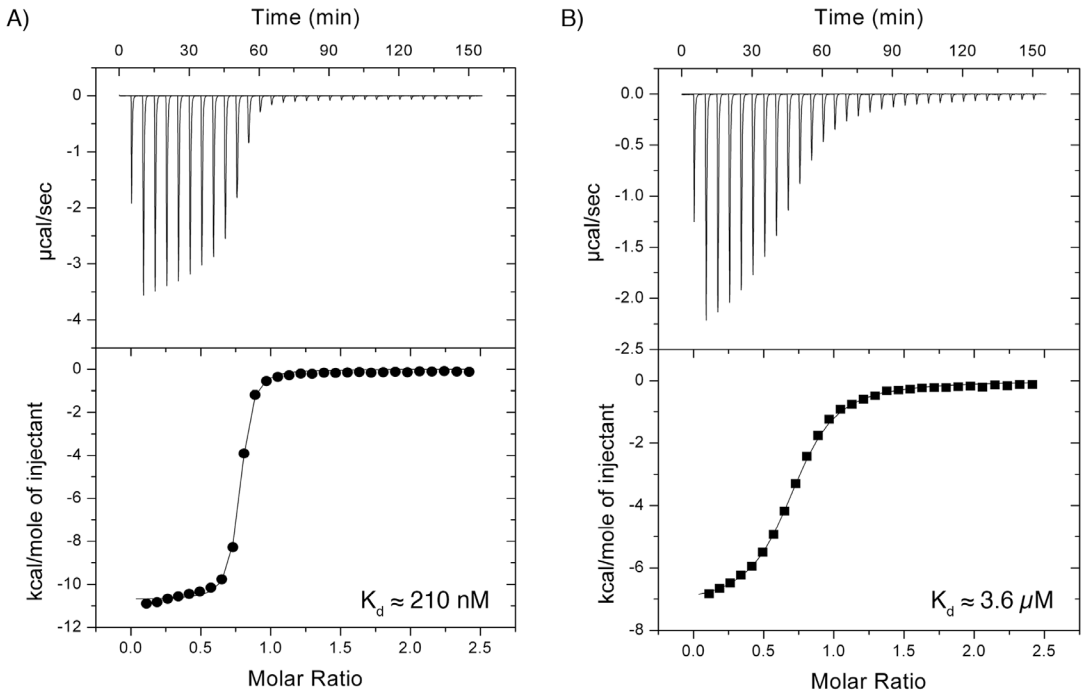

Figure 4.17: Competitive interaction between the ADX and the TD for binding to the PBD2. A) and B) ITC analysis of the TD interaction with the PBD2 and the PBD2-ADX complex, respectively.

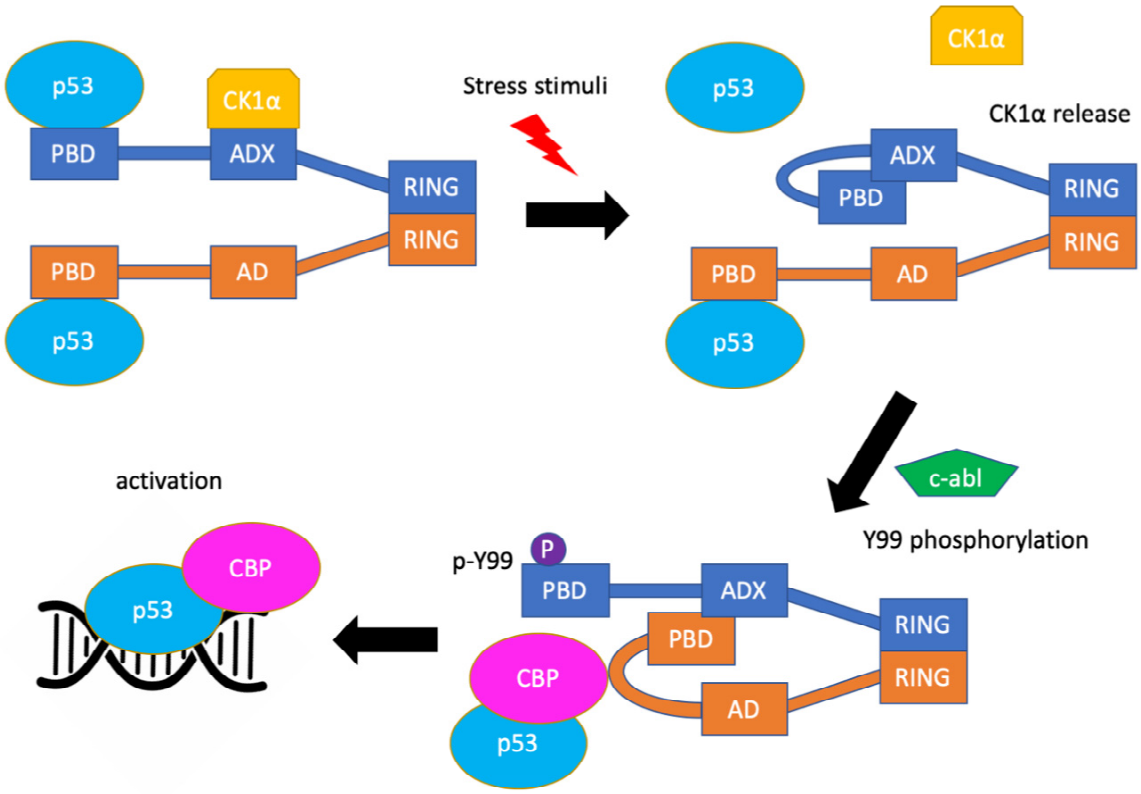

Figure 4.18: Proposed mechanism of p53 activation. Under normal condition, p53 is constantly suppressed by MDM2 and MDMX, where the MDMX-CK1α interaction facilitate the formation of p53-MDMX complex. Stress stimulation causes CK1α dissociation from MDMX and weakens the p53-MDMX interaction by promoting the intramolecular interaction between the PBD and the ADX. The MDMX PBD is phosphorylated by c-abl at Y99, which weakens its interaction with the ADX. Free ADX then could interact with the MDM2 PBD and compete with p53, reducing the affinity for the MDM2-p53 interaction. Meanwhile, the transcription co-activators (such as CBP) could bind the p53 to promote p53 activation.

CHAPTER 5: CONCLUSIONS

5.1 Summary of key research findings

In this work, I detail a series of studies that describe and evaluate the interactions between different domains of p53, MDM2 and MDMX. In chapter 2, I demonstrated that the MDM2 AD is an important sequence that interacts with two distinct domains (the DBD and the RD) of p53 and remains dynamic even in the bound form. I further identified that the AD binds the structurally destabilized zinc-free DBD with much greater affinity. In chapter 3, I discovered that the p53 TD, specifically the TD2 motif, binds the DBD and compete with the AD. I found that the MDM2 PBD binds the TD and reduced its affinity towards the DBD. In chapter 4, I showed that the ADX (MDMX residue 180 – 300) is a disordered region with residual α-helical propensity. I demonstrated that the ADX binds the MDM2 PBD and directly competes with the TD. Finally, I identified two distinct motifs of the ADX that can bind the hydrophobic pocket of the PBD that is responsible for TD binding.

5.2 Significance of current work

One of the many questions that has not been addressed in the literature is the steps that are required for the RING domain to catalyze ubiquitin transfer onto the substrate p53 molecule. Better understanding of the pathway can potentially lead to development of new and more specific therapeutic agents to disrupt this pathway for cancer therapy. To date, there is no direct evidence that the catalytic RING domain can interact with p53, nor does the isolated RING domain ubiquitinate p53. Instead, three early studies showed that the AD is crucial for the E3 ubiquitin ligase activity of MDM2 (Kawai, Wiederschain & Yuan,

2003; Meulmeester et al., 2003 and Ma et al., 2006). Moreover, MDM2 that lacks the PBD is still functionally active and able to efficiently ubiquitinate p53 (Ma et al., 2006). Coupled to this, a recent study showed that the AD binds the RING domain and can bind the E2-bound RING domain more tightly to promote ubiquitin discharge (Cheng et al., 2014). Thus, the AD is functionally important in allowing MDM2 to efficiently ubiquitinate p53. Building on these prior studies, I have filled in one of the missing steps in p53 ubiquitination: namely, that the AD serves to bridge from the enzyme (MDM2) to the substrate (p53). In this process, the AD retains structural disorder to facilitate dynamic interactions to promote p53 ubiquitination (Figure 2.22).

I have also shown that the structurally destabilized DBD has a clear advantage over the WT DBD by forming a tight interaction with the AD. If my proposed mechanism of action is correct, the direct impact of this tight interaction would be the disruption of the dynamic interaction network, directly affecting p53 ubiquitination. Indeed, several studies have shown that p53 missense mutants with a structurally destabilized DBD are resistant to MDM2-mediated ubiquitination (Natalia & Karen, 2007; Peng et al., 2001 and Yang et al., 2019). Moreover, the accumulation of p53 missense mutants inside the cell is commonly observed in cancers (Bartek et al., 1991). Ultimately, gain of function mutations to p53 confer a significant advantage for survival, growth and invasion of cancer cells (Dong et al., 2009; Gualberto et al., 1998; Hanel et al., 2013; Lawrence et al., 2019; Muller et al., 2011 and Olive et al., 2004). Thus, sequestration of the AD may be a common mechanism for cancers to inactivate MDM2 and to promote the pro-survival effects exerted by mutant p53, suggesting that the AD would be a valuable therapeutic target to reactivate MDM2 for treatment of cancers expressing mutant p53.

In addition to the role of the AD in p53 ubiquitination, the AD also directly inhibits the DNA binding activity of p53. A previous study showed that the AD binds to the DBD to inhibit DNA binding (Cross et al., 2011). Here, I have shown that the AD also binds the RD. The RD was shown to bind non-specifically to DNA to promote p53 one-dimensional sliding on DNA and is crucial for establishing a stable DNA contact (Friedler et al., 2005; Laptenko et al., 2015; Richard et al., 2004; Tafvizi et al., 2011 and Terakawa et al., 2012). Through direct interaction with the RD, the AD is fully capable of disrupting the p53-DNA interaction and likely represents a means by which MDM2 can exert another layer of control over p53 activity.

The direct interaction between the TD2 motif and the DBD adds another layer of complexity to the interaction of the DBD with the AD. The results presented herein demonstrate that the TD is a direct competitor for the AD-DBD interaction. Taking into consideration the fact that p53 predominantly exists as a dimer in normal cell and transitions into the tetrameric form when the cell is stressed (Gaglia et al., 2013), this interaction may be considerably stronger owing to a high local concentration of the TD2 motif that can potentially participate in intra- and inter-molecular interactions with the DBD. In order to circumvent this inhibitory effect being exerted on MDM2, our data suggest that the PBD can bind to and sequester the TD2 motif while bringing the AD into spatial proximity with the DBD. This bifunctional interaction would then allow the AD to efficiently inhibit p53 DNA-binding activity and promote p53 ubiquitination (Figure 3.11).

Making the story even more complicated, maximal activity of MDM2 requires heterodimerization with its close homolog MDMX (Badciong & Haas, 2002; Huang et al, 2011; Kawai et al., 2007; Linares et al., 2003 and Wang, Wang & Jiang, 2011). Of note,

MDMX also contains an AD (ADX), but the sequence is completely different from the MDM2 AD. This domain cannot perform the same task as the MDM2 AD in promoting p53 ubiquitination. In contrast, it exerts an auto-regulatory effect that modulates the MDMX-p53 interaction (Bista, Petrovich & Fersht, 2013). Based on the results presented herein, I further expanded the context for this auto-regulatory effect onto MDM2, where the ADX also binds to the MDM2 PBD to modulate the MDM2-p53 interaction and may result in p53 activation (Figure 4.18). To circumvent this auto-inhibitory effect, a previous study suggested that CK1α can bind the ADX to promote MDMX-p53 interaction (Wu et al., 2012). Moreover, CK1α was also found to bind the MDM2 to inhibit p53 activity (Huart et al., 2012). Thus, inhibiting the activity of CK1α is likely to be a promising approach to stimulate the activity of p53 for cancer therapy.

5.7 Potential future directions

Following directly from the studies I have detailed, many unanswered questions arise. I would have been personally interested in answering many of these but could not do so due to time constraints. This section details the research questions following from my work that I feel are most worthwhile to pursue in the future.

In order to better understand the pathway that ultimately lead to p53 ubiquitination, it will be important to comprehensively explore each of the individual steps within this pathway. A key piece of information that I took from the literature was the demonstration of a direct interaction between the AD and the RING domain from an in vivo study conducted by Cheng et al. The authors found that the AD not only binds the RING domain, but also selectively promotes RING binding to ubiquitin-charged E2-conjugating enzyme

without affecting binding to uncharged E2 (Cheng et al., 2014). In this work, I further expanded the AD interaction to the DBD and the RD and proposed a model that the AD is a key sequence element to promote enzyme-substrate recognition to facilitate subsequent ubiquitination. Unfortunately, it remains unclear how the AD binds to the RING domain and whether the AD-RING domain interaction is sufficient to promote ubiquitination of the DBD and the RD. Thus, structural and functional characterization of the AD-RING domain interaction is urgently needed to further define the role of the AD.

To achieve this goal, I suggest performin NMR experiments to evaluate the direct interaction between the AD and the RING in *cis* (using a MDM2 construct that contains both the AD and the RING) and *in trans* (using two separate MDM2 constructs that contain individual domains). Moreover, the ubiquitin ligase activity of the RING could be studied using a combination of proteins including ubiquitin-activating enzyme (E1), ubiquitin-conjugating enzyme (E2), ubiquitin and the RING. Specifically, the ubiquitin ligase activity should be measured for the DBD and the RING in presence and absence of the AD. Furthermore, proteins that sequester the AD, such as retinoblastoma protein and p14arf, could be introduced to evaluate their potential inhibitory effects on the AD and the ubiquitin ligase activity of the RING.

My thesis work has highlighted the role of AD phosphorylation as an important event in promoting the interaction with the DBD and the RD. The AD is hyperphosphorylated in vivo and hypo-phosphorylation of the AD weakens the E3 ubiquitin ligase activity of MDM2 (Blatter et al., 2002). Based on the current information from PhosphoSitePlus (Hornbeck et al., 2014), the AD contains 16 phosphorylation sites and it is not known which of these are crucial for the activity of the AD. Due to time

constraints, only one AD phosphomimic mutant (five serine residues mutated to glutamate) was tested. In addition, these phosphomimetic mutations may not be fully representative of phosphorylation. Thus, it would be desirable to comprehensively study these domain-domain interactions using chemically synthesized AD that contains different numbers of phosphorylated residues to investigate the effects of phosphorylation on the interaction with the DBD, the RD and the RING domain. Furthermore, it would be valuable to evaluate the effect of phosphorylation on AD activity. This could be achieved via the *in vitro* ubiquitination experiments mentioned previously, but instead using chemically-synthesized AD. Moreover, the effect of phosphorylation could be studied *in vivo* by mutating the appropriate serine and threonine residues to glutamate and comparing these to alanine mutations (to prevent phosphorylation).

Finally, our data suggest that the ADs of MDM2 and MDMX are crucial elements that regulate the activity of MDM2 and MDMX. Given the importance of these sequences, it is crucial to understand how they are regulated. Previous studies showed that CK1α stably associates with the ADs, which stimulate MDM2-mediated p53 degradation and promotes the MDMX-p53 interaction (Huart et al., 2012 and Wu et al., 2012). Thus, biophysical characterization of the interaction between CK1α and the ADs is necessary to understand how CK1α can promote the activity of both MDM2 and MDMX. Notably, the NMR and calorimetric techniques used in this thesis are perfectly suited to study these interactions and to identify the potential binding site on these proteins.

BIBLIOGRAPHY

1. Friedler A, Veprintsev DB, Rutherford T, von Glos KI, Fersht AR. Binding of Rad51 and other peptide sequences to a promiscuous, highly electrostatic binding site in p53. J Biol Chem. 2005 March 04;280(9):8051-9.

2. Marblestone JG, Edavettal SC, Lim Y, Lim P, Zuo X, Butt TR. Comparison of SUMO fusion technology with traditional gene fusion systems: enhanced expression and solubility with SUMO. Protein Sci. 2006 January 01;15(1):182-9.

3. Huang L, Yan Z, Liao X, Li Y, Yang J, Wang ZG, et al. The p53 inhibitors MDM2/MDMX complex is required for control of p53 activity in vivo. Proc Natl Acad Sci U S A. 2011 July 19;108(29):12001-6.

4. Wang X, Wang J, Jiang X. MdmX protein is essential for Mdm2 protein-mediated p53 polyubiquitination. J Biol Chem. 2011 July 08;286(27):23725-34.

5. Muller PA, Vousden KH, Norman JC. P53 and its Mutants in Tumor Cell Migration and Invasion. J Cell Biol. 2011 January 24;192(2):209-18.

6. Huart AS, MacLaine NJ, Narayan V, Hupp TR. Exploiting the MDM2-CK1alpha protein-protein interface to develop novel biologics that induce UBL-kinase-modification and inhibit cell growth. PLoS One. 2012;7(8):e43391.

7. Leavitt S, Freire E. Direct measurement of protein binding energetics by isothermal titration calorimetry. Curr Opin Struct Biol. 2001 October 01;11(5):560-6.

8. Di Lello P, Jenkins LM, Jones TN, Nguyen BD, Hara T, Yamaguchi H, et al. Structure of the Tfb1/p53 complex: Insights into the interaction between the p62/Tfb1 subunit of TFIIH and the activation domain of p53. Mol Cell. 2006 June 23;22(6):731-40.

9. Feng J, Tamaskovic R, Yang Z, Brazil DP, Merlo A, Hess D, et al. Stabilization of Mdm2 via Decreased Ubiquitination Is Mediated by Protein Kinase B/Akt-dependent Phosphorylation. J Biol Chem. 2004 08/20/;279(34):35510-7.

10. Battiste JL, Wagner G. Utilization of site-directed spin labeling and high-resolution heteronuclear nuclear magnetic resonance for global fold determination of large proteins with limited nuclear overhauser effect data. Biochemistry. 2000 May 09;39(18):5355-65.

11. Friedler A, Veprintsev DB, Hansson LO, Fersht AR. Kinetic Instability of p53 Core Domain Mutants IMPLICATIONS FOR RESCUE BY SMALL MOLECULES. J Biol Chem. 2003 06/27/;278(26):24108-12.

12. Tjandra N, Feller SE, Pastor RW, Bax A. Rotational diffusion anisotropy of human ubiquitin from 15N NMR relaxation. J Am Chem Soc. 1995 -12-01;117(50):12562-6.

13. Yao J, Dyson HJ, Wright PE. Chemical shift dispersion and secondary structure prediction in unfolded and partly folded proteins. FEBS Lett. 1997 Dec 15,;419(2-3):285-9.

14. Williamson MP. Using chemical shift perturbation to characterise ligand binding. Prog Nucl Magn Reson Spectrosc. 2013 August 01;73:1-16.

15. Farrow NA, Muhandiram R, Singer AU, Pascal SM, Kay CM, Gish G, et al. Backbone dynamics of a free and phosphopeptide-complexed Src homology 2 domain studied by 15N NMR relaxation. Biochemistry. 1994 May 17;33(19):5984-6003.

16. Wishart DS, Bigam CG, Yao J, Abildgaard F, Dyson HJ, Oldfield E, et al. 1H, 13C and 15N chemical shift referencing in biomolecular NMR. J Biomol NMR. 1995 Sep;6(2):135-40.

17. Markley JL, Bax A, Arata Y, Hilbers CW, Kaptein R, Sykes BD, et al. Recommendations for the presentation of NMR structures of proteins and nucleic acids--IUPAC-IUBMB-IUPAB Inter-Union Task Group on the standardization of data bases of protein and nucleic acid structures determined by NMR spectroscopy. Eur J Biochem. 1998 Aug 15,;256(1):1-15.

18. Delaglio F, Grzesiek S, Vuister GW, Zhu G, Pfeifer J, Bax A. NMRPipe: a multidimensional spectral processing system based on UNIX pipes. J Biomol NMR. 1995 November 01;6(3):277-93.

19. Gilkes DM, Chen L, Chen J. MDMX regulation of p53 response to ribosomal stress. EMBO J. 2006 Nov 29,;25(23):5614-25.

20. Nicholls CD, McLure KG, Shields MA, Lee PWK. Biogenesis of p53 involves cotranslational dimerization of monomers and posttranslational dimerization of dimers. Implications on the dominant negative effect. J Biol Chem. 2002 Apr 12,;277(15):12937-45.

21. Anil B, Riedinger C, Endicott JA, Noble MEM. The structure of an MDM2-Nutlin-3a complex solved by the use of a validated MDM2 surface-entropy reduction mutant. Acta Crystallogr D Biol Crystallogr. 2013 Aug;69(Pt 8):1358-66.

22. Jurrus E, Engel D, Star K, Monson K, Brandi J, Felberg LE, et al. Improvements to the APBS biomolecular solvation software suite. Protein Sci. 2018 January 01;27(1):112-28.

23. Micsonai A, Wien F, Bulyaki E, Kun J, Moussong E, Lee YH, et al. BeStSel: a web server for accurate protein secondary structure prediction and fold recognition from the circular dichroism spectra. Nucleic Acids Res. 2018 July 02;46(W1):W315-22.

24. Vranken WF, Boucher W, Stevens TJ, Fogh RH, Pajon A, Llinas M, et al. The CCPN data model for NMR spectroscopy: development of a software pipeline. Proteins. 2005 June 01;59(4):687-96.

25. Stad R, Little NA, Xirodimas DP, Frenk R, van der Eb, A J, Lane DP, et al. Mdmx stabilizes p53 and Mdm2 via two distinct mechanisms. EMBO Rep. 2001 November 01;2(11):1029-34.

26. Kadakia M, Brown TL, McGorry MM, Berberich SJ. MdmX inhibits Smad transactivation. Oncogene. 2002 Dec 12,;21(57):8776-85.

27. Mancini F, Gentiletti F, D'Angelo M, Giglio S, Nanni S, D'Angelo C, et al. MDM4 (MDMX) Overexpression Enhances Stabilization of Stress-induced p53 and Promotes Apoptosis. J Biol Chem. 2004 02/27/;279(9):8169-80.

28. Wiedemann C, Bellstedt P, Görlach M. CAPITO--a web server-based analysis and plotting tool for circular dichroism data. Bioinformatics. 2013 Jul 15,;29(14):1750-7.

29. Camilloni C, De Simone A, Vranken WF, Vendruscolo M. Determination of secondary structure populations in disordered states of proteins using nuclear magnetic resonance chemical shifts. Biochemistry. 2012 March 20;51(11):2224-31.

30. Yang Y, Ludwig RL, Jensen JP, Pierre SA, Medaglia MV, Davydov IV, et al. Small molecule inhibitors of HDM2 ubiquitin ligase activity stabilize and activate p53 in cells. Cancer Cell. 2005 Jun;7(6):547-59.

31. Herman AG, Hayano M, Poyurovsky MV, Shimada K, Skouta R, Prives C, et al. Discovery of Mdm2-MdmX E3 Ligase Inhibitors Using a Cell-Based Ubiquitination Assay. Cancer Discov. 2011 -09-01 00:00:00;1(4):312-25.

32. Chang YS, Graves B, Guerlavais V, Tovar C, Packman K, To K, et al. Stapled α–helical peptide drug development: A potent dual inhibitor of MDM2 and MDMX for p53-dependent cancer therapy. PNAS. 2013 -09-03 00:00:00;110(36):E3445-54.

33. Graves B, Thompson T, Xia M, Janson C, Lukacs C, Deo D, et al. Activation of the p53 pathway by small-molecule-induced MDM2 and MDMX dimerization. Proc Natl Acad Sci U S A. 2012 Jul 17,;109(29):11788-93.

34. Zhang Q, Zeng SX, Lu H. Targeting p53-MDM2-MDMX loop for cancer therapy. Subcell Biochem. 2014;85:281-319.

35. Liu Y, Wang X, Wang G, Yang Y, Yuan Y, Ouyang L. The past, present and future of potential small-molecule drugs targeting p53-MDM2/MDMX for cancer therapy. Eur J Med Chem. 2019 Aug 15,;176:92-104.

36. Vassilev LT, Vu BT, Graves B, Carvajal D, Podlaski F, Filipovic Z, et al. In vivo activation of the p53 pathway by small-molecule antagonists of MDM2. Science. 2004 Feb 06,;303(5659):844-8.

37. Egorova O, Mis M, Sheng Y. A site-directed mutagenesis study of the MdmX RING domain. Biochem Biophys Res Commun. 2014 May 16,;447(4):696-701.

38. Kosztyu P, Slaninová I, Valčíková B, Verlande A, Müller P, Paleček JJ, et al. A Single Conserved Amino Acid Residue as a Critical Context-Specific Determinant of the Differential Ability of Mdm2 and MdmX RING Domains to Dimerize. Front Physiol. 2019;10:390.

39. Tanimura S, Ohtsuka S, Mitsui K, Shirouzu K, Yoshimura A, Ohtsubo M. MDM2 interacts with MDMX through their RING finger domains. FEBS Lett. 1999 Mar 19,;447(1):5-9.

40. Gilkes DM, Chen L, Chen J. MDMX regulation of p53 response to ribosomal stress. EMBO J. 2006 November 29;25(23):5614-25.

41. Zheng J, Lang Y, Zhang Q, Cui D, Sun H, Jiang L, et al. Structure of human MDM2 complexed with RPL11 reveals the molecular basis of p53 activation. Genes Dev. 2015 Jul 15,;29(14):1524-34.

42. Dias SS, Hogan C, Ochocka A, Meek DW. Polo-like kinase-1 phosphorylates MDM2 at Ser260 and stimulates MDM2-mediated p53 turnover. FEBS Lett. 2009 Nov 19,;583(22):3543-8.

43. Winter M, Milne D, Dias S, Kulikov R, Knippschild U, Blattner C, et al. Protein kinase CK1delta phosphorylates key sites in the acidic domain of murine double-minute clone 2 protein (MDM2) that regulate p53 turnover. Biochemistry. 2004 Dec 28,;43(51):16356-64.

44. Allende-Vega N, Dias S, Milne D, Meek D. Phosphorylation of the acidic domain of Mdm2 by protein kinase CK2. Mol Cell Biochem. 2005 Jun;274(1-2):85-90.

45. Hornbeck PV, Zhang B, Murray B, Kornhauser JM, Latham V, Skrzypek E. PhosphoSitePlus, 2014: mutations, PTMs and recalibrations. Nucleic Acids Res. 2015 Jan;43(Database issue):512.

46. Worrall EG, Worrall L, Blackburn E, Walkinshaw M, Hupp TR. The effects of phosphomimetic lid mutation on the thermostability of the N-terminal domain of MDM2. J Mol Biol. 2010 May 07,;398(3):414-28.

47. Li C, Pazgier M, Li C, Yuan W, Liu M, Wei G, et al. Systematic mutational analysis of peptide inhibition of the p53-MDM2/MDMX interactions. J Mol Biol. 2010 Apr 30,;398(2):200-13.

48. Thut CJ, Goodrich JA, Tjian R. Repression of p53-mediated transcription by MDM2: a dual mechanism. Genes Dev. 1997 Aug 01,;11(15):1974-86.

49. Pazgier M, Liu M, Zou G, Yuan W, Li C, Li C, et al. Structural basis for high-affinity peptide inhibition of p53 interactions with MDM2 and MDMX. PNAS. 2009 -03-24 00:00:00;106(12):4665-70.

50. Parant J, Chavez-Reyes A, Little NA, Yan W, Reinke V, Jochemsen AG, et al. Rescue of embryonic lethality in Mdm4-null mice by loss of Trp53 suggests a nonoverlapping pathway with MDM2 to regulate p53. Nat Genet. 2001 Sep;29(1):92-5.

51. Migliorini D, Lazzerini Denchi E, Danovi D, Jochemsen A, Capillo M, Gobbi A, et al. Mdm4 (Mdmx) regulates p53-induced growth arrest and neuronal cell death during early embryonic mouse development. Mol Cell Biol. 2002 Aug;22(15):5527-38.

52. Phillips A, Teunisse A, Lam S, Lodder K, Darley M, Emaduddin M, et al. HDMX-L is expressed from a functional p53-responsive promoter in the first intron of the HDMX gene and participates in an autoregulatory feedback loop to control p53 activity. J Biol Chem. 2010 Sep 17,;285(38):29111-27.

53. Wei C, Wu Q, Vega VB, Chiu KP, Ng P, Zhang T, et al. A global map of p53 transcription-factor binding sites in the human genome. Cell. 2006 Jan 13,;124(1):207-19.

54. Oliner JD, Saiki AY, Caenepeel S. The Role of MDM2 Amplification and Overexpression in Tumorigenesis. Cold Spring Harb Perspect Med. 2016 06 01,;6(6).

55. Cahilly-Snyder L, Yang-Feng T, Francke U, George DL. Molecular analysis and chromosomal mapping of amplified genes isolated from a transformed mouse 3T3 cell line. Somat Cell Mol Genet. 1987 May;13(3):235-44.

56. Montes de Oca Luna, R., Wagner DS, Lozano G. Rescue of early embryonic lethality in mdm2-deficient mice by deletion of p53. Nature. 1995 Nov 09,;378(6553):203-6.

57. Jones SN, Roe AE, Donehower LA, Bradley A. Rescue of embryonic lethality in Mdm2-deficient mice by absence of p53. Nature. 1995 Nov 09,;378(6553):206-8.

58. Fakharzadeh SS, Trusko SP, George DL. Tumorigenic potential associated with enhanced expression of a gene that is amplified in a mouse tumor cell line. EMBO J. 1991 Jun;10(6):1565-9.

59. Wade M, Li Y, Wahl GM. MDM2, MDMX and p53 in oncogenesis and cancer therapy. Nat Rev Cancer. 2013 Feb;13(2):83-96.

60. Haupt S, Buckley D, Pang J-B, Panimaya J, Paul PJ, Gamell C, et al. Targeting Mdmx to treat breast cancers with wild-type p53. Cell Death Dis. 2015 Jul 16,;6:e1821.

61. Feeley KP, Adams CM, Mitra R, Eischen CM. Mdm2 Is Required for Survival and Growth of p53-Deficient Cancer Cells. Cancer Res. 2017 -07-15 00:00:00;77(14):3823-33.

62. Wiech M, Olszewski MB, Tracz-Gaszewska Z, Wawrzynow B, Zylicz M, Zylicz A. Molecular mechanism of mutant p53 stabilization: the role of HSP70 and MDM2. PLoS ONE. 2012;7(12):e51426.

63. Fontemaggi G, Dell'Orso S, Trisciuoglio D, Shay T, Melucci E, Fazi F, et al. The execution of the transcriptional axis mutant p53, E2F1 and ID4 promotes tumor neo-angiogenesis. Nat Struct Mol Biol. 2009 Oct;16(10):1086-93.

64. Dong P, Xu Z, Jia N, Li D, Feng Y. Elevated expression of p53 gain-of-function mutation R175H in endometrial cancer cells can increase the invasive phenotypes by activation of the EGFR/PI3K/AKT pathway. Mol Cancer. 2009 Nov 16,;8:103.

65. Robles AI, Harris CC. Clinical outcomes and correlates of TP53 mutations and cancer. Cold Spring Harb Perspect Biol. 2010 Mar;2(3):a001016.

66. Wang M, Yang C, Zhang X, Li X. Characterizing genomic differences of human cancer stratified by the TP53 mutation status. Mol Genet Genomics. 2018 Jun;293(3):737-46.

67. Donehower LA, Soussi T, Korkut A, Liu Y, Schultz A, Cardenas M, et al. Integrated Analysis of TP53 Gene and Pathway Alterations in The Cancer Genome Atlas. Cell Rep. 2019 Jul 30,;28(5):1370,1384.e5.

68. van Oijen MG, Slootweg PJ. Gain-of-function mutations in the tumor suppressor gene p53. Clin Cancer Res. 2000 Jun;6(6):2138-45.

69. Oren M, Rotter V. Mutant p53 gain-of-function in cancer. Cold Spring Harb Perspect Biol. 2010 Feb;2(2):a001107.

70. Eldar A, Rozenberg H, Diskin-Posner Y, Rohs R, Shakked Z. Structural studies of p53 inactivation by DNA-contact mutations and its rescue by suppressor mutations via alternative protein–DNA interactions. Nucleic Acids Res. 2013 /10/01;41(18):8748-59.

71. Friedler A, DeDecker BS, Freund SMV, Blair C, Rüdiger S, Fersht AR. Structural distortion of p53 by the mutation R249S and its rescue by a designed peptide: implications for "mutant conformation". J Mol Biol. 2004 Feb 06,;336(1):187-96.

72. Ng JWK, Lama D, Lukman S, Lane DP, Verma CS, Sim AYL. R248Q mutation—Beyond p53-DNA binding. Proteins: Structure, Function, and Bioinformatics. 2015;83(12):2240-50.

73. Mello SS, Attardi LD. Not all p53 gain-of-function mutants are created equal. Cell Death & Differentiation. 2013 -07;20(7):855-7.

74. Olivier M, Hollstein M, Hainaut P. TP53 mutations in human cancers: origins, consequences, and clinical use. Cold Spring Harb Perspect Biol. 2010 Jan;2(1):a001008.

75. Jabbur JR, Tabor AD, Cheng X, Wang H, Uesugi M, Lozano G, et al. Mdm-2 binding and TAF(II)31 recruitment is regulated by hydrogen bond disruption between the p53 residues Thr18 and Asp21. Oncogene. 2002 Oct 10,;21(46):7100-13.

76. Schon O, Friedler A, Bycroft M, Freund SMV, Fersht AR. Molecular mechanism of the interaction between MDM2 and p53. J Mol Biol. 2002 Oct 25,;323(3):491-501.

77. Shi D, Pop MS, Kulikov R, Love IM, Kung AL, Kung A, et al. CBP and p300 are cytoplasmic E4 polyubiquitin ligases for p53. Proc Natl Acad Sci U S A. 2009 Sep 22,;106(38):16275-80.

78. Wang X, Wang J, Jiang X. MdmX protein is essential for Mdm2 protein-mediated p53 polyubiquitination. J Biol Chem. 2011 Jul 08,;286(27):23725-34.

79. Badciong JC, Haas AL. MdmX is a RING finger ubiquitin ligase capable of synergistically enhancing Mdm2 ubiquitination. J Biol Chem. 2002 December 20;277(51):49668-75.

80. Hershko A, Ciechanover A. The ubiquitin system. Annu Rev Biochem. 1998;67:425-79.

81. Glickman MH, Ciechanover A. The ubiquitin-proteasome proteolytic pathway: destruction for the sake of construction. Physiol Rev. 2002 Apr;82(2):373-428.

82. Thomasova D, Bruns HA, Kretschmer V, Ebrahim M, Romoli S, Liapis H, et al. Murine Double Minute-2 Prevents p53-Overactivation-Related Cell Death (Podoptosis) of Podocytes. JASN. 2015 -07-01 00:00:00;26(7):1513-23.

83. Thomasova D, Ebrahim M, Fleckinger K, Li M, Molnar J, Popper B, et al. MDM2 prevents spontaneous tubular epithelial cell death and acute kidney injury. Cell Death Dis. 2016 11 24,;7(11):e2482.

84. Hall PA, Lane DP. Tumour suppressors: A developing role for p53? Current Biology. 1997 March 1,;7(3):R144-7.

85. Ebrahim M, Mulay SR, Anders H, Thomasova D. MDM2 beyond cancer: podoptosis, development, inflammation, and tissue regeneration. Histol Histopathol. 2015 Nov;30(11):1271-82.

86. Vogelstein B, Lane D, Levine AJ. Surfing the p53 network. Nature. 2000 November 16;408(6810):307-10.

87. Lev Bar-Or R, Maya R, Segel LA, Alon U, Levine AJ, Oren M. Generation of oscillations by the p53-Mdm2 feedback loop: a theoretical and experimental study. Proc Natl Acad Sci U S A. 2000 Oct 10,;97(21):11250-5.

88. Zhang X, Liu F, Wang W. Two-phase dynamics of p53 in the DNA damage response. Proc Natl Acad Sci U S A. 2011 May 31,;108(22):8990-5.

89. Terakawa T, Kenzaki H, Takada S. p53 searches on DNA by rotation-uncoupled sliding at C-terminal tails and restricted hopping of core domains. J Am Chem Soc. 2012 Sep 05,;134(35):14555-62.

90. Tafvizi A, Huang F, Fersht AR, Mirny LA, van Oijen AM. A single-molecule characterization of p53 search on DNA. Proc Natl Acad Sci U S A. 2011 Jan 11,;108(2):563-8.

91. McKinney K, Mattia M, Gottifredi V, Prives C. p53 linear diffusion along DNA requires its C terminus. Mol Cell. 2004 November 05;16(3):413-24.

92. Friedler A, Veprintsev DB, Freund SMV, von Glos KI, Fersht AR. Modulation of binding of DNA to the C-terminal domain of p53 by acetylation. Structure. 2005 Apr;13(4):629-36.

93. Zhou X, Wang XW, Xu L, Hagiwara K, Nagashima M, Wolkowicz R, et al. COOH-Terminal Domain of p53 Modulates p53-mediated Transcriptional Transactivation, Cell Growth, and Apoptosis. Cancer Res. 1999 -02-15 00:00:00;59(4):843-8.

94. Hamard P, Lukin DJ, Manfredi JJ. p53 Basic C Terminus Regulates p53 Functions through DNA Binding Modulation of Subset of Target Genes. J Biol Chem. 2012 06/22/;287(26):22397-407.

95. Mujtaba S, He Y, Zeng L, Yan S, Plotnikova O, Sachchidanand n, et al. Structural mechanism of the bromodomain of the coactivator CBP in p53 transcriptional activation. Mol Cell. 2004 Jan 30,;13(2):251-63.

96. Lowe ED, Tews I, Cheng KY, Brown NR, Gul S, Noble MEM, et al. Specificity determinants of recruitment peptides bound to phospho-CDK2/cyclin A. Biochemistry. 2002 Dec 31,;41(52):15625-34.

97. Avalos JL, Celic I, Muhammad S, Cosgrove MS, Boeke JD, Wolberger C. Structure of a Sir2 enzyme bound to an acetylated p53 peptide. Mol Cell. 2002 Sep;10(3):523-35.

98. DeHart CJ, Chahal JS, Flint SJ, Perlman DH. Extensive post-translational modification of active and inactivated forms of endogenous p53. Mol Cell Proteomics. 2014 Jan;13(1):1-17.

99. Meek DW, Anderson CW. Posttranslational Modification of p53: Cooperative Integrators of Function. Cold Spring Harb Perspect Biol. 2009 12/01/;1(6):a000950.

100. Kruse JP, Gu W. Modes of p53 regulation. Cell. 2009 May 15;137(4):609-22.

101. Yakovleva T, Pramanik A, Kawasaki T, Tan-No K, Gileva I, Lindegren H, et al. p53 Latency. C-terminal domain prevents binding of p53 core to target but not to nonspecific DNA sequences. J Biol Chem. 2001 May 11,;276(19):15650-8.

102. Laptenko O, Shiff I, Freed-Pastor W, Zupnick A, Mattia M, Freulich E, et al. The p53 C terminus controls site-specific DNA binding and promotes structural changes within the central DNA binding domain. Mol Cell. 2015 Mar 19,;57(6):1034-46.

103. Weinberg RL, Freund SMV, Veprintsev DB, Bycroft M, Fersht AR. Regulation of DNA Binding of p53 by its C-terminal Domain. Journal of Molecular Biology. 2004 September 17,;342(3):801-11.

104. Kim H, Kim K, Choi J, Heo K, Baek HJ, Roeder RG, et al. p53 Requires an Intact C-Terminal Domain for DNA Binding and Transactivation. Journal of Molecular Biology. 2012 February 3,;415(5):843-54.

105. Rajagopalan S, Jaulent AM, Wells M, Veprintsev DB, Fersht AR. 14-3-3 activation of DNA binding of p53 by enhancing its association into tetramers. Nucleic Acids Res. 2008 Oct;36(18):5983-91.

106. Foo RS-, Nam Y, Ostreicher MJ, Metzl MD, Whelan RS, Peng C, et al. Regulation of p53 tetramerization and nuclear export by ARC. Proc Natl Acad Sci U S A. 2007 Dec 26,;104(52):20826-31.

107. Stommel JM, Marchenko ND, Jimenez GS, Moll UM, Hope TJ, Wahl GM. A leucine-rich nuclear export signal in the p53 tetramerization domain: regulation of subcellular localization and p53 activity by NES masking. EMBO J. 1999 Mar 15,;18(6):1660-72.

108. Kawaguchi T, Kato S, Otsuka K, Watanabe G, Kumabe T, Tominaga T, et al. The relationship among p53 oligomer formation, structure and transcriptional activity using a comprehensive missense mutation library. Oncogene. 2005 Oct 20,;24(46):6976-81.

109. Weinberg RL, Veprintsev DB, Fersht AR. Cooperative binding of tetrameric p53 to DNA. J Mol Biol. 2004 Aug 27,;341(5):1145-59.

110. Rajagopalan S, Huang F, Fersht AR. Single-Molecule characterization of oligomerization kinetics and equilibria of the tumor suppressor p53. Nucleic Acids Res. 2011 Mar;39(6):2294-303.

111. Davison TS, Nie X, Ma W, Lin Y, Kay C, Benchimol S, et al. Structure and functionality of a designed p53 dimer. J Mol Biol. 2001 Mar 23,;307(2):605-17.

112. Clore GM, Omichinski JG, Sakaguchi K, Zambrano N, Sakamoto H, Appella E, et al. High-resolution structure of the oligomerization domain of p53 by multidimensional NMR. Science. 1994 Jul 15,;265(5170):386-91.

113. Veprintsev DB, Freund SMV, Andreeva A, Rutledge SE, Tidow H, Cañadillas JMP, et al. Core domain interactions in full-length p53 in solution. Proc Natl Acad Sci U S A. 2006 Feb 14,;103(7):2115-9.

114. Malecka KA, Ho WC, Marmorstein R. Crystal structure of a p53 core tetramer bound to DNA. Oncogene. 2009 Jan 22,;28(3):325-33.

115. Wang Y, Schwedes JF, Parks D, Mann K, Tegtmeyer P. Interaction of p53 with its consensus DNA-binding site. Mol Cell Biol. 1995 Apr;15(4):2157-65.

116. Cañadillas JMP, Tidow H, Freund SMV, Rutherford TJ, Ang HC, Fersht AR. Solution structure of p53 core domain: Structural basis for its instability. PNAS. 2006 -02-14 00:00:00;103(7):2109-14.

117. Cho Y, Gorina S, Jeffrey PD, Pavletich NP. Crystal structure of a p53 tumor suppressor-DNA complex: understanding tumorigenic mutations. Science. 1994 Jul 15,;265(5170):346-55.

118. Pavletich NP, Chambers KA, Pabo CO. The DNA-binding domain of p53 contains the four conserved regions and the major mutation hot spots. Genes Dev. 1993 Dec;7(12B):2556-64.

119. Berger M, Vogt Sionov R, Levine AJ, Haupt Y. A role for the polyproline domain of p53 in its regulation by Mdm2. J Biol Chem. 2001 February 09;276(6):3785-90.

120. Edwards SJ, Hananeia L, Eccles MR, Zhang YF, Braithwaite AW. The proline-rich region of mouse p53 influences transactivation and apoptosis but is largely dispensable for these functions. Oncogene. 2003 -07;22(29):4517-23.

121. Zhu J, Jiang J, Zhou W, Zhu K, Chen X. Differential regulation of cellular target genes by p53 devoid of the PXXP motifs with impaired apoptotic activity. Oncogene. 1999 Mar 25,;18(12):2149-55.

122. Toledo F, Krummel KA, Lee CJ, Liu C, Rodewald L, Tang M, et al. A mouse p53 mutant lacking the proline-rich domain rescues Mdm4 deficiency and provides insight into the Mdm2-Mdm4-p53 regulatory network. Cancer Cell. 2006 April 1,;9(4):273-85.

123. Dornan D, Shimizu H, Burch L, Smith AJ, Hupp TR. The proline repeat domain of p53 binds directly to the transcriptional coactivator p300 and allosterically controls DNA-dependent acetylation of p53. Mol Cell Biol. 2003 December 01;23(23):8846-61.

124. Huang F, Rajagopalan S, Settanni G, Marsh RJ, Armoogum DA, Nicolaou N, et al. Multiple conformations of full-length p53 detected with single-molecule fluorescence resonance energy transfer. PNAS. 2009 -12-08 00:00:00;106(49):20758-63.

125. Baptiste N, Friedlander P, Chen X, Prives C. The proline-rich domain of p53 is required for cooperation with anti-neoplastic agents to promote apoptosis of tumor cells. Oncogene. 2002 -01;21(1):9-21.

126. Teufel DP, Freund SM, Bycroft M, Fersht AR. Four domains of p300 each bind tightly to a sequence spanning both transactivation subdomains of p53. Proc Natl Acad Sci U S A. 2007 April 24;104(17):7009-14.

127. Lee H, Mok KH, Muhandiram R, Park KH, Suk JE, Kim DH, et al. Local structural elements in the mostly unstructured transcriptional activation domain of human p53. J Biol Chem. 2000 Sep 22,;275(38):29426-32.

128. Zhu J, Zhou W, Jiang J, Chen X. Identification of a novel p53 functional domain that is necessary for mediating apoptosis. J Biol Chem. 1998 May 22,;273(21):13030-6.

129. Candau R, Scolnick DM, Darpino P, Ying CY, Halazonetis TD, Berger SL. Two tandem and independent sub-activation domains in the amino terminus of p53 require the adaptor complex for activity. Oncogene. 1997 Aug 14,;15(7):807-16.

130. Raj N, Attardi LD. The Transactivation Domains of the p53 Protein. Cold Spring Harb Perspect Med. 2017 January 03;7(1):10.1101/cshperspect.a026047.

131. Gaglia G, Guan Y, Shah JV, Lahav G. Activation and control of p53 tetramerization in individual living cells. Proc Natl Acad Sci U S A. 2013 September 17;110(38):15497-501.

132. Lebedeva MA, Eaton JS, Shadel GS. Loss of p53 causes mitochondrial DNA depletion and altered mitochondrial reactive oxygen species homeostasis. Biochim Biophys Acta. 2009 May 01;1787(5):328-34.

133. Kulawiec M, Ayyasamy V, Singh KK. p53 regulates mtDNA copy number and mitocheckpoint pathway. J Carcinog. 2009;8:8.

134. Wong TS, Rajagopalan S, Townsley FM, Freund SM, Petrovich M, Loakes D, et al. Physical and functional interactions between human mitochondrial single-stranded DNA-binding protein and tumour suppressor p53. Nucleic Acids Res. 2009 Feb;37(2):568-81.

135. Bakhanashvili M, Grinberg S, Bonda E, Rahav G. Excision of nucleoside analogs in mitochondria by p53 protein. AIDS. 2009 Apr 27,;23(7):779-88.

136. Achanta G, Sasaki R, Feng L, Carew JS, Lu W, Pelicano H, et al. Novel role of p53 in maintaining mitochondrial genetic stability through interaction with DNA Pol gamma. EMBO J. 2005 October 05;24(19):3482-92.

137. Chen D, Yu Z, Zhu Z, Lopez CD. The p53 pathway promotes efficient mitochondrial DNA base excision repair in colorectal cancer cells. Cancer Res. 2006 April 01;66(7):3485-94.

138. de Souza-Pinto NC, Harris CC, Bohr VA. p53 functions in the incorporation step in DNA base excision repair in mouse liver mitochondria. Oncogene. 2004 August 26;23(39):6559-68.

139. Gupta S, De S, Srivastava V, Hussain M, Kumari J, Muniyappa K, et al. RECQL4 and p53 potentiate the activity of polymerase gamma and maintain the integrity of the human mitochondrial genome. Carcinogenesis. 2014 January 01;35(1):34-45.

140. Wong TS, Rajagopalan S, Freund SM, Rutherford TJ, Andreeva A, Townsley FM, et al. Biophysical characterizations of human mitochondrial transcription factor A and its binding to tumor suppressor p53. Nucleic Acids Res. 2009 November 01;37(20):6765-83.

141. Yoshida Y, Izumi H, Torigoe T, Ishiguchi H, Itoh H, Kang D, et al. P53 physically interacts with mitochondrial transcription factor A and differentially regulates binding to damaged DNA. Cancer Res. 2003 July 01;63(13):3729-34.

142. Bakhanashvili M, Grinberg S, Bonda E, Simon AJ, Moshitch-Moshkovitz S, Rahav G. p53 in mitochondria enhances the accuracy of DNA synthesis. Cell Death and Differentiation. 2008 Dec;15(12):1865-74.

143. Bergeaud M, Mathieu L, Guillaume A, Moll UM, Mignotte B, Le Floch N, et al. Mitochondrial p53 mediates a transcription-independent regulation of cell respiration and interacts with the mitochondrial F_1F0-ATP synthase. Cell Cycle. 2013 Sep 01,;12(17):2781-93.

144. Zhuang J, Wang PY, Huang X, Chen X, Kang JG, Hwang PM. Mitochondrial disulfide relay mediates translocation of p53 and partitions its subcellular activity. Proc Natl Acad Sci U S A. 2013 October 22;110(43):17356-61.

145. Boopathi E, Srinivasan S, Fang JK, Avadhani NG. Bimodal protein targeting through activation of cryptic mitochondrial targeting signals by an inducible cytosolic endoprotease. Mol Cell. 2008 October 10;32(1):32-42.

146. De S, Kumari J, Mudgal R, Modi P, Gupta S, Futami K, et al. RECQL4 is essential for the transport of p53 to mitochondria in normal human cells in the absence of exogenous stress. J Cell Sci. 2012 May 15;125(Pt 10):2509-22.

147. Mathew R, Khor S, Hackett SR, Rabinowitz JD, Perlman DH, White E. Functional role of autophagy-mediated proteome remodeling in cell survival signaling and innate immunity. Mol Cell. 2014 Sep 18,;55(6):916-30.

148. White E. The role for autophagy in cancer. J Clin Invest. 2015 Jan;125(1):42-6.

149. Mrakovcic M, Fröhlich LF. p53-Mediated Molecular Control of Autophagy in Tumor Cells. Biomolecules. 2018 03 21,;8(2).

150. White E. Autophagy and p53. Cold Spring Harb Perspect Med. 2016 Apr 01,;6(4):a026120.

151. Giorgi C, Bonora M, Sorrentino G, Missiroli S, Poletti F, Suski JM, et al. p53 at the endoplasmic reticulum regulates apoptosis in a Ca2 -dependent manner. PNAS. 2015 -02-10 00:00:00;112(6):1779-84.

152. Deng X, Gao F, Flagg T, Anderson J, May WS. Bcl2's flexible loop domain regulates p53 binding and survival. Mol Cell Biol. 2006 Jun;26(12):4421-34.

153. Follis AV, Llambi F, Merritt P, Chipuk JE, Green DR, Kriwacki RW. Pin1-Induced Proline Isomerization in Cytosolic p53 Mediates BAX Activation and Apoptosis. Mol Cell. 2015 Aug 20,;59(4):677-84.

154. Leu JI-, Dumont P, Hafey M, Murphy ME, George DL. Mitochondrial p53 activates Bak and causes disruption of a Bak-Mcl1 complex. Nat Cell Biol. 2004 May;6(5):443-50.

155. Chipuk JE, Bouchier-Hayes L, Kuwana T, Newmeyer DD, Green DR. PUMA couples the nuclear and cytoplasmic proapoptotic function of p53. Science. 2005 Sep 09,;309(5741):1732-5.

156. Follis AV, Chipuk JE, Fisher JC, Yun M, Grace CR, Nourse A, et al. PUMA binding induces partial unfolding within BCL-xL to disrupt p53 binding and promote apoptosis. Nat Chem Biol. 2013 Mar;9(3):163-8.

157. Moll UM, Marchenko N, Zhang X-. p53 and Nur77/TR3 - transcription factors that directly target mitochondria for cell death induction. Oncogene. 2006 Aug 07,;25(34):4725-43.

158. Arima Y, Nitta M, Kuninaka S, Zhang D, Fujiwara T, Taya Y, et al. Transcriptional blockade induces p53-dependent apoptosis associated with translocation of p53 to mitochondria. J Biol Chem. 2005 May 13,;280(19):19166-76.

159. Ding HF, McGill G, Rowan S, Schmaltz C, Shimamura A, Fisher DE. Oncogene-dependent regulation of caspase activation by p53 protein in a cell-free system. J Biol Chem. 1998 Oct 23,;273(43):28378-83.

160. Haupt Y, Rowan S, Shaulian E, Vousden KH, Oren M. Induction of apoptosis in HeLa cells by trans-activation-deficient p53. Genes Dev. 1995 Sep 01,;9(17):2170-83.

161. Caelles C, Helmberg A, Karin M. p53-dependent apoptosis in the absence of transcriptional activation of p53-target genes. Nature. 1994 Jul 21,;370(6486):220-3.

162. Lane DP. Cancer. p53, guardian of the genome. Nature. 1992 Jul 02,;358(6381):15-6.

163. Huang P. Excision of mismatched nucleotides from DNA: a potential mechanism for enhancing DNA replication fidelity by the wild-type p53 protein. Oncogene. 1998 Jul 23,;17(3):261-70.

164. Skalski V, Lin ZY, Choi BY, Brown KR. Substrate specificity of the p53-associated 3′-5′ exonuclease. Oncogene. 2000 Jul 6,;19(29):3321-9.

165. Lilling G, Elena N, Sidi Y, Bakhanashvili M. p53-associated 3′→5′ exonuclease activity in nuclear and cytoplasmic compartments of cells. Oncogene. 2003 Jan 16,;22(2):233-45.

166. Williams AB, Schumacher B. p53 in the DNA-Damage-Repair Process. Cold Spring Harb Perspect Med. 2016 05 02,;6(5).

167. Xing J, Sheppard HM, Corneillie SI, Liu X. p53 Stimulates TFIID-TFIIA-promoter complex assembly, and p53-T antigen complex inhibits TATA binding protein-TATA interaction. Mol Cell Biol. 2001 Jun;21(11):3652-61.

168. Louder RK, He Y, López-Blanco JR, Fang J, Chacón P, Nogales E. Structure of promoter-bound TFIID and model of human pre-initiation complex assembly. Nature. 2016 03 31,;531(7596):604-9.

169. Xiao H, Pearson A, Coulombe B, Truant R, Zhang S, Regier JL, et al. Binding of basal transcription factor TFIIH to the acidic activation domains of VP16 and p53. Mol Cell Biol. 1994 Oct;14(10):7013-24.

170. Thut CJ, Chen JL, Klemm R, Tjian R. p53 transcriptional activation mediated by coactivators TAFII40 and TAFII60. Science. 1995 Jan 06,;267(5194):100-4.

171. Farmer G, Colgan J, Nakatani Y, Manley JL, Prives C. Functional interaction between p53, the TATA-binding protein (TBP), andTBP-associated factors in vivo. Mol Cell Biol. 1996 Aug;16(8):4295-304.

172. Coleman RA, Qiao Z, Singh SK, Peng CS, Cianfrocco M, Zhang Z, et al. p53 Dynamically Directs TFIID Assembly on Target Gene Promoters. Mol Cell Biol. 2017 June 15;37(13):10.1128/MCB.00085,17. Print 2017 Jul 1.

173. Truant R, Xiao H, Ingles CJ, Greenblatt J. Direct interaction between the transcriptional activation domain of human p53 and the TATA box-binding protein. J Biol Chem. 1993 Feb 05,;268(4):2284-7.

174. Liu X, Miller CW, Koeffler PH, Berk AJ. The p53 activation domain binds the TATA box-binding polypeptide in Holo-TFIID, and a neighboring p53 domain inhibits transcription. Mol Cell Biol. 1993 Jun;13(6):3291-300.

175. Chen X, Farmer G, Zhu H, Prywes R, Prives C. Cooperative DNA binding of p53 with TFIID (TBP): a possible mechanism for transcriptional activation. Genes Dev. 1993 Oct;7(10):1837-49.

176. Ard PG, Chatterjee C, Kunjibettu S, Adside LR, Gralinski LE, McMahon SB. Transcriptional regulation of the mdm2 oncogene by p53 requires TRRAP acetyltransferase complexes. Mol Cell Biol. 2002 Aug;22(16):5650-61.

177. Wang T, Kobayashi T, Takimoto R, Denes AE, Snyder EL, el-Deiry WS, et al. hADA3 is required for p53 activity. EMBO J. 2001 Nov 15,;20(22):6404-13.

178. Avantaggiati ML, Ogryzko V, Gardner K, Giordano A, Levine AS, Kelly K. Recruitment of p300/CBP in p53-dependent signal pathways. Cell. 1997 Jun 27,;89(7):1175-84.

179. An W, Kim J, Roeder RG. Ordered cooperative functions of PRMT1, p300, and CARM1 in transcriptional activation by p53. Cell. 2004 Jun 11,;117(6):735-48.

180. Barlev NA, Liu L, Chehab NH, Mansfield K, Harris KG, Halazonetis TD, et al. Acetylation of p53 activates transcription through recruitment of coactivators/histone acetyltransferases. Mol Cell. 2001 Dec;8(6):1243-54.

181. Scolnick DM, Chehab NH, Stavridi ES, Lien MC, Caruso L, Moran E, et al. CREB-binding Protein and p300/CBP-associated Factor Are Transcriptional Coactivators of the p53 Tumor Suppressor Protein. Cancer Res. 1997 -09-01 00:00:00;57(17):3693-6.

182. Beckerman R, Prives C. Transcriptional regulation by p53. Cold Spring Harb Perspect Biol. 2010 Aug;2(8):a000935.

183. Fischer M. Census and evaluation of p53 target genes. Oncogene. 2017 07 13,;36(28):3943-56.

184. Tebaldi T, Zaccara S, Alessandrini F, Bisio A, Ciribilli Y, Inga A. Whole-genome cartography of p53 response elements ranked on transactivation potential. BMC Genomics. 2015 Jun 17,;16:464.

185. Andrysik Z, Galbraith MD, Guarnieri AL, Zaccara S, Sullivan KD, Pandey A, et al. Identification of a core TP53 transcriptional program with highly distributed tumor suppressive activity. Genome Res. 2017 Oct,;27(10):1645-57.

186. Chipuk JE, Kuwana T, Bouchier-Hayes L, Droin NM, Newmeyer DD, Schuler M, et al. Direct activation of Bax by p53 mediates mitochondrial membrane permeabilization and apoptosis. Science. 2004 Feb 13,;303(5660):1010-4.

187. Yamaguchi T, Matsuda K, Sagiya Y, Iwadate M, Fujino MA, Nakamura Y, et al. p53R2-dependent Pathway for DNA Synthesis in a p53-regulated Cell Cycle Checkpoint. Cancer Res. 2001 -11-15 00:00:00;61(22):8256-62.

188. He G, Siddik ZH, Huang Z, Wang R, Koomen J, Kobayashi R, et al. Induction of p21 by p53 following DNA damage inhibits both Cdk4 and Cdk2 activities. Oncogene. 2005 Apr 21,;24(18):2929-43.

189. Vaseva AV, Moll UM. The mitochondrial p53 pathway. Biochim Biophys Acta. 2009 May;1787(5):414-20.

190. Essmann F, Pohlmann S, Gillissen B, Daniel PT, Schulze-Osthoff K, Jänicke RU. Irradiation-induced translocation of p53 to mitochondria in the absence of apoptosis. J Biol Chem. 2005 Nov 04,;280(44):37169-77.

191. Brown CJ, Lain S, Verma CS, Fersht AR, Lane DP. Awakening guardian angels: drugging the p53 pathway. Nat Rev Cancer. 2009 December 01;9(12):862-73.

192. Marchenko ND, Hanel W, Li D, Becker K, Reich N, Moll UM. Stress-mediated nuclear stabilization of p53 is regulated by ubiquitination and importin-alpha3 binding. Cell Death Differ. 2010 February 01;17(2):255-67.

193. Chernov MV, Bean LJ, Lerner N, Stark GR. Regulation of ubiquitination and degradation of p53 in unstressed cells through C-terminal phosphorylation. J Biol Chem. 2001 August 24;276(34):31819-24.

194. Price BD, Calderwood SK. Increased sequence-specific p53-DNA binding activity after DNA damage is attenuated by phorbol esters. Oncogene. 1993 Nov;8(11):3055-62.

195. Maltzman W, Czyzyk L. UV irradiation stimulates levels of p53 cellular tumor antigen in nontransformed mouse cells. Mol Cell Biol. 1984 September 01;4(9):1689-94.

196. Schärer E, Iggo R. Mammalian p53 can function as a transcription factor in yeast. Nucleic Acids Res. 1992 Apr 11,;20(7):1539-45.

197. Pietenpol JA, Tokino T, Thiagalingam S, el-Deiry WS, Kinzler KW, Vogelstein B. Sequence-specific transcriptional activation is essential for growth suppression by p53. Proc Natl Acad Sci U S A. 1994 Mar 15,;91(6):1998-2002.

198. Farmer G, Bargonetti J, Zhu H, Friedman P, Prywes R, Prives C. Wild-type p53 activates transcription in vitro. Nature. 1992 July 02;358(6381):83-6.

199. Kern SE, Kinzler KW, Bruskin A, Jarosz D, Friedman P, Prives C, et al. Identification of p53 as a sequence-specific DNA-binding protein. Science. 1991 June 21;252(5013):1708-11.

200. Fields S, Jang SK. Presence of a potent transcription activating sequence in the p53 protein. Science. 1990 August 31;249(4972):1046-9.

201. Raycroft L, Wu HY, Lozano G. Transcriptional activation by wild-type but not transforming mutants of the p53 anti-oncogene. Science. 1990 August 31;249(4972):1049-51.

202. Donehower LA, Harvey M, Slagle BL, McArthur MJ, Montgomery CA, Butel JS, et al. Mice deficient for p53 are developmentally normal but susceptible to spontaneous tumours. Nature. 1992 March 19;356(6366):215-21.

203. Li FP, Fraumeni JF. Prospective study of a family cancer syndrome. JAMA. 1982 May 21;247(19):2692-4.

204. Pirollo K, Srivastava S, Blattner W, Zou Z, Chang EH. Germ-line transmission of a mutated p53 gene in a cancer-prone family with Li-Fraumeni syndrome. Nature. 1990 Dec 27,;348(6303):747-9.

205. Malkin D, Li FP, Strong LC, Fraumeni JF, Nelson CE, Kim DH, et al. Germ line p53 mutations in a familial syndrome of breast cancer, sarcomas, and other neoplasms. Science. 1990 Nov 30,;250(4985):1233-8.

206. Li FP, Fraumeni JF. Soft-tissue sarcomas, breast cancer, and other neoplasms. A familial syndrome? Ann Intern Med. 1969 Oct;71(4):747-52.

207. Hinds P, Finlay C, Levine AJ. Mutation is required to activate the p53 gene for cooperation with the ras oncogene and transformation. J Virol. 1989 Feb;63(2):739-46.

208. Finlay CA, Hinds PW, Tan TH, Eliyahu D, Oren M, Levine AJ. Activating mutations for transformation by p53 produce a gene product that forms an hsc70-p53 complex with an altered half-life. Mol Cell Biol. 1988 Feb;8(2):531-9.

209. Eliyahu D, Goldfinger N, Pinhasi-Kimhi O, Shaulsky G, Skurnik Y, Arai N, et al. Meth A fibrosarcoma cells express two transforming mutant p53 species. Oncogene. 1988 Sep;3(3):313-21.

210. Ben David Y, Prideaux VR, Chow V, Benchimol S, Bernstein A. Inactivation of the p53 oncogene by internal deletion or retroviral integration in erythroleukemic cell lines induced by Friend leukemia virus. Oncogene. 1988 Aug;3(2):179-85.

211. Wolf D, Rotter V. Inactivation of p53 gene expression by an insertion of Moloney murine leukemia virus-like DNA sequences. Mol Cell Biol. 1984 Jul;4(7):1402-10.

212. Mowat M, Cheng A, Kimura N, Bernstein A, Benchimol S. Rearrangements of the cellular p53 gene in erythroleukaemic cells transformed by Friend virus. Nature. 1985 Apr 18-24;314(6012):633-6.

213. Parada LF, Land H, Weinberg RA, Wolf D, Rotter V. Cooperation between gene encoding p53 tumour antigen and ras in cellular transformation. Nature. 1984 Dec 13-19;312(5995):649-51.

214. Jenkins JR, Rudge K, Currie GA. Cellular immortalization by a cDNA clone encoding the transformation-associated phosphoprotein p53. Nature. 1984 Dec 13-19;312(5995):651-4.

215. Eliyahu D, Raz A, Gruss P, Givol D, Oren M. Participation of p53 cellular tumour antigen in transformation of normal embryonic cells. Nature. 1984 Dec 13-19;312(5995):646-9.

216. Kress M, May E, Cassingena R, May P. Simian virus 40-transformed cells express new species of proteins precipitable by anti-simian virus 40 tumor serum. J Virol. 1979 Aug;31(2):472-83.

217. DeLeo AB, Jay G, Appella E, Dubois GC, Law LW, Old LJ. Detection of a transformation-related antigen in chemically induced sarcomas and other transformed cells of the mouse. Proc Natl Acad Sci U S A. 1979 May;76(5):2420-4.

218. Linzer DI, Levine AJ. Characterization of a 54K dalton cellular SV40 tumor antigen present in SV40-transformed cells and uninfected embryonal carcinoma cells. Cell. 1979 May;17(1):43-52.

219. Lane DP, Crawford LV. T antigen is bound to a host protein in SV40-transformed cells. Nature. 1979 Mar 15,;278(5701):261-3.

220. Nigro JM, Baker SJ, Preisinger AC, Jessup JM, Hostetter R, Cleary K, et al. Mutations in the p53 gene occur in diverse human tumour types. Nature. 1989 Dec 07,;342(6250):705-8.

221. Takahashi T, Nau MM, Chiba I, Birrer MJ, Rosenberg RK, Vinocour M, et al. p53: a frequent target for genetic abnormalities in lung cancer. Science. 1989 Oct 27,;246(4929):491-4.

222. Baker SJ, Fearon ER, Nigro JM, Hamilton SR, Preisinger AC, Jessup JM, et al. Chromosome 17 deletions and p53 gene mutations in colorectal carcinomas. Science. 1989 Apr 14,;244(4901):217-21.

223. Nakai H, Misawa S, Toguchida J, Yandell DW, Ishizaki K. Frequent p53 gene mutations in blast crisis of chronic myelogenous leukemia, especially in myeloid crisis harboring loss of a chromosome 17p. Cancer Res. 1992 Dec 01,;52(23):6588-93.

224. Hollstein MC, Metcalf RA, Welsh JA, Montesano R, Harris CC. Frequent mutation of the p53 gene in human esophageal cancer. Proc Natl Acad Sci U S A. 1990 Dec;87(24):9958-61.

225. Hollstein M, Sidransky D, Vogelstein B, Harris CC. p53 mutations in human cancers. Science. 1991 Jul 05,;253(5015):49-53.

226. Hanahan D, Weinberg RA. Hallmarks of cancer: the next generation. Cell. 2011 Mar 04,;144(5):646-74.

227. Tarini Sinha. Tumors: Benign and Malignant. 2018;10.

228. Klein G. Oncogenes and Tumor Suppressor Genes. Acta Oncol. 1988;27(4):427-37.

229. Lee, Eva Y. H. P., Muller WJ. Oncogenes and tumor suppressor genes. Cold Spring Harb Perspect Biol. 2010 Oct;2(10):a003236.

230. Roos WP, Thomas AD, Kaina B. DNA damage and the balance between survival and death in cancer biology. Nat Rev Cancer. 2016 January 01;16(1):20-33.

231. IARC monographs on the evaluation of carcinogenic risks to humans. Solar and ultraviolet radiation. IARC Monogr Eval Carcinog Risks Hum. 1992;55:1-316.

232. IARC Working Group on the Evaluation of Carcinogenic Risks to Humans. Tobacco smoke and involuntary smoking. IARC Monogr Eval Carcinog Risks Hum. 2004;83:1-1438.

233. Boffetta P. Involuntary smoking and lung cancer. Scand J Work Environ Health. 2002;28 Suppl 2:30-40.

234. Storz P. Reactive oxygen species in tumor progression. Front Biosci. 2005 May 01;10:1881-96.

235. Thomas DB, Rosenblatt K, Jimenez LM, McTiernan A, Stalsberg H, Stemhagen A, et al. Ionizing radiation and breast cancer in men (United States). Cancer Causes Control. 1994 January 01;5(1):9-14.

236. Hanahan D, Weinberg RA. The hallmarks of cancer. Cell. 2000 January 07;100(1):57-70.

237. Joerger AC, Fersht AR. The p53 Pathway: Origins, Inactivation in Cancer, and Emerging Therapeutic Approaches. Annu Rev Biochem. 2016 June 02;85:375-404.

238. Brenner DR, Weir HK, Demers AA, Ellison LF, Louzado C, Shaw A, et al. Projected estimates of cancer in Canada in 2020. CMAJ. 2020 March 02;192(9):E199-205.

239. Bouaoun L, Sonkin D, Ardin M, Hollstein M, Byrnes G, Zavadil J, et al. TP53 Variations in Human Cancers: New Lessons from the IARC TP53 Database and Genomics Data. Hum Mutat. 2016 09;37(9):865-76.

240. Wu H, Hu Z, Liu XQ. Protein trans-splicing by a split intein encoded in a split DnaE gene of Synechocystis sp. PCC6803. Proc Natl Acad Sci U S A. 1998 August 04;95(16):9226-31.

241. Liu D, Xu R, Cowburn D. Segmental isotopic labeling of proteins for nuclear magnetic resonance. Methods Enzymol. 2009;462:151-75.

242. Nomura K, Klejnot M, Kowalczyk D, Hock AK, Sibbet GJ, Vousden KH, et al. Structural analysis of MDM2 RING separates degradation from regulation of p53 transcription activity. Nat Struct Mol Biol. 2017 July 01;24(7):578-87.

243. Kostic M, Matt T, Martinez-Yamout MA, Dyson HJ, Wright PE. Solution structure of the Hdm2 C2H2C4 RING, a domain critical for ubiquitination of p53. J Mol Biol. 2006 October 20;363(2):433-50.

244. Kostic M, Matt T, Martinez-Yamout MA, Dyson HJ, Wright PE. Solution structure of the Hdm2 C2H2C4 RING, a domain critical for ubiquitination of p53. J Mol Biol. 2006 Oct 20,;363(2):433-50.

245. Joerger AC, Ang HC, Fersht AR. Structural basis for understanding oncogenic p53 mutations and designing rescue drugs. Proc Natl Acad Sci U S A. 2006 Oct 10,;103(41):15056-61.

246. Bullock AN, Henckel J, Fersht AR. Quantitative analysis of residual folding and DNA binding in mutant p53 core domain: definition of mutant states for rescue in cancer therapy. Oncogene. 2000 Mar 2,;19(10):1245-56.

247. Wong KB, DeDecker BS, Freund SM, Proctor MR, Bycroft M, Fersht AR. Hot-spot mutants of p53 core domain evince characteristic local structural changes. Proc Natl Acad Sci U S A. 1999 Jul 20,;96(15):8438-42.

248. Soong R, Robbins PD, Dix BR, Grieu F, Lim B, Knowles S, et al. Concordance between p53 protein overexpression and gene mutation in a large series of common human carcinomas. Hum Pathol. 1996 Oct;27(10):1050-5.

249. Inoue K, Kurabayashi A, Shuin T, Ohtsuki Y, Furihata M. Overexpression of p53 protein in human tumors. Med Mol Morphol. 2012 June 01;45(3):115-23.

250. Iggo R, Gatter K, Bartek J, Lane D, Harris AL. Increased expression of mutant forms of p53 oncogene in primary lung cancer. Lancet. 1990 March 24;335(8691):675-9.

251. Gannon JV, Greaves R, Iggo R, Lane DP. Activating mutations in p53 produce a common conformational effect. A monoclonal antibody specific for the mutant form. EMBO J. 1990 May 01;9(5):1595-602.

252. Rodrigues NR, Rowan A, Smith ME, Kerr IB, Bodmer WF, Gannon JV, et al. P53 Mutations in Colorectal Cancer. Proc Natl Acad Sci U S A. 1990 October 01;87(19):7555-9.

253. Bartek J, Bartkova J, Vojtesek B, Staskova Z, Lukas J, Rejthar A, et al. Aberrant expression of the p53 oncoprotein is a common feature of a wide spectrum of human malignancies. Oncogene. 1991 September 01;6(9):1699-703.

254. Lukashchuk N, Vousden KH. Ubiquitination and degradation of mutant p53. Mol Cell Biol. 2007 Dec;27(23):8284-95.

255. Burgess A, Chia KM, Haupt S, Thomas D, Haupt Y, Lim E. Clinical Overview of MDM2/X-Targeted Therapies. Front Oncol. 2016;6:7.

256. Jackson MW, Berberich SJ. MdmX protects p53 from Mdm2-mediated degradation. Mol Cell Biol. 2000 Feb;20(3):1001-7.

257. Uhrinova S, Uhrin D, Powers H, Watt K, Zheleva D, Fischer P, et al. Structure of free MDM2 N-terminal domain reveals conformational adjustments that accompany p53-binding. J Mol Biol. 2005 Jul 15,;350(3):587-98.

258. Chemes LB, Alonso LG, Noval MG, de Prat-Gay G. Circular dichroism techniques for the analysis of intrinsically disordered proteins and domains. Methods Mol Biol. 2012;895:387-404.

259. Laurie NA, Donovan SL, Shih C, Zhang J, Mills N, Fuller C, et al. Inactivation of the p53 pathway in retinoblastoma. Nature. 2006 Nov 02,;444(7115):61-6.

260. Wei X, Wu S, Song T, Chen L, Gao M, Borcherds W, et al. Secondary interaction between MDMX and p53 core domain inhibits p53 DNA binding. Proc Natl Acad Sci U S A. 2016 May 10;113(19):2558.

261. Lum JK, Neuweiler H, Fersht AR. Long-range modulation of chain motions within the intrinsically disordered transactivation domain of tumor suppressor p53. J Am Chem Soc. 2012 January 25;134(3):1617-22.

262. Wells M, Tidow H, Rutherford TJ, Markwick P, Jensen MR, Mylonas E, et al. Structure of tumor suppressor p53 and its intrinsically disordered N-terminal transactivation domain. Proc Natl Acad Sci U S A. 2008 April 15;105(15):5762-7.

263. Jin A, Itahana K, O'Keefe K, Zhang Y. Inhibition of HDM2 and activation of p53 by ribosomal protein L23. Mol Cell Biol. 2004 Sep;24(17):7669-80.

264. Dai M, Zeng SX, Jin Y, Sun X, David L, Lu H. Ribosomal protein L23 activates p53 by inhibiting MDM2 function in response to ribosomal perturbation but not to translation inhibition. Mol Cell Biol. 2004 Sep;24(17):7654-68.

265. Lohrum MA, Ludwig RL, Kubbutat MH, Hanlon M, Vousden KH. Regulation of HDM2 activity by the ribosomal protein L11. Cancer Cell. 2003 June 01;3(6):577-87.

266. Marechal V, Elenbaas B, Piette J, Nicolas JC, Levine AJ. The ribosomal L5 protein is associated with mdm-2 and mdm-2-p53 complexes. Mol Cell Biol. 1994 November 01;14(11):7414-20.

267. Dai MS, Lu H. Inhibition of MDM2-mediated p53 ubiquitination and degradation by ribosomal protein L5. J Biol Chem. 2004 October 22;279(43):44475-82.

268. Lindstrom MS, Jin A, Deisenroth C, White Wolf G, Zhang Y. Cancer-associated mutations in the MDM2 zinc finger domain disrupt ribosomal protein interaction and attenuate MDM2-induced p53 degradation. Mol Cell Biol. 2007 February 01;27(3):1056-68.

269. Honda R, Tanaka H, Yasuda H. Oncoprotein MDM2 is a ubiquitin ligase E3 for tumor suppressor p53. FEBS Lett. 1997 December 22;420(1):25-7.

270. Saito S, Goodarzi AA, Higashimoto Y, Noda Y, Lees-Miller SP, Appella E, et al. ATM mediates phosphorylation at multiple p53 sites, including Ser(46), in response to ionizing radiation. J Biol Chem. 2002 April 12;277(15):12491-4.

271. She QB, Chen N, Dong Z. ERKs and p38 kinase phosphorylate p53 protein at serine 15 in response to UV radiation. J Biol Chem. 2000 July 07;275(27):20444-9.

272. Bulavin DV, Saito S, Hollander MC, Sakaguchi K, Anderson CW, Appella E, et al. Phosphorylation of human p53 by p38 kinase coordinates N-terminal phosphorylation and apoptosis in response to UV radiation. EMBO J. 1999 December 01;18(23):6845-54.

273. Zhao H, Traganos F, Darzynkiewicz Z. Phosphorylation of p53 on Ser15 during cell cycle caused by Topo I and Topo II inhibitors in relation to ATM and Chk2 activation. Cell Cycle. 2008 October 01;7(19):3048-55.

274. Loughery J, Cox M, Smith LM, Meek DW. Critical role for p53-serine 15 phosphorylation in stimulating transactivation at p53-responsive promoters. Nucleic Acids Res. 2014 July 01;42(12):7666-80.

275. Jabbur JR, Huang P, Zhang W. DNA damage-induced phosphorylation of p53 at serine 20 correlates with p21 and Mdm-2 induction in vivo. Oncogene. 2000 December 14;19(54):6203-8.

276. Chehab NH, Malikzay A, Stavridi ES, Halazonetis TD. Phosphorylation of Ser-20 mediates stabilization of human p53 in response to DNA damage. Proc Natl Acad Sci U S A. 1999 November 23;96(24):13777-82.

277. Feng L, Hollstein M, Xu Y. Ser46 phosphorylation regulates p53-dependent apoptosis and replicative senescence. Cell Cycle. 2006 December 01;5(23):2812-9.

278. Chao C, Herr D, Chun J, Xu Y. Ser18 and 23 phosphorylation is required for p53-dependent apoptosis and tumor suppression. EMBO J. 2006 June 07;25(11):2615-22.

279. Chao C, Hergenhahn M, Kaeser MD, Wu Z, Saito S, Iggo R, et al. Cell type- and promoter-specific roles of Ser18 phosphorylation in regulating p53 responses. J Biol Chem. 2003 October 17;278(42):41028-33.

280. Armata HL, Garlick DS, Sluss HK. The ataxia telangiectasia-mutated target site Ser18 is required for p53-mediated tumor suppression. Cancer Res. 2007 December 15;67(24):11696-703.

281. Pavithra L, Mukherjee S, Sreenath K, Kar S, Sakaguchi K, Roy S, et al. SMAR1 forms a ternary complex with p53-MDM2 and negatively regulates p53-mediated transcription. J Mol Biol. 2009 May 15;388(4):691-702.

282. Cai X, Liu X. Inhibition of Thr-55 phosphorylation restores p53 nuclear localization and sensitizes cancer cells to DNA damage. Proc Natl Acad Sci U S A. 2008 November 04;105(44):16958-63.

283. Petitjean A, Mathe E, Kato S, Ishioka C, Tavtigian SV, Hainaut P, et al. Impact of mutant p53 functional properties on TP53 mutation patterns and tumor phenotype: lessons from recent developments in the IARC TP53 database. Hum Mutat. 2007 June 01;28(6):622-9.

284. Teufel DP, Bycroft M, Fersht AR. Regulation by phosphorylation of the relative affinities of the N-terminal transactivation domains of p53 for p300 domains and Mdm2. Oncogene. 2009 May 21;28(20):2112-8.

285. Rustandi RR, Baldisseri DM, Weber DJ. Structure of the negative regulatory domain of p53 bound to S100B(betabeta). Nat Struct Biol. 2000 July 01;7(7):570-4.

286. Tong Q, Cui G, Botuyan MV, Rothbart SB, Hayashi R, Musselman CA, et al. Structural plasticity of methyllysine recognition by the tandem tudor domain of 53BP1. Structure. 2015 February 03;23(2):312-21.

287. Miller Jenkins LM, Feng H, Durell SR, Tagad HD, Mazur SJ, Tropea JE, et al. Characterization of the p300 Taz2-p53 TAD2 complex and comparison with the p300 Taz2-p53 TAD1 complex. Biochemistry. 2015 March 24;54(11):2001-10.

288. Krois AS, Ferreon JC, Martinez-Yamout MA, Dyson HJ, Wright PE. Recognition of the disordered p53 transactivation domain by the transcriptional adapter zinc finger domains of CREB-binding protein. Proc Natl Acad Sci U S A. 2016 March 29;113(13):1853.

289. Lee CW, Martinez-Yamout MA, Dyson HJ, Wright PE. Structure of the p53 transactivation domain in complex with the nuclear receptor coactivator binding domain of CREB binding protein. Biochemistry. 2010 November 23;49(46):9964-71.

290. Harris CC. P53: at the Crossroads of Molecular Carcinogenesis and Risk Assessment. Science. 1993 December 24;262(5142):1980-1.

291. Oda E, Ohki R, Murasawa H, Nemoto J, Shibue T, Yamashita T, et al. Noxa, a BH3-only member of the Bcl-2 family and candidate mediator of p53-induced apoptosis. Science. 2000 May 12;288(5468):1053-8.

292. Nakano K, Vousden KH. PUMA, a novel proapoptotic gene, is induced by p53. Mol Cell. 2001 March 01;7(3):683-94.

293. Miyashita T, Reed JC. Tumor suppressor p53 is a direct transcriptional activator of the human bax gene. Cell. 1995 January 27;80(2):293-9.

294. Selvakumaran M, Lin HK, Miyashita T, Wang HG, Krajewski S, Reed JC, et al. Immediate early up-regulation of bax expression by p53 but not TGF beta 1: a paradigm for distinct apoptotic pathways. Oncogene. 1994 June 01;9(6):1791-8.

295. Miyashita T, Krajewski S, Krajewska M, Wang HG, Lin HK, Liebermann DA, et al. Tumor suppressor p53 is a regulator of bcl-2 and bax gene expression in vitro and in vivo. Oncogene. 1994 June 01;9(6):1799-805.

296. Stambolic V, MacPherson D, Sas D, Lin Y, Snow B, Jang Y, et al. Regulation of PTEN transcription by p53. Mol Cell. 2001 August 01;8(2):317-25.

297. Hoffman WH, Biade S, Zilfou JT, Chen J, Murphy M. Transcriptional repression of the anti-apoptotic survivin gene by wild type p53. J Biol Chem. 2002 February 01;277(5):3247-57.

298. Bartke T, Siegmund D, Peters N, Reichwein M, Henkler F, Scheurich P, et al. p53 upregulates cFLIP, inhibits transcription of NF-kappaB-regulated genes and induces caspase-8-independent cell death in DLD-1 cells. Oncogene. 2001 February 01;20(5):571-80.

299. Marchenko ND, Zaika A, Moll UM. Death signal-induced localization of p53 protein to mitochondria. A potential role in apoptotic signaling. J Biol Chem. 2000 May 26;275(21):16202-12.

300. Mihara M, Erster S, Zaika A, Petrenko O, Chittenden T, Pancoska P, et al. P53 has a Direct Apoptogenic Role at the Mitochondria. Mol Cell. 2003 March 01;11(3):577-90.

301. Chang BD, Xuan Y, Broude EV, Zhu H, Schott B, Fang J, et al. Role of p53 and p21waf1/cip1 in senescence-like terminal proliferation arrest induced in human tumor cells by chemotherapeutic drugs. Oncogene. 1999 August 26;18(34):4808-18.

302. Brown JP, Wei W, Sedivy JM. Bypass of senescence after disruption of p21CIP1/WAF1 gene in normal diploid human fibroblasts. Science. 1997 August 08;277(5327):831-4.

303. Harper JW, Adami GR, Wei N, Keyomarsi K, Elledge SJ. The p21 Cdk-interacting protein Cip1 is a potent inhibitor of G1 cyclin-dependent kinases. Cell. 1993 November 19;75(4):805-16.

304. Finlay CA, Hinds PW, Levine AJ. The p53 proto-oncogene can act as a suppressor of transformation. Cell. 1989 June 30;57(7):1083-93.

305. el-Deiry WS, Tokino T, Velculescu VE, Levy DB, Parsons R, Trent JM, et al. WAF1, a potential mediator of p53 tumor suppression. Cell. 1993 November 19;75(4):817-25.

306. Fang S, Jensen JP, Ludwig RL, Vousden KH, Weissman AM. Mdm2 is a RING finger-dependent ubiquitin protein ligase for itself and p53. J Biol Chem. 2000 March 24;275(12):8945-51.

307. Wiech M, Olszewski MB, Tracz-Gaszewska Z, Wawrzynow B, Zylicz M, Zylicz A. Molecular mechanism of mutant p53 stabilization: the role of HSP70 and MDM2. PLoS One. 2012;7(12):e51426.

308. Muller P, Ceskova P, Vojtesek B. Hsp90 is essential for restoring cellular functions of temperature-sensitive p53 mutant protein but not for stabilization and activation of wild-type p53: implications for cancer therapy. J Biol Chem. 2005 February 25;280(8):6682-91.

309. Park SJ, Kostic M, Dyson HJ. Dynamic Interaction of Hsp90 with Its Client Protein p53. J Mol Biol. 2011 August 05;411(1):158-73.

310. Ayrault O, Godeny MD, Dillon C, Zindy F, Fitzgerald P, Roussel MF, et al. Inhibition of Hsp90 via 17-DMAG induces apoptosis in a p53-dependent manner to prevent medulloblastoma. Proc Natl Acad Sci U S A. 2009 October 06;106(40):17037-42.

311. Muller P, Hrstka R, Coomber D, Lane DP, Vojtesek B. Chaperone-dependent stabilization and degradation of p53 mutants. Oncogene. 2008 May 29;27(24):3371-83.

312. Peng Y, Chen L, Li C, Lu W, Chen J. Inhibition of MDM2 by hsp90 contributes to mutant p53 stabilization. J Biol Chem. 2001 November 02;276(44):40583-90.

313. Nagata Y, Anan T, Yoshida T, Mizukami T, Taya Y, Fujiwara T, et al. The stabilization mechanism of mutant-type p53 by impaired ubiquitination: the loss of wild-type p53 function and the hsp90 association. Oncogene. 1999 October 28;18(44):6037-49.

314. Menon AG, Anderson KM, Riccardi VM, Chung RY, Whaley JM, Yandell DW, et al. Chromosome 17p deletions and p53 gene mutations associated with the formation of malignant neurofibrosarcomas in von Recklinghausen neurofibromatosis. Proc Natl Acad Sci U S A. 1990 July 01;87(14):5435-9.

315. Kotler E, Shani O, Goldfeld G, Lotan-Pompan M, Tarcic O, Gershoni A, et al. A Systematic p53 Mutation Library Links Differential Functional Impact to Cancer Mutation Pattern and Evolutionary Conservation. Mol Cell. 2018 September 06;71(5):873.

316. Kato S, Han SY, Liu W, Otsuka K, Shibata H, Kanamaru R, et al. Understanding the function-structure and function-mutation relationships of p53 tumor suppressor protein by high-resolution missense mutation analysis. Proc Natl Acad Sci U S A. 2003 July 08;100(14):8424-9.

317. El-Hizawi S, Lagowski JP, Kulesz-Martin M, Albor A. Induction of gene amplification as a gain-of-function phenotype of mutant p53 proteins. Cancer Res. 2002 June 01;62(11):3264-70.

318. Gualberto A, Aldape K, Kozakiewicz K, Tlsty TD. An oncogenic form of p53 confers a dominant, gain-of-function phenotype that disrupts spindle checkpoint control. Proc Natl Acad Sci U S A. 1998 April 28;95(9):5166-71.

319. Kern SE, Kinzler KW, Baker SJ, Nigro JM, Rotter V, Levine AJ, et al. Mutant p53 proteins bind DNA abnormally in vitro. Oncogene. 1991 January 01;6(1):131-6.

320. Shaulsky G, Goldfinger N, Rotter V. Alterations in tumor development in vivo mediated by expression of wild type or mutant p53 proteins. Cancer Res. 1991 October 01;51(19):5232-7.

321. Valenti F, Ganci F, Fontemaggi G, Sacconi A, Strano S, Blandino G, et al. Gain of function mutant p53 proteins cooperate with E2F4 to transcriptionally downregulate RAD17 and BRCA1 gene expression. Oncotarget. 2015 March 20;6(8):5547-66.

322. Polotskaia A, Xiao G, Reynoso K, Martin C, Qiu WG, Hendrickson RC, et al. Proteome-wide analysis of mutant p53 targets in breast cancer identifies new levels of gain-of-function that influence PARP, PCNA, and MCM4. Proc Natl Acad Sci U S A. 2015 March 17;112(11):1220.

323. Roy S, Tomaszowski KH, Luzwick JW, Park S, Li J, Murphy M, et al. p53 orchestrates DNA replication restart homeostasis by suppressing mutagenic RAD52 and POLtheta pathways. Elife. 2018 January 15;7:10.7554/eLife.31723.

324. Pfister NT, Prives C. Chromatin dysregulation by mutant p53. Oncotarget. 2016 May 24;7(21):29875-6.

325. Liu K, Lin FT, Graves JD, Lee YJ, Lin WC. Mutant p53 perturbs DNA replication checkpoint control through TopBP1 and Treslin. Proc Natl Acad Sci U S A. 2017 May 09;114(19):E3766-75.

326. Pfister NT, Fomin V, Regunath K, Zhou JY, Zhou W, Silwal-Pandit L, et al. Mutant p53 cooperates with the SWI/SNF chromatin remodeling complex to regulate VEGFR2 in breast cancer cells. Genes Dev. 2015 June 15;29(12):1298-315.

327. Do PM, Varanasi L, Fan S, Li C, Kubacka I, Newman V, et al. Mutant p53 cooperates with ETS2 to promote etoposide resistance. Genes Dev. 2012 April 15;26(8):830-45.

328. Weissmueller S, Manchado E, Saborowski M, Morris JP, Wagenblast E, Davis CA, et al. Mutant p53 drives pancreatic cancer metastasis through cell-autonomous PDGF receptor beta signaling. Cell. 2014 April 10;157(2):382-94.

329. Subramanian M, Francis P, Bilke S, Li XL, Hara T, Lu X, et al. A mutant p53/let-7i-axis-regulated gene network drives cell migration, invasion and metastasis. Oncogene. 2015 February 26;34(9):1094-104.

330. Song H, Hollstein M, Xu Y. p53 gain-of-function cancer mutants induce genetic instability by inactivating ATM. Nat Cell Biol. 2007 May 01;9(5):573-80.

331. Song H, Xu Y. Gain of function of p53 cancer mutants in disrupting critical DNA damage response pathways. Cell Cycle. 2007 July 01;6(13):1570-3.

332. Xu Y. Induction of genetic instability by gain-of-function p53 cancer mutants. Oncogene. 2008 June 05;27(25):3501-7.

333. Liu DP, Song H, Xu Y. A common gain of function of p53 cancer mutants in inducing genetic instability. Oncogene. 2010 February 18;29(7):949-56.

334. Hanel W, Marchenko N, Xu S, Yu SX, Weng W, Moll U. Two hot spot mutant p53 mouse models display differential gain of function in tumorigenesis. Cell Death Differ. 2013 July 01;20(7):898-909.

335. Olive KP, Tuveson DA, Ruhe ZC, Yin B, Willis NA, Bronson RT, et al. Mutant p53 gain of function in two mouse models of Li-Fraumeni syndrome. Cell. 2004 December 17;119(6):847-60.

336. Kollareddy M, Dimitrova E, Vallabhaneni KC, Chan A, Le T, Chauhan KM, et al. Regulation of nucleotide metabolism by mutant p53 contributes to its gain-of-function activities. Nat Commun. 2015 June 12;6:7389.

337. Freed-Pastor WA, Mizuno H, Zhao X, Langerod A, Moon SH, Rodriguez-Barrueco R, et al. Mutant p53 disrupts mammary tissue architecture via the mevalonate pathway. Cell. 2012 January 20;148(1-2):244-58.

338. Zhang C, Liu J, Liang Y, Wu R, Zhao Y, Hong X, et al. Tumour-associated mutant p53 drives the Warburg effect. Nat Commun. 2013;4:2935.

339. Chavez-Perez VA, Strasberg-Rieber M, Rieber M. Metabolic utilization of exogenous pyruvate by mutant p53 (R175H) human melanoma cells promotes survival under glucose depletion. Cancer Biol Ther. 2011 October 01;12(7):647-56.

340. Kalo E, Kogan-Sakin I, Solomon H, Bar-Nathan E, Shay M, Shetzer Y, et al. Mutant p53R273H attenuates the expression of phase 2 detoxifying enzymes and promotes the survival of cells with high levels of reactive oxygen species. J Cell Sci. 2012 November 15;125(Pt 22):5578-86.

341. Zhu J, Sammons MA, Donahue G, Dou Z, Vedadi M, Getlik M, et al. Gain-of-function p53 mutants co-opt chromatin pathways to drive cancer growth. Nature. 2015 September 10;525(7568):206-11.

342. Eriksson M, Ambroise G, Ouchida AT, Lima Queiroz A, Smith D, Gimenez-Cassina A, et al. Effect of Mutant p53 Proteins on Glycolysis and Mitochondrial Metabolism. Mol Cell Biol. 2017 November 28;37(24):10.1128/MCB.00328,17. Print 2017 Dec 15.

343. Kupryjanczyk J, Thor AD, Beauchamp R, Merritt V, Edgerton SM, Bell DA, et al. P53 Gene Mutations and Protein Accumulation in Human Ovarian Cancer. Proc Natl Acad Sci U S A. 1993 June 01;90(11):4961-5.

344. Xu HJ, Cagle PT, Hu SX, Li J, Benedict WF. Altered retinoblastoma and p53 protein status in non-small cell carcinoma of the lung: potential synergistic effects on prognosis. Clin Cancer Res. 1996 July 01;2(7):1169-76.

345. Elledge RM, Clark GM, Fuqua SA, Yu YY, Allred DC. P53 Protein Accumulation Detected by Five Different Antibodies: Relationship to Prognosis and Heat Shock Protein 70 in Breast Cancer. Cancer Res. 1994 July 15;54(14):3752-7.

346. Thor AD, Moore DH, Edgerton SM, Kawasaki ES, Reihsaus E, Lynch HT, et al. Accumulation of p53 tumor suppressor gene protein: an independent marker of prognosis in breast cancers. J Natl Cancer Inst. 1992 June 03;84(11):845-55.

347. Quinn DI, Henshall SM, Head DR, Golovsky D, Wilson JD, Brenner PC, et al. Prognostic significance of p53 nuclear accumulation in localized prostate cancer treated with radical prostatectomy. Cancer Res. 2000 March 15;60(6):1585-94.

348. Wu W, Xu C, Ling X, Fan C, Buckley BP, Chernov MV, et al. Targeting RING domains of Mdm2-MdmX E3 complex activates apoptotic arm of the p53 pathway in leukemia/lymphoma cells. Cell Death Dis. 2015 December 31;6:e2035.

349. Patton JT, Mayo LD, Singhi AD, Gudkov AV, Stark GR, Jackson MW. Levels of HdmX expression dictate the sensitivity of normal and transformed cells to Nutlin-3. Cancer Res. 2006 March 15;66(6):3169-76.

350. Wade M, Wong ET, Tang M, Stommel JM, Wahl GM. Hdmx modulates the outcome of p53 activation in human tumor cells. J Biol Chem. 2006 November 03;281(44):33036-44.

351. Hu B, Gilkes DM, Farooqi B, Sebti SM, Chen J. MDMX overexpression prevents p53 activation by the MDM2 inhibitor Nutlin. J Biol Chem. 2006 November 03;281(44):33030-5.

352. Popowicz GM, Czarna A, Holak TA. Structure of the human Mdmx protein bound to the p53 tumor suppressor transactivation domain. Cell Cycle. 2008 August 01;7(15):2441-3.

353. Zuckerman V, Lenos K, Popowicz GM, Silberman I, Grossman T, Marine JC, et al. c-Abl phosphorylates Hdmx and regulates its interaction with p53. J Biol Chem. 2009 February 06;284(6):4031-9.

354. Chen L, Li C, Pan Y, Chen J. Regulation of p53-MDMX interaction by casein kinase 1 alpha. Mol Cell Biol. 2005 August 01;25(15):6509-20.

355. Wu S, Chen L, Becker A, Schonbrunn E, Chen J. Casein kinase 1alpha regulates an MDMX intramolecular interaction to stimulate p53 binding. Mol Cell Biol. 2012 December 01;32(23):4821-32.

356. Gu J, Kawai H, Nie L, Kitao H, Wiederschain D, Jochemsen AG, et al. Mutual dependence of MDM2 and MDMX in their functional inactivation of p53. J Biol Chem. 2002 May 31;277(22):19251-4.

357. Okamoto K, Taya Y, Nakagama H. Mdmx enhances p53 ubiquitination by altering the substrate preference of the Mdm2 ubiquitin ligase. FEBS Lett. 2009 September 03;583(17):2710-4.

358. O'Keefe K, Li H, Zhang Y. Nucleocytoplasmic shuttling of p53 is essential for MDM2-mediated cytoplasmic degradation but not ubiquitination. Mol Cell Biol. 2003 September 01;23(18):6396-405.

359. Linares LK, Hengstermann A, Ciechanover A, Muller S, Scheffner M. HdmX stimulates Hdm2-mediated ubiquitination and degradation of p53. Proc Natl Acad Sci U S A. 2003 October 14;100(21):12009-14.

360. Li M, Brooks CL, Wu-Baer F, Chen D, Baer R, Gu W. Mono- versus polyubiquitination: differential control of p53 fate by Mdm2. Science. 2003 December 12;302(5652):1972-5.

361. Kawai H, Lopez-Pajares V, Kim MM, Wiederschain D, Yuan ZM. RING domain-mediated interaction is a requirement for MDM2's E3 ligase activity. Cancer Res. 2007 July 01;67(13):6026-30.

362. Linke K, Mace PD, Smith CA, Vaux DL, Silke J, Day CL. Structure of the MDM2/MDMX RING domain heterodimer reveals dimerization is required for their ubiquitylation in trans. Cell Death Differ. 2008 May 01;15(5):841-8.

363. Danovi D, Meulmeester E, Pasini D, Migliorini D, Capra M, Frenk R, et al. Amplification of Mdmx (or Mdm4) directly contributes to tumor formation by inhibiting p53 tumor suppressor activity. Mol Cell Biol. 2004 July 01;24(13):5835-43.

364. Shvarts A, Bazuine M, Dekker P, Ramos YF, Steegenga WT, Merckx G, et al. Isolation and identification of the human homolog of a new p53-binding protein, Mdmx. Genomics. 1997 July 01;43(1):34-42.

365. Shvarts A, Steegenga WT, Riteco N, van Laar T, Dekker P, Bazuine M, et al. MDMX: a novel p53-binding protein with some functional properties of MDM2. EMBO J. 1996 October 01;15(19):5349-57.

366. Sharp DA, Kratowicz SA, Sank MJ, George DL. Stabilization of the MDM2 oncoprotein by interaction with the structurally related MDMX protein. J Biol Chem. 1999 December 31;274(53):38189-96.

367. Stad R, Ramos YF, Little N, Grivell S, Attema J, van Der Eb, A J, et al. Hdmx stabilizes Mdm2 and p53. J Biol Chem. 2000 September 08;275(36):28039-44.

368. Oliner JD, Pietenpol JA, Thiagalingam S, Gyuris J, Kinzler KW, Vogelstein B. Oncoprotein MDM2 conceals the activation domain of tumour suppressor p53. Nature. 1993 April 29;362(6423):857-60.

369. Wu Y, Lin JC, Piluso LG, Dhahbi JM, Bobadilla S, Spindler SR, et al. Phosphorylation of p53 by TAF1 inactivates p53-dependent transcription in the DNA damage response. Mol Cell. 2014 January 09;53(1):63-74.

370. Follis AV, Llambi F, Ou L, Baran K, Green DR, Kriwacki RW. The DNA-binding domain mediates both nuclear and cytosolic functions of p53. Nat Struct Mol Biol. 2014 June 01;21(6):535-43.

371. Rajagopalan S, Andreeva A, Rutherford TJ, Fersht AR. Mapping the physical and functional interactions between the tumor suppressors p53 and BRCA2. Proc Natl Acad Sci U S A. 2010 May 11;107(19):8587-92.

372. Moynahan ME, Pierce AJ, Jasin M. BRCA2 is required for homology-directed repair of chromosomal breaks. Mol Cell. 2001 February 01;7(2):263-72.

373. Yu VP, Koehler M, Steinlein C, Schmid M, Hanakahi LA, van Gool AJ, et al. Gross chromosomal rearrangements and genetic exchange between nonhomologous chromosomes following BRCA2 inactivation. Genes Dev. 2000 June 01;14(11):1400-6.

374. Bochkareva E, Kaustov L, Ayed A, Yi GS, Lu Y, Pineda-Lucena A, et al. Single-stranded DNA mimicry in the p53 transactivation domain interaction with replication protein A. Proc Natl Acad Sci U S A. 2005 October 25;102(43):15412-7.

375. Rajagopalan S, Andreeva A, Teufel DP, Freund SM, Fersht AR. Interaction between the transactivation domain of p53 and PC4 exemplifies acidic activation domains as single-stranded DNA mimics. J Biol Chem. 2009 August 07;284(32):21728-37.

376. Rodriguez MS, Desterro JM, Lain S, Lane DP, Hay RT. Multiple C-terminal lysine residues target p53 for ubiquitin-proteasome-mediated degradation. Mol Cell Biol. 2000 November 01;20(22):8458-67.

377. Nakamura S, Roth JA, Mukhopadhyay T. Multiple lysine mutations in the C-terminal domain of p53 interfere with MDM2-dependent protein degradation and ubiquitination. Mol Cell Biol. 2000 December 01;20(24):9391-8.

378. Ito A, Kawaguchi Y, Lai CH, Kovacs JJ, Higashimoto Y, Appella E, et al. MDM2-HDAC1-mediated deacetylation of p53 is required for its degradation. EMBO J. 2002 November 15;21(22):6236-45.

379. Gu W, Roeder RG. Activation of p53 sequence-specific DNA binding by acetylation of the p53 C-terminal domain. Cell. 1997 August 22;90(4):595-606.

380. Li M, Luo J, Brooks CL, Gu W. Acetylation of p53 inhibits its ubiquitination by Mdm2. J Biol Chem. 2002 December 27;277(52):50607-11.

381. Ferreon JC, Lee CW, Arai M, Martinez-Yamout MA, Dyson HJ, Wright PE. Cooperative regulation of p53 by modulation of ternary complex formation with CBP/p300 and HDM2. Proc Natl Acad Sci U S A. 2009 April 21;106(16):6591-6.

382. Grossman SR, Perez M, Kung AL, Joseph M, Mansur C, Xiao ZX, et al. p300/MDM2 complexes participate in MDM2-mediated p53 degradation. Mol Cell. 1998 October 01;2(4):405-15.

383. Ito A, Lai CH, Zhao X, Saito S, Hamilton MH, Appella E, et al. p300/CBP-mediated p53 acetylation is commonly induced by p53-activating agents and inhibited by MDM2. EMBO J. 2001 March 15;20(6):1331-40.

384. Midgley CA, Desterro JM, Saville MK, Howard S, Sparks A, Hay RT, et al. An N-terminal p14ARF peptide blocks Mdm2-dependent ubiquitination in vitro and can activate p53 in vivo. Oncogene. 2000 May 04;19(19):2312-23.

385. Inoue T, Geyer RK, Howard D, Yu ZK, Maki CG. MDM2 can promote the ubiquitination, nuclear export, and degradation of p53 in the absence of direct binding. J Biol Chem. 2001 November 30;276(48):45255-60.

386. Kulikov R, Letienne J, Kaur M, Grossman SR, Arts J, Blattner C. Mdm2 facilitates the association of p53 with the proteasome. Proc Natl Acad Sci U S A. 2010 June 01;107(22):10038-43.

387. Fuchs SY, Adler V, Buschmann T, Wu X, Ronai Z. Mdm2 association with p53 targets its ubiquitination. Oncogene. 1998 November 12;17(19):2543-7.

388. Carter S, Bischof O, Dejean A, Vousden KH. C-terminal modifications regulate MDM2 dissociation and nuclear export of p53. Nat Cell Biol. 2007 April 01;9(4):428-35.

389. Lohrum MA, Woods DB, Ludwig RL, Balint E, Vousden KH. C-terminal ubiquitination of p53 contributes to nuclear export. Mol Cell Biol. 2001 December 01;21(24):8521-32.

390. Nie L, Sasaki M, Maki CG. Regulation of p53 nuclear export through sequential changes in conformation and ubiquitination. J Biol Chem. 2007 May 11;282(19):14616-25.

391. Chan WM, Mak MC, Fung TK, Lau A, Siu WY, Poon RY. Ubiquitination of p53 at multiple sites in the DNA-binding domain. Mol Cancer Res. 2006 January 01;4(1):15-25.

392. Peng Y, Chen L, Li C, Lu W, Agrawal S, Chen J. Stabilization of the MDM2 oncoprotein by mutant p53. J Biol Chem. 2001 March 02;276(9):6874-8.

393. Stephen CW, Lane DP. Mutant conformation of p53. Precise epitope mapping using a filamentous phage epitope library. J Mol Biol. 1992 June 05;225(3):577-83.

394. Sdek P, Ying H, Zheng H, Margulis A, Tang X, Tian K, et al. The central acidic domain of MDM2 is critical in inhibition of retinoblastoma-mediated suppression of E2F and cell growth. J Biol Chem. 2004 December 17;279(51):53317-22.

395. Bothner B, Lewis WS, DiGiammarino EL, Weber JD, Bothner SJ, Kriwacki RW. Defining the molecular basis of Arf and Hdm2 interactions. J Mol Biol. 2001 November 23;314(2):263-77.

396. Zhang Y, Wolf GW, Bhat K, Jin A, Allio T, Burkhart WA, et al. Ribosomal protein L11 negatively regulates oncoprotein MDM2 and mediates a p53-dependent ribosomal-stress checkpoint pathway. Mol Cell Biol. 2003 December 01;23(23):8902-12.

397. Meplan C, Richard MJ, Hainaut P. Metalloregulation of the tumor suppressor protein p53: zinc mediates the renaturation of p53 after exposure to metal chelators in vitro and in intact cells. Oncogene. 2000 November 02;19(46):5227-36.

398. Hainaut P, Milner J. A structural role for metal ions in the "wild-type" conformation of the tumor suppressor protein p53. Cancer Res. 1993 April 15;53(8):1739-42.

399. Butler JS, Loh SN. Structure, function, and aggregation of the zinc-free form of the p53 DNA binding domain. Biochemistry. 2003 March 04;42(8):2396-403.

400. Yu X, Blanden AR, Narayanan S, Jayakumar L, Lubin D, Augeri D, et al. Small molecule restoration of wildtype structure and function of mutant p53 using a novel zinc-metallochaperone based mechanism. Oncotarget. 2014 October 15;5(19):8879-92.

401. Nikolova PV, Henckel J, Lane DP, Fersht AR. Semirational design of active tumor suppressor p53 DNA binding domain with enhanced stability. Proc Natl Acad Sci U S A. 1998 December 08;95(25):14675-80.

402. Bullock AN, Henckel J, DeDecker BS, Johnson CM, Nikolova PV, Proctor MR, et al. Thermodynamic stability of wild-type and mutant p53 core domain. Proc Natl Acad Sci U S A. 1997 December 23;94(26):14338-42.

403. Rasquinha JA, Bej A, Dutta S, Mukherjee S. Intrinsic Differences in Backbone Dynamics between Wild Type and DNA-Contact Mutants of the p53 DNA Binding Domain Revealed by Nuclear Magnetic Resonance Spectroscopy. Biochemistry. 2017 September 19;56(37):4962-71.

404. Tompa P, Fuxreiter M. Fuzzy complexes: polymorphism and structural disorder in protein-protein interactions. Trends Biochem Sci. 2008 January 01;33(1):2-8.

405. Hellman M, Tossavainen H, Rappu P, Heino J, Permi P. Characterization of intrinsically disordered prostate associated gene (PAGE5) at single residue resolution by NMR spectroscopy. PLoS One. 2011;6(11):e26633.

406. Kay LE, Torchia DA, Bax A. Backbone dynamics of proteins as studied by 15N inverse detected heteronuclear NMR spectroscopy: application to staphylococcal nuclease. Biochemistry. 1989 November 14;28(23):8972-9.

407. Zhu G, Xia Y, Nicholson LK, Sze KH. Protein dynamics measurements by TROSY-based NMR experiments. J Magn Reson. 2000 April 01;143(2):423-6.

408. Sattler M, Schleucher J, Griesinger C. Heteronuclear multidimensional NMR experiments for the structure determination of proteins in solution employing pulsed field gradients. Progress in Nuclear Magnetic Resonance Spectroscopy. 1999 March 19,;34(2):93-158.

409. Cheng Q, Song T, Chen L, Chen J. Autoactivation of the MDM2 E3 ligase by intramolecular interaction. Mol Cell Biol. 2014 August 01;34(15):2800-10.

410. Ma J, Martin JD, Zhang H, Auger KR, Ho TF, Kirkpatrick RB, et al. A second p53 binding site in the central domain of Mdm2 is essential for p53 ubiquitination. Biochemistry. 2006 August 01;45(30):9238-45.

411. Reifenberger G, Liu L, Ichimura K, Schmidt EE, Collins VP. Amplification and overexpression of the MDM2 gene in a subset of human malignant gliomas without p53 mutations. Cancer Res. 1993 June 15;53(12):2736-9.

412. Leach FS, Tokino T, Meltzer P, Burrell M, Oliner JD, Smith S, et al. p53 Mutation and MDM2 amplification in human soft tissue sarcomas. Cancer Res. 1993 May 15;53(10 Suppl):2231-4.

413. Patterson H, Barnes D, Gill S, Spicer J, Fisher C, Thomas M, et al. Amplification and Over-Expression of the MDM2 Gene in Human Soft Tissue Tumours. Sarcoma. 1997;1(1):17-22.

414. Bond GL, Hu W, Bond EE, Robins H, Lutzker SG, Arva NC, et al. A single nucleotide polymorphism in the MDM2 promoter attenuates the p53 tumor suppressor pathway and accelerates tumor formation in humans. Cell. 2004 November 24;119(5):591-602.

415. Momand J, Jung D, Wilczynski S, Niland J. The MDM2 gene amplification database. Nucleic Acids Res. 1998 August 01;26(15):3453-9.

416. Oliner JD, Kinzler KW, Meltzer PS, George DL, Vogelstein B. Amplification of a gene encoding a p53-associated protein in human sarcomas. Nature. 1992 July 02;358(6381):80-3.

417. Roth J, Dobbelstein M, Freedman DA, Shenk T, Levine AJ. Nucleo-cytoplasmic shuttling of the hdm2 oncoprotein regulates the levels of the p53 protein via a pathway used by the human immunodeficiency virus rev protein. EMBO J. 1998 January 15;17(2):554-64.

418. Honda R, Yasuda H. Activity of MDM2, a ubiquitin ligase, toward p53 or itself is dependent on the RING finger domain of the ligase. Oncogene. 2000 March 09;19(11):1473-6.

419. Dolezelova P, Cetkovska K, Vousden KH, Uldrijan S. Mutational analysis reveals a dual role of Mdm2 acidic domain in the regulation of p53 stability. FEBS Lett. 2012 July 30;586(16):2225-31.

420. Cross B, Chen L, Cheng Q, Li B, Yuan ZM, Chen J. Inhibition of p53 DNA binding function by the MDM2 protein acidic domain. J Biol Chem. 2011 May 06;286(18):16018-29.

421. Kussie PH, Gorina S, Marechal V, Elenbaas B, Moreau J, Levine AJ, et al. Structure of the MDM2 oncoprotein bound to the p53 tumor suppressor transactivation domain. Science. 1996 November 08;274(5289):948-53.

422. Xiao ZX, Chen J, Levine AJ, Modjtahedi N, Xing J, Sellers WR, et al. Interaction between the retinoblastoma protein and the oncoprotein MDM2. Nature. 1995 June 22;375(6533):694-8.

423. Chen J, Lin J, Levine AJ. Regulation of transcription functions of the p53 tumor suppressor by the mdm-2 oncogene. Mol Med. 1995 January 01;1(2):142-52.

424. Momand J, Zambetti GP, Olson DC, George D, Levine AJ. The mdm-2 oncogene product forms a complex with the p53 protein and inhibits p53-mediated transactivation. Cell. 1992 June 26;69(7):1237-45.

425. Picksley SM, Lane DP. The p53-mdm2 autoregulatory feedback loop: a paradigm for the regulation of growth control by p53? Bioessays. 1993 October 01;15(10):689-90.

426. Wu X, Bayle JH, Olson D, Levine AJ. The p53-mdm-2 autoregulatory feedback loop. Genes Dev. 1993 July 01;7(7A):1126-32.

427. Barak Y, Juven T, Haffner R, Oren M. Mdm2 Expression is Induced by Wild Type P53 Activity. EMBO J. 1993 February 01;12(2):461-8.

428. Midgley CA, Lane DP. p53 protein stability in tumour cells is not determined by mutation but is dependent on Mdm2 binding. Oncogene. 1997 Sep 4,;15(10):1179-89.

429. Zhang Y, Xiong Y, Yarbrough WG. ARF promotes MDM2 degradation and stabilizes p53: ARF-INK4a locus deletion impairs both the Rb and p53 tumor suppression pathways. Cell. 1998 March 20;92(6):725-34.

430. Haupt Y, Maya R, Kazaz A, Oren M. Mdm2 promotes the rapid degradation of p53. Nature. 1997 May 15;387(6630):296-9.

431. Kubbutat MH, Jones SN, Vousden KH. Regulation of p53 stability by Mdm2. Nature. 1997 May 15;387(6630):299-303.

432. Buttgereit P, Schakowski F, Marten A, Brand K, Renoth S, Ziske C, et al. Effects of adenoviral wild-type p53 gene transfer in p53-mutated lymphoma cells. Cancer Gene Ther. 2001 June 01;8(6):430-9.

433. Shaw P, Bovey R, Tardy S, Sahli R, Sordat B, Costa J. Induction of apoptosis by wild-type p53 in a human colon tumor-derived cell line. Proc Natl Acad Sci U S A. 1992 May 15;89(10):4495-9.

434. Yonish-Rouach E, Resnitzky D, Lotem J, Sachs L, Kimchi A, Oren M. Wild-type p53 induces apoptosis of myeloid leukaemic cells that is inhibited by interleukin-6. Nature. 1991 July 25;352(6333):345-7.

435. Wagner AJ, Kokontis JM, Hay N. Myc-mediated apoptosis requires wild-type p53 in a manner independent of cell cycle arrest and the ability of p53 to induce p21waf1/cip1. Genes Dev. 1994 December 01;8(23):2817-30.

436. Brugarolas J, Chandrasekaran C, Gordon JI, Beach D, Jacks T, Hannon GJ. Radiation-induced cell cycle arrest compromised by p21 deficiency. Nature. 1995 October 12;377(6549):552-7.

437. Levine AJ. P53, the Cellular Gatekeeper for Growth and Division. Cell. 1997 February 07;88(3):323-31.

438. Sandor J, Ambrus T, Ember I. The function of the p53 gene suppressor in carcinogenesis. Orv Hetil. 1995 August 27;136(35):1875-83.

439. Wang XW. Role of p53 and apoptosis in carcinogenesis. Anticancer Res. 1999 December 01;19(6A):4759-71.

440. Vousden KH, Lu X. Live or let die: the cell's response to p53. Nat Rev Cancer. 2002 August 01;2(8):594-604.

441. Blattner C, Hay T, Meek DW, Lane DP. Hypophosphorylation of Mdm2 augments p53 stability. Mol Cell Biol. 2002 September 01;22(17):6170-82.

442. Kawai H, Wiederschain D, Yuan ZM. Critical contribution of the MDM2 acidic domain to p53 ubiquitination. Mol Cell Biol. 2003 July 01;23(14):4939-47.

443. Pomerantz J, Schreiber-Agus N, Liegeois NJ, Silverman A, Alland L, Chin L, et al. The Ink4a tumor suppressor gene product, p19Arf, interacts with MDM2 and neutralizes MDM2's inhibition of p53. Cell. 1998 March 20;92(6):713-23.

444. Hsieh JK, Chan FS, O'Connor DJ, Mittnacht S, Zhong S, Lu X. RB regulates the stability and the apoptotic function of p53 via MDM2. Mol Cell. 1999 February 01;3(2):181-93.

445. Argentini M, Barboule N, Wasylyk B. The contribution of the acidic domain of MDM2 to p53 and MDM2 stability. Oncogene. 2001 March 15;20(11):1267-75.

446. Yang L, Song T, Cheng Q, Chen L, Chen J. Mutant p53 Sequestration of the MDM2 Acidic Domain Inhibits E3 Ligase Activity. Mol Cell Biol. 2019 February 04;39(4):10.1128/MCB.00375,18. Print 2019 Feb 15.

447. Popowicz GM, Czarna A, Rothweiler U, Szwagierczak A, Krajewski M, Weber L, et al. Molecular basis for the inhibition of p53 by Mdmx. Cell Cycle. 2007 October 01;6(19):2386-92.

448. Chen X, Gohain N, Zhan C, Lu WY, Pazgier M, Lu W. Structural basis of how stress-induced MDMX phosphorylation activates p53. Oncogene. 2016 April 14;35(15):1919-25.

449. Shan B, Li DW, Bruschweiler-Li L, Bruschweiler R. Competitive binding between dynamic p53 transactivation subdomains to human MDM2 protein: implications for regulating the p53.MDM2/MDMX interaction. J Biol Chem. 2012 August 31;287(36):30376-84.

450. He F, Borcherds W, Song T, Wei X, Das M, Chen L, et al. Interaction between p53 N terminus and core domain regulates specific and nonspecific DNA binding. Proc Natl Acad Sci U S A. 2019 April 30;116(18):8859-68.

451. Lamiable A, Thevenet P, Rey J, Vavrusa M, Derreumaux P, Tuffery P. PEP-FOLD3: faster de novo structure prediction for linear peptides in solution and in complex. Nucleic Acids Res. 2016 July 08;44(W1):449.

452. Krois AS, Dyson HJ, Wright PE. Long-range regulation of p53 DNA binding by its intrinsically disordered N-terminal transactivation domain. Proc Natl Acad Sci U S A. 2018 November 27;115(48):E11302-10.

453. Pervushin K, Riek R, Wider G, Wuthrich K. Attenuated T2 relaxation by mutual cancellation of dipole-dipole coupling and chemical shift anisotropy indicates an avenue

to NMR structures of very large biological macromolecules in solution. Proc Natl Acad Sci U S A. 1997 November 11;94(23):12366-71.

454. Salzmann M, Pervushin K, Wider G, Senn H, Wuthrich K. TROSY in triple-resonance experiments: new perspectives for sequential NMR assignment of large proteins. Proc Natl Acad Sci U S A. 1998 November 10;95(23):13585-90.

455. Pervushin K, Riek R, Wider G, Wüthrich K. Transverse Relaxation-Optimized Spectroscopy (TROSY) for NMR Studies of Aromatic Spin Systems in13C-Labeled Proteins. Journal of the American Chemical Society. 1998 Jul;120(25):6394-400.

456. Yu GW, Rudiger S, Veprintsev D, Freund S, Fernandez-Fernandez MR, Fersht AR. The central region of HDM2 provides a second binding site for p53. Proc Natl Acad Sci U S A. 2006 January 31;103(5):1227-32.

457. Han JC, Han GY. A procedure for quantitative determination of tris(2-carboxyethyl)phosphine, an odorless reducing agent more stable and effective than dithiothreitol. Anal Biochem. 1994 July 01;220(1):5-10.

458. Bista M, Petrovich M, Fersht AR. MDMX contains an autoinhibitory sequence element. Proc Natl Acad Sci U S A. 2013 October 29;110(44):17814-9.

459. Canadillas JM, Tidow H, Freund SM, Rutherford TJ, Ang HC, Fersht AR. Solution structure of p53 core domain: structural basis for its instability. Proc Natl Acad Sci U S A. 2006 February 14;103(7):2109-14.

APPENDIX A PRIMERS, PCR CONDITIONS AND PLASMID CONSTRUCTS

Table A1: Primer sequences.

Primer	Sequence	T_M (°C)
A100	AAAACATATGGAGGAGCCGCAGTCAGATCCTAG	71.1
A101	AAAACCGGATCCCTATTAGGTGTTGTTGGGCAG	71.8
A102	AAAACATATGGATGAAGCTCCCAGAATGCCAGAGGCTG	71.3
A103	AAAAGGATCCTTACAGGGGCCAGGAGGGGGCTG	73.3
A104	AAAAGCTCTTCAGGAATGGAGGAGCCGCAGTCAGATCC TAGCG	73.1
A105	AAAAGCTCTTCAGGAAGTACTGGTACCCCGAGCAATCC GGAC	71.7
A106	AAAAGCCGGATCCTTAGGCCAGGCTAATTTCC	71.2
A107	GGGAGCAGGGCTCACTCCAGC	70.8
A108	TCCACCAATCTGTTCTCTGTGAGCCTCAATAATATCG	70.8
A109	TGAACCGCGTGGCACCAGCCCGTCTGAGTCAGGCCCTTC TGTCTTGAAC	69.3
A110	CATCACCATCACCATCATAGTGGGGACTACAAGGACGA CGACGACAAGTG	67.7
A111	TGCGATAGCGTGAGCGATCAGTTCAGTGTG	68.1
A112	GTCCAGCCAATCACCGCTGTG	67.7
A113	TGCGATACCGACAGCTTTGAAGAAGATCCGGAAATTAG	69.2
A114	TTCGCCGGCTTGATACACGGTC	68.7
A115	AAAAGCTCTTCAGGAATGTGCAACACCAATATGAGCGT GCC	69.5
A116	AAAAGGATCCTTAGTTTTCGCTAACACTTGTGCCGCTAT C	67.8
A117	AAAAGCTCTTCAGGAGATGAAACCAGCCGTCTGGACCT GG	70.1
A118	AAAAGGATCCTTAGCTGGTCACTTCCACGTCGGTATCAT C	70
A119	ACC CCG CGC AGC AAT GGT AG	69.5
A120	GCGTTTTTAGGTAATCTGCGCAGCAATTACACC	67.8
A121	GGCCGGCAGACCAGCCACATCCC	69.4

Table A2: Standard PCR conditions.

Normal PCR			
Step	Temperature (°C)	Time (second)	
Denaturation	98	30	
Denaturation	98	15	
Annealing	65 - 72	15	30 cycles
Extension	72	30	
Final extension	72	300	

Inverse PCR			
Step	Temperature (°C)	Time (second)	
Denaturation	98	30	
Denaturation	98	15	
Annealing	65 - 72	15	30 cycles
Extension	72	180	
Final extension	72	600	

Table A3: Plasmid constructs.

Name	Vector	Resistance	Inductant	Fusion Gene	Protein sequence
pE53D	pET-32	ampicillin	IPTG	His_6-Thrombin-p53DBD	MGSSHHHHHHSSGLVPRGSHMSSSV PSQKTYQGSYGFRLGFLHSGTAKSV TCTYSPALNKMFCQLAKTCPVQLWV DSTPPPGTRVRAMAIYKQSQHMTEV VRRCPHHERCSDSDGLAPPQHLIRVE GNLRVEYLDDRNTFRHSVVVPYEPP EVGSDCTTIHYNYMCNSSCMGGMN RRPILTIITLEDSSGNLLGRNSFEVRV CVCPGRDRRTEEENLRKKGEPHHEL PPGSTKRALPNNT
pEM2AD	pET-32	ampicillin	IPTG	His_6-SUMO-MDM2AD	MGHHHHHHGSDSEVNQEAKPEVKP EVKPETHINLKVSDGSSEIFFKIKKTT PLRRLMEAFAKRQGKGMDSLRFLYD GIRIQADQTPEDLDMEDNDIIEAHRE QIGGSTGTPSNPDLDAGVSEHSGDW LDQDSVSDQFSVEFEVESLDSEDYSL SEEGQELSDEDDEVYQVTVYQAGES DTDSFEEDPEISLA
pEM2QC	pET-32	ampicillin	IPTG	His_6-SUMO-MDM2ADQ238C	MGHHHHHHGSDSEVNQEAKPEVKP EVKPETHINLKVSDGSSEIFFKIKKTT PLRRLMEAFAKRQGKGMDSLRFLYD GIRIQADQTPEDLDMEDNDIIEAHRE QIGGSTGTPSNPDLDAGVSEHSGDW LD***C***DSVSDQFSVEFEVESLDSEDYSL SEEGQELSDEDDEVYQVTVYQAGES DTDSFEEDPEISLA
pEM2SC	pET-32	ampicillin	IPTG	His_6-SUMO-MDM2ADS286C	MGHHHHHHGSDSEVNQEAKPEVKP EVKPETHINLKVSDGSSEIFFKIKKTT PLRRLMEAFAKRQGKGMDSLRFLYD GIRIQADQTPEDLDMEDNDIIEAHRE QIGGSTGTPSNPDLDAGVSEHSGDW LDQDSVSDQFSVEFEVESLDSEDYSL SEEGQELSDEDDEVYQVTVYQAGE***C*** DTDSFEEDPEISLA
pEM2M5	pET-32	ampicillin	IPTG	His_6-SUMO-MDM2ADS240ES242ES246ES252ES256E	MGHHHHHHGSDSEVNQEAKPEVKP EVKPETHINLKVSDGSSEIFFKIKKTT PLRRLMEAFAKRQGKGMDSLRFLYD GIRIQADQTPEDLDMEDNDIIEAHRE QIGGSTGTPSNPDLDAGVSEHSGDW LDQDEVEDQFEVEFEVEELDEEDYSL SEEGQELSDEDDEVYQVTVYQAGES DTDSFEEDPEISLA

pE53RD	pET-32	ampicillin	IPTG	CBD-SUMO-p53RD-Thrombin-His_6-FLAG	MKIEEGKLTNPGVSAWQVNTAYTA GQLVTYNGKTYKCLQPHTSLAGWEP SNVPALWQLQNNHGSDSEVNQEAK PEVKPEVKPETHINLKVSDGSSEIFFK IKKTTPLRRLMEAFAKRQGKGMDSL RFLYDGIRIQADQTPEDLDMEDNDII EAHREQIGGGKEPGGSRAHSSHLKS KKGQSTSRHKKLMFKTEGPDSDGLV PRGSHHHHHHSGDYKDDDDK
pE53TPD	pET-32	ampicillin	IPTG	His_6-Thrombin-p53TPD	MGSSHHHHHHSSGLVPRGSHMEEPQ SDPSVEPPLSQETFSDLWKLLPENNV LSPLPSQAMDDLMLSPDDIEQWFTE DPGPDEAPRMPEAAPRVAPAPAAPT PAAPAPAPSWPLSSSVPSQKTYQGSY GFRLGFLHSGTAKSVTCTYSPALNK MFCQLAKTCPVQLWVDSTPPPGTRV RAMAIYKQSQHMTEVVRRCPHHER CSDSDGLAPPQHLIRVEGNLRVEYLD DRNTFRHSVVVPYEPPEVGSDCTTIH YNYMCNSSCMGGMNRRPILTIITLED SSGNLLGRNSFEVRVCVCPGRDRRT EEENLRKKGEPHHELPPGSTKRALPN NT
pE53T2PD	pET-32	ampicillin	IPTG	His_6-Thrombin-p53T2PD	MGSSHHHHHHSSGLVPRGSHMSPLP SQAMDDLMLSPDDIEQWFTEDPGPD EAPRMPEAAPRVAPAPAAPTPAAPA PAPSWPLSSSVPSQKTYQGSYGFRLG FLHSGTAKSVTCTYSPALNKMFCQL AKTCPVQLWVDSTPPPGTRVRAMAI YKQSQHMTEVVRRCPHHERCSDSDG LAPPQHLIRVEGNLRVEYLDDRNTFR HSVVVPYEPPEVGSDCTTIHYNYMC NSSCMGGMNRRPILTIITLEDSSGNLL GRNSFEVRVCVCPGRDRRTEEENLR KKGEPHHELPPGSTKRALPNNT
pE53PD	pET-32	ampicillin	IPTG	His_6-Thrombin-p53PD	MGSSHHHHHHSSGLVPRGSHDEAPR MPEAAPRVAPAPAAPTPAAPAPAPS WPLSSSVPSQKTYQGSYGFRLGFLHS GTAKSVTCTYSPALNKMFCQLAKTC PVQLWVDSTPPPGTRVRAMAIYKQS QHMTEVVRRCPHHERCSDSDGLAPP QHLIRVEGNLRVEYLDDRNTFRHSV VVPYEPPEVGSDCTTIHYNYMCNSSC MGGMNRRPILTIITLEDSSGNLLGRN SFEVRVCVCPGRDRRTEEENLRKKG EPHHELPPGSTKRALPNNT

pE53T	pET-32	ampicillin	IPTG	His_6-SUMO-p53TP	MGHHHHHHGSDSEVNQEAKPEVKPEVKPETHINLKVSDGSSEIFFKIKKTTPLRRLMEAFAKRQGKGMDSLRFLYDGIRIQADQTPEDLDMEDNDIIEAHREQIGGMEEPQSDPSVEPPLSQETFSDLWKLLPENNVLSPLPSQAMDDLMLSPDDIEQWFTEDPGPDEAPRMPEAAPRVAPAPAAPTPAAPAPAPSWPL
pEM2PBD	pET-32	ampicillin	IPTG	His_6-SUMO-MDM2PBD	MGHHHHHHGSDSEVNQEAKPEVKPEVKPETHINLKVSDGSSEIFFKIKKTTPLRRLMEAFAKRQGKEMDSLRFLYDGIRIQADQTPEDLDMEDNDIIEAHREQIGGMCNTNMSVPTDGAVTTSQIPASEQETLVRPKPLLLKLLKSVGAQKDTYTMKEVLFYLGQYIMTKRLYDEKQQHIVYCSNDLLGDLFGVPSFSVKEHRKIYTMIYRNLVVVNQQESSDSGTSVSEN
pEMXAD	pET-32	ampicillin	IPTG	His_6-SUMO-MDMXAD	MGHHHHHHGSDSEVNQEAKPEVKPEVKPETHINLKVSDGSSEIFFKIKKTTPLRRLMEAFAKRQGKGMDSLRFLYDGIRIQADQTPEDLDMEDNDIIEAHREQIGGDETSRLDLGFEEWDVAGLPWWFLGNLRSNYTPRSNGSTDLQTNQDVGTAIVSDTTDDLWFLNESVSEQLGVGIKVEAADTEQTSEEVGKVSDKKVIEVGKNDDLEDSKSLSDDTDVEVTS
pEMXADAA	pET-32	ampicillin	IPTG	His_6-SUMO-MDMXADW200AW201A	MGHHHHHHGSDSEVNQEAKPEVKPEVKPETHINLKVSDGSSEIFFKIKKTTPLRRLMEAFAKRQGKGMDSLRFLYDGIRIQADQTPEDLDMEDNDIIEAHREQIGGDETSRLDLGFEEWDVAGLPAAFLGNLRSNYTPRSNGSTDLQTNQDVGTAIVSDTTDDLWFLNESVSEQLGVGIKVEAADTEQTSEEVGKVSDKKVIEVGKNDDLEDSKSLSDDTDVEVTS

Red: hexahistidine tag Blue: thrombin cleavage site Green: SUMO-tag Orange: CBD-tag Purple: FLAG-tag

APPENDIX B BUFFER COMPOSITIONS

Table B1: Buffer compositions.

Name	Composition
1x minimum medium	83.3 mM NaH_2PO_4, 34.4 mM K_2HPO_4, 17.1 mM NaCl, 0.25x vitamin mix, 0.25x trace element, 4 mM $MgSO_4$, 1.8 mM $FeSO_4$, 0.1 mM $CaCl_2$, pH 7.4
1000x trace element solution	50mM $FeCl_3$, 20 mM $CaCl_2$, 10 mM $MnCl_2$, 10 mM $ZnSO_4$, 2 mM each of the $CoCl_2$, $CuCl_2$, $NiCl_2$, Na_2MoO_4, Na_2SeO_3 and H_3BO_3, 50 mM HCl
Lysis buffer	50 mM NaH_2PO_4, 300 mM NaCl, 20 mM imidazole, pH 7.5
Elution buffer	50 mM NaH_2PO_4, 300 mM NaCl, 300 mM imidazole, pH 7.5
Denaturing lysis buffer	50 mM NaH_2PO_4, 4 M gunidinium chloride, 20 mM imidazole, pH 7.5
Cleavage buffer	20 mM NaH_2PO_4, 100 mM NaCl, 2 mM β-mercaptoethanol, pH 7.0
Buffer A	25 mM NaH_2PO_4, pH 6.5
Buffer B	25 mM NaH_2PO_4, 1 M NaCl, pH 6.5
NMR buffer	20 mM NaH_2PO_4, 40 mM NaCl, 1 mM TCEP, 1 mM DSS, 0.2% w/v NaN_3, pH 7.0
ITC buffer	20 mM NaH_2PO_4, 40 mM NaCl, 1 mM TCEP, pH 7.0
5x SDS-PAGE loading buffer	250 mM Tris–HCl (pH 6.8), 8% w/v sodium dodecyl sulphate, 0.2% w/v bromophenol blue, 40% v/v glycerol, 20% v/vβ-mercaptoethanol

APPENDIX C NMR EXPERIMENT PARAMETERS.

Table C1: NMR experiment parameters.

Experiment (293K)	Recycling delay (s)	# of scans	Dimension	# of complex points	Sweep width (ppm)	Spectrum center position (ppm)	Proton frequency (MHz)	Notes
Chapter 2								
MDM2 AD								
^{1}H-^{15}N HSQC (gNhsqcA.c)	1	2	^{1}H	1024	16	4.832	500[1]	AD 800 µM
			^{15}N	256	21	117.543		
HNCACB (ghn_cacbA.c)	1	4	^{1}H	1024	16	4.832		
			^{15}N	80	21	117.543		
			^{13}C	100	70	45.7		
CBCACONH (gcbca_co_nhA.c)	1	2	^{1}H	1024	16	4.832		
			^{15}N	80	21	117.543		
			^{13}C	100	70	45.7		
HNCACO (ghn_cacbA.c)	1	8	^{1}H	1024	16	4.832		
			^{15}N	80	21	117.543		
			^{13}C	40	10	176.3		
HNCO (ghn_coA.c)	1	2	^{1}H	1024	16	4.832		
			^{15}N	80	21	117.543		
			^{13}C	40	10	176.3		
^{1}H-^{15}N hetNOE (hsqcnoef3gpsi)	5	24	^{1}H	2048	16	4.814	700[2]	
			^{15}N	512	11	120.617		
MDM2 AD titration (DBD)								
^{1}H-^{15}N HSQC (hsqcetfpgpsi2)	1	8	^{1}H	2048	16	4.819	500[3]	AD 150 µM
			^{15}N	196	21	119.471		
^{1}H-^{15}N HSQC (hsqcetfpgpsi2)	1	8	^{1}H	2048	16	4.819		AD 150 µM DBD 150 µM
			^{15}N	196	21	119.471		
MDM2 AD titration (DBD) low salt								
^{1}H-^{15}N HSQC (hsqcetfpgpsi2)	1	8	^{1}H	2048	16	4.818	500[3]	AD 150 µM
			^{15}N	196	21	119.471		
^{1}H-^{15}N HSQC (hsqcetfpgpsi2)	1	8	^{1}H	2048	16	4.818		AD 150 µM DBD 150 µM
			^{15}N	196	21	119.471		
MDM2 AD (DBD bound)								
^{1}H-^{15}N HSQC (hsqcetfpgpsi2)	1	2	^{1}H	2048	16	4.83	700[2]	AD 300 µM DBD 330 µM
			^{15}N	128	11	120.638		
HNCA (hncagpwg3d)	1	24	^{1}H	2048	16	4.83		Nus amount: 20% Nus points: 256
			^{15}N	40	16.5	120.635		
			^{13}C	128	30	53.336		

HNCO (hncogp3d)	1	8	^{1}H	2048	16	4.83		Nus amount: 8% Nus points: 102
			^{15}N	40	16.5	120.635		
			^{13}C	128	10	174.137		
^{1}H-^{15}N hetNOE (hsqcnoef3gpsi)	5	36	^{1}H	2048	16	4.83		
			^{15}N	256	11	120.638		
p53 DBD								
^{1}H-^{15}N TROSY (trosyetf3gpsi2)	1	4	^{1}H	2048	16	4.89	700^{2}	DBD 300 µM
			^{15}N	256	32	118.696		
TROSY-HNCA (trhncaetgp3d)	1.3	32	^{1}H	2048	18	4.89		Nus amount: 12.5% Nus points: 576
			^{15}N	72	26	120.696		
			^{13}C	128	30	53.393		
TROSY-HNCOCACB (trhncocacbgp2h3d)	1.3	48	^{1}H	2048	18	4.89		Nus amount: 20% Nus points: 461
			^{15}N	72	26	120.696		
			^{13}C	256	80	43.194		
^{1}H-^{15}N TROSY hetNOE (trnoef3gpsi)	5	40	^{1}H	2048	16	4.89		
			^{15}N	256	24.5	119.947		
p53 DBD (AD bound)								
^{1}H-^{15}N TROSY (trosyetf3gpsi2)	1	4	^{1}H	2048	16	4.83	800^{4}	DBD 300 µM AD 600 µM
			^{15}N	256	32	120.635		
TROSY-HNCA (trhncaetgp3d)	1.3	16	^{1}H	2048	18	4.832		Nus amount: 25% Nus points: 432
			^{15}N	72	26	120.635		
			^{13}C	96	30	53.335		
TROSY-HNCACB (trhncacbgp2h3d)	1.3	48	^{1}H	2048	18	4.83		Nus amount: 12.5% Nus points: 450
			^{15}N	72	26	120.635		
			^{13}C	200	80	43.135		
^{1}H-^{15}N TROSY hetNOE (trnoef3gpsi)	5	48	^{1}H	2048	16	4.83	700^{2}	
			^{15}N	320	24.5	119.889		
p53 DBD PRE experiments								
^{1}H-^{15}N TROSY (oxi/red) (trosyetf3gpsi2)	1.3	32	^{1}H	2048	16	4.83	700^{2}	DBD 160 µM ADSC 200 µM
			^{15}N	256	25	120.135		
^{1}H-^{15}N TROSY (oxi/red) (trosyetf3gpsi2)	1.3	40	^{1}H	2048	16	4.83		DBD 160 µM ADQC 200 µM
			^{15}N	256	25	120.139		
p53 RD HSQC experiments								
^{1}H-^{15}N HSQC (hsqcetfpgpsi2)	1	8	^{1}H	2048	16	4.814	700^{2}	AD 150 µM
			^{15}N	196	21	116.614		
^{1}H-^{15}N HSQC (hsqcetfpgpsi2)	1	8	^{1}H	2048	16	4.814		AD 150 µM RD 150 µM
			^{15}N	196	21	116.614		
^{1}H-^{15}N HSQC (hsqcetfpgpsi2)	1	8	^{1}H	2048	16	4.814		AD 150 µM RD 300 µM
			^{15}N	196	21	116.614		
^{1}H-^{15}N HSQC	1	8	^{1}H	2048	16	4.814		AD 150 µM

(hsqcetfpgpsi2)			^{15}N	196	21	116.614		RD 600 µM
Chapter 3								
p53 TD								
^{1}H-^{15}N HSQC (hsqcetfpgpsi2)	1	4	^{1}H	2048	16	4.819	700[2]	TD 800 µM
			^{15}N	256	24	120.125		
HNCACB (hncacbgp3d)	1	8	^{1}H	2048	16	4.819		
			^{15}N	64	24	120.125		
			^{13}C	96	65	45.29		
CCCONH (hccconhgp3d3)	1	8	^{1}H	1024	16	4.819		
			^{15}N	80	24	120.125		
			^{13}C	128	80	42.79		
HNCACO (hncacogp3d)	1	8	^{1}H	2048	16	4.819		
			^{15}N	64	24	120.125		
			^{13}C	96	10	175.262		
HNCO (hncogp3d)	1	4	^{1}H	2048	7	4.819		
			^{15}N	64	24	120.125		
			^{13}C	96	7	175.262		
p53 TD HSQC experiments								
^{1}H-^{15}N HSQC (hsqcetfpgpsi2)	1	8	^{1}H	2048	16	4.817	500[3]	TD 150 µM
			^{15}N	196	25	119.355		
^{1}H-^{15}N HSQC (hsqcetfpgpsi2)	1	8	^{1}H	2048	16	4.817		TD 150 µM DBD 150 µM
			^{15}N	196	25	119.355		
p53 TD PRE experiments								
^{1}H-^{15}N HSQC (hsqcetfpgpsi2)	1	16	^{1}H	2048	16	4.819	700[2]	TD 150 µM DBD^{Zn} 225 µM
			^{15}N	196	22	119.613		
^{1}H-^{15}N HSQC (hsqcetfpgpsi2)	1	16	^{1}H	2048	16	4.819		TD 150 µM DBD^{Co} 225 µM
			^{15}N	196	22	119.613		
MDM2 AD HSQC experiment								
^{1}H-^{15}N HSQC (hsqcetfpgpsi2)	1	4	^{1}H	2048	16	4.819	500[3]	AD 150 µM
			^{15}N	196	25	119.471		
^{1}H-^{15}N HSQC (hsqcetfpgpsi2)	1	8	^{1}H	2048	16	4.819		AD 150 µM TPD 150 µM
			^{15}N	196	25	119.471		
^{1}H-^{15}N HSQC (hsqcetfpgpsi2)	1	8	^{1}H	2048	16	4.819		AD 150 µM T2PD 150 µM
			^{15}N	196	25	119.471		
^{1}H-^{15}N HSQC (hsqcetfpgpsi2)	1	8	^{1}H	2048	16	4.819		AD 150 µM PD 150 µM
			^{15}N	196	25	119.471		
^{1}H-^{15}N HSQC (hsqcetfpgpsi2)	1	8	^{1}H	2048	16	4.819		AD 150 µM DBD 150 µM
			^{15}N	196	25	119.471		
p53 DBD TROSY experiment								

^{1}H-^{15}N TROSY (trosyetf3gpsi2)	1	12	^{1}H	2048	16	4.819		DBD 200 µM
			^{15}N	256	32	118.618		
^{1}H-^{15}N TROSY (trosyetf3gpsi2)	1	16	^{1}H	2048	16	4.819	700[2]	DBD 200 µM TD 220 µM
			^{15}N	256	32	118.618		
^{1}H-^{15}N TROSY (trosyetf3gpsi2)	1	16	^{1}H	2048	16	4.819		DBD 200 µM TD 220 µM PBD 300 µM
			^{15}N	256	32	118.618		
Chapter 4								
MDMX ADX backbone resonance assignment								
^{1}H-^{15}N HSQC (hsqcetfpgpsi2)	1	2	^{1}H	2048	16	4.833		ADX 380 µM
			^{15}N	200	22.5	116.886		
HNCACB (hncacbgp3d)	1	8	^{1}H	2048	16	4.833		Nus amount: 12.5% Nus points: 523
			^{15}N	88	22.5	116.848		
			^{13}C	190	70	45.813		
CBCACONH (cbcaconhgp3d)	1	2	^{1}H	2048	16	4.833		Nus amount: 12.5% Nus points: 523
			^{15}N	88	21	116.848	800[4]	
			^{13}C	190	70	45.813		
HNCACO (hncacogp3d)	1	16	^{1}H	1024	16	4.833		Nus amount: 25% Nus points: 264
			^{15}N	88	22.5	116.886		
			^{13}C	48	6.5	176.3		
HNCO (hncogp3d)	1	8	^{1}H	1024	16	4.833		Nus amount: 12.5% Nus points: 132
			^{15}N	88	22.5	116.886		
			^{13}C	48	6.5	176.3		
MDMX ADX HSQC experiments								
^{1}H-^{15}N HSQC (hsqcetfpgpsi2)	1	16	^{1}H	2048	16	4.819		ADX 150 µM
			^{15}N	196	23	116.614		
^{1}H-^{15}N HSQC (hsqcetfpgpsi2)	1	16	^{1}H	2048	16	4.819		ADX 150 µM PBD2 300 µM
			^{15}N	196	23	116.614	700[2]	
^{1}H-^{15}N HSQC (hsqcetfpgpsi2)	1	16	^{1}H	2048	16	4.819		ADX 150 µM PBD2 150 µM TD 225 µM
			^{15}N	196	23	116.614		
MDMX ADX_{AA} HSQC experiments								
^{1}H-^{15}N HSQC (hsqcetfpgpsi2)	1	16	^{1}H	2048	16	4.819		ADX_{AA} 150 µM
			^{15}N	196	23	116.614		
^{1}H-^{15}N HSQC (hsqcetfpgpsi2)	1	16	^{1}H	2048	16	4.819	700[2]	ADX_{AA} 150 µM PBD2 300 µM
			^{15}N	196	23	116.614		
^{1}H-^{15}N HSQC	1	8	^{1}H	2048	16	4.815	500[3]	

(hsqcetfpgpsi2)			^{15}N	196	25	119.472		ADX_{AA} 100 µM
MDMX ADXD HSQC experiments								
^{1}H-^{15}N HSQC (hsqcetfpgpsi2)	1	8	^{1}H	2048	16	4.815	500[3]	ADXD 100 µM
			^{15}N	196	25	119.472		
^{1}H-^{15}N HSQC (hsqcetfpgpsi2)	1	8	^{1}H	2048	16	4.815		ADXD 100 µM PBD2 110 µM
			^{15}N	196	25	119.472		
MDM2 PBD2 backbone resonance assignment								
^{1}H-^{15}N HSQC (hsqcetfpgpsi2)	1	4	^{1}H	2048	16	4.839	700[2]	PBD2 400 µM
			^{15}N	256	24	117.123		
HNCACB (hncacbgp3d)	1	32	^{1}H	2048	16	4.839		Nus amount: 25% Nus points: 512
			^{15}N	64	24	117.123		
			^{13}C	128	75	41.808		
CBCACONH (cbcaconhgp3d)	1	16	^{1}H	2048	16	4.839		Nus amount: 13% Nus points: 266
			^{15}N	64	24	116.848		
			^{13}C	128	75	41.808		
HNCACO (hncacogp3d)	1	24	^{1}H	2048	16	4.839		Nus amount: 10% Nus points: 256
			^{15}N	80	24	117.123		
			^{13}C	128	12	176.761		
HNCO (hncogp3d)	1	12	^{1}H	2048	16	4.839		Nus amount: 6% Nus points: 154
			^{15}N	80	24	116.886		
			^{13}C	128	12	176.761		
MDM2 PBD2 HSQC experiments								
^{1}H-^{15}N HSQC (hsqcetfpgpsi2)	1	36	^{1}H	2048	16	4.839	700[2]	PBD2 100 µM
			^{15}N	196	21	116.614		
^{1}H-^{15}N HSQC (hsqcetfpgpsi2)	1	36	^{1}H	2048	16	4.839		PBD2 100 µM ADX 300 µM
			^{15}N	196	21	116.614		
^{1}H-^{15}N HSQC (hsqcetfpgpsi2)	1	36	^{1}H	2048	16	4.839		PBD2 100 µM TD 300 µM
			^{15}N	196	21	116.614		
^{1}H-^{15}N HSQC (hsqcetfpgpsi2)	1	36	^{1}H	2048	16	4.839		PBD2 100 µM ADXD 300 µM
			^{15}N	196	21	116.614		

1: Varian 500 MHz INOVA spectrometer equipped with an HCN room temperature probe (Quebec/Eastern Canada High Field NMR facility (QANUC; Montreal, QC).

2: Bruker Avance III 700 MHz spectrometer equipped with a 5mm triple resonance inverse cryoprobe with a z-axis gradient (Bruker Canada; Biomolecular Magnetic Resonance Facility (BMRF), National Research Council (NRC)).

3: Burker Avance 500 MHz spectrometer equipped with a room temperature 5 mm broadband fluorine observe (BBFO) SmartProbe with a z-axis gradient (Bruker Canada; NMR3 facility, Dalhousie University).

4: Bruker Avance III 800 MHz spectrometer equipped with a TCI cyroprobe and a z-axis gradient (Bruker Canada; Quebec/Eastern Canada High Field NMR facility (QANUC); Montreal, QC).

APPENDIX D ASSIGNED CHEMICAL SHIFTS (PPM) OF VARIOUS PROTEINS AND PROTEINS IN COMPLEXES

Table D1: H_N, N, C', C_α, and C_β chemical shifts (ppm) of the DBD in NMR buffer at 293K.

Residue number	Amino acid	H_N	N	C'	C_α	C_β
L1*	Gly	-	-	-	-	-
L2*	Ser	-	-	-	-	-
L3*	His	-	-	174.58	55.97	30.22
L4*	Met	8.24	121.47	175.96	53.75	32.12
94	Ser	8.93	117.95	175.01	57.36	63.61
95	Ser	8.25	118.46	174.11	57.94	63.44
96	Ser	8.21	117.03	173.23	56.95	64.38
97	Val	8.36	122.47	-	58.97	-
98	Pro	-	-	175.33	61.94	31.22
99	Ser	8.36	115.33	174.83	57.89	63.07
100	Gln	8.54	121.14	175.82	53.78	29.66
101	Lys	7.8	124.23	176.79	56.78	32.14
102	Thr	8.93	126.12	174.2	64.33	68.52
103	Tyr	9.38	129.3	174.49	55.73	-
104	Gln	9.35	129.07	179.05	58.2	28.12
105	Gly	7.48	105.74	174.4	44.76	-
106	Ser	9.25	117.19	175.06	60.29	62.19
107	Tyr	8.58	118.11	175.77	57.68	34.89
108	Gly	7.43	110.45	173.3	47.72	-
109	Phe	8.16	119.76	174.8	56.25	39.33
110	Arg	9.06	128.85	172.75	54.57	31.99
111	Leu	7.6	116.69	177.64	51.87	42.9
112	Gly	8.46	108.58	169.29	43.41	-
113	Phe	7.79	116.29	175.79	55.97	42.1
114	Leu	9.09	123.63	177.3	54.27	41.86
115	His	8.72	122.74	180.06	55.95	-
116	Ser	8.83	120.97	174.52	57.96	-
117	Gly	8.78	111.59	174.29	44.67	-
118	Thr	8.38	110.16	174.13	60.04	69.08
119	Ala	8.2	124.54	-	52.94	-
120	Lys	-	-	177.01	-	-
121	Ser	7.67	112.49	174.6	57.33	63.08
122	Val	7.82	123.34	176.23	62.44	-
123	Thr	8.5	115.46	174.72	62.49	69.04
124	Cys	7.37	120.72	172.78	58.33	27.55

125	Thr	9.57	124.27	170.17	59.7	68.37
126	Tyr	8.83	129.95	173.08	55.87	40.75
127	Ser	8.33	120.54	-	52.81	-
128	Pro	-	-	179.46	63.86	31.23
129	Ala	8.12	119.5	179.49	54.38	18.02
130	Leu	7	113.61	176.61	53.36	43.25
131	Asn	7.93	119.99	173.13	53.07	36.06
132	Lys	6.8	118.33	172.41	53.66	32.39
133	Met	9.47	129.39	172.77	53.71	35.18
134	Phe	9.24	126.63	174.58	54.94	40.36
135	Cys	9.26	120.05	171.96	54.57	32.54
136	Gln	7.79	118.43	176.52	53.94	31.14
137	Leu	8.58	126.14	177.02	56.72	41.15
138	Ala	8.94	124	175.75	54.31	17.1
139	Lys	7.43	118.37	177.36	53.49	32.28
140	Thr	8.11	118.09	173.96	65.45	68.56
141	Cys	9.25	127.31	-	55.11	-
142	Pro	-	-	175.75	61.71	30.76
143	Val	9.04	126	174.4	61.63	34.49
144	Gln	8.36	122.47	175.51	53.04	29.15
145	Leu	9.4	120.54	175.61	53.05	41.26
146	Trp	9.03	127.7	174.64	55.81	29.31
147	Val	8.17	112.46	176.48	58.67	34.21
148	Asp	9.06	122.96	176.66	55.28	41.31
149	Ser	7.79	113.81	172.45	56.53	64.12
150	Thr	8.2	118.07	-	61.51	-
151	Pro	-	-	-	-	-
152	Pro	-	-	-	-	-
153	Pro	-	-	177.81	63.43	30.76
154	Gly	8.79	113.83	174.3	44.71	-
155	Thr	7.62	118.68	174.23	64.31	67.93
156	Arg	9.65	129.02	173.35	54.92	33.88
157	Val	9.05	120.77	175.48	60.33	-
158	Arg	9.54	133.26	173.27	54.07	32.2
159	Ala	8.72	127.61	175.58	50.01	-
160	Met	8.1	118.92	172.53	53.96	-
161	Ala	9.48	128.1	175.87	49.31	20.79
162	Ile	8.41	112.16	175.1	59.04	-
163	Tyr	9.17	123.17	174.46	60.62	36.69
164	Lys	7.66	119.39	177.42	57.45	-
165	Gln	9.05	116.97	-	55.23	-
166	Ser	-	-	176.68	61.69	-
167	Gln	9.26	119.76	175.72	57.47	26.33

168	His	7.56	116.86	176.5	54.88	31.57
169	Met	7.41	119.45	179.14	60.25	32.82
170	Thr	8.45	110.83	173.09	63.09	68.45
171	Glu	8.05	125.01	176.15	56.07	29.31
172	Val	8.74	127.7	177.31	63.97	-
173	Val	8.59	130.21	175.2	63.08	30.21
174	Arg	7.96	127.3	174.36	54.18	32.34
175	Arg	7.95	116.92	176.19	56.9	-
176	Cys	8.58	125.21	-	56	-
177	Pro	-	-	178.7	65.24	31.1
178	His	7.87	116.27	177.89	59.32	29.8
179	His	8.99	120.76	177.81	62.23	29.33
180	Glu	8.75	120.66	177.77	58.75	28.97
181	Arg	7.15	115.25	176.97	55.82	29.86
182	Cys	7.4	119.17	174.77	59.44	-
183	Ser	8.31	118.96	174.61	57.53	61.63
184	Asp	7.98	122.31	177.72	52.42	40.51
185	Ser	8.41	116.69	175.11	58.76	62.99
186	Asp	8.12	125.28	176.84	53.3	40.26
187	Gly	8.48	109.89	173.58	44.82	-
188	Leu	8.22	122.39	176.87	55.38	-
189	Ala	8.94	125.26	-	49.44	-
190	Pro	-	-	-	-	-
191	Pro	-	-	176.39	64.77	31.83
192	Gln	8.63	114.04	176.94	56.95	27.74
193	His	7.2	119.09	-	57.52	-
194	Leu	-	-	174.52	57.85	-
195	Ile	7.72	116	175.95	60.64	37.78
196	Arg	8.78	122.33	176.1	53.43	34.11
197	Val	7.25	117.97	175.46	60.83	33.43
198	Glu	8.58	129.44	176.73	54.1	30.98
199	Gly	8.74	111.31	174.06	46.21	-
200	Asn	8.19	117.82	175.74	52.07	39.99
201	Leu	8.92	126.93	177.88	55.78	40.66
202	Arg	8.53	119.22	174.42	55.06	28.38
203	Val	6.8	118.82	172.99	60.5	32.3
204	Glu	8.66	126.41	173.81	54.58	32.73
205	Tyr	8.88	123.62	175.57	57.93	38.79
206	Leu	9.31	126.68	174.93	53.86	43.58
207	Asp	8.36	123.14	175.36	52.23	41.08
208	Asp	8.17	124.44	178.71	55.12	43.21
209	Arg	9.08	128.37	175.38	57.5	29.13
210	Asn	8.7	115.04	176.04	54.11	39.63

211	Thr	8.68	109.97	175.74	61.21	69.96
212	Phe	7.47	114.11	174.49	58.16	35.77
213	Arg	7.55	116.5	176.76	55.95	-
214	His	7.85	123.72	176.95	52.39	32.23
215	Ser	9.35	115.67	171.3	58.6	65.72
216	Val	8.39	116.59	174.4	58.05	33.01
217	Val	9.19	131.02	174.67	59.16	-
218	Val	8.31	117.48	-	56.93	-
219	Pro	-	-	177.59	62.37	30.87
220	Tyr	8.59	124.46	174.01	59.05	37.28
221	Glu	7.15	131.63	-	51.62	-
222	Pro	-	-	-	-	-
223	Pro	-	-	176.99	62.21	31.3
224	Glu	8.38	123.24	176.16	55.26	29.43
225	Val	8.3	122.01	177.92	64.44	30.56
226	Gly	8.85	116.72	174.02	44.58	-
227	Ser	8.28	116.92	173.08	56.61	64.2
228	Asp	8.45	120.46	174.31	53.81	42.28
229	Cys	7.45	112.81	171.87	54.47	27.73
230	Thr	7.78	120.04	173.13	61.74	70.11
231	Thr	8.78	124.68	173.33	62.2	69.18
232	Ile	9.06	130.21	173.23	59.47	39.25
233	His	8.43	125.29	173.38	53.49	30.05
234	Tyr	8.34	123.45	176.41	57.58	40.78
235	Asn	8.98	117.88	172.15	52.03	43.81
236	Tyr	10.02	122.07	178.38	57.8	40.76
237	Met	8.54	117.23	175.06	53.73	28.49
238	Cys	7.26	120.58	173.6	60.68	-
239	Asn	8.4	118.6	177.81	53.47	39.83
240	Ser	9.57	120.69	174.43	63.7	-
241	Ser	8.09	109.98	175.43	57.94	63.18
242	Cys	7.73	122.46	178.19	64.27	28.96
243	Met	9.05	130.09	177.6	56.72	-
244	Gly	8.86	110.96	173.66	45	-
245	Gly	7.3	109.1	-	43.53	-
246	Met	-	-	179.43	59.31	33.51
247	Asn	8.57	118.58	173.62	54.51	36.76
248	Arg	9.28	108.24	176.19	57.48	26.44
249	Arg	7.81	123.99	-	53.68	-
250	Pro	-	-	177.57	62.44	33.09
251	Ile	7.03	112.57	174.65	58.59	-
252	Leu	9.23	118.77	178.29	52.73	-
253	Thr	8.86	114.77	171.59	61.97	69.32

254	Ile	9.31	127.11	176.08	59.86	-
255	Ile	9.17	130.5	176.15	57.81	-
256	Thr	9.55	117.24	172.86	57.87	69.64
257	Leu	8.11	124.22	176.11	52.13	42.82
258	Glu	9.16	125.92	175.31	53.49	34.09
259	Asp	8.4	120	177.97	52.26	40.82
260	Ser	8.6	113.67	175.54	60.84	62.4
261	Ser	8.04	117.45	174.1	58.02	63.38
262	Gly	7.99	109.55	174.61	44.45	-
263	Asn	8.68	121.21	175.27	53.2	37.57
264	Leu	8.6	123.97	176.93	56.02	41.58
265	Leu	9.58	124.52	178.21	54.27	42.72
266	Gly	7.87	106.9	170.76	45.55	-
267	Arg	10.16	125.34	174.48	56.34	34.24
268	Asn	9.56	127.41	172.41	52.93	44.4
269	Ser	9.39	114.14	172.85	57.67	66.47
270	Phe	8.09	113.98	172.94	56.02	39.48
271	Glu	8.56	123.66	174.82	55.28	29.53
272	Val	7.98	123.8	174.53	60.22	34.99
273	Arg	8.49	128.04	173.14	54.65	33.07
274	Val	8.54	130.4	177.68	59.66	31
275	Cys	9.92	124.79	172.96	54.99	-
276	Ala	8.56	123.04	179.29	54.63	18.82
277	Cys	8.76	116.72	-	54.87	-
278	Pro	-	-	177.13	66.09	32.14
279	Gly	8.96	104.95	175.5	46.78	-
280	Arg	7.18	122.37	178.64	58.28	29.48
281	Asp	8.12	121.56	177.42	57.23	38.64
282	Arg	7.73	121.12	177	58.85	27.64
283	Arg	7.27	118.39	179.17	59.1	28.85
284	Thr	8.38	116.68	176.67	65.92	68.38
285	Glu	8.14	121.61	180.61	60.53	28.89
286	Glu	8.6	120.73	179.61	59.45	28.22
287	Glu	8.35	122.05	178.87	58.59	28.18
288	Asn	7.98	118.2	177.27	54.98	37.46
289	Leu	7.5	121.11	178.69	56.81	40.88
290	Arg	7.72	119.79	177.97	57.51	29.31
291	Lys	7.94	119.83	177.45	57.04	31.78
292	Lys	7.89	120.97	177.42	56.85	31.74
293	Gly	8.04	108.79	173.8	44.58	-
294	Glu	8	122.37	-	53.91	-
295	Pro	-	-	176.64	62.76	31.22
296	His	8.428	120.06	-	55.55	-

297	His	-	-	174.68	55.36	30.04
298	Glu	8.49	123.17	176.06	55.69	29.52
299	Leu	8.4	125.71	-	52.5	-
300	Pro	-	-	-	-	-
301	Pro	-	-	177.85	63.21	31.11
302	Gly	8.57	110.37	174.57	44.85	-
303	Ser	8.07	116.11	174.92	58.35	63.31
304	Thr	8.22	116.79	174.49	61.65	69.25
305	Lys	8.27	124.55	176.32	55.89	31.99
306	Arg	8.28	123.51	175.76	55.42	30.1
307	Ala	8.33	126.59	177.33	51.7	18.38
308	Leu	8.26	123.89	-	52.51	-
309	Pro	-	-	176.66	62.72	31.2
310	Asn	8.49	119.16	174.93	52.84	38.2
311	Asn	8.39	120.05	174.5	53.12	38.39
312	Thr	7.73	119.57	-	63.03	-

*L1 – L4: linker residues from thrombin cleavage.

Table D2: H_N, N, C', C_α, and C_β chemical shifts (ppm) of the DBD in complex with the AD in NMR buffer at 293K.

Residue number	Amino acid	H_N	N	C'	C_α	C_β
L1*	Gly	-	-	-	-	-
L2*	Ser	-	-	-	-	-
L3*	His	-	-	-	-	-
L4*	Met	8.21	121.45	175.98	53.96	-
94	Ser	8.87	117.81	174.92	57.42	63.67
95	Ser	8.22	118.3	174.13	58.03	63.32
96	Ser	8.18	116.93	173.37	57.1	64.32
97	Val	8.31	122.6	-	59.02	33.27
98	Pro	-	-	175.34	61.92	31.23
99	Ser	8.3	115.18	174.79	57.91	63.05
100	Gln	8.52	121.08	-	53.87	29.59
101	Lys	7.77	123.97	176.84	56.79	31.96
102	Thr	8.89	125.77	174.16	64.33	68.62
103	Tyr	9.36	129.07	174.45	55.78	39.72
104	Gln	9.34	128.94	179.07	58.24	28.1
105	Gly	7.51	105.6	174.34	44.77	-
106	Ser	9.22	117.06	175.06	60.35	-
107	Tyr	8.56	118.03	175.76	57.71	34.98
108	Gly	7.41	110.33	173.33	47.71	-
109	Phe	8.14	119.67	-	56.22	39.16
110	Arg	9.06	128.84	172.85	54.57	32.19
111	Leu	7.6	116.67	177.52	51.9	-
112	Gly	8.45	108.35	-	43.39	-
113	Phe	-	-	175.63	-	-
114	Leu	9.02	123.34	-	54.22	-
115	His	8.67	122.88	-	56.11	-
116	Ser	8.88	120.76	174.25	61.67	-
117	Gly	8.59	111.25	174.05	44.64	-
118	Thr	8.36	110.32	174.04	60.02	69.06
119	Ala	8.17	124.33	-	53.04	18.25
120	Lys	-	-	176.92	-	-
121	Ser	7.66	112.47	174.47	57.41	63.15
122	Val	7.82	123.44	176.16	62.45	31.96
123	Thr	8.48	115.59	174.77	62.51	69.17
124	Cys	7.35	120.58	172.77	58.35	27.47
125	Thr	9.55	124.1	170.25	59.78	68.34
126	Tyr	8.67	129.6	173.06	55.86	40.79
127	Ser	8.31	120.42	-	52.79	64.04

128	Pro	-	-	179.32	63.86	-
129	Ala	8.1	119.42	179.33	54.4	18.07
130	Leu	6.98	113.44	176.6	53.42	-
131	Asn	7.91	119.81	173.07	53.17	36.17
132	Lys	6.78	118.22	172.42	53.71	-
133	Met	9.45	129.29	172.77	53.73	35.14
134	Phe	9.18	126.49	174.61	55.03	40.26
135	Cys	9.25	119.95	171.95	54.63	32.58
136	Gln	7.76	118.27	176.55	53.96	31.17
137	Leu	8.55	125.97	176.97	56.73	41.26
138	Ala	8.92	123.87	175.77	54.32	17.17
139	Lys	7.41	118.3	177.37	53.59	32.31
140	Thr	8.08	117.97	173.94	65.48	68.58
141	Cys	9.23	127.2	-	55.13	27.73
142	Pro	-	-	175.69	-	-
143	Val	9.02	125.99	174.43	61.63	34.26
144	Gln	8.37	122.4	175.46	53.12	29.25
145	Leu	9.35	120.49	-	53.11	41.32
146	Trp	9.02	127.68	174.63	55.92	-
147	Val	8.13	112.49	176.47	58.75	34.15
148	Asp	9.03	122.88	176.69	55.31	41.29
149	Ser	7.77	113.65	172.45	56.56	64.25
150	Thr	8.16	117.93	-	61.49	69.45
151	Pro	-	-	-	-	-
152	Pro	-	-	-	-	-
153	Pro	-	-	177.83	63.33	-
154	Gly	8.75	113.68	174.29	44.73	-
155	Thr	7.6	118.59	174.22	64.35	67.97
156	Arg	9.62	128.86	173.32	54.89	33.81
157	Val	9.03	120.69	175.51	60.38	32.38
158	Arg	9.52	133.12	173.29	54.05	32.35
159	Ala	8.7	127.48	175.62	50.05	21.26
160	Met	8.08	118.77	172.49	53.97	-
161	Ala	9.45	127.9	175.84	49.29	20.84
162	Ile	8.39	112.14	175.03	59.08	-
163	Tyr	9.14	123.06	-	60.61	-
164	Lys	7.63	119.27	177.34	57.43	-
165	Gln	9.03	116.79	-	55.26	29
166	Ser	-	-	176.67	-	-
167	Gln	9.24	119.63	175.7	57.5	-
168	His	7.53	116.73	176.5	54.92	31.59
169	Met	7.4	119.36	179.08	60.26	32.76
170	Thr	8.42	110.7	173.2	63.1	68.37

171	Glu	8.04	124.91	176.14	56.06	29.38
172	Val	8.71	127.53	177.22	63.99	31.79
173	Val	8.56	130.08	175.22	63.13	30.2
174	Arg	7.93	127.2	174.34	54.2	32.46
175	Arg	7.92	116.9	176.16	56.79	-
176	Cys	8.56	125.17	-	56.07	-
177	Pro	-	-	178.7	65.27	31.13
178	His	7.86	116.19	177.75	59.26	29.57
179	His	8.97	120.64	177.78	62.24	29.4
180	Glu	8.71	120.61	177.75	58.82	28.95
181	Arg	7.14	115.19	176.9	55.96	29.76
182	Cys	7.39	118.99	174.76	59.44	26.8
183	Ser	8.25	118.79	174.59	57.6	-
184	Asp	7.99	122.25	177.64	52.56	40.61
185	Ser	8.38	116.6	175.03	58.77	63.1
186	Asp	8.11	125.09	176.82	53.38	40.28
187	Gly	8.44	109.79	173.6	44.83	-
188	Leu	8.2	122.29	176.89	55.46	43.37
189	Ala	8.89	125.04	-	49.46	17.62
190	Pro	-	-	-	-	-
191	Pro	-	-	176.35	64.61	-
192	Gln	8.57	113.82	176.93	56.98	27.73
193	His	7.18	118.97	-	57.54	31.05
194	Leu	-	-	-	-	-
195	Ile	-	-	175.97	-	-
196	Arg	8.77	122.23	176.07	53.44	34.11
197	Val	7.23	117.91	175.43	60.82	33.48
198	Glu	8.56	129.3	176.77	54.19	30.99
199	Gly	8.7	111.2	174.05	46.18	-
200	Asn	8.16	117.75	175.68	52.11	39.87
201	Leu	8.87	126.76	177.83	55.79	40.81
202	Arg	8.51	119.18	174.4	55.07	28.37
203	Val	6.78	118.74	173.07	60.52	32.2
204	Glu	8.64	126.22	173.83	54.62	32.62
205	Tyr	8.84	123.49	175.58	57.98	38.71
206	Leu	9.29	126.56	174.98	53.89	43.64
207	Asp	8.32	122.84	175.37	52.23	41.08
208	Asp	8.17	124.34	178.6	55.07	43.16
209	Arg	9.03	128.17	175.35	57.51	29.11
210	Asn	8.67	114.94	176.08	54.15	39.62
211	Thr	8.65	109.83	175.68	61.3	-
212	Phe	7.46	114.07	174.48	58.25	35.65
213	Arg	7.53	116.41	176.66	56.08	30.16

214	His	7.83	123.6	176.89	52.54	-
215	Ser	9.32	115.55	171.3	58.62	65.74
216	Val	8.38	116.59	174.43	58.11	32.76
217	Val	9.16	130.82	174.71	59.23	34.86
218	Val	8.3	117.43	-	56.93	32.69
219	Pro	-	-	177.52	62.4	30.9
220	Tyr	8.56	124.32	174.01	59.09	37.2
221	Glu	7.13	131.52	-	51.64	30.17
222	Pro	-	-	-	-	-
223	Pro	-	-	177	62.23	31.28
224	Glu	8.34	123.11	176.18	55.3	29.44
225	Val	8.26	121.85	177.86	64.43	30.53
226	Gly	8.8	116.54	174.04	44.61	-
227	Ser	8.25	116.83	173.1	56.68	64.26
228	Asp	8.43	120.39	174.24	53.88	42.36
229	Cys	7.44	112.69	171.9	54.53	27.76
230	Thr	7.74	119.88	173.11	61.77	70.1
231	Thr	8.73	124.53	173.32	62.2	69.2
232	Ile	9.03	130.06	173.25	59.47	39.31
233	His	8.38	125.21	173.37	53.57	29.95
234	Tyr	8.32	123.34	176.36	57.6	40.74
235	Asn	8.96	117.78	172.16	51.98	43.9
236	Tyr	10	122.04	-	57.83	-
237	Met	8.53	117.11	175.11	53.76	-
238	Cys	7.24	120.43	173.55	60.8	34.32
239	Asn	8.41	118.49	177.76	53.4	39.67
240	Ser	9.55	120.58	174.42	53.41	62.7
241	Ser	8.06	109.88	175.34	58.02	63.19
242	Cys	7.71	122.21	178.2	64.25	28.97
243	Met	9.02	129.99	177.64	56.75	39.34
244	Gly	8.85	110.83	173.69	45.04	-
245	Gly	7.28	109.03	-	43.54	-
246	Met	-	-	179.42	-	-
247	Asn	8.58	118.62	-	54.51	36.9
248	Arg	9.23	108.17	176.03	57.53	-
249	Arg	7.76	123.48	-	53.68	30.39
250	Pro	-	-	177.59	-	-
251	Ile	7.01	112.49	174.66	58.63	42.68
252	Leu	9.21	118.6	178.35	52.75	44
253	Thr	8.84	114.59	171.59	62.02	69.33
254	Ile	9.28	126.99	176.07	59.89	38.59
255	Ile	9.16	130.37	176.13	57.9	-
256	Thr	9.53	117.14	172.86	57.94	69.49

257	Leu	8.08	123.95	176.1	52.12	42.77
258	Glu	9.14	125.75	175.3	53.52	33.98
259	Asp	8.37	119.89	177.93	52.25	40.76
260	Ser	8.57	113.52	175.53	60.85	62.5
261	Ser	8.02	117.37	174.1	58.04	63.41
262	Gly	7.98	109.46	174.59	44.47	-
263	Asn	8.65	121.07	175.25	53.19	37.58
264	Leu	8.57	123.88	176.85	56.04	41.53
265	Leu	9.55	124.38	178.21	54.25	-
266	Gly	7.89	106.74	170.78	45.55	-
267	Arg	10.14	125.29	174.38	56.35	34.23
268	Asn	9.53	127.14	172.45	53.02	44.63
269	Ser	9.34	114.09	172.93	57.6	66.54
270	Phe	8.08	114.02	172.9	56.06	39.62
271	Glu	8.54	123.54	174.82	55.29	29.57
272	Val	7.97	123.72	174.52	60.25	34.97
273	Arg	8.47	127.93	173.12	54.66	32.93
274	Val	8.51	130.26	177.64	59.68	32.89
275	Cys	9.89	124.67	172.91	54.97	31.14
276	Ala	8.53	122.9	179.19	54.69	-
277	Cys	8.78	116.53	-	54.77	27.21
278	Pro	-	-	177.16	65.95	32.01
279	Gly	9.01	104.75	175.47	46.76	-
280	Arg	7.2	122.41	178.62	58.34	29.41
281	Asp	8.09	121.47	177.33	57.3	38.67
282	Arg	7.69	120.95	-	58.92	27.63
283	Arg	7.26	118.35	179.14	59.09	28.81
284	Thr	8.37	116.66	176.66	65.95	68.34
285	Glu	8.14	121.59	180.54	60.59	28.86
286	Glu	8.59	120.62	179.56	59.56	28.11
287	Glu	8.33	121.95	178.84	58.6	28.1
288	Asn	7.97	118.22	177.37	55.18	37.5
289	Leu	7.5	121.03	178.84	57	40.85
290	Arg	7.71	119.78	178.25	57.81	29.46
291	Lys	7.92	119.42	177.59	57.29	31.75
292	Lys	7.81	120.46	177.45	57	31.76
293	Gly	7.97	108.43	173.77	44.6	-
294	Glu	7.95	122.24	-	53.94	28.94
295	Pro	-	-	176.66	62.81	31.12
296	His	8.39	119.76	-	55.46	29.4
297	His	-	-	174.57	-	-
298	Glu	8.45	122.96	176.02	55.79	29.67
299	Leu	8.35	125.51	-	52.5	40.57

300	Pro	-	-	-	-	-
301	Pro	-	-	177.83	63.09	31.04
302	Gly	8.54	110.23	174.58	44.89	-
303	Ser	8.04	115.99	174.9	58.42	63.34
304	Thr	8.19	116.61	174.47	61.66	69.21
305	Lys	8.24	124.33	176.31	55.92	32.01
306	Arg	8.24	123.25	175.59	55.47	30.05
307	Ala	8.29	126.38	177.27	51.69	18.48
308	Leu	8.22	123.74	-	52.53	40.6
309	Pro	-	-	176.65	62.74	31.14
310	Asn	8.45	119.04	174.91	52.86	38.27
311	Asn	8.36	119.97	174.47	53.03	38.36
312	Thr	7.7	119.51	-	63.02	70.26

*L1 – L4: linker residues from thrombin cleavage.

Table D3: H_N, N, C', C_α, and C_β chemical shifts (ppm) of the AD in NMR buffer at 293K.

Residue number	Amino acid	H_N	N	C'	C_α	C_β
215	Ser	-	-	-	-	-
216	Thr	-	-	-	-	-
217	Gly	8.53	111.56	173.91	45.12	-
218	Thr	8.14	116.59	173.01	59.72	69.69
219	Pro	-	-	176.92	63.4	32.13
220	Ser	8.42	116.1	173.92	58.33	63.84
221	Asn	8.43	121.12	173.49	51.17	39.01
222	Pro	-	-	176.73	63.71	32.16
223	Asp	8.27	119.36	176.53	54.63	40.92
224	Leu	7.96	122.03	177.34	55.42	42.36
225	Asp	8.25	120.97	176.18	54.56	41.19
226	Ala	8.17	124.59	178.43	52.94	19.13
227	Gly	8.4	107.81	174.33	45.42	-
228	Val	7.92	119.12	176.39	62.3	32.82
229	Ser	8.41	119.38	174.51	58.24	63.86
230	Glu	8.45	123.01	176.16	56.69	30.24
231	His	8.37	119.59	174.84	55.46	30.02
232	Ser	8.33	117.66	175.01	58.51	63.85
233	Gly	8.45	110.8	173.93	45.41	-
234	Asp	8.19	120.43	176.1	54.45	40.98
235	Trp	8.03	121.29	175.94	57.5	29.35
236	Leu	7.87	124.19	176.54	54.91	42.66
237	Asp	8.13	121.32	176.37	54.28	41
238	Gln	8.28	120.86	175.98	56.09	29.51
239	Asp	8.41	121.07	176.41	54.81	41.14
240	Ser	8.15	115.88	174.59	58.48	63.89
241	Val	8.12	121.51	176.35	62.31	32.77
242	Ser	8.36	119.26	174.45	58.37	63.86
243	Asp	8.36	122.72	176.32	54.43	41.07
244	Gln	8.23	120.05	175.68	56.04	29.27
245	Phe	8.19	120.66	175.66	57.61	39.51
246	Ser	8.13	117.58	174.22	58.12	63.87
247	Val	8.14	121.66	175.94	62.21	32.85
248	Glu	8.37	124.15	175.94	56.47	30.41
249	Phe	8.13	120.95	175.29	57.39	39.91
250	Glu	8.33	123.17	175.99	56.19	30.48
251	Val	8.24	121.97	176.14	62.22	32.96
252	Glu	8.56	125.26	176.33	56.59	30.52
253	Ser	8.44	117.75	174.4	57.92	63.75

254	Leu	8.41	125.04	177.17	55.03	42.42
255	Asp	8.38	121.57	176.29	54.38	41.23
256	Ser	8.25	116.27	174.63	58.35	63.92
257	Glu	8.44	122.81	175.82	56.55	30.28
258	Asp	8.26	121.16	176.11	54.07	41.14
259	Tyr	8.19	122.2	176.11	57.98	38.47
260	Ser	8.3	117.73	174.4	58.72	63.77
261	Leu	8.14	123.93	177.46	55.16	42.26
262	Ser	8.25	116.74	174.61	58.28	63.92
263	Glu	8.49	123.21	176.51	56.55	30.38
264	Glu	8.45	121.99	177.17	56.87	30.35
265	Gly	8.52	110.35	174.15	45.41	-
266	Gln	8.2	119.74	175.88	55.56	29.84
267	Glu	8.61	122.73	176.29	56.47	30.1
268	Leu	8.4	124.22	177.26	54.91	42.5
269	Ser	8.46	117.4	174.3	57.84	64.1
270	Asp	8.49	123.29	176.41	54.45	41.27
271	Glu	8.38	120.89	176.3	56.63	30.43
272	Asp	8.37	121.51	176.49	54.44	41.3
273	Asp	8.28	121.39	176.51	54.54	41.32
274	Glu	8.36	121.51	176.11	56.84	30.22
275	Val	8.09	121.15	176.05	62.65	32.6
276	Tyr	8.22	124.15	175.58	57.95	38.8
277	Gln	8.18	122.71	175.38	55.4	29.67
278	Val	8.17	122.03	176.25	62.43	32.85
279	Thr	8.29	119.75	174.07	62.18	69.83
280	Val	8.19	123.8	175.56	62.06	32.93
281	Tyr	8.36	125.27	175.47	58.01	38.99
282	Gln	8.28	123.96	174.94	55.1	29.79
283	Ala	8.36	126.34	178.2	52.74	19.22
284	Gly	8.43	108.69	174.24	45.15	-
285	Glu	8.33	120.63	176.67	56.61	30.47
286	Ser	8.43	116.36	174.27	58.12	63.98
287	Asp	8.45	122.79	176.49	54.48	41.08
288	Thr	8.13	113.74	174.45	61.85	69.8
289	Asp	8.34	123.03	176.12	54.56	41.3
290	Ser	8.15	115.9	174.01	58.26	63.79
291	Phe	8.27	122.49	175.39	57.59	39.72
292	Glu	8.26	123.12	175.74	56.05	30.76
293	Glu	8.36	122.52	175.82	56.1	30.76
294	Asp	8.56	123.69	174.72	52.32	41.01
295	Pro	-	-	177.17	63.34	32.24
296	Glu	8.5	120.32	176.72	56.75	29.98

297	Ile	8	121.71	176.17	61.08	38.77
298	Ser	8.36	119.96	174.45	58.06	63.74
299	Leu	8.36	125.69	176.18	55	42.27
300	Ala	7.85	110.55	172.52	53.85	20.15

Table D4: H_N, N, C' and C_α chemical shifts (ppm) of the AD in complex with the DBD in NMR buffer at 293K.

Residue number	Amino acid	H_N	N	C'	C_α
215	Ser	-	-	-	-
216	Thr	-	-	-	-
217	Gly	-	-	173.86	45.15
218	Thr	8.11	116.79	-	59.75
219	Pro	-	-	176.95	63.43
220	Ser	8.39	116.29	173.92	58.47
221	Asn	8.4	121.31	-	51.19
222	Pro	-	-	176.75	63.72
223	Asp	8.24	119.54	176.51	54.66
224	Leu	7.93	122.22	177.34	55.43
225	Asp	8.22	121.16	176.18	54.53
226	Ala	8.14	124.77	178.43	52.94
227	Gly	8.38	107.99	174.34	45.45
228	Val	7.89	119.29	176.39	62.34
229	Ser	8.38	119.55	174.56	58.33
230	Glu	8.43	123.21	176.15	56.79
231	His	8.34	119.82	-	55.53
232	Ser	-	-	175	58.56
233	Gly	8.42	110.99	173.92	45.43
234	Asp	8.16	120.67	176.11	54.44
235	Trp	8	121.42	175.97	57.53
236	Leu	7.85	124.2	176.58	54.95
237	Asp	8.11	121.46	176.39	54.29
238	Gln	8.25	121.00	175.98	56.18
239	Asp	8.39	121.22	176.42	54.8
240	Ser	8.12	116.01	174.65	58.56
241	Val	8.08	121.6	176.36	62.39
242	Ser	8.32	119.31	174.47	58.46
243	Asp	8.32	122.86	176.34	54.47
244	Gln	8.2	120.18	175.73	56.11
245	Phe	8.15	120.67	175.67	57.67
246	Ser	8.09	117.64	174.29	58.18
247	Val	8.11	121.76	175.96	62.24
248	Glu	8.34	124.16	175.97	56.56
249	Phe	8.09	120.97	175.33	57.46
250	Glu	8.3	123.19	176.04	56.26
251	Val	8.19	121.92	176.16	62.32
252	Glu	8.54	125.17	176.36	56.71

253	Ser	8.39	117.72	174.5	58.08
254	Leu	8.35	125.16	177.17	55.15
255	Asp	8.33	121.69	176.29	54.44
256	Ser	8.19	116.48	174.7	58.5
257	Glu	8.39	123.03	175.86	56.6
258	Asp	8.2	121.41	176.15	54.14
259	Tyr	8.13	122.32	176.09	58.09
260	Ser	8.28	117.72	174.5	58.86
261	Leu	8.09	124.16	177.48	55.22
262	Ser	8.2	116.84	174.69	58.41
263	Glu	8.44	123.44	176.64	56.69
264	Glu	8.39	122.15	177.18	56.94
265	Gly	8.46	110.63	174.2	45.47
266	Gln	8.14	119.97	175.88	55.66
267	Glu	8.57	122.86	176.32	56.56
268	Leu	8.35	124.29	177.27	54.92
269	Ser	8.4	117.64	174.34	57.99
270	Asp	8.45	123.58	176.4	54.5
271	Glu	8.33	121.14	176.33	56.77
272	Asp	8.3	121.64	176.08	54.55
273	Asp	8.23	121.66	176.52	54.61
274	Glu	8.31	121.79	176.59	56.99
275	Val	8.03	121.26	176.08	62.75
276	Tyr	8.14	124.22	175.57	58.01
277	Gln	8.14	122.66	175.43	55.52
278	Val	8.11	122.08	176.19	62.39
279	Thr	8.23	119.93	-	62.35
280	Val	-	-	175.49	62.09
281	Tyr	8.29	125.34	-	58.02
282	Gln	-	-	175.1	55.31
283	Ala	8.36	126.5	178.2	52.75
284	Gly	8.4	108.82	174.23	45.19
285	Glu	8.28	120.98	176.66	56.62
286	Ser	8.39	116.75	174.29	58.23
287	Asp	8.41	123.14	176.52	54.5
288	Thr	8.08	114.04	174.46	61.92
289	Asp	8.29	123.34	176.09	54.58
290	Ser	8.1	116.23	174.03	58.21
291	Phe	8.22	122.81	175.4	57.65
292	Glu	8.21	123.39	175.75	56.11
293	Glu	8.31	122.84	175.84	56.15
294	Asp	8.51	124.01	-	52.34
295	Pro	-	-	177.16	63.35

296	Glu	8.45	120.7	176.74	56.81
297	Ile	7.95	121.99	176.15	61.11
298	Ser	8.3	120.29	174.43	58.11
299	Leu	8.31	126.01	176.16	55.03
300	Ala	7.8	115.46	-	53.85

Table D5: H_N, N, C', C_α, and C_β chemical shifts (ppm) of the TD in NMR buffer at 293K.

Residue number	Amino acid	H_N	N	C'	C_α	C_β
1	Met	-	-	-	-	-
2	Glu	-	-	175.79	56.42	30.4
3	Glu	8.6	124.08	174.46	54.55	29.64
4	Pro	-	-	176.81	63.14	32.16
5	Gln	8.56	121.13	175.95	55.47	29.76
6	Ser	8.4	117.92	173.71	58.3	64
7	Asp	8.45	123.75	174.65	52.18	40.76
8	Pro	-	-	177.04	63.61	32.28
9	Ser	8.51	116.14	174.45	58.97	63.84
10	Val	7.87	121.25	175.81	61.68	32.82
11	Glu	8.35	126.36	173.83	54.18	29.69
12	Pro	-	-	-	-	-
13	Pro	-	-	176.87	62.91	32.32
14	Leu	8.36	122.58	177.57	55.24	42.24
15	Ser	8.34	116.87	174.54	58.26	63.74
16	Gln	8.5	122.63	175.96	55.94	29.48
17	Glu	8.47	122.08	176.53	56.85	29.87
18	Thr	8.11	115.1	174.31	61.95	69.81
19	Phe	8.24	122.4	175.85	58.22	39.26
20	Ser	8.1	116.84	174.41	58.53	63.86
21	Asp	8.28	122.22	176.87	55.06	40.58
22	Leu	7.93	121.21	178.06	56.63	41.6
23	Trp	7.85	119.49	176.74	57.88	28.71
24	Lys	7.55	120.57	176.11	56.85	32.79
25	Leu	7.81	120.76	177.08	55.03	42.16
26	Leu	7.91	123.82	175.47	53.12	41.3
27	Pro	-	-	177.45	63.91	32.19
28	Glu	8.73	119.87	176.28	57	29.7
29	Asn	8.27	118.93	174.69	53.32	38.41
30	Asn	8.27	119.69	174.81	53.39	39.01
31	Val	8.04	120.38	176.03	62.64	32.54
32	Leu	8.3	125.73	177.05	55.04	42.21
33	Ser	8.24	118.28	172.33	56.39	63.16
34	Pro	-	-	176.69	63.04	32.2
35	Leu	8.32	123.87	175.46	53.28	41.44
36	Pro	-	-	176.96	63.29	32.16

37	Ser	8.35	115.87	174.6	58.48	63.72
38	Gln	8.39	122.38	175.53	55.61	29.55
39	Ala	8.32	125.37	177.82	52.54	19.08
40	Met	8.34	119.65	176.19	55.53	32.81
41	Asp	8.25	121.13	176.13	55	40.93
42	Asp	8.23	120.35	176.35	54.82	40.92
43	Leu	8.08	121.83	177.34	55.3	41
44	Met	8.24	120.43	175.88	55.31	32.42
45	Leu	8.09	123.26	177.08	55.06	42.42
46	Ser	8.53	118.58	173.16	56.17	63.48
47	Pro	-	-	176.91	63.96	32.31
48	Asp	8.21	118.98	176.13	54.95	40.92
49	Asp	8.09	120.34	176.27	54.65	41.01
50	Ile	7.85	120.31	176.38	61.56	38.81
51	Glu	8.34	123.89	176.46	56.94	29.88
52	Gln	8.15	120.55	175.36	55.7	29.51
53	Trp	7.97	121.56	175.62	56.99	29.68
54	Phe	7.98	121.63	175.28	57.58	39.74
55	Thr	7.98	116.42	173.69	61.56	69.9
56	Glu	8.31	123.47	175.72	56.24	30.57
57	Asp	8.45	123.53	174.39	52.21	40.89
58	Pro	-	-	177.27	63.42	32.41
59	Gly	8.41	109.38	172.12	44.29	-
60	Pro	-	-	177.01	63.56	32.3
61	Asp	8.45	119.91	176.07	54.55	40.84
62	Glu	8.1	120.87	175.76	56.15	30.55
63	Ala	8.27	126.71	175.24	50.54	17.81
64	Pro	-	-	176.72	63.05	32.15
65	Arg	8.47	122.07	176.24	56.05	30.89
66	Met	8.48	123.39	174.28	53.3	30.89
67	Pro	-	-	176.81	63.24	32.15
68	Glu	8.54	121.25	176.08	56.57	30.17
69	Ala	8.31	125.48	176.98	52.05	19.25
70	Ala	8.22	124.81	175.32	50.39	17.9
71	Pro	-	-	-	-	-
72	Arg	-	-	-	-	-
73	Val	8.19	122.25	175.35	61.6	32.92
74	Ala	8.45	129.99	175.18	50.38	17.97
75	Pro	-	-	-	-	-
76	Ala	-	-	-	-	-

77	Pro	-	-	-	-	-
78	Ala	-	-	-	-	-
79	Ala	-	-	-	-	-
80	Pro	-	-	176.75	62.99	32.3
81	Thr	8.33	117.66	172.86	60.01	69.69
82	Pro	-	-	-	-	-
83	Ala	-	-	-	-	-
84	Ala	-	-	-	-	-
85	Pro	-	-	-	-	-
86	Ala	-	-	-	-	-
87	Pro	-	-	-	-	-
88	Ala	-	-	-	-	-
89	Pro	-	-	-	63.05	32.05
90	Ser	8.13	115.89	173.49	58.11	63.8
91	Trp	8.03	123.98	174.1	54.85	29.2
92	Pro	-	-	175.89	63.14	31.92
93	Leu	7.84	128.45	175.3	56.75	43.21

Table D6: H_N, N, C', C_α and C_β chemical shifts (ppm) of the ADX in NMR buffer at 293K.

Residue #	Amino acid	H_N	N	C'	C_α	C_β
181	Asp	-	-	-	-	-
182	Glu	-	-	176.75	-	-
183	Thr	8.35	115.19	174.84	62.58	69.76
184	Ser	8.34	118.58	174.52	58.6	63.79
185	Arg	8.35	123.14	173.22	56.31	30.81
186	Leu	8.25	122.98	177.05	55.45	42.39
187	Asp	8.32	120.73	176.14	54.22	40.95
188	Leu	8.06	122.13	177.82	55.37	42.33
189	Gly	8.39	108.9	174.03	45.37	-
190	Phe	7.9	119.39	175.82	57.79	39.54
191	Glu	8.48	121.76	176.55	56.92	29.97
192	Glu	8.25	120.6	176.27	56.97	30.07
193	Trp	7.85	120.44	175.97	57.01	29.8
194	Asp	8.16	121.93	176.71	54.3	41.02
195	Val	7.88	119.68	176.37	62.88	32.3
196	Ala	8.18	124.79	178.26	53.07	18.93
197	Gly	8.07	107.06	173.87	45.13	-
198	Leu	7.71	122.02	174.87	52.84	41.63
199	Pro	-	-	177.93	62.65	-
200	Trp	7.96	120.38	176.93	58.65	-
201	Trp	6.48	117.95	176.38	57.29	27.62
202	Phe	7.21	121.54	176	58.78	39.3
203	Leu	7.77	121.39	177.97	55.8	42.03
204	Gly	7.86	107.47	174.3	45.92	-
205	Asn	8.09	118.46	175.48	53.62	38.83
206	Leu	8.05	121.42	177.6	55.79	42.25
207	Arg	8.17	120.29	176.62	56.59	30.62
208	Ser	8.15	115.61	173.37	58.8	63.81
209	Asn	8.3	119.78	174.55	53.36	38.83
210	Tyr	8.03	120.72	175.18	58.11	38.98
211	Thr	7.94	120.2	178.5	59.37	70.16
212	Pro	-	-	176.76	63.02	32.15
213	Arg	8.41	121.26	176.5	56.13	30.95
214	Ser	8.39	116.98	174.5	58.26	63.95
215	Asn	8.57	121.22	175.79	53.4	38.86
216	Gly	8.42	109.31	174.31	45.47	-
217	Ser	8.24	115.7	175.13	58.54	63.95
218	Thr	8.28	115.46	174.38	62.08	69.72
219	Asp	8.32	122.72	176.18	54.56	41.09

220	Leu	8.18	122.35	177.52	55.47	42.26
221	Gln	8.41	120.83	176.32	56.02	29.39
222	Thr	8.16	114.76	174.44	62.03	69.86
223	Asn	8.47	120.85	175.19	53.51	38.81
224	Gln	8.39	120.65	175.64	56.01	29.47
225	Asp	8.42	121.8	176.47	54.51	41.16
226	Val	8.11	119.92	176.89	62.59	32.51
227	Gly	8.49	111.84	174.38	45.44	-
228	Thr	8	113.94	174.24	61.87	69.88
229	Ala	8.29	126.98	177.4	52.48	19.24
230	Ile	8.19	121.24	176.35	61.08	38.62
231	Val	8.31	125.57	175.97	62.15	32.89
232	Ser	8.44	120.3	174.09	58.12	64.09
233	Asp	8.45	123.04	176.48	54.43	41.27
234	Thr	8.2	114.16	174.88	61.71	69.81
235	Thr	8.23	116.04	174.49	62.23	69.81
236	Asp	8.29	122.73	176.11	54.62	41.3
237	Asp	8.3	120.78	176.6	54.92	40.98
238	Leu	8.1	121.48	177.69	55.54	41.64
239	Trp	7.9	120.75	176.32	58.11	29.2
240	Phe	7.42	119.51	175.56	57.87	39.03
241	Leu	7.76	122.55	177.01	55.44	42.21
242	Asn	8.14	119.27	175.38	53.54	39.01
243	Glu	8.34	121.4	176.66	57.03	30.31
244	Ser	8.32	116.63	174.85	58.77	63.72
245	Val	8.11	121.59	176.51	62.69	32.65
246	Ser	8.31	118.84	174.98	58.87	63.78
247	Glu	8.43	123.04	176.68	57.11	30.18
248	Gln	8.34	120.89	176.37	56.04	29.23
249	Leu	8.25	122.96	178.05	55.46	42.4
250	Gly	8.4	109.54	174.23	45.45	-
251	Val	7.95	118.84	176.79	62.48	32.64
252	Gly	8.5	112.44	173.85	45.23	-
253	Ile	7.93	120.37	176.07	61	38.84
254	Lys	8.44	126.64	176.16	56.07	33.13
255	Val	8.33	123.7	176.1	62.28	32.97
256	Glu	8.58	125.76	176.02	56.23	30.41
257	Ala	8.42	126.01	177.37	52.41	19.4
258	Ala	8.36	123.72	177.62	52.44	19.43
259	Asp	8.37	119.79	176.67	54.46	41.07
260	Thr	8.07	113.95	174.8	62.06	69.87
261	Glu	8.44	123.26	176.56	56.77	30.21
262	Gln	8.44	121.8	176.26	55.86	29.52

263	Thr	8.33	115.91	174.69	61.85	69.95
264	Ser	8.44	118.22	174.75	58.54	63.9
265	Glu	8.51	123.02	176.58	56.86	30.34
266	Glu	8.42	122.06	176.78	56.75	30.3
267	Val	8.16	121.62	177.03	63.02	32.51
268	Gly	8.52	112.22	174.09	45.37	-
269	Lys	8.05	121.08	176.87	56.27	33.23
270	Val	8.27	122.1	176.37	62.47	32.79
271	Ser	8.43	119.55	174.36	58.33	63.96
272	Asp	8.36	123.19	176.18	54.4	41.1
273	Lys	8.19	121.6	176.47	56.33	32.9
274	Lys	8.35	123.22	176.46	56.3	32.99
275	Val	8.23	122.82	175.99	62.49	32.75
276	Ile	8.26	125.68	175.99	60.9	38.63
277	Glu	8.52	126.37	176.18	56.18	30.56
278	Val	8.3	122.41	176.78	62.67	32.7
279	Gly	8.6	113.02	173.96	45.24	-
280	Lys	8.18	121.03	176.36	56.15	33.26
281	Asn	8.6	120.52	175.01	53.27	39.08
282	Asp	8.37	121.1	175.98	54.66	41.2
283	Asp	8.32	120.3	176.42	54.63	41.05
284	Leu	8.15	121.9	177.81	55.43	42.27
285	Glu	8.35	121.51	176.54	56.91	30.24
286	Asp	8.38	121.57	176.6	54.54	41.16
287	Ser	8.28	116.5	174.93	58.82	63.69
288	Lys	8.28	123.15	176.81	56.53	32.86
289	Ser	8.33	116.96	174.68	58.46	63.77
290	Leu	8.31	124.38	177.51	55.32	42.34
291	Ser	8.26	116.21	174.23	58.26	64.04
292	Asp	8.36	122.73	176.07	54.44	41.29
293	Asp	8.34	121.06	176.54	54.48	41.07
294	Thr	8.13	114.13	174.45	62.36	69.89
295	Asp	8.41	123.37	176.09	54.43	41.07
296	Val	7.98	119.97	176.09	62.19	32.92
297	Glu	8.47	125.09	176.37	56.51	30.38
298	Val	8.34	122.9	176.47	62.37	32.78
299	Thr	8.35	118.75	173.87	61.62	70.03
300	Ser	8.03	123.88	-	60.04	64.9

Table D7: H_N, N, C', C_α and C_β chemical shifts (ppm) of the PBD2 in NMR buffer at 293K.

Residue #	Amino acid	H_N	N	C'	C_α	C_β
2	Cys	-	-	-	-	-
3	Asn	-	-	175.84	53.33	38.5
4	Thr	8.09	113.92	174.48	62.73	69.89
5	Asn	8.49	120.65	175.09	53.36	38.63
6	Met	8.29	120.69	175.98	55.96	32.72
7	Ser	8.27	116.46	173.96	58.64	63.81
8	Val	7.95	122.06	-	59.71	32.69
9	Pro	-	-	177.22	-	-
10	Thr	8.27	114.13	174.49	61.97	69.8
11	Asp	8.32	122.3	176.69	54.56	41.09
12	Gly	8.3	109.37	173.81	45.42	-
13	Ala	8.05	123.19	177.79	52.6	19.45
14	Val	8.14	119.22	176.58	62.41	32.84
15	Thr	8.3	117.94	174.85	61.97	69.72
16	Thr	8.2	116.03	174.68	61.65	69.7
17	Ser	8.33	118.21	-	61.98	63.73
18	Gln	-	-	-	-	-
19	Ile	-	-	-	-	-
20	Pro	-	-	177.28	-	-
21	Ala	8.81	126.82	179.38	54.97	18.56
22	Ser	8.55	111.57	-	60.12	62.42
23	Glu	-	-	178.46	58.2	30
24	Gln	7.89	118.95	-	58.14	29.24
25	Glu	-	-	175.94	55.64	29.93
26	Thr	7.53	117.48	173.12	64.53	70.37
27	Leu	8.48	128.05	177.04	54.78	43.35
28	Val	9.79	117.03	174.02	59.26	36.44
29	Arg	9.21	121.67	-	52.51	32.42
30	Pro	-	-	-	-	-
31	Lys	-	-	-	-	-
32	Pro	-	-	179.02	67.39	32.64
33	Leu	8.9	118.49	178.33	58.24	41.61
34	Leu	7.42	118.36	177.9	56.83	40.8
35	Leu	8.6	120.15	-	58.19	41.41

36	Lys	-	-	-	-	-
37	Leu	7.31	121.21	179.93	59.67	41.13
38	Leu	8.18	120.48	-	58.06	39.74
39	Lys	-	-	180.37	-	-
40	Ser	7.88	116.79	175.38	61.68	62.92
41	Val	7.27	112.67	175.67	60.64	30.93
42	Gly	7.5	111.45	174.51	45.58	-
43	Ala	7.34	125	178.11	53.3	18.47
44	Gln	8.75	118.02	172.06	55.82	31.25
45	Lys	7.36	118.18	175.74	55.67	34.64
46	Asp	-	-	175.74	55.03	42.27
47	Thr	6.99	111.11	172.27	60.6	71.82
48	Tyr	8.73	119.88	175.88	57.35	45.78
49	Thr	9.02	110.73	-	61.12	71.04
50	Met	-	-	-	-	-
51	Lys	-	-	-	-	-
52	Glu	7.91	120.1	178.54	-	-
53	Val	8.3	119.64	-	67.98	30.78
54	Leu	-	-	-	-	-
55	Phe	8.09	121.84	178.56	62.47	32.36
56	Tyr	8.53	119.9	178.37	62.9	38.92
57	Leu	8.9	121.23	178.97	58.19	41.97
58	Gly	8.28	106.56	176.18	47.55	-
59	Gln	7.69	120.5	178.97	58.43	28.51
60	Tyr	8.75	124.41	-	62.8	38.52
61	Ile	-	-	177.64	66.07	-
62	Met	7.89	115.75	179.92	58.32	32.31
63	Thr	8.57	116.23	-	66.21	69.24
64	Lys	-	-	174.89	-	-
65	Arg	7.6	116.16	176.29	56.73	26.52
66	Leu	7.63	115.03	176.21	54.82	42.28
67	Tyr	6.88	114.44	175.84	56.12	39.19
68	Asp	8.64	123.64	176.65	54.32	42.94
69	Glu	8.63	124.06	-	59.34	30.01
70	Lys	-	-	177.2	-	-
71	Gln	8.39	121.03	175.21	54.49	29.47
72	Gln	8.29	119.06	174.76	58.84	27.84
73	His	7.84	112.64	173.68	56.4	30.7

74	Ile	7.72	122.51	173.91	59.77	37.14
75	Val	8.39	126.33	174.66	60.92	32.86
76	Tyr	8.36	125.9	175.33	57.78	38.66
77	Cys	8.41	117.46	173.82	55.96	29.52
78	Ser	7.7	116.63	174.75	60.48	63.43
79	Asn	8.75	118.17	173.01	53.28	38.12
80	Asp	7.67	118.52	175.13	53.3	47.38
81	Leu	8.43	128.9	178.06	58.16	47.35
82	Leu	9.85	118.56	178.28	58.19	42.51
83	Gly	7.77	106.61	177.21	48.02	-
84	Asp	7.53	123.05	178.77	56.88	40.25
85	Leu	8.09	118.93	-	57.24	41.87
86	Phe	-	-	176.78	-	-
87	Gly	8.31	108.34	174.1	46.55	-
88	Val	7.11	108.48	-	56.99	34.78
89	Pro	-	-	176.78	63.13	32.03
90	Ser	7.23	111.14	172.52	56.7	65.18
91	Phe	8.23	114.62	171.48	56.79	39.77
92	Ser	8.81	113	178.28	54.7	63.79
93	Val	9.5	122.64	-	64.65	31.66
94	Lys	-	-	-	-	-
95	Glu	7.37	120	-	54.7	27.86
96	His	-	-	-	-	-
97	Arg	-	-	-	-	-
98	Lys	-	-	-	-	-
99	Ile	-	-	-	-	-
100	Tyr	8.62	121.27	177.01	62.83	38.61
101	Thr	8.17	114.19	176.42	67.33	69.02
102	Met	7.88	120.34	-	59.68	31.22
103	Ile	-	-	178.71	-	-
104	Tyr	8.87	119.75	-	61.31	37.68
105	Arg	-	-	-	-	-
106	Asn	-	-	-	-	-
107	Leu	-	-	175.6	-	-
108	Val	8.73	127.86	-	63.1	32.49
109	Val	8.16	119.19	176.21	63.11	32.57
110	Val	8.42	127.04	175.64	63.09	32.41
111	Asn	8.6	122.64	175.04	53.21	38.9

112	Gln	8.48	121.56	175.86	56.31	29.57
113	Gln	8.46	121.29	176.02	56.25	29.51
114	Glu	8.45	122.27	176.55	56.61	30.4
115	Ser	8.42	116.99	174.73	58.24	63.96
116	Ser	8.46	118.14	174.41	58.45	63.94
117	Asp	8.39	122.49	176.5	54.58	41.24
118	Ser	8.34	116.6	175.29	59	63.82
119	Gly	8.5	110.93	174.43	45.52	-
120	Thr	8.05	113.62	174.63	61.83	69.94
121	Ser	8.4	118.87	174.45	58.26	63.87
122	Val	8.25	121.89	176.12	62.16	32.82
123	Ser	8.39	119.65	174.32	58.19	64.01
124	Glu	8.5	123.59	175.34	56.61	30.56
125	Asn	8.04	124.53	-	54.84	40.54